INVESTIGATION OF THE LIQUEFACTION

OF A

SOIL PROFILE

USING

IN SITU TESTS

CLIFFORD ALAN JESSETT

DOCTOR OF PHILOSOPHY

CITY UNIVERSITY, LONDON

DEPARTMENT OF CIVIL ENGINEERING

GEOTECHNICAL ENGINEERING RESEARCH CENTRE

JUNE 1992

LIST OF CONTENTS

LIST OF TABLES

LIST OF FIGURES

ACKNOWLEDGEMENTS

The author wishes to acknowledge the Science and Engineering Research Council and Sir William Halcrow and Partners for jointly funding the research in the form of a Cooperative Award in Science and Engineering. The interest and support of colleagues, particularly that of Dr Nick Brut, at Sir William Halcrow and Partners was of great value. Gratitude is also expressed to others, such as Hans Erwig (Associate of Fugro McClelland), that have contributed to the research by their discussion and suggestions.

Greatest thanks is given to Professor John Atkinson. Without his guidance and enthusiasm it is certain that the project would not have reached this point. The author also wishes to thank all of his colleagues at the research centre for their advice, technical assistance and friendship.

This dissertation has been completed while the author was a member of the Newcastle upon Tyne office of Ove Arup and Partners. The assistance of both Ove Arup and Partners and individual colleagues in completing the dissertation is gratefully acknowledged. In particular the author wishes to thank David Williams for proof-reading the final text and Karen Clift for her patience when typing the document.

Finally the author wishes to thank his wife, Sue, and young daughters, Amy and Katie, for allowing him the time to complete this project.

DECLARATION

I grant powers of discretion to the University Librarian to allow this thesis to be copied in whole or in part without further reference to me. This permission covers copies made for study purposes, subject to normal conditions of acknowledgement.

ABSTRACT

Liquefaction is defined here as a sudden reduction in soil strength and stiffness resulting from a rapid increase in pore pressure. It is a behaviour typically associated with extensive deposits of fine granular soils. The mechanisms of liquefaction are identified as the generation and dissipation of excess pore pressures. Failure due to liquefaction can occur at the point of excess pore pressure generation (coincident liquefaction), or elsewhere in a soil profile or structure (non-coincident liquefaction). Existing methods available to the engineer for assessing the likelihood of liquefaction have been reviewed. None of these appear correctly to assess excess pore pressure generation and dissipation within real soil profiles. Therefore, these cannot always correctly predict liquefaction behaviour. A new approach based upon an in situ test is proposed.

New laboratory equipment was built which enabled the rapid preparation of uniform beds of soil and the monitoring of pore pressure generation and dissipation. It was used to study aspects of excess pore pressure generation due to rapid single increment loading and their subsequent dissipation. Two mechanisms of dissipation are identified; one-dimensional consolidation and hindered settling. The latter would appear to be relevant in correctly understanding liquefaction failure.

The same equipment was used to assess which type of in situ instrument is able to determine in situ soil state. The research indicates that testing with a piezovane is potentially the best way of determining soil state and excess pore pressure dissipation characteristics throughout real soil profiles. It is proposed that the use of this approach in conjunction with correct numerical modelling of excess pore pressure dissipation should be developed as an appropriate engineering method of assessing the likelihood of liquefaction at a site.

SYMBOLS AND ABBREVIATIONS

a	soil particle radius (m)
c_p'	Hvorslev cohesion intercept
c_v	coefficient of consolidation (m^2 year $^{-1}$)
d	maximum drainage path (m)
e	void ratio
g	acceleration due to gravity (9.81 m s^{-2})
h	horizontal displacement, direct shear box tests (mm)
k	permeability (m s^{-1})
i	hydraulic gradient
m	hindered settling constant (function of soil particle shape, size distribution and Reynolds number)
q	applied load
r	internal radius of sand column (0.094m)
t	elapse time or time (seconds)
u_o	initial soil pore pressure (kPa)
$\bar{u}$	excess pore pressure (kPa)
v	vertical displacement, direct shear tests (mm)
v_s	terminal settling velocity of a single sphere through a fluid (m s^{-1})
v_{hs}	terminal settling velocity of particles forming a concentration falling through a fluid (m s^{-1})
z	depth (m)

C	concentration of a suspension, volume of solid particles per unit volume of suspension
CSL	critical state line
D_r	relative density (%)
D_{10}, D_{50}	effective particle size (mm)
G_s	specific gravity of soil particles
H	static head of water (m)
K	Stokes number, a correction factor
M	mass of soil particles forming a soil bed in the sand column (kg)
N	Standard Penetration Test value or resistance
NCL	normal consolidation (compression) line
N_1	Modified Standard Penetration Test Resistance

O — digital output of monitoring system (millivolts) corresponding to a miniature electrical pore pressure transducer

R_e — Reynolds number, $\frac{2av_s}{\mu}$

T — thickness of soil bed in the sand column (m)

T_1 — thickness of initial very loose soil bed in the sand column prior to vibration (m)

T_2 — thickness of soil bed produced by prolonged vibration (m)

T_v — time factor

U — soil particle size uniformity coefficient

U — degree of consolidation

V — supply voltage to instrumentation (volts)

γ_{sus} — unit weight of soil suspension (kN m^{-3})

γ_w — unit weight of pore fluid (water) (kN m^{-3})

ε — strain

λ — slope of critical state line

μ — fluid dynamic viscosity (N s m^{-2} or kg m^{-1} s^{-1})

ρ — surface settlement (mm)

ρ_s — density of soil particles (kg m^{-3})

ρ_w — density of pore fluid (kg m^{-3})

σ_n, σ_n' — total and effective normal stress (kN m^{-2})

σ'_{vo} — initial vertical effective stress (kN m^{-2})

τ, τ' — total and effective shear stress (kN m^{-2})

τ'_{crit} — effective shear stress at critical state (kN m^{-2})

τ'_{peak} — effective shear stress at peak state (kN m^{-2})

υ — specific volume

Γ — specific volume of soil at critical state with $\sigma_n' = 1.0$ kN m^{-2}

ϕ'_{cs} — critical state or ultimate angle of friction

ϕ'_p — Hvorslev friction angle

CHAPTER 1 INTRODUCTION

Liquefaction is a soil behaviour generally associated with extensive deposits of loose cohesionless materials. It is caused by a sudden reduction in effective stresses due to a rapid increase in pore pressure. A sufficient reduction in effective stresses results in failure attributed to liquefaction. This can take many forms and is frequently large scale, for example; bearing capacity and flotation failures, large settlements, slope and lateral ground movements. Liquefaction failures have become associated with a wide range of loading environments, eg. rapid single load increments, earthquakes, wave, shock and vibration loading. A common feature of many case histories is a delay between the triggering event and failure, together with the ejection of soil and water at ground level for a period after the initial disturbance. Many approaches, adopting various methods, have been proposed for assessing the likelihood of liquefaction failure at a site.

The thesis examined in this dissertation is that existing approaches are not appropriate for assessing the potential for liquefaction damage in a complete soil deposit. The generation and dissipation of excess pore pressures throughout the deposit are recognised as controlling factors in any liquefaction failure. A new approach is proposed based upon the in situ determination of soil state to assess excess pore pressure generation capacity, together with numerical modelling of excess pore pressure dissipation to examine possible liquefaction failure throughout the deposit.

In this dissertation modern soil mechanics theory is used to understand the mechanics of liquefaction. The generation of excess pore pressures, their dissipation and soil failure are considered. Excess pore pressures generated by a single rapid loading increment are studied in detail. Excess pressures generated by cyclic loading are not considered in detail because a large body of literature already exists. However this is commented upon since many of the processes discussed in this dissertation are common to both cases. Two mechanisms of excess pore pressure dissipation are identified; consolidation and hindered settling or resedimentation. The mechanics of hindered settling are drawn from applied physics and hydraulics theory. Liquefaction failures result from a reduction in soil strength and stiffness associated with reduced effective stresses. Liquefaction is therefore an expression of the principle of effective stress and can be explained using modern soil mechanics theory. It is not a special soil behaviour.

Examples of failures attributed to liquefaction are described and common aspects highlighted to illustrate the nature of liquefaction. The various approaches that have been proposed are outlined and critically reviewed in the light of modern theory. These include field, laboratory and numerical modelling based approaches. A combination of these are often used at a particular site. It is this discussion that identifies the need for a new approach. The suggestion is made that this should be based upon the in situ determination of excess pore pressure generation capacity by defining soil state relative to its critical state, together with the modelling of excess pressure dissipation leading to possible failure.

The remainder of the dissertation describes and discusses the laboratory based research that was carried out to identify and develop such an approach. This consisted essentially of laboratory scale model tests on soil beds prepared in loose and dense states. These had two objectives. Firstly the study of the mechanics of liquefaction by investigating excess pore pressure generation and dissipation. Secondly the identification of an appropriate in situ method for determining soil state using various model instruments, namely cones, vanes and expanding membrane probes. It is fully appreciated that field trials of an in situ method are essential once a correct theoretical approach has been confirmed, however it was felt that initially progress could be best achieved in the laboratory.

A new method for preparing beds of a uniform fine sand in various states was developed. The equipment used to achieve this was known as a sand column. This is described together with the electrical transducer and computer based system assembled to monitor excess pore pressure generation and dissipation within soil beds. The accuracy and performance of the laboratory equipment and its components are discussed in some detail.

From the large number of tests that were performed it was possible to recognise a number of different types of soil behaviour. These are defined on the basis of the excess pore pressures recorded and other basic observations. They depend upon a number of factors but principally on relative density, and as such are a basis for determining in situ soil state.

The findings of the research are discussed under a number of headings. The basic properties and behaviour of the soil used in the majority of the tests are considered. This includes the excess pore pressures generated by the soil when subjected to rapid loading. The two mechanisms of excess pore pressure dissipation are identified and discussed. Different types of soil behaviour were recorded with each of the model instruments. The reasons for this are considered in detail. The significance of factors such as instrument geometry, rate of loading and, where appropriate, disturbance due to installation are discussed. On the basis of these discussions a piezovane is proposed as the most suitable means of establishing in situ soil state. How the use of this instrument might be incorporated into a new approach for assessing the risks of liquefaction failure at a site is considered. It is noted that an instrument capable of determining the in situ state of granular soils may have wider applications beyond assessing the likelihood of liquefaction failure.

The project was initiated from discussions between Sir Alan Muir Wood and Professor John Atkinson. The research was supported jointly by Sir William Halcrow and Partners and the Science and Engineering Research Council (SERC) in the form of a CASE (Cooperative Award in Science and Engineering) award. It was carried out by the author as a member of the Geotechnical Engineering Research Centre of City University, London.

CHAPTER 2 MECHANICS OF LIQUEFACTION

The basic concepts of modern or critical state soil mechanics are presented in this chapter. Particular attention is given to the mechanisms that are involved in liquefaction. The chapter also outlines relevant theory that is not normally associated with critical state soil mechanics. For example the mechanics of hindered settling can be used to describe the process of sedimentation from a concentrated suspension.

The theory presented in this chapter is used in subsequent parts of the dissertation to review critically existing approaches and discuss the results of the laboratory research.

The chapter has four principal sections, the first of which outlines the general framework of critical state soil mechanics. This is used in the subsequent section to define and discuss liquefaction. A specific aspect of liquefaction that is considered is the possibility that failure may occur remote from the point of excess pore pressure generation. This highlights the need to understand fully the mechanics of excess pore pressure generation and dissipation within a soil profile. These mechanisms are considered in the final two sections of the chapter.

2.1 Basic soil mechanics

This chapter is not intended to be a comprehensive introduction to critical state soil mechanics, but rather an outline of the theory relevant to liquefaction. The subject of critical state soil mechanics is discussed more thoroughly by texts such as Atkinson and Bransby (1978).

2.1.1 Soil states and stress paths.

Soil may exist in a wide range of states from very dense to very loose and with a range of effective stresses from very small (eg. near the surface) to relatively large (eg. of the order of 500 kPa at a depth of 50m). The behaviour of a soil under load is dependent upon the initial state of the soil. This is defined by effective stress and specific volume. It is important to consider both stress and specific volume together to describe soil state. Figure 2.1 shows the results of similar drained shear tests performed at the same effective stress on two samples, one initially loose and the other dense.

Two points may be noted. Firstly the dense sample exhibits a peak strength, and secondly both samples approach a similar ultimate or critical state strength. At this stage the soil deforms plastically at constant stress and volume. Taylor's model (refer Atkinson and Bransby, 1978) suggests that the additional strength achieved at peak states with dense samples is a result of soil dilation during shearing. This accounts for peak strengths coinciding with the maximum rate of dilation as observed in direct shear tests with relatively dense samples.

By plotting the results of similar drained shear tests against axes of shear stress, effective normal stress and specific volume it can be demonstrated that the critical states of a soil lie on a unique line referred to as the critical state line (CSL). Figure 2.2 shows the state paths for the two tests presented in Figure 2.1. Path AC represents the stress path of the loose sample and BPC that of the dense sample. These stress paths and those discussed subsequently in this chapter correspond to isotropic elastic soils.

2.1.2 State boundary surface

A surface defining the boundary of possible soil states can be shown to exist (Atkinson and Bransby, 1978). This is referred to as the state boundary surface, Figure 2.3 shows an example. Possible soil states lie either on or beneath the surface. It may also be used to distinguish between elastic and plastic behaviours. Changes in state beneath the surface cause elastic deformations while changes that traverse the surface include plastic deformation.

In Figure 2.3 AB represents the critical state line and CD the normal compression (consolidation) line as defined in conventional oedometer tests. The curved surface ABCD is termed the Roscoe surface. State paths traversing this surface result in plastic deformations with a combination of positive excess pore pressure generation and soil compression. The surface ABFE is known as the Hvorslev surface. It represents the locus of all potential peak states in stress space. The plastic deformations that occur as a state path traverses the surface are associated with a combination of negative excess pore pressure generation and soil dilation.

Uncemented soils are unable to sustain tensile stresses. The surface EFHG represents this condition and is referred to as the no tension cut off. The line EF is simply the intersection of this plane and the Hvorslev surface. A full description of the state boundary surface and how it may be defined for a particular soil are discussed in standard texts such as Atkinson and Bransby (1978).

2.1.3 Wet and dry states

Soil states that lie beneath the Roscoe surface (ie. above and to the right of the critical state line in Figure 2.4a) are described as wet of critical. This is because drained loading of soil in these states results in a net flow of water out of the sample as the state path approaches the critical state line, AC in Figure 2.4b. Undrained loading of similar soils generates positive excess pore pressures as soil states follow the path AD and the soil attempts to compress.

Similarly soil states that lie beneath the Hvorslev surface (ie. below and to the left of the critical state line in Figure 2.4a) are referred to as dry of critical. Drained loading of soil in these states causes dilation as soil strengths pass through peak values. This behaviour corresponds to the state path BPC in Figure 2.4c with peak strengths achieved at P and a critical state reached at C. Undrained loading of a similar soil element would generate negative excess pore pressures as the soil state follows the path BE and attempts to dilate.

2.2 Liquefaction within critical state soil mechanics

Liquefaction is defined here as a sudden reduction in soil strength and stiffness resulting from a rapid increase in soil pore pressures. It is implicit from this definition that positive excess pore pressures can be generated at the point of liquefaction or, conversely, elsewhere in a soil profile and migrate to the point of observed failure. Liquefaction failure occurs when the reduction in soil strength and stiffness is sufficient to cause unacceptable structural movement or displacements in a soil structure.

This section considers basic liquefaction behaviours within the framework of critical state soil mechanics. Two aspects are considered in some detail, liquefaction at large effective stresses and the mechanisms of liquefaction failure occurring at a point remote from the zone of excess pore pressure generation. This latter behaviour is referred to in this dissertation as non-coincident liquefaction failure and it explains the common field observation of delayed failure. In cases where excess pore pressure generation and failure occur at the same point this is referred to as coincident liquefaction.

Soil failures resulting from an increase in pore pressures may be divided into two types. These can be understood by considering two examples, a lightly overconsolidated soil (A, wet of critical) and a heavily over consolidated soil (B, dry of critical) subjected to similar loading. Figure 2.5 shows the initial states of these soil elements and their subsequent state paths. In each case the soil is subjected to an increase in pore pressure and then shear loading. At this stage it is not necessary to define how the positive excess pore pressures are generated. This is considered in section 2.3. The reduction in effective stresses in both soil elements causes a reduction in strength and stiffness. Consequently a failure mechanism may begin to develop.

Reduced effective stresses followed by increased shear stresses applied to soil element A produces the state path ACD in Figure 2.5a. As the soil state traverses the Roscoe surface the soil generates additional positive excess pore pressures. In the case of sands these excess pore pressures can be very large. This is discussed further in section 2.3.1. In these soils the result is a rapid and significant reduction in effective stresses as the state path approaches the critical state line at E. Soil failures caused by this behaviour can be catastrophic and when associated with fine granular soils it is generally referred to as liquefaction.

Similar initial increases in the pore pressure and shear stress applied to soil element B produces the state path BFG in Figure 2.5b. In this case, unlike that described above, negative excess pore pressures are generated as the soil attempts to approach the critical state line by traversing the Hvorslev surface, ie. state path GH. This results in increased effective stresses and the stabilisation of any potential failure mechanism. With time the negative excess pressures will dissipate, effective stresses will reduce and further limited strain failure may occur.

To summarise liquefaction failures result from the progressive rapid generation of large positive excess pore pressures as soil states approach the critical state line. For liquefaction failure to occur at the point of excess pore pressure generation, as described above, the initial soil state must be wet of critical. Consequently soil states that are wet of critical are highly susceptible to liquefaction failure while those dry of critical are unlikely to exhibit such failures.

2.2.1 Liquefaction at large effective stresses

It is commonly believed that liquefaction failures only occur when excess pore pressures reduce effective stresses to a low, near zero value. The example that follows illustrates that liquefaction failure can also occur at large effective stresses. The mechanisms and parameters that control the generation of positive excess pore pressures are discussed in subsequent sections of this chapter.

Figure 2.6 shows two similar foundations, one lightly loaded and the other heavily loaded. A soil element (A) beneath the heavily loaded foundation is closer to failure at C than the corresponding element (B) beneath the lightly loaded footing which reaches the critical state line at F. A similar positive excess pore pressure ($\bar{u}_c$) applied to each element would result in liquefaction failure of soil A as its stress path reaches the critical state line at C (following dilation and a reduction in effective normal stress) while soil B, after limited elastic deformation remains stable at E. For soil B to be brought to failure large excess pore pressures ($\bar{u}_f$) must be generated and the soil must dilate in order to move the soil state from B to F.

This example illustrates that liquefaction failure can occur at high shear stresses while similar elements at low effective stresses remain stable.

2.2.2 Non-coincident liquefaction

It is commonly assumed that liquefaction failure occurs at the point at which excess pore pressures are generated. This has been defined earlier in the chapter as coincident liquefaction or the coincident model. In many cases this may not be realistic since pore pressures dissipating from one point can induce a rise in pore pressure at other points and consequently may result in failure at a point remote from the zone of excess pore pressure generation. The examples which follow illustrate this possible mechanism.

Figure 2.7 shows a simple soil profile consisting of a thick deposit of loose sand resting on a bedrock and with a less permeable near surface layer. This profile is typical of the type associated with many liquefaction failures. The behaviour of two soil elements, A and B, can be considered. Undrained loading of the soil profile from the base generates positive excess pore pressures throughout the loose sand bed. Largest excess pressures are created at A where initial effective stresses are high and shearing is most intense. Excess pore pressures at A rise rapidly to a peak value ($\bar{u}_A$) during shearing. The maximum value is equivalent to the initial vertical effective stress acting prior to loading. The excess pore pressures may be sufficient to induce coincident liquefaction failure.

The initial effective stresses at B are less than those at A. It is also isolated from the shearing perturbation by the softened zone at the base of the profile. As a result the excess pore pressures generated within element B ($\bar{u}_B$) are relatively small and the soil state might migrate from B to F. With time the excess pore pressures dissipate upwards towards the free surface. The effective stresses at A therefore increase as the excess pore pressures reduce from their peak values. This redistribution can result in a rise in pore pressures at B (eg. to $\bar{u}_C$). If the increase is sufficient then liquefaction failure occurs as the stress path moves towards the critical state line at C. Clearly time is required for the excess pressures generated at A to redistribute to cause failure of B. This accounts for the delay frequently noted between the onset of an earthquake tremor and the first signs of a liquefaction failure.

Figure 2.8 shows the second example with a loaded foundation resting on relatively loose sands. Two elements of soil are shown, A and B. Beneath the foundation at A high effective normal stresses exist. B lies at the edge of the foundation where effective normal stresses are lower but shear stresses are high. Undrained loading of the foundation would create positive excess pore pressures within the profile. These are greatest beneath the foundation in the region of high initial effective stresses. The stress path of soil A would therefore move towards the critical state line via C. Smaller excess pressures are generated at B ($\bar{u}_b$) moving the stress path to a point such as D. After the initial loading excess pore pressures dissipate as pore water flows towards the free surface. At A effective stresses increase as excess pore pressures dissipate to zero. This is likely to cause a rise in the pore pressures at B. The stress path of this element will move from D towards the critical state line at E. Liquefaction failure is likely in this zone of high shear stress.

The examples considered have shown that liquefaction failure at one location in a soil profile can be caused by the generation of positive excess pore pressures elsewhere in the profile. This non-coincident model of liquefaction accounts for the delayed failure often associated with this soil behaviour. Examples of delayed failures are described in Chapter 3. Clearly for the mechanics of non-coincident liquefaction to be fully understood it must be recognised that both the generation and redistribution of excess pore pressures are important factors.

2.3 Generation of large positive excess pore pressures

Liquefaction can only occur when relatively large positive excess pore pressures are generated within a soil profile. In Section 2.1.3 it is concluded that only wet of critical soils subjected to rapid, undrained, loading are capable of creating these pressures. However previous researchers have demonstrated that dry of critical soils can also generate positive excess pore pressure when subjected to rapid cyclic loading, eg. by an earthquake. These two sources of large positive excess pore pressures are considered in the sections that follow.

2.3.1 Excess pore pressures generated by a single rapid loading increment

Large positive pressures are generated as the stress path of a soil element traverses the Roscoe surface towards the critical state line, AD in Figure 2.4a (refer section 2.1.3). The theoretical maximum value of the excess pressure, $\bar{u}_{AD}$, is a function of the initial soil state and the geometry of the state boundary surface, in particular the position of the critical state line in effective stress space. Clearly the closer the initial soil state to the critical state line the smaller the excess pore pressures that may be generated. The position of the critical state line is defined by the equation;

$$\upsilon = \Gamma - \lambda \ln \sigma'_n \qquad 2.1$$

Figure 2.9 shows the various parameters

The gradient of the critical state line against the axes of specific volume and the logarithm of effective normal stresses may be defined by λ. The maximum excess pore pressures that can be generated by undrained loading of a soil are therefore a function of λ and generally the smaller the value of λ the larger the excess pore pressures that may be generated. The fine granular soils that are typically associated with liquefaction failure exhibit very low λ - values. It is this characteristic that enables these soils to generate the large positive excess pore pressures that are necessary for liquefaction failure provided they are initially in a wet of critical state.

2.3.2 Excess pore pressures generated by cyclic loading

The basic liquefaction behaviour of soil in a cyclic loading environment may be demonstrated by considering two soil elements, one wet of critical (A) and the other dry (I). Each is subjected to rapid cyclic shearing followed by a large increase in average shear stress. The initial soil states and subsequent stress paths that they follow are shown in Figure 2.10

The theory presented earlier in the chapter predicts that the wet of critical soil element follows the stress path ABCD during the early stages of cyclic loading. Positive excess pore pressures are generated as the soil state traverses the Roscoe surface, BC, to the point where peak cyclic shear stresses are applied at C. Subsequent stress cycles are within the state boundary surface and soil behaviour should therefore be elastic. The stress path followed by such a soil would be expected to oscillate between C and D with no further excess pore pressures generated. However, laboratory cyclic loading tests (eg. Yoshimi, 1977 and Prakash, 1981) demonstrate that excess pore pressures continue to be generated. This results in the effective stress state migrating from CD towards the origin. It is a logarithmic movement of the stress state with the stress path approaching a constant effective normal stress at E. This produces a weaker and less stiff soil. Application of a large shear stress produces the stress path EFG. Further positive excess pressures are generated as the soil state traverses the Roscoe surface towards the critical state line at G. Clearly this form of soil behaviour is similar to that described in section 2.2 with large positive excess pressures generated which may result in liquefaction failure.

In the case of the dry of critical soil element, I, basic theory predicts a stress path that oscillates between J and K, Figure 2.10b. However, as above, laboratory cyclic loading tests show a similar but less pronounced logarithmic migration of the stress path towards the origin (eg. to L) as positive excess pore pressures are generated. Effective stresses are reduced and the soil becomes weaker and less stiff. Application of a large shear stress to this soil element produces the stress path LMN as the soil state moves towards the critical state line. Negative excess pore pressures are generated as the soil attempts to dilate while traversing the Hvorslev surface, MN. This results in increased effective stresses and the soil stabilises at N. Hence although positive excess pore pressures may be generated during cyclic loading of dry of critical soil, subsequent shearing as a failure mechanism develops generates negative excess pore pressures which prevent liquefaction failure.

It is important to note that although these examples reiterate that only soils wet of critical may be easily liquefied cyclic loading of dry of critical soils can generate positive excess pore pressures. The example has shown that the dry of critical soil that generates these pressures is unlikely to exhibit liquefaction failure. However, these positive excess pore pressures may redistribute and cause failure elsewhere in the soil profile

2.4 Mechanics of excess pore pressure dissipation

In section 2.2.2 it is concluded that the way in which excess pore pressures dissipate or redistribute through a soil profile is a significant factor in the mechanics of liquefaction. In soil mechanics this is generally associated with the process of consolidation. Many recorded cases of liquefaction failure are associated with one-dimensional dissipation of excess pore pressures. The laboratory research described in this dissertation also considers essentially one-dimensional dissipation of excess pore pressures. One-dimensional consolidation theory is therefore outlined in this section as a potential mechanism.

There is strong evidence that the large positive excess pore pressures that were associated with liquefaction failures may redistribute by a different mechanism. This is discussed in detail in subsequent parts of the dissertation. In this section the basic theory of the alternative mechanism, hindered settling, is introduced. It is derived from hydraulics and applied physics theory where it is used to describe the settling of solid particles through a fluid.

2.4.1 One-dimensional dissipation of excess pore pressure by consolidation

In soil mechanics the dissipation of excess pore pressures is generally associated with the process of consolidation. For the one-dimensional case this is described by the differential equation given below and attributed to Terzaghi (refer Atkinson and Bransby, 1978).

$$c_V \frac{\partial^2 \bar{u}}{\partial z^2} = \frac{\partial \bar{u}}{\partial t} \qquad 2.2$$

Where c_v is a soil parameter known as the coefficient of consolidation. If the boundary conditions and the initial distribution of excess pore pressures are known an exact solution of Equation 2.2 may be obtained. A solution gives the variation in excess pore pressures with time throughout a consolidating soil layer. Two related parameters may be defined, average degree of consolidation (U) and time factor (T_v). The degree of consolidation at a particular level in a consolidating soil layer and time (t) is given by;

$$\text{degree of consolidation} = \frac{\bar{u}_o - \bar{u}_t}{\bar{u}_o} \qquad 2.3$$

The average degree of consolidation is the average of the above values throughout the consolidating layer. Time factor is given by;

$$T_v = \frac{c_v t}{H^2} \qquad 2.4$$

where H = shortest drainage path

The relationship between the average degree of consolidation and time factor values is a function of the initial distribution of excess pore pressures and the drainage paths. Exact solutions have been produced for various combinations of excess pore pressure distribution and drainage paths, eg. Atkinson and Bransby, 1978. It is possible to use these solutions to compare theoretical and recorded laboratory test results in order to derive a value of the coefficient of consolidation.

In the case where a liquefied sand layer rests on an impermeable rock base the boundary condition is that of one-way drainage towards the upper surface of the layer. The excess pore pressures created by a disturbance are generally proportional to the initial effective overburden stress. The initial distribution of excess pore pressure is therefore triangular, increasing with depth. The solution to Equation 2.2 for this case is summarised by Figures 2.11a and b. These show the solution in the form of an isochrone plot and the relationship between surface settlement, or average degree of consolidation, and time.

The rate and nature of the dissipation is significantly different if alternative boundary conditions apply for the same initial distribution of excess pore pressures. One-way drainage towards the base of the bed and two-way drainage result in increased rates of dissipation. In these cases a 50% degree of consolidation is achieved in approximately 31% and 15% respectively of the time required for the case of one-way drainage towards the upper surface. The difference in the nature of the dissipation is shown by Figures 2.11c and d. Two points may be noted, excess pore pressures at the base of the soil bed dissipate to zero very rapidly, and elsewhere in the profile excess pore pressures may actually rise before dissipating to zero (Figure 2.11c).

2.4.2 One-dimensional dissipation of excess pore pressures by hindered settling

The terminal velocity of a particle settling through a fluid is given by a relatively complex equation. This simplifies to the equation given below for the range of Reynolds number (R_e) where Stokes Law holds, ie.

$R_e < 1$ (after Graf, 1984).

$$v_s = \frac{2}{9} a^2 g \frac{\rho_s - \rho_w}{\mu} \qquad 2.5$$

(after Graf, 1984)

where v_s = terminal settling velocity of a single spherical soil particle through a fluid ($m\ s^{-1}$)

a = particle radius (m)

g = acceleration due to gravity ($9.81 m\ s^{-2}$)

μ = fluid dynamic viscosity ($kg\ m^{-1}s^{-1}$)

ρ_s = density of particle ($kg\ m^{-3}$)

ρ_w = density of fluid ($kg\ m^{-3}$)

Graf (1984) describes a series of corrections that are applied to the settling velocity derived from Equation 2.5. These correct for particle shape, proximity to a solid boundary, a concentration of particles, particle roughness, particle rotation and turbulence effects. Only one of these corrections are used in this research, that for the settlement of dispersed particles or concentrations. The first extensive study of this aspect of hindered settling was presented by Maude and Whitmore (1958). It was proposed that the terminal settling velocity of particles within a concentration, referred to as the hindered settling velocity (v_{hs}), may be derived by applying a correction to the terminal settling velocity of a single particle (v_s), as set out below;

$$v_{hs} = K(v_s) \qquad 2.6$$

$$\text{where} \quad K = (1 - C)^m \qquad 2.7$$

(after Maude and Whitmore, 1958)

and C = concentration of particles per unit volume, ie. the inverse of specific volume

m = a coefficient dependent upon parameters including Reynolds number (R_e) and particle shape

= 4.5 for $R_e < 1$ (after Graf, 1984).

In hydraulics these equations are used to define the theoretical settling velocity of particles through a fluid. They may also be adopted to describe the sedimentation of a concentration of particles to form a soil bed. This starts from the base of the fluidised layer or concentration as particles settle out of the fluid. The boundary between the loose bed and the fluidised layer above progresses upwards as the process continues. Where the concentration is uniform and contains particles of similar geometry and composition the rate at which this interface moves upwards will be constant. Throughout the period of sedimentation all the particles within the fluidised layer continue to settle. The rate at which the upper surface of the fluidised layer moves downwards is equal to the hindered settling velocity of the near surface particles and is linear with time as shown in Figure 2.12a.

The excess pore pressures within the fluidised layer and the bed beneath are as shown in Figure 2.12b. This shows the total, steady state and the excess pore pressure distribution at a particular point during the sedimentation process. The excess pore pressures within the concentration are similar to those in a heavy fluid, increasing linearly with depth. Within the soil bed pore pressures are hydrostatic and therefore excess pore pressures are constant with depth.

As noted above, with time the interface between the fluidised layer and the soil bed progresses upwards. Figure 2.12c shows how the distribution of excess pore pressures varies with time in the form of an isochrone plot. It begins with a triangular distribution increasing with depth. Excess pore pressures dissipate from the base with isochrones remaining vertical in the soil bed and increasing linearly with depth in the fluidised layer above.

There are clear differences between the mechanism of hindered settling and that of consolidation described in section 2.4.1. For example the degree of consolidation and surface settlement are linear with the root of time in the case of consolidation (Figure 2.11b) and linear with time for hindered settling (Figure 2.12a). In addition the form of isochrone plots for the two mechanisms differ significantly. In the case of consolidation the rate of change in excess pore pressure varies with depth. Conversely where the mechanism is hindered settling the rates of change are constant with depth, however there is an abrupt change at the boundary between the two states.

CHAPTER 3 PREVIOUS STUDIES AND OBSERVATIONS OF LIQUEFACTION

Since the first geotechnical use of the term by Hazen in 1920 (Poulos et at, 1985) various forms of failure have been attributed to liquefaction. Partly as a result of this many different methods have been proposed to assess the likelihood of liquefaction failure at a site. This chapter sets out to critically review these in the light of the theory presented in Chapter 2 and observations made in the field. To achieve this the first part of the chapter provides a brief description of a selection of liquefaction failures and highlights some of their common features. Each of the approaches that have been proposed are outlined in the second section of the chapter. The third and final section summarises some of the common features of liquefaction failures before reviewing each of the proposed approaches. It is concluded that a new method is required and suggested how this might be achieved. Although a thorough literature review was undertaken, only selected papers are quoted in this chapter.

3.1 Field observations

Failures attributed to liquefaction have been reported in a number of different environments and have taken various forms. The examples outlined in this section were selected to illustrate these points. Recorded case histories are referred to under four headings within the section. These illustrate the soils and soil profiles that have been associated with liquefaction, the wide range of environments where failures have been observed or considered a potential hazard, and the nature of liquefaction failures. A common feature of many failures is a delay between the triggering event and observations of failure at ground level. This behaviour is highlighted under the final heading of the section.

3.1.1 Soils and soil profiles

Liquefaction is generally thought to be a phenomenon associated with extensive homogeneous deposits of saturated, loose, uniform fine to medium sands. In reality soil profiles are not uniform and there is some evidence to suggest that layered soil profiles can also be susceptible to liquefaction failure. To illustrate this point the examples that follow describe soil profiles in which liquefaction failures have been observed.

Lindenberg and Koning (1981), and Castro (1969) described large scale flow slide failures of loose sand deposits on the Dutch coast. Figure 3.1 shows a sketch section through such a failure. Results of site investigations in the area are presented by Delft (1984) and summarised in Figure 3.2 which shows a typical soil profile with saturated sands and sandy silt layers. The grading of selected samples are presented in Figure 3.3. This shows highly uniform fine and medium sands with small percentages of silt. Lindenberg and Koning (1981), and Castro (1969) described similar failures in the banks of the Mississippi River, USA. In this case the soil profile consisted of a layer of loose uniform fine sands beneath a surface layer of clay.

Ishihara and Perlea (1984) presented examples of liquefaction failures that were observed in the area of Bucharest, Rumania in 1977. In areas where failure was observed the profile consisted of loose saturated sands beneath thin near surface layers of sandy silts and silty clays, Figure 3.4. The grading of the principal sand layer is shown in Figure 3.5. The soil profile of an adjacent area that showed no signs of liquefaction failure is shown in Figure 3.6. Ishihara and Perlea (1984) attributed the difference in behaviour to the thickness of the near surface layer of silty clay.

The widespread liquefaction failures observed after the 1964 Niigata (Japan) earthquake were reported by the Japanese Society of Soil Mechanics and Foundation Engineering (1966). The city of Niigata is built on thick deposits of alluvial material and recently placed made ground. A large proportion of the soil profile consisted of saturated loose uniform fine to medium sands. Figure 3.7 shows examples of the grading of these soils. Typical soil profiles from areas where liquefaction was observed are illustrated in Figures 3.8 to 3.10. These show several common features. Firstly a high proportion of loose uniform sands beneath the water table and secondly the presence of a less permeable near surface layer. For example Figures 3.9 and 3.10 show layers of sandy silts and sandy clays.

Casagrande (1936, 1975) described the liquefaction failure of several man-made structures. These included the partial collapse of the Fort Peck Dam, Montana, USA in 1938 (Figure 3.11). The structure was founded on alluvial sands with a core constructed of hydraulically placed sand.

Other authors have described the collapse of dams, for example Seed (1979b) and Castro et al (1992) discussed the failure of the Lower San Fernando Dam in 1971. Figure 3.12 shows a section through the structure before failure. The dam was founded on alluvium and consisted of a clay core with shoulders of hydraulically placed sand. The crest consisted of shale and rolled fill. Failure resulted from the liquefaction of parts of the material forming the upstream shoulder (Seed,1979b).

These examples have shown that liquefaction failure is a phenomenon generally associated with deposits of saturated loose uniform fine or medium sands. No cases were found in the literature where liquefaction occurred in soils which contained no saturated, loose uniform fine or medium sands. However, it noted that other soil types are frequently present, namely silts and clays, and that these may have a significant influence upon the mechanisms that act to cause failure.

3.1.2 Environment

Recorded case histories of failures have been associated with both rapid single increments of load and cyclic loading. The examples that follow illustrate the wide range of environments in which liquefaction has been considered, and the events that caused failure.

The large scale movements of Dutch coastal deposits was discussed by Lindenberg and Koning (1981). It was concluded that the flow slides were caused by tidal scour and seepage forces along the banks of major tidal channels. This induced minor bank failures which triggered the larger flow slides. Soil piping is also an example of liquefaction. In this case it is caused by a critical hydraulic gradient which is a result of large static water pressures, for example associated with a coffer dam.

Failures induced by cyclic loading include those described by Ishihara and Perlea (1984), The Japanese Society of Soil Mechanics and Foundation Engineering (1966) and Seed (1979a). In each of these examples failure was caused or triggered by an earthquake tremor. There is an extensive literature in this area. Further examples of earthquake induced liquefaction failure are presented by Marsal (1961), Seed (1970), Youd and Bennett (1983) and Seed et al (1981).

Casagrande (1936) described the failure of a large dam induced by a blasting operation to remove a nearby coffer dam. In recent years blast induced liquefaction has also been studied by the military and the designers of nuclear power plants.

Similarities between the cyclic loading induced by earthquakes and that of wave loading in a marine environment has led engineers to consider the possibility of wave induced liquefaction failure. Examples of case histories and methods are described by Bjerrum (1973), Lee and Focht (1975), and Finn et al (1983).

In Chapter 2 it is recognised that large positive excess pore pressures are necessary to cause liquefaction failure. The examples that have been described above show that these pressures may be generated by either a rapid single increment of load or by cyclic loading.

3.1.3 Nature of failures

Liquefaction failures are frequently large scale, occur over a relatively short period (ie. seconds or minutes) and generally involve significant ground movements. The examples that follow illustrate these points and demonstrate the various forms of failure that have been attributed to liquefaction.

The flow slides described by Lindenberg and Koning (1981) propagated rapidly with up to 4 x $10^6 m^3$ of sand displaced over large distances. The failed material appeared to flow as a heavy liquid and came to rest with ground surfaces generally less than six degrees from horizontal. It was reported that 229 similar failures were recorded in Holland between 1881 and 1946 involving some 25 x $10^6 m^3$ of sand and the loss of Ha 264 (660 acres) of land.

The Vrance Earthquake resulted in liquefaction failures in the area of Bucharest, Rumania (Ishihara and Perlea, 1984). Structural damage was caused by differential settlements. This was associated with surface cracking and the flow of water and sand from sand volcanoes or vents at ground level. This began shortly after the earthquake.

The failures induced by the Niigate earthquake of 1964 were described by the Japanese Society of Soil Mechanics and Foundation Engineering (1966) and discussed by Seed (1970). Examples included bearing capacity failures, flotation failures (eg. a large sewage treatment tank floated to the surface), and lateral movement of bridge abutments leading to collapse, slope failures and large surface settlements. These were associated with surface cracking and the flow of soil and water from sand vents. Figures 3.13 and 3.14 show examples of these features. Table 3.2 outlines the sequence of events observed during and after the earthquake.

Figure 3.11 shows a section through the Fort Peck Dam after its partial collapse. Failure involved the rapid collapse of a 520m section of the upstream face. Approximately $8 \times 10^6 m^3$ of sand travelled up to 400m in three minutes. During the failure the displaced material behaved as a heavy flowing liquid, coming to rest at very low angles. Casagrande (1975) attributed collapse to the liquefaction of the hydraulically placed sand of the upstream shoulder of the dam.

A section through the Lower San Fernando Dam, following its collapse, is shown in Figure 3.15. The structure began to fail approximately 40 seconds after a major earth tremor and came to rest after a further 50 seconds. The figure shows the failed material to consist of a series of blocks and wedges. Inspection of the structure revealed the blocks to be separated by zones of loose sand. Seed (1979b) concluded that failure was caused by the liquefaction of a zone within the hydraulically placed sand forming the upstream shoulder.

From the examples presented above it is apparent that liquefaction failure can take many forms and that it has been observed in both natural soil profiles and man-made structures.

3.1.4 Delayed failures and excess pore pressure dissipation

Several authors have described liquefaction failures in which ground movements and failure occurred a period after the trigger event. In this section a selection of these failures are described and their significance briefly discussed.

Ishihara and Perlea (1984) noted that the failures associated with the 1977 Vrance Earthquake started after the tremor. These included the settlement of buildings, settlement and cracking of the ground surface, and the ejection of soil and water to form sand volcanoes, as described in section 3.1.3. It was reported that in some cases the flow of water continued for an hour after the tremor. Ishihara and Perlea compared areas where failures were observed with those where no evidence of liquefaction was seen. They concluded that where failures had not been observed a thick near surface layer of silty clay prevented excess pore pressures generated at depth from reaching ground level.

Both Yoshimi (1977) and Seed et al (1975) discussed the delayed failures associated with the 1964 Niigata Earthquake. Table 3.1 outlines the sequence of events observed during and after the tremor. These were described in detail by the Japanese Society of Soil Mechanics and Foundation Engineering (1966). Eyewitness accounts state that settlements, ground cracking and sand volcanoes began some time after the initial tremor and continued long after the event. Seed et al (1975) demonstrated, using a numerical model, that these failures were a result of the dissipation of excess pore pressures generated at depth to cause failure close to ground level. Seed has also considered the delayed partial collapse of the Lower San Fernando Dam following an earthquake (Seed, 1979b). The failure is described in section 3.1.3 and summarised in Table 3.3. Seed concluded that the delayed movements resulted from the redistribution of excess pore pressures generated within the structure by the earthquake tremor.

These and other examples demonstrate clearly that there can be a delay between the triggering event and observations of liquefaction failure. This is consistent with the non-coincident model of liquefaction introduced in Chapter 2. This predicts that the large positive excess pore pressures necessary for liquefaction failure may be generated in zones of high effective stress (eg. at depth). These then redistribute within a soil profile or structure and may cause failure elsewhere, such as beneath foundations close to ground level.

3.2 Methods of investigating liquefaction behaviour

Many approaches have been proposed for determining the likelihood of liquefaction failure at a particular site and to study the controlling factors. These include theoretically based and empirical approaches which use field, laboratory and numerical techniques. A combination of techniques is often applied with a particular approach. This has resulted in a large and often confusing and at times conflicting literature.

The various approaches and combinations of techniques are outlined in this section before being critically reviewed in section 3.3 which follows. The approaches and techniques are presented in the following sequence; theoretical, physical modelling, numerical modelling, and empirical. There is no significance in the order of presentation. A summary of the approaches and the techniques they use is set out in Table 3.1.

As noted above, cataloguing the various methods in this way simplifies the situation. In many cases a combination of approaches has been adopted, for example modelling techniques have been used to support theoretical approaches.

3.2.1 Critical void ratio and critical state

Casagrande first introduced the concept of a critical density or critical void ratio when discussing the liquefaction of embankments of loose sand in the mid 1930's (Casagrande, 1936). He proposed the existence of a critical void ratio line within void ratio - effective stress space for each soil type. An example is shown in Figure 3.16. Casagrande used drained direct shear tests to demonstrate that the critical void ratio line separated two soil behaviours. Drained loading of soil with an initial state above the critical void ratio line resulted in compression of the sample. Similarly, soils with states below or to the left of the line dilated when loaded. Figure 3.16 summarises the results of these early tests.

Castro (1969) was later able to perform consolidated undrained, load controlled, triaxial tests with pore pressure measurement. These illustrated that the critical void ratio line also separated different undrained behaviours. Undrained loading of soil with an initial state above the critical void ratio line (ie. relatively loose) resulted in the generation of high positive excess pore pressures. This caused the sudden failure of test samples, described by Castro as liquefaction. Similarly soil at a state below the critical void ratio line (ie. relatively dense) generated negative excess pore pressures when loaded. Figure 3.17 shows a typical set of Castro's results. Castro defined liquefaction failure as that in which a loss of strength is caused by a large increase in pore pressure which is maintained during subsequent soil shearing. He concluded that collapse results from the greatly reduced effective stresses acting within the soil and noted that it was not necessary for effective stresses to be reduced to zero for failure to occur.

Casagrande (1936, 1975), Castro (1969, 1975) and Poulos et al (1985) concluded that only soil with an initial state above the critical void ratio line could suffer liquefaction failure. Although the concept of a critical void ratio line was first demonstrated by performing static loading tests, Castro (1969) suggested that the theory was equally applicable to cases of cyclic loading.

Two methods have been used to apply the critical void ratio approach. The first and most simple involves subjecting representative samples to consolidated undrained triaxial testing. If any of the samples liquefy, as defined by Castro (1969), the initial state of the samples are assumed to have been wet or critical and the profile is considered to be potentially liquefiable.

The second method has been adopted by the site investigation company Delft (1984) to establish the stability of Dutch coastal deposits with respect to liquefaction. For each sand present in a soil profile a series of reconstituted samples were subjected to consolidated undrained triaxial tests. These enabled the critical void ratio line of each soil to be defined. An example is shown in Figure 3.18. The susceptibility of a soil profile to liquefaction is assessed by determining the in situ soil state and effective stress level. Corresponding values were then plotted relative to the appropriate critical void ratio line. If any of the plotted points lie above or to the right of the critical void ratio line then the soil profile is considered to be potentially liquefiable. In situ soil states are determined using an electrical resistivity technique which exploits the relationship between soil density and resistivity.

Clearly the theoretical framework developed by Casagrande and Castro is similar to that of critical state soil mechanics. Recent studies have adopted this framework to examine liquefaction failure in the field, and to interpret the results of centrifuge model tests.

Schofield (1981) used the critical state model or framework together with a series of conceptual models to discuss aspects of liquefaction failure within a soil profile. He proposed two forms of liquefaction failure. The first corresponds with the approach of Casagrande and Castro, and that presented in Chapter 2, ie. only soil wet of critical can exhibit liquefaction failure.

Schofield (1981) demonstrated the second form of failure, termed clastic liquefaction, with the model shown in Figure 3.19. This presents a soil profile consisting of wet of critical sands overlying bedrock with a surface layer of low permeability dry of critical soil eg. desiccated clay. Disturbance of the profile results in the fluidisation of the sand layer. The sand begins to resediment, starting at the base. Schofield suggested that the stress path of elements within the clay layer will migrate towards the no tension cut-off, OA in Figure 3.19. When the stress path intersects this boundary it is suggested that it suffers hydraulic fracture, cracking into blocks with fluidised sand rising through the clastic debris. Clearly this form of failure is similar to that discussed in section 2.2 with excess pressures generated at one point redistributing to cause failure elsewhere in a soil profile. Similar mechanisms were identified by Seed (1987) when describing observations made in vibrating table tests.

Critical state or steady state soil mechanics is increasingly being adopted to examine the mechanisms of liquefaction and explain previous failures. For example Castro et al (1992) used the concept of steady state soil strength to re-evaluate the partial collapse of the Lower San Fernando Dam in 1971, refer section 3.3.

3.2.2 Equivalent stress path

Seed and various co-workers (eg. Seed and Idriss, 1967) have considered observations of liquefaction in earthquake regions. Engineering interest in this area first began in the early 1960's. More recently the approach proposed by Seed has been used to assess the likelihood of liquefaction failure associated with shock and wave loading. Reviews of the approach were presented by Seed (1979a) and Prakash (1981).

The approach is relatively straightforward with undisturbed soil samples subjected to an equivalent design cyclic loading. The stress history applied to a soil profile by an earthquake is generally complex. Seed (1979a) described a procedure for selecting an equivalent uniform cyclic stress history or stress path. For engineering design purposes representative undisturbed samples from a soil profile were consolidated and then subjected to the equivalent undrained (constant volume) stress path. Loading was applied by either triaxial or simple shear apparatus suitably modified for rapid cyclic loading. The excess pore pressures generated within samples during loading were used to assess the likelihood of liquefaction in the soil profile under investigation. To do this Seed (1979a) defined the following terms.

a) Peak cyclic pore pressure ratio of 100% (formally termed initial liquefaction): a condition where during the course of cyclic loading, the residual pore pressure on completion of any full stress cycle becomes equal to the applied confining pressure; the development of a peak excess pore pressure of 100% has no implication on the magnitude of the deformation that the soil might undergo.

b) Cyclic Mobility (or Peak cyclic pore pressure ratio of 100% with limited strain potential, formally termed cyclic liquefaction with limited strain potential): a condition where cyclic loading generates a peak cyclic excess pore pressure ratio of 100% and subsequent cyclic loading results in limited strains either because of the remaining resistance of the soil to deformation or because the soil dilates, the pore pressure drops, and the soil stabilizes under the applied load.

If the number of uniform stress cycles necessary to induce a peak pore pressure ratio of 100% or an unacceptable level of cyclic strain is less than that of the equivalent design disturbance then liquefaction is considered a hazard.

The true triaxial and hollow cylinder apparatus have been used by researchers to study the influence of complex three-dimensional cyclic stress paths upon the liquefaction characteristics of soil elements.

In may respects the methods used are similar to those described above.

Ishihara and Yamada (1981) presented the results of tests performed in the true triaxial apparatus. Similarly Ishihara and Yasuda (1975) described tests carried out with a hollow cylinder apparatus. In both cases reconstituted samples were subjected to consolidated undrained three-dimensional cyclic loading. Various types of stress path were applied. These included uniform and irregular stress histories to assess the validity of applying an equivalent uniform stress path. Test samples were assumed to have liquefied when and if initial liquefaction occurred, as defined by Seed (1979a) and summarised above.

3.2.3 Critical strain

Dobry et al (1981) proposed the use of a strain value to assess the likelihood of liquefaction failure in earthquake environments. It was suggested that soil exhibits a threshold strain below which no excess pore pressure is generated. Dobry et al proposed that the susceptibility of a soil profile to liquefaction failure may be assessed by comparing the threshold strain of a soil with the strain induced by a disturbance. They concluded that liquefaction can only occur if the strain induced by the disturbance exceeds the threshold value since only then can the excess pore pressure necessary for liquefaction failure be generated.

A field method has been proposed for applying this approach. Dobry et al (1981) demonstrated that a threshold strain value is associated with a threshold acceleration and that this may be determined by in situ measurements of shear wave velocity. Essentially the method involves measurement of shear wave velocity throughout a soil profile. These values are used to estimate the threshold acceleration of soils in the profile. If the peak acceleration of the design disturbance exceeds the threshold acceleration of any soil present positive excess pore pressures will be generated. Dobry et al (1981) concluded that if this is the case then liquefaction failure should be considered a hazard.

3.2.4 Physical modelling

Scaled models of soil profiles or structures have been used in a number of studies to examine liquefaction failures. Such a study is described by Eckersley (1990). In this case flow slides were induced in small, instrumented coking coal stockpiles by slowly raising the water table.

Vibrating table tests and more recently centrifuge testing have been used by researchers to study the mechanics of liquefaction in cyclic loading environments. This is achieved by subjecting a model soil profile or structure to a scaled cyclic loading. Yoshimi (1977) and Prakash (1981) have presented reviews of vibrating table tests. Schofield (1981) described the development of the geotechnical centrifuge and its use in the study of cyclic soil behaviour. Theoretically, only centrifuge modelling allows the correct scaling of all relevant parameters, and is therefore the most accurate method of modelling liquefaction behaviour in the laboratory.

Figures 3.20 and 3.21 show the results of vibrating table tests reported by Yoshimi (1977), and Florin and Ivanov (1961). Figure 3.20 shows the excess pore pressure response observed in a fine sand layer subjected to horizontal vibrations from the base. The figure also shows predicted excess pore pressure values calculated by an analytical method similar to that described by Seed et al (1975) and discussed in section 3.2.5. In the tests described by Florin and Ivanov excess pore pressures were generated by shock or impact loading a bed of loose sand. Figure 3.21 shows the initial distribution of excess pore pressures and their subsequent dissipation in the form of isochrones. The excess pore pressure dissipation behaviour observed in these tests is similar to that introduced in Chapter 2 and referred to as hindered settling or resedimentation.

Lee and Schofield (1984 and 1988) presented the results of centrifuge tests to study the stability of artificial sand islands in an earthquake environment. The centrifuge facility used for these tests was that described by Schofield (1981). Figure 3.22 shows a section through the model structure which was constructed of fine Leighton Buzzard sand by pluvation through silicone oil. Tests were carried out at 40g with the model subjected to an equivalent full scale earthquake. Figure 3.23 presents selected results of one of these tests. Pore pressure transducer PPT 2338 located centrally beneath the crest of the model showed a rapid increase in excess pore pressure during the tremor. Similar transducers situated in the shoulders of the structure (eg. PPT's 68, 2335, 2252 and 2331) showed lower excess pore pressures during the earthquake. These increased steadily after the tremor as the high excess pressures generated beneath the crest dissipated laterally. Lee and Schofield (1984) noted similarities between this behaviour and the delayed failure of the Lower San Fernando Dam which was attributed to the dissipation of excess pore pressures generated by a tremor, refer section 3.1.

3.2.5 Numerical modelling

Various numerical modelling methods have been developed to study and describe liquefaction behaviour. Four broad groups of methods can be defined ranging from the relatively simple seismic coefficient method to the complex modelling of coupled excess pore pressure generation and dissipation to examine liquefaction behaviour in an earthquake environment. More recently similar methods have been proposed for assessing the likelihood of liquefaction failure resulting from wave or shock loading. The majority of the numerical modelling methods are now computer based.

The use of seismic coefficient in pseudostatic analysis to access slope stability during earthquakes was outlined by Seed (1970). This is an elementary method which dose not consider the effects of excess pore pressure generation upon the controlling factor of effective stresses within the soil slope. Consequently, in many cases it is an inaccurate method. It is based upon conventional static slope stability analysis with an additional horizontal force representing the disturbing effect of the earthquake. The magnitude of the additional force is given by the product of the weight of the failing body of soil and a seismic coefficient. As with conventional slope stability analysis, if the factor of safety derived from calculations is below an accepted value the slope is assumed to be susceptible to collapse, in this case as a result of liquefaction failure. Seed (1970) introduced various empirical and analytical procedures for determining an appropriate value of the seismic coefficient. Empirically derived values typically range from 0.05 to 0.15 in the USA and 0.12 to 0.25 in Japan. The exact value adopted depends upon various factors including seismicity, foundation conditions and the geometry of the slope.

Numerical modelling of excess pore pressure generation associated with liquefaction failure was initially developed for earthquake environments where the relatively rapid loading of soils could be assumed to be undrained, ie. no excess pore pressure dissipation takes place during loading. An example of one of these methods was described by Martin et al (1975). This predicted the progressive generation of excess pressures throughout a soil profile due to a random stress history. The method was reported to be based upon a fundamental understanding of soil behaviour and the mechanisms of liquefaction. It is a complex computer based approach which requires a large number of parameters to be defined accurately for each of the soils present.

Several authors have considered the mechanics of .excess pore pressure dissipation within a soil profile leading to possible liquefaction failure, eg. Ambrasseys and Sarma (1969), and Yoshimi and Kuwabara (1973). In both of these cases an initial excess pressure distribution was assumed and Terzaghi one-dimensional consolidation theory adopted to predict dissipation. Studies included dissipation within simple two layer profiles, with various distributions of initial excess pore pressure. It was concluded that liquefaction of the surface layer could result from the dissipation of excess pressures generated in the lower layer, provided that the permeability and compressibility of the upper layer were sufficiently low compared with that of the layer beneath.

A number of computer based methods have been developed which model coupled excess pore pressure generation and dissipation specifically to assess the likelihood of liquefaction failure (ie. pressures are able to dissipate during and after loading). Examples include the programs developed to study earthquake induced liquefaction (Seed et al, 1975), to predict wave induced failure (Finn et al, 1983) and to assess the likelihood of liquefaction in both earthquake and marine environments (Martin et al, 1980).

Seed et al (1975) modelled the events of the 1964 Niigata earthquake. The results of this study are summarised in Table 3.2. There appears to be a good agreement between the behaviour predicted by the numerical model and the observed events. In particular the program predicted the upward dissipation of excess pore pressures resulting in surface cracking and a flow of water at ground level several minutes after the tremor. Seed et al (1975) concluded that this type of numerical model had achieved an adequate level of sophistication considering the uncertainties of input data for irregular cyclic motions and in situ soil properties.

Yoshimi (1977) adopted the method presented by Seed et al (1975) to model the results of vibrating table tests. Figure 3.20 shows the results of the laboratory tests and the computer based prediction. There appears to be a good agreement between the observed and predicted behaviours. However, Yoshimi noted that the consolidation model adopted by Seed et al (1975) to model excess pore pressure dissipation required significant modification of coefficient of consolidation values at low effective stresses to produce the data shown in Figure 3.20.

3.2.6 Empirical field methods

Various existing in situ site investigation techniques have been proposed for predicting the likelihood of liquefaction failure. Examples include the standard penetration test (SPT), cone penetration test (CPT), self-boring pressuremeter and electrical resistivity methods. In each case the methods were first used in earthquake environments and a similar approach is used. In situ test values are plotted against a parameter representing the design disturbance, eg. cyclic stress ratio in Figures 3.24 to 3.27. Case histories are plotted against the same axes and used to define areas at risk from liquefaction failures as shown in Figures 3.24 to 3.27. If values derived from the site under investigation fall within this area liquefaction failure is considered a hazard. The use of each of the techniques that have been proposed is outlined below.

Seed et al (1983) reviewed the development of the SPT and the CPT as methods of assessing the likelihood of liquefaction in earthquake regions. The use of the CPT was also discussed by Robertson and Campenella (1985). Seed et al (1983) present a series of design charts which correlate a modified penetration resistance (N_1) or modified cone penetration resistance in the case of the CPT, against a design earthquake parameter. Figure 3.24 shows an example of a design chart for the SPT method. Similar curves are proposed by Seed for different earthquake magnitudes and other soil types. The design charts proposed by Seed et al (1983) for use with CPT data were adapted from earlier SPT charts. This was achieved by assuming a constant correlation between the cone penetration resistance gained from CPT and N-values derived from the SPT. Figure 3.25 presents examples of charts prepared in this way. Alternatively, Seed suggest producing design charts at each new site by performing CPTs and SPTs in parallel to gain a better CPT-SPT correlation factor. The procedure for deriving modified penetration values and the selection of a design earthquake are provided by Seed et al (1983).

A variation in the SPT method has been proposed by Law et al (1990). They suggested that it is more appropriate and straight forward to plot modified or corrected penetration resistance against an energy parameter, rather than the conventional stress parameter.

The self-boring pressuremeter was developed by Hughes and described by Hughes et al (1977). Vaid et al (1981) suggested its use as a technique for studying the likelihood of liquefaction failure at a site. This was discussed further by Morris (1983). In situ tests with the instrument enable the shearing resistance and dilation angle of a soil to be determined by the methods outlined by Hughes et al (1977). Vaid et al (1981) presented a design chart using these parameters, this is shown in Figure 3.27. It correlates soil dilation angle with an earthquake parameter. The design curves were based upon data previously presented by Seed et al (1983) for the SPT method and would be used in a similar manner.

Arulmoli et al (1981, 1985) proposed a correlation between an electrical parameter, derived from in situ resistivity testing, and an earthquake parameter similar to that adopted for penetration test method outlined above. A series of design curves are proposed for various earthquake magnitudes: Figure 3.36 shows an example. These are used in a similar manner to the charts proposed for the SPT and CPT methods with values of the electrical parameter determined by the procedure presented by Arulmoli et al (1981, 1985). This approach has been developed further by Arulanandan and Muraleetharan (1988 a and b).

3.2.7 Field simulation

Various authors have described field methods of simulating rapid cyclic loading by using buried explosive chargers. These are generally referred to as blasting techniques. Similar procedures have been described by Florin and Ivanov (1961), Kummenje and Eide (1961), Prakash (1981), and more recently Charlie et al (1992). A series of explosive charges are detonated at a point in a soil profile. A sufficient period is allowed between successive blasts to ensure excess pore pressures dissipate fully. The depth, position and energy of the blast varies between the various authors, as does the criteria for assessing the likelihood of liquefaction failure. Florin and Ivanov (1961) and Ivanov and Sinitsyn (1977) make this assessment on the basis of the surface settlements caused by each blast. If the total settlement induced by three successive blasts exceeded 80 to 100mm the authors assume liquefaction failure is a hazard. Both Kummenje and Eide (1961) and Prakash (1981) adopt a criteria based upon the excess pore pressures measured within the soil profile and observations of surface settlement. Liquefaction failure is considered to be a hazard if the maximum excess pore pressure observed within the profile equals the initial effective overburden stress, ie. vertical effective stresses become zero.

3.3 Existing methods in the light of theory and field observations

Liquefaction failures are caused by a sudden reduction in effective stresses due to a rapid increase in pore pressures. This significantly reduces soil strength and stiffness thereby causing failure. It is therefore not a special soil behaviour but simply an example of the principle of effective stress. Case histories show that failures are associated with soil profiles with a high proportion of fine granular soils. Basic critical state soil mechanics theory suggests that only soil elements wet of critical can generate the large positive excess pore pressures necessary for liquefaction failure. However, laboratory testing has shown that cyclic loading of dry of critical soil may also generate these positive excess pore pressures. On shearing these soil elements will dilate resulting in limited strain failure. To distinguish between these two behaviours the term cyclic mobility has been proposed to describe the limited strain behaviour caused by the undrained cyclic loading of dry of critical soil (Castro 1975). Field observations, theory and modelling, both physical and numerical, suggest that large positive excess pore pressures generated at one point can redistribute within a soil profile to cause liquefaction elsewhere in the profile.

An accurate method of assessing the likelihood of liquefaction failure must therefore determine the following. Firstly, whether large positive excess pore pressures can be generated in a soil profile or structure. Secondly, are these excess pressures sufficient to cause failure at the point of generation or elsewhere in the soil profile as they dissipate. Various methods have been proposed for assessing the likelihood of liquefaction failure at a site. These are outlined earlier in this chapter and are reviewed in this section.

Critical void ratio theory has developed into the critical state soil mechanics model which can be used to correctly predict excess pore pressure generation. It may also be adopted to understand the redistribution of pore pressures within a soil profile or structure, and potential failure mechanisms. However, the approach is not in general use by practising engineers possibly for several reasons as follows. Extensive sampling and testing would be required to establish the state boundary surface of each soil present in a profile. Secondly, an accurate in situ test would be required to establish in situ soil state. Although an electrical resistivity technique has been proposed for determining soil state in situ this is relatively complex. This together with the need for extensive field testing and laboratory testing makes the approach expensive and probably impractical.

The equivalent stress path approach is perhaps more readily understood and has become the most widely adopted theoretically based approach. Laboratory testing gives an understanding of the excess pore pressures that can be generated within a soil element. However, the soils typically associated with liquefaction are highly susceptible to disturbance during sampling and preparation even by supposedly "undisturbed" methods. Alternatively samples have to be reconstituted and this requires an accurate knowledge of in situ soil state and stress history. These are frequently not known or are assumed on the basis of conventional site investigation data. In addition, laboratory tests are described as undrained. In reality this is not the case since the relatively high permeability of the soils results in local drainage and the collection of a layer of free water at the top of a sample during loading. This behaviour has been demonstrated by various workers, eg. Gilbert and Marcuson (1988). Tests would therefore be more accurately described as constant volume rather than undrained. Another relevant factor is that large positive excess pore pressures and free water generated in soil elements would significantly influence the behaviour of adjacent soil in a profile. Constant volume laboratory testing prevents drainage beyond the boundary of the sample. It therefore cannot be used to understand excess pore pressure dissipation during or after loading, and the possibility of liquefaction failure elsewhere in a soil profile.

The critical strain approach suggests that most granular soils, irrespective of their state are capable of generating large positive excess pore pressures and can therefore be associated with liquefaction failure. However, the theory presented in Chapter 2 suggests that only soils wet of critical can be liquefied, although dry of critical soils are able to generate positive excess pore pressures which may dissipate to cause failure elsewhere. The approach fails to consider the possibility of this non-coincident model of liquefaction. In practice the method involves measuring shear wave velocities throughout a profile to derive ground accelerations. This uses relatively complex equations and parameters, some of which are assumed, or are approximations. There is no evidence to suggest that this method has been widely adopted by practising engineers.

Physical modelling, especially centrifuge testing, represents an excellent research tool for examining and understanding the mechanics of excess pore pressure generation, dissipation and liquefaction failure. However, it is cumbersome, time consuming and difficult to model real and complex soil profiles or structures. These methods are therefore of limited value to the engineer examining a specific site, although they are of considerable value to those studying the processes of liquefaction

As with physical modelling, numerical modelling is a powerful tool for studying the mechanics of liquefaction. For numerical methods to be accurate adequate correct input data is required together with a correct analytical model. In practice, input data is often based upon the results of conventional site investigation data and laboratory testing which may not be of sufficient accuracy. The most suitable type of numerical model is the coupled type which allow excess pore pressure dissipation during, as well as after, soil loading. This is significant when studying liquefaction because the soils present, although loaded rapidly, are also of a relatively high permeability allowing drainage to occur during loading and rapid redistribution of excess pore pressures after loading. Consolidation theory is generally adopted to describe the dissipation of excess pore pressures in these analyses. However, the results of work by previous researchers, and the theory presented in Chapter 2 suggests an alternative mechanism may also act, that of hindered settling. If this is correct numerical models should incorporate both mechanisms in order to predict liquefaction behaviour accurately.

The field methods that have been proposed (ie. SPT, CPT and self-boring pressuremeter) determine the relative density of a soil and not its' state relative to the critical state line of the soil. The theory in Chapter 2 indicates that the it is soil state relative to the critical state line that is relevant to the generation of excess pore pressures and therefore the likelihood of liquefaction failure. However, the methods, especially SPT and increasingly CPT, are familiar to the practising engineer, there is a large volume of case history data, and well documented procedures have been published for earthquake environments. For these reasons the methods have become widely adopted. There is no evidence that the use of the self-boring pressuremeter has been widely used. For each method the correlation between test values and an earthquake parameter is empirical and based upon highly scattered case history data. This has been attributed principally to a poor level of standardisation of SPT methods. This has remained a problem despite attempts to standardise procedures and equipment, eg. Seed et al (1985) and Skempton (1986). Results can therefore be inconsistent between different operators. It is also important to note that these approaches cannot take account of the possibility of a non-coincident model for liquefaction failure. This probably accounts for a large amount of the scatter seen in the case history data used to define design charts.

Field simulation of rapid cyclic loading events using explosive charges might be considered to be full scale model testing. However, the approach is empirical with various authors using different charges placed at a variety of depths in a soil profile. It is suggested that a large number of charges at various depths would be needed fully to investigate a site. This in itself would significantly alter the properties of the soils present. The approach has the advantage that it allows excess pore pressures generated at one location to dissipate through the profile under investigation, and more recently workers have proposed measuring the pore pressures generated throughout a soil profile to assess the likelihood of liquefaction failure.

It would appear that none of the currently proposed methods offer the engineer an accurate and practical means of assessing the likelihood of liquefaction failure at a site. There is therefore a need for an appropriate new approach. Such a method should assess the excess pore pressure generation capacity of soils throughout a profile, how these might dissipate or redistribute within a profile, and potential failure mechanisms. This can best be achieved by recognising that liquefaction and liquefaction failure is controlled by excess pore pressure generation and dissipation. Determining the excess pore pressure generation characteristics of soils throughout a profile by sampling and laboratory testing is impractical due to sample disturbance and drainage during loading. An accurate in situ technique of assessing excess pore pressure generation therefore has clear advantages.

Critical state soil mechanics provides a comprehensive model of soil behaviour. This predicts that only soils wet of critical are able to generate the large positive excess pressures necessary for liquefaction failure. It is also recognised that positive excess pore pressures generated by cyclic loading of dry of critical soils can dissipate to cause failure elsewhere in a profile. This case is not considered in detail in this document although it is noted that once excess pore pressures have been generated the potential mechanisms of dissipation and failure are common to both cases.

The remainder of this dissertation describes the laboratory research carried out by the author to identify and develop an appropriate in situ technique for determining soil state relative to its critical state line and therefore the potential of the soil to generate positive excess pore pressures. To make a complete assessment of the likelihood of liquefaction failure various scenarios of excess pore pressure generation, dissipation and failure need to be considered. It is suggested that this is best achieved by numerical modelling incorporating accurate soil data, and correct excess pore pressure dissipation and failure mechanisms. Soil state would be provided by the new in situ technique. Models of excess pore pressure dissipation appear to exist in the form of consolidation and hindered settling. Finally, critical state soil mechanisms provides the overall framework for describing these behaviours and potential failure mechanisms.

CHAPTER 4 EQUIPMENT AND MATERIALS

The discussion in Chapter 3 has demonstrated the need for a new approach. Liquefaction failure is controlled by excess pore pressure generation and dissipation. It is suggested that an in situ method is the best means of determining the excess pore pressure generation potential throughout a soil profile. The excess pore pressures that can be generated by a soil are dependent upon the relative positions of the in situ soil state and its critical state line. An accurate in situ method should therefore determine this relative position. The mechanisms of liquefaction, especially the dissipation of excess pore pressures, were also identified as important in Chapter 3. This chapter describes the laboratory equipment and materials that were used by the author to study these mechanisms and identify and develop a suitable in situ method.

The research described in the dissertation was carried out in the laboratory for several reasons. These include a good control and knowledge of conditions, materials and parameters, which is rarely possible in the field. However, it is fully appreciated that before an in situ testing method could be generally adopted a comprehensive programme of field testing would be required. This is discussed briefly in Chapter 8.

This chapter is divided into six sections, the first of these considers in more detail the intended use of the equipment and the requirements placed upon it. The principal components of the equipment are described in subsequent sections. These were the soil used, a new apparatus for preparing soil beds termed a sand column, an electrical transducer-computer based monitoring system and model in situ instruments. The final section reviews the performance of the equipment, some of the problems encountered and how these might be overcome.

4.1 Laboratory based research

The laboratory research had two principal aims; to study the mechanics of liquefaction and to identify and develop an appropriate in situ field instrument. To achieve both these aims it was necessary to create model soil profiles or beds in the laboratory. In order to perform a complete study it was considered equally important for both non-liquefiable and liquefiable beds to be produced. This would provide a better understanding of the mechanics of liquefaction and an assessment of whether an instrument was capable of distinguishing the two conditions.

Beds had to be in a known state and be reproducible. The shape and dimensions of the beds needed to be such that testing could be easily performed and monitored, eg. the penetration of an instrument into a profile or the dissipation of excess pore pressures through a model profile. A bed thickness of approximately 1m was considered appropriate. A further consideration was the time required to prepare beds. Conventional methods involve the sedimentation of soil particles through water. This requires beds to be excavated from an apparatus and resedimented before each test. This is both time consuming and cumbersome if large volumes of soil are involved. A new piece of equipment, termed a sand column, was designed and built to overcome these problems and enable the rapid preparation of uniform soil beds. Very loose beds were produced by fluidising the soil with a large hydraulic gradient applied upwards through the bed. On removing the hydraulic gradient the soil resettled to form a very loose bed. Dense beds were created by prolonged vibration of very loose beds. In order to assess whether these methods successfully formed uniform beds of known state a series of tests were carried out. These are described in Appendix D.

Perhaps the most significant component of the equipment was the soil used. The principal requirement was that the soil should be capable of being easily prepared in liquefiable and non-liquefiable states. Soils associated with this behaviour are typically uniformly graded loose fine sands. Liquefaction results from the generation of high positive excess pore pressures when these soils are disturbed. This does not occur if these soils exist in a dense state, since undrained shearing generates negative excess pressures. Clearly, permeability is also an important parameter since it controls the rate of excess pore pressure dissipation during and following loading. For high excess pore pressures to be generated soil permeability must be low relative to the rate of loading. Field evidence indicates that the excess pore pressures associated with liquefaction failures can dissipate relatively rapidly to cause failure remote from the point of excess pore pressure generation. This suggests relatively high permeability values. The permeability of fine sands

($1x10^{-4}$m s^{-1} to $1x10^{-5}$ m s^{-1}), is such that both these conditions may be satisfied provided loading is rapid. Case histories show that this is typically the case for liquefaction failures. The soil selected for testing showed a strong tendency to generate large positive excess pore pressures when loaded rapidly in a loose state and the opposite behaviour when relatively dense. It exhibited these characteristics at low effective stresses. This was relevant because test beds prepared in the sand column were approximately one metre thick.

In order to study the mechanics of liquefaction and soil behaviour adjacent to model instruments in the sand column a pore pressure monitoring system was required. The system had to exhibit a rapid response and provide continuous and simultaneous reading of pore pressures within a soil bed and on the surface of model instruments. An accuracy of 1% of the maximum excess pore pressure to be generated was considered appropriate for the system. The one metre bed proposed meant that changes in pore pressures of the order of 10 kPa were anticipated. The accuracy required of the monitoring system was therefore $\pm$ 0.1 kPa. Further considerations were that the system should be flexible (ie. easily modified and adjusted to enable monitoring at any location within a bed or on the surface of a model instrument) and have a minimal influence upon test results. A digital data storage system was desirable since this would enable the rapid analysis and plotting of potentially large quantities of data. The system that was assembled to fulfil these requirements is described in section 4.4.

In situ instruments can be used to load soil in one of three ways: by applying normal stresses, shear stresses, or a combination of the two. Three basic types of instrument exist which apply these loads: expanding membrane probes or pressuremeters, vanes and cones respectively. Models were built of each type of instrument to enable tests to be performed to determine whether any were able to distinguish liquefiable and non-liquefiable soil profiles. It is noted above that the excess pore pressures that a soil can generate is a function of its soil state relative to the critical state line. Conversely, if a known stress path is applied to a soil element and excess pore pressures are monitored, the initial state of the soil state relative to its critical state line may be established. It should therefore be possible to use an instrument incorporating pore pressure measurement to determine the potential of soils within a profile to generate excess pore pressures. The various model instruments that were built to assess this approach are described in section 4.5. The principal requirements that were placed upon the instruments were that they should be relatively straightforward and therefore easily modified and that they would work in conjunction with the sand column and monitoring system.

4.2 Soil selected for testing

The soil used to form beds in the sand column was described as a white, very uniform, very silty, fine quartz sand. It was chosen from an initial sample of thirty soils selected from a variety of natural and industrial sources. Of these thirty samples the soil selected was designated soil 23. This soil was chosen on the basis of its particle size distribution, permeability and its behaviour, especially excess pore pressure generation, under shear loading. The conventional laboratory tests that were used to investigate each of these characteristics are described in Appendix A. This includes a discussion of the results and the selection of soil 23. The basic properties of the soil are summarised in Table 4.1 and Figure A.1 shows its particle size distribution curve.

4.3 Sand column apparatus

The sand column apparatus, shown in Figure 4.1, enabled the rapid preparation of soil beds in various states. It was designed to enable two types of laboratory tests. Firstly, to study the mechanics of liquefaction, and secondly the identification and development of a suitable in situ instrument. The apparatus consisted of two principal components: the sand column in which soil beds were created, and a vibrating table upon which the sand column stood. Secondary components included a static head reservoir which enabled the generation of excess pore pressures at the base of beds, a surface surcharge load for testing at increased effective stress levels, and an impermeable near surface layer to enable simple layered soil profiles to be modelled. Each of the components is described in more detail in the following sections.

4.3.1 Sand column

The sand column, shown in Figure 4.1, consisted of a vertical cylinder standing on a base with a removable head on the top. The cylinder was made of transparent perspex, 1140mm in length with an internal diameter of 188mm (external diameter 200mm). A base filter of a fine geotextile material was clamped between two perforated plates at the bottom of the column. The plates were bolted together and sealed with a 230mm diameter 'o' ring. A mains water supply was connected to the cylinder beneath the base filter, with flow rates controlled by a standard disc valve.

The removable head was made up of a 16 standard wire gauge brass plate, with a maximum diameter of 400mm, tapering to 188mm at its base, where it was attached to the sand column by eight bolts. Each bolt passed through a brass flange at the base of the head, a rubber seal and a perspex flange on top of the cylinder. A drainage pipe was connected to the side of the head, close to the top.

A guiding gantry was housed in the removable head. This consisted of two brass bars (25mm by 12.5mm by 400mm) bolted across the diameter of the head, one vertically above the other. Vertical holes, 16mm in diameter, in the centre of each bar were designed to guide model instruments into soil beds prepared lower in the column. A total of sixteen smaller vertical holes (8mm in diameter), situated in each bar, were designed to hold instrumentation tubes in position. These are described in section 4.4.1 and were held in position by cap head screws threaded into the upper bar of the gantry.

4.3.2 Vibrating table

The vibrating table, shown in Figure 4.2, consisted of two 17mm thick sheets of marine plywood (560mm by 740mm). These were separated by four heavy duty springs, one at each corner of the table. The distance between the two plywood sheets was approximately 40mm.

Vibration was produced by a BKB electric motor which operated at 1425 revolutions per minute. This was bolted to the upper surface of the table with its axis vertical. The spindle of the motor passed through the upper plywood sheet, where it was connected to an eccentric weight. This rotated between the two plywood sheets, as illustrated by Figure

4.3.

The 242 gram eccentric weight or arm was made of a 135mm length of 3/4 inch Whitworth steel studding. A 2mm by 2mm slot was machined across the diameter of one end of the weight. It was held in position by a cap head screw as shown in Figure 4.3. A calibration was produced which related the energy level of the vibrating table (ie. the eccentricity of the arm) to the final density of a bed formed in the sand column. The arm eccentricity was defined as the horizontal distance between the centre of gravity of the arm and the vertical axis of the vibrating table motor. The calibration curve is reproduced in Figure 4.4 with the period of vibration required to produce uniform soil beds indicated.

4.3.3 Static head reservoir

The static head reservoir comprised a 9 litre water reservoir connected via a disc valve to the base of the sand column, as illustrated in Figure 4.1. The reservoir was attached to an adjustable wall mounting so that the elevation of the reservoir could be readily varied and measured.

4.3.4 Surcharge load

The surcharge load was designed to be placed inside the sand column and to rest on the surface of a soil bed. Figure 4.5 shows the surcharge load apparatus. It consisted of a perspex disc or plate, two PVC silos, each sealed at one end and a maximum of 28 kg of 1mm to 2mm diameter lead shot. The silos were made of drainpipe with an external diameter of 68mm and were 1000mm in length.

The disc was 188mm in diameter and 10mm thick, with seven holes across the diameter. Five of the holes were of 10mm diameter to allow instrumentation tubes to pass through the disc. A further hole of 7mm diameter was designed to enable a miniature pore pressure transducer to be attached directly to the disc. A 19mm hole in the centre of the disc was extended upwards by a perspex sleeve to enable the driving rod of a model instrument to pass through the disc. Steel cables were attached to the disc at four points by means of brass bosses threaded into the top surface of the plate.

4.3.5 Impermeable near surface layer

A layer of low permeability was created near to the surface of a sand bed by the sedimentation of a clay layer. Once this had settled and consolidated under its own weight, a surface layer of sand was placed very slowly over the clay. Care was taken not to disturb the very soft clay layer by placing the overlying sand too rapidly. The clay used to form the impermeable layer was ground London Clay, which was sieved through a 0.425mm British Standard sieve.

4.4 Monitoring System

The system that was used to monitor pore pressures in the sand column consisted of several components. The principal parts comprised miniature electrical pore pressure transducers which formed the instrumentation, and a computer controlled data logger that processed and recorded the output of the instrumentation. These components are described in greater detail in the sub-sections that follow.

To ensure that the combined system achieved the required level of accuracy a series of tests were performed. These are described in Appendix C. The use of a computer based system enabled very rapid, accurate, recording of test data, ie. approximately 2800 values in a typical 500 second test. It also enabled this large volume of data to be analyzed and plotted conveniently.

4.4.1 Instrumentation

Pore pressures were monitored in the sand column using miniature electrical resistance pore pressure transducers. These were generally sealed into the end of brass instrumentation tubes (1520mm long with an outside diameter of 8mm) with the supply/output cable passing through the bore of the tubing as shown by Figure 4.6. The instrumentation tubes were held in position by the guiding gantry which is described in section 4.3.1. Alternatively, transducers were housed within model instruments or attached to the surcharge load disc. These methods are described in sections 4.5 and 4.3.4 respectively. The specifications of the transducers are set out in Table 4.2. The supply voltage to the instrumentation, typically five volts, was provided by the logging system.

Initially the miniature pore pressure transducers proved problematic. In particular de-airing to prevent air bubbles forming in or behind the ceramic filter provided with the transducers. This was a problem because of the relatively low pore pressures within soil beds and the use of a mains water supply, ie. the water used was not de-aired. Air bubbles trapped between the outer face of the filter and the silicon membrane of a transducer can have two effects. Firstly, changes in pore pressure result in changes in the volume of the bubble. This will increase the response time of the transducer. Secondly, if a bubble completely spans the bore of the transducer between the filter and the membrane of the transducer then its' surface tension is able to support a pressure difference. This means the instrument may not measure the full pressure change that occurs in the adjacent soil. This problem was overcome by replacing the ceramic filters with ones of cintered bronze, and regularly calibrating the instrumentation.

4.4.2 Computer controlled data logging and analysis system

The electrical output from the instrumentation was conditioned and logged by a BBC model B microcomputer and a purpose developed software package, together with a 16 channel 3D interface. The interface was made up of a multiplexer, an amplification unit and an analogue to digital convertor. The latter reduced the analogue output of the instrumentation (pore pressure transducers and potentiometer, refer section 4.5.2) into a digital signal of a suitable range for handling by the computer.

The computer controlled the logging process and recorded test data on disc for subsequent analysis and plotting. Ancillary equipment included an 80-track disc-drive, an Epsom LX-80 dot matrix printer and a monochrome monitor. The assembled system is shown in Figure 4.7 The software package, developed by the author, permitted four operations to be performed. These were the continuous logging of the instrumentation output to enable calibration, logging during a test, the analysis of data and the plotting of results. Appendix B describes the programs in detail and section 5.2 outlines how they were used during a typical test procedure.

4.5 Model in situ instruments and control mechanisms

The various model instruments that were built for use with the sand column apparatus are described in this section. Three basic types of model instrument were built: cones, vanes and an expanding membrane probe. For ease of manufacture and modification, and to avoid problems of corrosion the model instruments were made principally of brass. Where other materials were used these are described in the appropriate sections that follow.

Each instrument was designed to be attached to a standard driving rod, which passed through the guiding gantry of the sand column, as shown in Figure 4.1. The driving rod consisted of a 1.50m length of 5/8 inch by 9 Standard Wire Gauge brass tubing (external diameter 15.8mm, internal diameter 6.4mm). Instruments were attached to the driving rod by a 1/4 inch British Standard Pipe Thread as shown in Figure 4.8.

4.5.1 Cones and piezocones

A total of four cones were built. Each had an overall length of 113mm and a shaft diameter of 15.8mm. Three of the instruments were simple cones with machined tip angles of 30°, 60° and 90°. The fourth instrument was a simple piezocone with a tip angle of 60°. A miniature pore pressure transducer was sealed into the end of the driving rod to enable pore pressures to be measured at one of the four positions shown in Figure 4.8. The remaining three positions were sealed with electrical solder.

4.5.2 Cone driving mechanism

Cones were driven by a dead weight system of up to 97.5N attached to the top of the vertical driving rod. The rate of penetration was controlled manually by the apparatus shown in Figures 4.1 and 4.9. This consisted of a simple winch, with a friction mechanism to counteract the weight of the dead load, the driving rod and a cone or piezocone. The system was also used with other instruments either to drive them into soil beds or to hold them stationary at a given vertical position.

A device was developed which enabled the vertical position of a piezocone to be determined. It consisted of a Reliance ten turn precision potentiometer attached to the winch via a band drive. The apparatus is shown in Figure 4.1 and in greater detail in Figure 4.9. The potentiometer was provided with a five volt power supply and its output processed by the BBC microcomputer via the interface.

4.5.3 Vanes and piezovanes

Three simple four bladed vanes were built with a shaft diameter of 15.8mm and tip angles of 60°. Two of the vanes had an overall length of 113mm. These were constructed with blade aspect ratios of 1 : 2 (diameter 59mm, height 29.5mm) and 1 : 1 (diameter 46mm, height 46mm). These are shown in Figure 4.10. The third vane had an overall length of 250mm and a blade aspect ratio of 2 : 1 (diameter 37.5mm, height 75mm).

Two simple piezovanes were built. In both cases these were adaptions of the 1 : 1 ratio vane described above. The modification enabled pore pressures to be measured either on the shaft of the vane or on the edge of a vane blade. The adapted vane is shown in Figure 4.10. As with the piezocone described above, pore pressures were measured by a miniature pore pressure transducer sealed into the end of the driving rod.

4.5.4 Vane rotating mechanism

Vanes were rotated manually via a steel lever arm (length 330mm, diameter 8mm) located in one of two holes machined in the top of the driving rod. This is shown in Figure 4.11. The holes were horizontal and passed through the axis of the driving rod.

4.5.5 Expanding membrane probe

A simple expanding membrane probe was constructed which utilised the piezocone described in section 4.5.1. The membrane consisted of a cylindrical balloon (12mm internal diameter) with both ends removed. Four 'o' rings (12mm in diameter) were used to seal the membrane onto the body of the probe as shown in Figure 4.12. The pressure required to expand the probe was supplied through the bore of the driving rod and via two of the piezocone's four filter positions. The remaining two filter positions were sealed with electrical solder.

4.5.6 Pressure system for expanding membrane probe

Air pressure was provided by a Medcalf Model B Hyflo pump via a 245cc brass cylinder as shown in Figure 4.13. Two standard ball valves controlled the flow of air into and out of the pressure cylinder. Air pressure was transferred from the pressure vessel to the probe through a length of nylon tubing. This passed through the bore of the driving rod to be sealed inside the base of the rod by two 'o' rings as shown in Figure 4.12.

Before a test a pressure was generated by the pump and sealed into the cylinder by closing the two ball valves. The pressure in the cylinder was measured via a Bourdon pressure gauge. During a test pressure was applied to the membrane by opening the ball valve to the probe. The valve remained open enabling the pressure applied to the membrane to be monitored via the gauge.

4.6 Summary

This chapter has described the equipment used in the laboratory research. It was designed by the author and manufactured by the technicians of the Geotechnical Research Centre. The main components of the apparatus, shown in Figure 4.14, worked well. It proved to be robust and simple to modify. The sand column and vibrating table enabled uniform beds of soil to be formed relatively quickly. Soil 23 was suitable, with rapid loading resulting in the generation of large excess pore pressures which then redistributed within the soil bed. The instrumentation and logging system functioned satisfactorily producing accurate and reproducible results. The microcomputer based logging system also enabled the rapid analysis and plotting of the 2800 data points recorded during a typical 500 second test.

Some difficulties were encountered. For example the interface component of the data logging system had been designed for use by previous researchers and lacked a comprehensive user manual. In order to ensure that it worked correctly and to a sufficient accuracy the unit was thoroughly checked and calibrated. Details of these checks are included in Appendix C. It was noted in section 4.4.1 that the filters supplied with the miniature pore pressure transducers were initially a problem. This was due to air bubbles forming in or behind the filters. It was overcome by replacing the ceramic filters with ones of cintered bronze. To ensure that similar problems did not occur with the piezovanes and piezocones they were assembled under water, and calibrated before and after each test. These instruments were also dismantled and reassembled between tests to enable a visual inspection for air bubbles.

Problems were also encountered with the control mechanisms used with the various model instruments. The method of driving instruments into soil beds proved to be rather crude and lacked the force to achieve full penetration in dense beds. The potentiometer used to determine the vertical position of an instrument within a bed was also a problem. The method of rotating the vane was somewhat crude and lacked a quantitive means of determining the torque applied. These problems were mechanical and could be overcome by constructing more powerful and slightly more sophisticated equipment. For example, a greater dead load or a hydraulic system could be used to drive instruments into soil beds.

The surcharge apparatus did not work well. It was possible to generate the expected large excess pore pressures within the soil bed beneath the surcharge disc. However, this resulted in fluidised sand passing between the disc and the sides of the sand column. Consequently, the disc and column became locked together and thereby transferred the surcharge load from the soil to the perspex cylinder of the sand column. This equipment was designed in an attempt to study liquefaction behaviour at larger effective stresses than were achievable in a one metre soil bed. However, it was obviously not very successful. Several alternatives exist: a taller column could be built although this would have physical limitations, or the surcharge method could be modified to prevent locking against the sides of the column, eg. lead shot could be placed directly onto a geofabric filter resting on the soil bed.

The formation of simple layered soil profiles in the sand column was straightforward although time consuming. The use of a clay to form layers of low permeability caused contamination of the fine sands which was difficult to remove. For this reason only a few tests were carried out with layered soil profiles, and this was done at the end of the testing program.

CHAPTER 5 PROCEDURES ADOPTED DURING SAND COLUMN TESTS

The various tests carried out in the sand column apparatus are described in this chapter. Two broad categories of tests were performed; those to study the mechanics of liquefaction, and those to assess whether an in situ instrument might be used in a new method to establish the susceptibility of a soil profile to liquefaction failure. The equipment referred to in this chapter is described in detail in Chapter 4.

This chapter is divided into six principal sections. The first of these sets out a schedule for the sand column tests performed and briefly discusses the purpose of the various types of test. A relatively large number of tests were carried out and many followed a common or general procedure which is outlined in the second section. The third section describes the tests undertaken to study the mechanics of liquefaction. The remaining three sections present the tests carried out with the three types of model instruments considered, ie. vanes, expanding membrane probe and cones. The results of the tests described in this chapter are presented in Chapter 6 and discussed in Chapter 7.

5.1 Testing schedule

The various sets or suites of tests that were performed in the sand column and described in this chapter are summarised in Table 5.1. This table refers to the appropriate sections of Chapter 6 which presents the results of testing.

The mechanics of liquefaction were studied to gain a clear understanding of the mode of failure and to demonstrate the theory proposed in Chapter 2 ie. that liquefaction failure may result from the redistribution of excess pore pressures within a soil profile. This was achieved by modelling the process of liquefaction in the sand column. This enabled the examination of the various factors that control the generation and subsequent redistribution of excess pore pressures within a soil profile. The parameters considered were; the magnitude of excess pore pressures initially generated, the period of excess pressure generation, soil state, effective stress level, and the influence of a non-uniform or layered soil profile.

In Chapter 3 it was suggested that a method incorporating an in situ instrument is the most appropriate approach to assess the susceptibility of a soil profile to liquefaction. Clearly, such a test should be able to identify the soil elements within a soil profile capable of generating large positive excess pore pressures. The test should also be able to monitor the subsequent dissipation or redistribution of these excess pressures.

There are three basic types of in situ soil loading; normal, shear or a combination of the two. Three forms of field instrument or probe exist which produce these types of loading. These are expanding membrane probes, vanes and cones respectively. Each of these types of instrument can be designed to measure pore pressures. In order to assess which of these instruments was able to fulfil the requirements stipulated above, sand column tests were performed with simplified models of each type of instrument. The tests were designed initially to assess the ability of each type of instrument to distinguish wet and dry soil states and to monitor pore pressure redistribution within a profile. Further testing with each type of instrument was carried out to determine which factors influenced the pore pressures observed when a soil element was loaded, eg. loading rate, disturbance due to placing the instrument, geometry and filter position.

5.2 General test procedure

The procedures common to the majority of sand column tests are set out in this section. Additions and deviations to these procedures for specific tests are detailed in the appropriate subsequent section of this chapter. The general method consisted of three parts; preparing and calibrating the apparatus, the test itself (the monitoring of excess pore pressure generation and dissipation resulting from a controlled perturbation), and finally post test procedures (recalibration, the dismantling of equipment or preparation for the next test, and the analysis and plotting of recorded data). These were subdivided into a number of elements to form the detailed test procedure. This is described in chronological order below.

5.2.1 Pre-test piping

To ensure the temperature of the sand column remained constant during a test the mains water supply valve was opened for a period of approximately thirty minutes prior to a test. The valve was then closed allowing the soil to settle forming a very loose bed.

5.2.2 Pre-test calibration

The monitoring system was calibrated before each test. This was carried out with the instrumentation immersed inside the sand column and used the appropriate continuous logging program (refer section B1 of Appendix B). Calibration involved lowering each of the pore pressure transducers into the column in 100mm increments. At each position the digital output of the monitoring system was recorded against the static water head acting upon each transducer. A record was made of the supply voltage to the instrumentation and the water temperature.

The calibration constant for each transducer was established by plotting static water head against the digital output (millivolts). Figure 5.1 shows an example of this type of plot. Constants were calculated by applying the equation;

$$\text{transducer constant} = \frac{\Delta 0}{\Delta H \; V \; \gamma_w} \qquad 5.1$$

where $\Delta 0$ = change in digital output (millivolts)

ΔH = change in static head (metres)

V = supply voltage to the instrumentation (volts)

γ_w = unit weight of water (9.81 kN m^{-3})

This produced constants with values in units of millivolts/kPa/volt.

5.2.3 Assembly of apparatus

This involved up to two operations; firstly, the positioning of the instrumentation and secondly, when appropriate, assembling model instruments.

Test beds were generally formed around the instrumentation. The position of the pore pressure transducers depended upon the type of test to be performed and the state of the soil bed to be created. The following guidelines were generally adopted.

In tests to study the mechanics of liquefaction and those where model instruments were driven into the bed, the instrumentation was distributed evenly throughout the soil profile. In cases where instruments were not driven (eg. vane and expanding membrane probe tests where the soil bed was formed around the instrument) approximately half the instrumentation was positioned close to the instruments' tip. The remainder of the transducers were distributed throughout the soil bed.

The basal filter of the sand column was used as a datum level during all tests. Transducer positions were recorded as an elevation above this datum. Graduations on the instrumentation tubes enabled transducers to be positioned by measuring down to the required level from the upper bar of the guiding gantry (1516mm above the basal filter), refer Figure 4.1.

The assembly of a model instrument involved the following. Instruments were attached to the driving rod in air with the thread sealed with a silicone rubber compound. This was done to prevent the flow of water into the bore of the driving rod. To ensure a good seal, the thread was cleaned and dried before applying the sealant. Sufficient time was allowed to permit the sealant to solidify before the instrument was immersed. This procedure was generally carried out inside the sand column with the water level lowered by siphoning.

For tests where the instrument was to be driven into the bed, the model instrument was suspended above the proposed soil level by the cone driving mechanism. For tests in which the bed was to be formed around the instrument, it was lowered into the column and held in place by the same mechanism. In these cases, the instrument was generally held with its tip 100mm above the basal filter of the column. The driving rod was clamped to prevent rotation during the formation of a soil bed.

5.2.4 Formation of soil beds

Having calibrated the monitoring system, positioned the instrumentation and where necessary assembled and positioned a model instrument, soil beds were formed by the following methods.

Very loose beds were created by opening the mains water supply valve, as shown in Figure 4.1. This lifted the soil particles into suspension. A flow rate in excess of 2 mm s^{-1} maintained for a period of ten minutes was necessary to completely fluidise the soil bed. On closing the valve the soil settled to produce a very loose bed with an average specific volume of 2.02. Medium to very dense beds were produced by prolonged vibration of initially loose beds. The vibration was applied by the calibrated vibrating table described in section 4.3.2. Prolonged vibration was required to ensure uniform soil beds were produced. This was a result of the densifying process.

Vibration of a very loose bed caused the entire bed to fluidise. Soil particles then resedimented in the higher energy environment. Resedimentation started at the base of the column and moved upwards. If the vibration was stopped before the resedimentation reached the surface of the bed, the material still in suspension settled to produce a very loose surface layer. The degree to which a soil bed densified depended upon the energy level of the vibrating table. The greater the eccentricity of the vibrating table arm, the more dense the bed produced. The time required to fully densify a bed also increased with the energy level. The calibration that was derived for the vibrating table is shown in Figure 4.4. This gives the final bed density for uniform beds against the eccentricity of the vibrating table. It also gives an indication of the time required to form a uniform soil bed.

To summarise, loose to very dense beds were created having selected the soil state required. The calibration shown in Figure 4.4 was then used to give the required eccentricity of the vibrating table, and an indication of the period of vibration necessary to form a uniform soil bed. The density, or state, of beds created by these methods were established as follows.

Initially, the average specific volume of soil beds was determined by adopting the equation;

$$\upsilon = \frac{T \pi r^2}{M} \rho_w G_s \qquad 5.2$$

where G_s= specific gravity of soil grains
ρ_w= density of water (1000 kg m^{-3})

M = mass of dry soil in column (kg)

T = thickness of soil bed (m)

r = internal radius of the sand column (0.094m)

It was found that very loose beds were consistently of a similar density of υ = 2.02. In later tests the density of beds was calculated by assuming the average specific volume of the initial very loose bed was 2.02 and applying the equation;

$$\upsilon = \frac{T_2}{T_1} 2.02 \qquad 5.3$$

where T_1 = thickness of the initial very loose bed (m)

T_2 = thickness of the test bed after prolonged vibration (m)

5.2.5 Sand column test

The principal objective of testing was to monitor the generation, distribution and dissipation of excess pore pressures within soil beds as a result of various forms of perturbation. This was achieved by using the monitoring system described in section 4.4 in conjunction with an appropriate software program (refer section B.2 of Appendix B). The duration of a sand column test varied depending upon the nature of the test, the soil profile and the state of the soils forming the profile. A test started with the beginning of the data logging program, and was considered to be complete, either when the program finished its recording sequence (typically 500 seconds), or when excess pore pressures had fully dissipated, whichever was the longer.

A typical test procedure was as follows; for the first thirty seconds the system was left static. At this point the soil was loaded by the application of a static water head or by one of the model instruments at the base of the sand column. Once the loading was completed the apparatus was left untouched until the end of the test. Throughout each test the thickness of the soil bed was observed through the side of the perspex cylinder and recorded. If the dissipation of excess pore pressures was not complete at the end of the logging operation, the test logging program was re-run or a continuous logging program was used to establish the end of dissipation.

5.2.6 Post-test calibration

The monitoring system was recalibrated after each sand column test. The procedure adopted was the same as that described above for pre-test calibration. The results of this calibration were compared with those of the initial calibration to assess any changes in the characteristics of the system during a test.

5.2.7 Dismantling the apparatus

The instrumentation and the model instrument (if applicable) were generally dismantled at the end of each series of tests or at the end of a days testing. Both were examined to assess any damage and to check the seal between the instrument and the driving rod.

5.2.8 Analysis of recorded data

On completion of a test, the recorded data was analyzed using the appropriate software program (refer section B.3 of Appendix B). This converted the digital output of the instrumentation into tabulated excess pore pressure values. An example of this output is shown in Figure B.8. The plotting programs (refer section B.4 of Appendix B) enabled the test data to be presented in graphical form against axes of excess pore pressure and time. An example of this form of output is shown in Figure B.11.

5.3 Tests to study the mechanics of liquefaction

In Chapter 2 it was suggested that liquefaction is controlled by the generation and dissipation of excess pore pressures. In order to understand and observe these mechanisms a number of sand column tests were carried out. In the majority of cases, liquefaction results from the generation of high excess pore pressures at the base of a soil profile. The tests described in this section are based upon modelling this process. The excess pressures were created either by applying a static water head or by shearing soil in a wet of critical state with a vane.

The tests are presented in three groups. The first group were conducted to examine factors that control the distribution and dissipation of excess pore pressures within uniform soil profiles. Tests included in the second group were designed to assess the effect of a surcharge load or higher effective stress levels upon the excess pressure generated and their dissipation. Finally, the third group consisted of a single test carried out to examine whether the same mechanisms act within layered soil profiles.

5.3.1 Distribution and dissipation of excess pore pressures within a uniform soil profile

Three suites of sand column tests were carried out to establish the factors which control excess pore pressure behaviour within a uniform soil profile. These are described in this section, and their details summarised in Table 5.2.

If large positive excess pore pressures are generated at depth, several factors will influence the subsequent redistribution of the excess pressures. These include the nature and state of the soil, the duration of the excess pore pressure generation and the magnitude of the excess pore pressures created. To study three of these factors, the static head apparatus was used in conjunction with the sand column to simulate the generation of excess pore pressures at the base of a soil profile.

The procedures outlined in section 5.2 were adopted for each test. A static water head was applied to the base of a soil bed thirty seconds after the start of the test. Tests A, D, F, I, L and O were conducted by E. Dwyer (1986). No observation of surface settlement were made in these tests.

Four tests were carried out to examine the effect of excess pore pressure magnitude, tests F, I, L and 42. Tests were performed with similar, very loose soil beds, with an average specific volume of 2.02. In each case the static water head was applied for a period of three seconds. The magnitude of the static head (expressed as a hydraulic gradient upwards through the test bed) varied from 0.25 to 1.5.

To simulate various periods of excess pressure generation the time for which the static head valve remained open was varied. Three tests were performed, A, 42 and D. In each case the soil bed was very loose (average specific volume 2.02) and the static head applied was equivalent to a hydraulic gradient of one.

Tests 0, 42, 43 and 44 were carried out to study the influence of soil state upon excess pore pressure generation and dissipation. For each test a static head equivalent to a hydraulic gradient of one was applied for a period of three seconds. The state of the beds (expressed as an average specific volume) ranged from 2.02 to 1.65.

5.3.2 Effective stress level

The majority of sand column tests were preformed with excess pore pressures generated at the base of soil beds (typically 700mm to 1000mm thick). The effective stress level at the base of these beds was therefore similar in each case. Three sand column tests (180, 181 and 186) were carried out to assess the influence of increased effective stress levels upon excess pore pressure response. Details of the tests are summarised in Table 5.3. In each case a dead load was applied to the surface of a very loose bed using the apparatus described in section 4.3.4. In tests 180 and 181, excess pore pressures were generated at the base of the bed by a 90° rotation of the 1:1 ratio piezovane (pore pressures were monitored on the blade edge). In test 186, excess pressures were created by shock loading. This was done by striking the base of the sand column manually with a steel edge.

The procedure adopted for each test was generally as that outlined in section 5.2. Five miniature pore pressure transducers were used in each test. Four were positioned in the soil bed and the fifth sealed into the piezovane. This required the driving rod and the instrumentation tubes to pass through the surcharge disc. The piezovane was then cleaned and flushed with water. Following this, the instrument was filled with water before being attached to the driving rod. These components were assembled inside the sand column and underwater.

Following pre-test calibrations, the piezovane was placed with its tip 116mm above the basal filter of the sand column and the instrumentation was positioned to monitor excess pressures throughout the proposed test bed. At this stage the surcharge disc was suspended directly beneath the lower guiding gantry. A very loose bed was then formed around the instrumentation and the piezovane.

Once the bed was formed and its thickness noted, the surcharge disc was lowered gently onto its surface. The two PVC silos were then lowered into the sand column on opposite sides of the guiding gantry. These were filled with water until they just touched the surcharge disc as shown in Figure 5.2. Lead shot was then added simultaneously to both silos at a slow rate. This continued until each of the silos contained 12 kg of lead shot (submerged weight 204 N), producing a surcharge load equivalent to 7.4 kN m^{-2}. The thickness of the bed was again recorded. Throughout the preparation period, disturbance of the soil bed was kept to a minimum. The generation of excess pore pressures caused by applying the surcharge load or other disturbances was monitored during this period using the continuous logging program CONLOG (refer section B.1 of Appendix B). Excess pore pressures generated by the gradual application of the surcharge load were limited to 0.2kPa at any location in the soil bed, ie. the loading was effectively a drained event.

During test 180, the surcharge disc appeared to lock against the sides of the sand column. This was due to fluidised sand passing between the disc and the wall of the column. In an attempt to prevent this the disc was modified before tests 181 and 186. The modification consisted of a strip of geofabric glued to the edge of the disc. This was designed to fill the gap thereby preventing sand particles passing the disc, but without stopping water flow or creating significant friction between the disc and the column. This last point was considered relevant since any friction would allow the surcharge load to be carried partially or wholly by the column and not be applied to the soil beneath.

5.3.3 Distribution and dissipation of excess pore pressures within a layered soil profile

A single sand column test was performed to study the generation and dissipation of excess pore pressures within a layered soil profile. The profile which was modelled consisted of a thick deposit of very loose sand beneath a thin clay layer and a further surface layer of very loose sand as shown in Figure 5.3. Excess pressures were created at the base of the profile by a 90° rotation of the 1:1 ratio piezovane. The test procedure was similar to that outlined in section 5.2, except preparation of the soil bed, which is described below.

Before pre-test calibrations were performed, a quantity of sand was removed from the sand column. The soil remaining in the apparatus was sufficient to form a very loose bed approximately 700mm thick. The piezovane was then assembled and pre-test calibrations carried out in a similar way to that described in section 5.3.2. The piezovane and the instrumentation were next positioned as shown in Figure 5.3.

The thick basal layer of very loose sand was formed in the normal way. This produced a bed 700.5mm thick. The impermeable layer was created by pumping a clay slurry on top of the basal sand. The slurry consisted of ground London Clay (passing 0.425mm sieve) mixed at a moisture content of 200%. This was allowed to sediment and consolidate under its own weight for a period of six hours forming a layer 12mm thick. Finally, the surface layer of very loose sand was formed by pluvation. This layer was formed at a very slow rate to avoid disturbance of the clay layer. The final average thickness of the surface layer was 105.5mm. The formation of this layer caused additional consolidation of the clay layer, with a final thickness of 11mm observed through the perspex sides of the sand column.

Twenty seconds after the test started, the excess pore pressures were generated by rotating the piezovane at the base of the profile. Throughout the test observations of surface settlement, settlement of the top of the thick basal sand layer and other movements within the profile were noted.

5.4 Vane and piezovane tests

Five suites of tests were performed with either vanes or piezovanes. The instruments and associated apparatus are described in sections 4.5.4 and 4.5.5. The tests were carried out for two reasons. Firstly to determine whether a vane is capable of distinguishing soil states. This was achieved by determining the excess pore pressure response of the adjacent soil when loaded in various initial states (section 5.4.2). The second objective was to establish which factors influence the observed excess pressures. Four factors were studied; the rate of vane rotation (section 5.4.1), vane geometry (section 5.4.3), the disturbance due to driving a vane into a soil bed (section 5.4.4), and finally the location of the point of pore pressure measurement or filter position on a piezovane (section 5.4.5).

The procedure adopted for each test was that outlined in section 5.2. Deviations from this are described in the appropriate sections. With the exception of the tests detailed in section 5.4.4, soil beds were created around the model instrument. The soil was loaded during a test by the manual rotation of the vane or piezovane.

5.4.1 Vane rotation rate

Five tests were conducted to examine the relationship between the rate of vane rotation and the measured pore pressure response. Details of these tests are set out in Table 5.4. Each test was carried out with the 1:1 ratio vane positioned at the base of very loose beds (average specific volume 2.02). The relationship was examined by repeating the test at various rates of rotation. These ranged from a 90° rotation in 0.5 seconds ($180°s^{-1}$) to a 90° rotation in 69 seconds ($1.3°s^{-1}$).

5.4.2 Soil state

The relationship between soil state and excess pore pressure for a vane was studied by performing a suite of seven tests with soil beds at various states. Table 5.5 shows the details of the tests. Each test was carried out with the 1:1 ratio vane. This was rotated through 90° at the base of the bed over a period of approximately 4 seconds ($22.5°s^{-1}$).

5.4.3 Vane geometry

The effect of vane geometry was studied indirectly by comparing the soil state - excess pore pressure relationship of three different vanes. The instruments are described in section 4.5.3 and had height to diameter ratios of 2:1, 1:1 and 1:2. The dimensions of the blades were such that the volume of soil within the cylinder defined by the rotating vane was similar for each instrument.

Three suites of tests were carried out, one with each vane geometry. All tests were conducted with the instrument tip 100mm above the basal filter of the sand column, and with a 90° vane rotation over 4 seconds ($22.5°s^{-1}$). Within a suite of tests the only variable was soil state. The tests performed with the 1:1 ratio vane are described in section 5.4.2 above, and summarised in Table 5.5. Details of the remaining tests are set out in Table 5.6

5.4.4 Vane rotation after driving into a soil bed

The effect of driving a vane into a soil bed upon the excess pore pressure response measured during subsequent rotation was studied indirectly. This was achieved by performing a series of tests in which the 1:1 ratio vane was driven into soil beds and subsequently rotated. The excess pore pressures generated by driving the vane were allowed to dissipate fully before it was rotated. Tests were carried out at various soil states. This enabled the soil state - excess pore pressure response relationship to be defined for both vane driving and vane rotation. The effect of driving the instrument may be studied by comparing the second of these relationships with that derived from the tests described in section 5.4.2. In these tests the soil beds were created around the vane and it may therefore be assumed that there was no effect due to driving the vane into the soil.

Tests were conducted in two stages. Each stage was recorded as a separate sand column test. Details of the tests are summarised in Tables 5.7 and 5.8. Before performing the first stage, the apparatus was assembled and calibrated as described in section 5.2. The soil bed was then formed with the vane suspended above the proposed soil level. During the first stage, the instrument was driven into the bed at a rate of approximately 20mm/second, initially entering the bed at an elapsed time of 30 seconds. It came to rest with its tip approximately 100mm above the basal filter of the sand column. For the remainder of the test stage observations of surface settlement were noted. At the end of this stage the vane and instrumentation were left in position.

The second stage started once the excess pore pressures generated in the first stage had dissipated or when the logging sequence of the first stage was complete, whichever was the longer. No adjustments or recalibrations of the apparatus were made between the two stages. Thirty seconds into the second stage the vane was rotated through 90° over a period of 4 seconds ($22.5°s^{-1}$). Observations of surface settlement were made for the remainder of the second stage. Following completion of this stage, post-test calibrations were performed, the apparatus dismantled and test data analyzed as described in section 5.2.

5.4.5 Piezovane filter position

These tests were carried out to establish the influence of filter position upon the excess pore pressures measured by a piezovane in a soil typical of those associated with liquefaction. This was achieved by comparing the soil state - excess pore pressure relationship for two different filter positions, one on the shaft of the vane and the other on the edge of a vane blade. The 1:1 ratio piezovane used in these tests is described in section 4.5.3.

Details of the sand column tests performed with the two piezovanes are summarised in Table 5.9. Variations from the general test procedure were as follows. Five miniature pore pressure transducers were used in each test. Four were positioned in the soil bed and the fifth sealed into the piezovane. Before a test, the model instrument was cleaned and flushed with water to remove any air bubbles. The water filled piezovane was then attached to the driving rod under water. This operation was carried out inside the sand column. Pre-test calibrations were performed with each of the five transducers in the normal way ie. including the transducer sealed into the piezovane. Soil beds were created around the piezovane with its tip 316mm above the basal filter of the sand column.

Thirty seconds after the start of a test the piezovane was rotated through 90° over 4 seconds (22.5°s^{-1}). Immediately after a test and the completion of post-test calibrations, the instrument was inspected to determine whether the point of pore pressure measurement had become blocked by either sand or an air bubble. If this occurred the piezovane was dismantled and cleaned, and the test repeated.

5.5 Expanding membrane tests

The expanding membrane probe and the associated pressure system are described in sections 4.5.5 and 4.5.6. Two suites of tests were performed with this instrument. The first of these was designed to establish the relationship between membrane pressure and soil excess pore pressure response. The second suite were carried out to determine whether an expanding membrane probe with pore pressure measurement is capable of distinguishing soil states, and in particular its ability to differentiate between dry and wet soil states.

The procedure adopted for each test was based upon that outlined in section 5.2. For expanding membrane probe tests this involved assembling the instrument as shown in Figure 4.12 before attaching it to the driving rod inside the sand column. In each case the soil bed was created around the instrument, with its tip 100mm above the basal filter of the sand column. The pressure to be applied to the membrane was generated in the pressure chamber prior to a test using the air pump. This was done with the valve to the probe closed. Once the required pressure was achieved the valve to the pump was closed, sealing the pressure chamber. The pump was then switched off for the remainder of the test. Thirty seconds into a test, the valve to the probe was opened and left open for the rest of the test. This resulted in a pressure being applied to the membrane and the adjacent soil. Observations of the probe/chamber pressure were made throughout a test. At the end of a test, the pressure in the probe was reduced to zero before dismantling and inspecting the probe to assess any damage, in particular to the membrane.

5.5.1 Membrane pressure

Five tests were conducted to establish the relationship between soil state and the excess pore pressure response of the adjacent soil when loaded. Test details are summarised in Table 5.10. In each case the test was performed in very loose soil beds with the model probe near to the base of a soil bed approximately 800mm thick. Initial chamber pressures ranged from 13.8kPa to 55.2kPa.

5.5.2 Soil state

Table 5.11 presents the details of the five tests carried out to study the relationship between soil state and excess pore pressure response for an expanding membrane probe. A standardised initial chamber pressure of 34.5kPa was adopted throughout the tests. This pressure was selected after performing the tests described in section 5.5.1. The average specific volume of the soil beds involved in the tests ranged from 2.02 to 1.71.

5.6 Cone and piezocone tests

Four sets of tests were performed with these model instruments which are described in section 4.5.1. Section 4.5.2 presents details of the associated cone driving apparatus. As with the other model instruments, tests were performed for two reasons, firstly to determine whether a cone is capable of distinguishing soil states wet of critical from those dry of critical. This was achieved by determining the soil state - excess pore pressure responses relationship for a cone driven into a soil (section 5.6.2). Secondly tests were carried out to study the factors which govern the excess pore pressures observed when a cone is driven into a soil profile. The following three factors were considered; penetration rate (section 5.6.1), cone geometry (section 5.6.3) and piezocone filter position (section 5.6.4).

The test procedure adopted for each test was similar to that outlined in section 5.2. Deviations from, and additions to, this are described in the appropriate sections that follow. In all cases soil beds were formed with the cone suspended above the proposed test bed. Testing involved monitoring the excess pore pressures generated as the cone or piezocone was driven into the soil bed.

5.6.1 Cone penetration rate

Three sets of tests were performed to examine the effect of penetration rate upon observed excess pore pressure response. All the tests were carried out with the 60° cone. The first set were performed in very loose soil beds, with the instrument driven into the bed at various rates ranging from 2mm/seconds to 300mm/seconds. The second set of tests were similar, except that the beds were in a medium dense state. The final set consisted of two tests, tests 69 and 70, in which the cone was driven into very loose beds in a sequence of 200mm stages. In test 69 the excess pore pressures created by one stage of penetration were allowed to dissipate fully before the next stage. In the other, test 70, excess pore pressures were allowed to dissipate to half their peak value before the next stage of penetration. Details of all the tests are summarised in Table 5.12.

5.6.2 Soil state

The relationship between soil state and excess pore pressure response for a cone was determined by performing a suite of seven tests. These were carried out with soil beds in various states. In each test, the 60° cone was driven into the bed at a constant rate of approximately 20mm/seconds. Details of individual tests are set out in Table 5.13.

5.6.3 Cone geometry

The influence of cone geometry was studied indirectly by comparing the soil state - excess pore pressure relationship of three different cones. The cones had tip angles of 30°, 60° and 90°. The relationship was determined for each cone by performing a suite of tests in which the instrument was driven into beds in various soil states. A standard rate of penetration of approximately 20mm/seconds was adopted for all tests. The tests carried out with the 60° cone are described in a previous section (section 5.6.2) and summarised in Table 5.13. Details of the remaining tests performed with the 30° and 90° cones are summarised in Table 5.14.

5.6.4 Piezocone filter position

Tests were carried out to study the effect of the filter position upon the excess pore pressures recorded when a simple 60° piezocone is driven into a soil bed. This was achieved by comparing the soil state - excess pore pressure relationship for three different filter positions. These were on the face, the shoulder and the shaft (position 2) of the piezocone shown in Figure 4.8. Summary details of the individual tests are presented in Table 5.15.

When a piezocone is driven into a soil profile the pore pressure measured by the model instrument is a combination of two factors. Firstly, a change in static head, and secondly, the excess pore pressures generated by the loading of the surrounding soil. In order to study the excess pore pressure response of the soil, it is necessary to subtract the component due to the change in static head. This requires the elevation of the instrument relative to the appropriate water table to be known throughout a test. In the sand column this was achieved by using the winch potentiometer apparatus described in section 4.5.2. During a test, the electrical output of the potentiometer was logged and recorded simultaneously with that of the pore pressure transducers by the computer program PEN2. The programs PEN3.1 and PEN4 enabled this test data to be analyzed and plotted. These programs are described in detail in Appendix B.

Five miniature pore pressure transducers were used in each of the tests. Four of these were positioned within the soil bed and the fifth was sealed into the piezocone. Before a test the model instrument was cleaned and flushed with water. It was then filled with water and attached to the driving rod. This was carried out inside the sand column and underwater. Pre-test calibrations were performed for each transducer and the winch potentiometer. Test beds were formed with the instrument suspended 850mm above the basal filter of the sand column. This position was used as a datum for the subsequent vertical movement of the model piezocone that took place during a test. In other respects the tests within each suite were similar to those described in section 5.6.2. Following a test and completion of post-test calibrations, the piezocone was examined to ensure the point of pore pressure measurement had not become blocked by either sand or an air bubble. If this had occurred the instrument would have been dismantled and cleaned, and the test repeated.

CHAPTER 6 RESULTS OF SAND COLUMN TESTS

The results of the sand column tests described in Chapter 5 are presented in this chapter. A discussion of the results is made in Chapter 7. This chapter is divided into four main sections, each of which describes the results of one of the principal types of test carried out. These comprised the tests to study the mechanics of liquefaction and the tests performed with the three types of model instruments (vanes, expanding membrane probe and cones) to assess whether any were able to distinguish liquefiable and non-liquefiable soil profiles. Corresponding sections of Chapter 5 are referred to in this chapter. Table 5.1 summarises the various sand column test that were performed and cross references the appropriate sections of Chapters 5 and 6.

The principal types of data recorded during sand column tests were pore pressures and observations of movements within soil beds made through the perspex side of the sand column. Surface settlements and movements within soil beds were measured using a 0.5mm graduated steel rule, attached to the external face of the sand column. By sighting across the surface of a bed it was possible to measure settlements to an accuracy of greater than 1mm.

For each type of test the results of many individual tests were similar. In order to avoid repetition, both in the presentation of results and subsequent discussion, classes of soil behaviour are defined for each of the four types of test. These are described, with the aid of examples, at the beginning of each of the four sections of the chapter. The results of individual sand column tests are presented in Tables 6.1 to 6.33 by reference to these classes of behaviour.

6.1 Results of tests to study liquefaction

The three groups of tests carried out to examine the mechanics of liquefaction are described in section 5.3. This section presents the results of these tests in six sub-sections. The first four of these give the results of the tests to study the distribution and dissipation of excess pore pressures in uniform soil beds. The first sub-section defines the various classes of soil behaviour observed in these tests. The remaining two sub-sections outline the results of the tests to examine the influence of effective stress level and the mechanics of liquefaction within layered soil profiles.

6.1.1 Classes of response in uniform soil profile tests

Two principal classes of soil behaviour were recorded during these tests. These are defined as Class I and Class II behaviours as follows.

In Class I tests large positive excess pore pressures were generated throughout the soil bed at the moment the static head valve was opened. An example of the excess pore pressures recorded in this type of test is shown in Figure 6.1. Maximum excess pore pressures increased with depth and were similar to initial vertical effective stresses. These remained relatively constant during the period the valve was open. Excess pore pressure decay began when the static head valve was closed. It started at the base of the soil bed and was characterised by a single dissipation curve. This behaviour is described by the following characteristics;

t_1 - start of excess pore pressure generation
$\bar{u}_1, t_2$ - peak excess pore pressure generated
t_3 - start of significant excess pore pressure dissipation
t_4 - full dissipation of excess pore pressure

<u>Characteristics of Class I tests, refer Figure 6.1</u>

In class II tests, as above, large excess pore pressures were generated as the static head valve was opened and were maintained for the period the valve remained open. Figure 6.2 shows an example of the excess pore pressures recorded in a Class II test. Generally the pressures were significantly less than the initial vertical effective stress. Excess pore pressures began to dissipate from throughout the soil bed at the moment the static head valve was closed, ie. excess pore pressure decay was not characterised by a single dissipation curve. This behaviour is described by the following characteristics;

t_1 - start of excess pore pressure generation

$\bar{u}_1, t_2$ - peak excess pore pressure generated

t_3 - start of significant excess pore pressure dissipation

t_4 - full dissipation of excess pore pressure

Characteristics of Class II tests, refer Figure 6.2

6.1.2 Excess pore pressure magnitude

The results of the four tests performed to study the influence of excess pore pressure magnitude are summarised in Table 6.1. Table 5.2 presents the initial conditions for these tests. Observations of surface settlement made during one of the tests, test 42, are shown in Figure 6.3.

6.1.3 Period of excess pore pressure generation

The period of excess pore pressure generation was simulated by varying the time for which a static head was applied to the base of a soil bed. The results of these tests are presented in Table 6.2. Table 5.2 presents the initial conditions for these tests. Figure 6.3 shows the observations of surface settlement made during test 42.

6.1.4 Soil state

Table 6.3 sets out the results of the sand column tests performed to study the influence of soil state upon soil behaviour. Table 5.2 summarises the initial conditions for these tests. Detailed observations of surface settlements recorded during three of the four tests are shown in Figure 6.3.

6.1.5 Effective stress level

Three tests, 180, 181 and 186, were performed with a surface charge load. These are described in section 5.3.2 and the excess pore pressure response recorded in the tests are presented in Figures 6.4, 6.5 and 6.6. The initial conditions in these tests are set out in Table 5.3. During each of these tests large positive excess pore pressures were generated throughout the test bed. Fluidised sand flowed past the surcharge disc as it sank downwards into the bed. A slight initial resistance to vane rotation was noted during tests 180 and 181. This reduced to zero with further vane rotation.

During test 180 the surcharge disc appeared to lock against the sides of the sand column. The settlement of the disc observed during tests 181 and 186 is shown in Figure 6.7. In both cases the end of settlement coincided with a rapid reduction in the excess pore pressures monitored throughout the soil bed. At the close of the tests 181 and 186, the sand which flowed past the surcharge plate settled to form a loose bed of sand on the top of the disc. This was approximately 20mm and 35mm thick in tests 181 and 186 respectively.

6.1.6 Liquefaction behaviour within a layered soil profile

The test described in section 5.3.3 of Chapter 5 lasted approximately 33 minutes. Excess pore pressures were monitored throughout the test by repeating the logging sequence four times in quick succession. These were designated test 182 - 185. The excess pore pressures recorded during the test are shown in Figure 6.8, while observations of settlement are plotted in Figure 6.9.

The 90° rotation of the piezovane, at 20 seconds, was achieved with little resistance. This caused the generation of large positive excess pore pressures within the thick basal layer of very loose sand. These began to dissipate at the end of vane movement, commencing at the base of the layer and being characterised by a single dissipation curve as shown in Figure 6.8. This was associated with settlements within the basal layer, which ceased by approximately 380 seconds. At this point the excess pore pressures throughout the layer stabilised at 0.66kPa. Rotation of the piezovane also created pore pressures within the thin surface layer of sand. These dissipated rapidly to zero by 45 seconds.

Figure 6.10 shows the behaviour of the clay layer observed during the test. Shortly after rotation of the piezovane, (from 30 seconds) free water was observed between the clay layer and the fluidised top of the basal sand layer. At the same time horizontal cracks began to form within the clay layer. This continued for some 25 minutes, with small blocks of clay falling from the clay layer to form slurry on top of the sand layer beneath. During this period the top surface of the clay layer showed a slight settlement of approximately 1mm.

At 26 minutes, a slight perturbation caused upward bulging of the clay layer at one location on the circumference of the sand column. This progressed rapidly, culminating in the rupture of the clay layer. Figures 6.10 and 6.11 show the structure that developed as fluidised sand and clay flowed rapidly, of the order of 10 to 100mm/second, to the surface of the model profile. Similar structures developed at other locations after the initial rupture. The clay layer fractured into blocks separated by clay slurry and fluidised sand. The material flowing through the initial major rupture formed a sand volcano structure at the surface. At the moment the clay layer fractured, a sudden increase in excess pore pressure was recorded within the surface sand layer. This is recorded in Figure 6.8. The flow of fluidised sand and clay continued for approximately 7 minutes and ended as the excess pore pressures throughout the profile dissipated to zero.

6.2 Results of vane and piezovane tests

The results presented below relate to the sand column tests performed with vanes and piezovanes. These are described in section 5.4.

6.2.1 Classes of response in vane and piezovane tests

The results of sand column tests conducted with vanes and piezovanes showed five principal classes of soil behaviour. In a Class I (vane) test large excess pore pressures were generated throughout the test bed, reaching peak values during the first 1 to 2 seconds of vane rotation. These increased with depth reaching maximum values similar to initial vertical effective stresses. An example of this behaviour is shown in Figure 6.12. Dissipation of excess pore pressures started at the end of vane rotation, beginning at the base of the soil bed. This was characterised by a single dissipation curve. This behaviour is described by the following characteristics;

t_1 - start of excess pore pressure generation
$\bar{u}_1, t_2$ - peak excess pore pressure generated
t_3 - start of significant excess pore pressure dissipation
t_4 - full excess pore pressure dissipation

Characteristics of Class I(vane) tests, refer Figure 6.12

Figure 6.13 shows an example of the excess pore pressures recorded in a Class Ia (vane) test. These are similar to that described above with the exception that a second peak of excess pore pressures was recorded at the end of vane rotation. These values were similar in magnitude to the initial peak values. However, the second peak values decayed more rapidly with the result that dissipating excess pore pressures regained the initial dissipation curve as shown in Figure 6.13. This behaviour is described by the characteristics set out below.

Surface settlements observed in Class I and I(a) vane tests were generally large, eg. 5mm to 27mm. Resistance to vane rotation was generally negligible.

t_1 - start of excess pore pressure generation

$\bar{u}_1, t_2$ - peak excess pore pressure generated

t_3 - start of significant excess pore pressure dissipation

t_4 - full dissipation of excess pore pressure

t_5 - start of second period of excess pore pressure generation

$\bar{u}_2, t_6$ - second peak excess pore pressure generated

t_7 - start of significant excess pore pressure dissipation, second peak

$\bar{u}_3, t_8$ - dissipating excess pore pressure rejoins initial dissipation curve

<u>Characteristics of Class Ia(vane) tests, refer Figure 6.13</u>

Test 117 was an example of a Class II (vane) test. The excess pore pressures recorded during this test are shown in Figure 6.14. Positive excess pore pressures were generated throughout the test bed during the period of vane rotation. Peak excess pore pressures increased with depth but were significantly less than initial vertical effective stresses. These began to dissipate throughout the soil bed at the end of vane rotation. This behaviour is described by the characteristics set out below.

Surface settlements recorded in this type of test were generally small eg. 1mm to 2mm, however 21mm was recorded in one test (Test 90). Resistance to vane rotation was generally zero or slight.

t_1 - start of excess pore pressure generation

$\bar{u}_1, t_2$ - peak excess pore pressure generated

t_3 - start of significant excess pore pressure dissipation

t_4 - full dissipation of excess pore pressure

Characteristics of Class II(vane) tests, refer Figure 6.14

An example of the excess pore pressures recorded during a Class III (vane) test is shown in Figure 6.15. Vane rotation resulted in a negligible excess pore pressure response for the period of perturbation. The end of rotation was marked by the rapid generation of small positive excess pore pressures throughout the bed. These then dissipated simultaneously reducing to zero over a short period. This behaviour is described by the characteristics set out below.

Surface settlements observed in Class III (vane) tests were very small (eg. 1mm) or zero. Resistance to vane rotation was recorded as slight to moderate.

t_1 to t_2 - period of vane rotation

t_2 - start of excess pore pressure generation

$\bar{u}_1, t_3$ - peak excess pore pressure generated

t_4 - full dissipation of excess pore pressure

Characteristics of Class III(vane) tests, refer Figure 6.15

Figure 6.16 shows an example of the excess pore pressures recorded during Class IV vane tests. The initial 1 to 2 seconds of vane rotation caused the generation of negative excess pore pressures throughout the bed. During the remaining 2 to 3 seconds of rotation, excess pressures decayed rapidly to zero and maintained this value through further vane movement. At the end of vane rotation, positive excess pressures developed at all levels in the bed. These appear to have increased in magnitude with depth or proximity to the vane, refer to Figure 6.16 and Table 6.5. Rapid dissipation of excess pressures then followed simultaneously throughout the soil bed. This behaviour is described by the characteristics set out below.

Surface settlements recorded in these tests were typically zero. Resistance to vane rotation was generally moderate or large. Occasionally a peak resistance was noted during the initial rotation of the vane, with a reduced resistance to further rotation. In some Class IV tests a small recoil, up to approximately 5° of the vane rotation mechanism, was observed at the end of rotation and on release of the lever arm.

t_1 - start of negative excess pore pressure generation

$\bar{u}_1, t_2$ - peak negative excess pore pressure generated

t_3 - full dissipation of negative excess pore pressure

t_4 - start of positive excess pore pressure generation

$\bar{u}_2, t_5$ - peak positive excess pore pressure generated

t_6 - full dissipation of positive excess pore pressure

Characteristics of Class IV(vane) tests, refer Figure 6.16

The excess pore pressure response shown in Figure 6.17 is an example of that recorded in a Class V (vane) sand column test. Negative excess pore pressures were observed throughout the test bed for the duration of vane rotation. The magnitude of the excess pressures increased with depth, ie. greatest negative excess pore pressures were created close to the vane. At the end of vane rotation the negative excess pressures reduced rapidly to zero before becoming positive. This appeared to coincide with the recoil of the vane control mechanism frequently noted during this class of test. The magnitude of the positive excess pressures increased with depth, but were a fraction of the initial vertical effective stress. These then decayed rapidly to zero. Considerable manual force was usually required to rotate the vane when this class of behaviour was observed. In some cases, it was not possible to attain a full 90° rotation. These tests were categorised as Class Va (vane). The excess pore pressures recorded in Class V (vane) tests are described by the characteristics set out below.

No surface settlements were observed in this class of behaviour. Resistance to vane rotation varied from slight to very large. As in Class IV (vane) tests a peak resistance was sometimes noted during initial rotation of the vane, and a recoil, up to approximately 10° of the vane control mechanism, was occasionally observed at the end of rotation.

t_1 - start of negative excess pore pressure generation

$\bar{u}_1, t_2$ - peak negative excess pore pressure generated

t_3 - dissipating excess pore pressure passes through zero

$\bar{u}_2, t_4$ - peak positive excess pore pressure generated

t_5 - full dissipation of positive excess pore pressure

<u>Characteristics of Class V(vane) tests, refer Figure 6.17</u>

6.2.2 Rate of rotation

The five tests performed to study the effect of vane rotation are described in section 5.4.1. Table 5.4 summarises the initial conditions of these tests. The results of these tests are presented in Table 6.4.

6.2.3 Soil state

The seven tests carried out to determine the effect of soil state upon excess pore pressure response are described in section 5.4.2. The 1:1 ratio vane was used in each test. Table 5.5 summarises the initial conditions of these tests. The results of the tests are set out in Tables 6.5 and 6.6.

6.2.4 Vane geometry

The influence of vane geometry was established by performing tests with vanes of different aspect ratios. A total of seventeen tests were carried out, and these are described in section 5.4.3. Tables 5.5 and 5.6 summarise the initial conditions of these tests. The results of the tests conducted with the 2:1 and 1:2 ratio vanes are summarised in Tables 6.7 and 6.8 respectively. The results of the tests conducted with the 1:1 ratio vane are referred to in section 6.2.3 and presented in Tables 6.5 and 6.6.

6.2.5 Installation disturbance

Section 5.4.4 describes the suite of tests in which the 1:1 ratio vane was driven into the soil beds and then rotated to examine the effect of installation disturbance. Table 5.7 summarises the initial conditions of these tests. The tests were performed in two stages, each stage was designated as a separate test. In the first of these the instrument was driven into a soil bed. The generation and dissipation of excess pore pressures and movements within the soil bed were monitored during this period. The results of these tests showed behaviours similar to those described in section 6.4 for cone and piezocone tests. Figures 6.18 and 6.19 show examples of the excess pore pressures recorded during two of these tests. The results of these tests are therefore classified by the behaviours described in section 6.4.1 for cone tests and not those defined in section 6.2.1 for vane tests. Table 6.9 summarises the results of these tests.

The second stage involved monitoring the soil behaviour associated with vane rotation. These were similar to those described in section 6.2.1. Table 6.10 sets out the results of these tests classified on this basis. Table 5.8 summarises the initial conditions in these tests. In three of the driving stages, tests 112, 114 and 118, only partial penetration of the vane into the soil bed was achieved. Consequently, in the stages that followed, tests 113, 115 and 119, the vane was not rotated at the base of the bed, but close to the surface. The excess pore pressures recorded during these tests were slightly different to those outlined in section 6.2.1. Figures 6.20 and 6.21 show two examples, while Figures 6.15 and 6.17 present the appropriate definitive examples. The results differ in that the excess pore pressures recorded in test 115 and test 113 are similar throughout each soil bed, while the examples referred to in section 6.2.1 show a variation in excess pore pressures with position in the soil bed.

6.2.6 Piezovane filter position

The two series of tests performed to examine the influence of filter position on a 1:1 ratio piezovane are described in section 5.4.5. Table 5.9 summarises the initial conditions in these tests. The results of the tests carried out with pore pressures monitored on the shaft of the vane are summarised in Tables 6.11 and 6.12. Similarly Tables 6.13 and 6.14 present the results of the tests in which pore pressures were measured on the edge of a vane blade.

6.3 Results of expanding membrane probe tests

The results presented below relate to the sand column tests performed with the expanding membrane probe. The tests are described in section 5.5.

6.3.1 Classes of response in expanding membrane probe tests

Three classes of behaviour were defined for the tests performed with this instrument. In a Class I (ex.mem.) test large positive excess pore pressures were generated throughout the soil bed at the moment the air pressure was applied to the membrane. An example of this is shown in Figure 6.22. Peak or maximum excess pressures were recorded within 1 to 2 seconds of the air pressure being applied. These increased linearly with depth and were similar in magnitude to initial vertical effective stresses. Decay of the excess pore pressures started at the base of the soil bed and was characterised by a single dissipation curve. This behaviour is described by the characteristics set out below.

Surface settlements observed in this class of test were typically relatively large eg. 17mm to 23mm.

t_1 - start of excess pore pressure generation
$\bar{u}_1, t_2$ - peak excess pore pressure generated
t_3 - start of significant excess pore pressure dissipation
t_4 - full dissipation of excess pore pressure

Characteristics of Class I(ex. mem.) tests, refer Figure 6.22

Figure 6.23 presents an example of the excess pore pressures recorded during a Class II (ex.mem.) test. Positive excess pressures were generated throughout the test bed at the moment pressure was applied to the membrane. Peak values increased with depth, but were significantly less than initial vertical effective stresses. Excess pressures then dissipated simultaneously from throughout the soil bed ie. decay was not characterised by a single dissipation curve. This behaviour is described by the characteristics set out below.

Surface settlements associated with Class II (ex.mem.) tests were zero or relatively small eg. 1mm.

t_1 - start of excess pore pressure generation

$\bar{u}_1, t_2$ - peak excess pore pressure generated

t_3 - full dissipation of excess pore pressure

Characteristics of Class II(ex. mem.) tests, refer Figure 6.23

In a number of tests no excess pore pressures were recorded when the air pressure was applied to the membrane. This was associated with no movement within the soil bed. Tests of this type are designated as Class III (ex.mem.).

6.3.2 Membrane pressure

Table 6.15 presents the results of the five tests performed to examine the influence of membrane pressure upon soil behaviour, especially excess pore pressure response. These results refer to the sand column tests described in section 5.5.1. Table 5.10 summarises the initial conditions of these tests.

6.3.3 Soil state

Section 5.5.2 describes the five tests conducted to establish the relationship between soil state and soil behaviour, in particular the excess pore pressures generated by an expanding membrane. Table 5.11 summarises the initial conditions in these tests. The results of these tests are set out in Table 6.16.

6.4 Results of cone and piezocone tests

The results carried out with cones and piezocones are presented in this section. Relevant sand column tests are described in section 5.6.

6.4.1 Classes of response in cone and piezocone tests

The results of sand column tests carried out with cones and piezocones fall into one of the following four classes of behaviour. Figures 6.24

and 6.25 show examples of the excess pore pressure response recorded in a Class I (cone) sand column test. This behaviour is described by the characteristics set out below.

Large positive excess pore pressures were generated throughout the bed as the instrument was driven into the soil. The rate at which the excess pore pressures increased was a function of penetration rate. In cases where this was relatively fast, excess pore pressures increased rapidly to a peak value eg. Figure 6.24, test 56 in which the rate of cone penetration was approximately 0.30m s^{-1}. Conversely, where the rate of penetration was relatively slow excess pore pressures increased over a longer period eg. Figure 6.25, test 57 in which the rate of cone penetration was approximately 0.007m s^{-1}. In all cases maximum excess pore pressures were similar to initial vertical effective stresses.

Dissipation of excess pressures began when the instrument came to rest at the base of the soil bed. Dissipation started at the base of the bed and was characterised by a single dissipation curve. The rate of dissipation was a function of penetration rate and soil state, principally the latter. The slower the rate of penetration, the shorter the period of dissipation after the cone came to rest, eg. 480 seconds in test 57 compared with 630 seconds in test 56, Figures 6.25 and 6.24 respectively. Dissipation rate increased with soil density, for example in sand column test 63 (Figure 6.26) peak excess pore pressures decayed to zero in 210 seconds. In this test the average specific volume of the soil bed was 1.85 compared with 2.02 for tests 56 and 57.

t_1 - start of excess pore pressure generation
$\bar{u}_1, t_2$ - peak excess pore pressure generated
t_3 - start of significant excess pore pressure dissipation
t_4 - full dissipation of excess pore pressure

<u>Characteristics of Class I(cone) tests, refer Figures 6.24 and 6.25</u>

Test 63 (Figure 6.26) was an example of a Class Ia (cone) behaviour. This was similar to that described above, with the exception that a sudden drop in the excess pore pressures in the soil bed was recorded at the moment cone penetration stopped. The sudden drop was particularly marked near to the base of the soil bed, ie. close to the cone tip. This behaviour is described by the characteristics set out

below.

The surface settlements observed in Class I (cone) tests ranged from 5mm to 33mm. In Class I(a) (cone) tests surface settlements were generally smaller with a range of 3mm to 15mm observed.

t_1 - start of excess pore pressure generation
$\bar{u}_1, t_2$ - peak excess pore pressure generated
t_3 - start of significant excess pore pressure dissipation
t_4 - full dissipation of excess pore pressure
$\bar{u}_2, t_5$ - rapid reduction of excess pore pressure at end of cone penetration

Characteristics of Class Ia(cone) tests, refer Figure 6.26

In Class II (cone) tests positive excess pore pressures were generated throughout the soil bed as a result of cone penetration. Examples of the excess pore pressures recorded in this type of test are shown in Figures 6.27 and 6.28. As with Class I tests, the rate at which excess pressures increased was a function of penetration rate. Peak excess pore pressures recorded in Class II tests increased with depth, but were significantly less than initial vertical effective stresses. These started to dissipate once cone penetration stopped. This behaviour is described by the characteristics set out below. In some cases (eg. test 67, Figure 6.27) this was less clear because of variations in the penetration rate.

Surface settlements recorded in this class of test were generally zero or small although in test 67 a surface settlement of 10mm was observed.

t_1 - start of excess pore pressure generation
$\bar{u}_1, t_2$ - peak excess pore pressure generated
t_3 - start of significant excess pore pressure dissipation
t_4 - full dissipation of excess pore pressure

Characteristics of Class II(cone) tests, refer Figures 6.27 and 6.28

Test 81 was an example of a Class III (cone) test. The excess pore pressures recorded during this test are shown in Figure 6.29. In this class of test only partial cone penetration was achieved ie. the cone did not reach the base of the soil bed. The excess pore pressures recorded during these tests were complex. Transducers above or close to the final position of the cone tip show an initial negative excess pressure response. The largest negative excess pressures were recorded close to the surface of the soil bed. At these points pore pressures then increased and continued to rise after excess pore pressures became positive. This continued until the cone came to rest. Below the final position of the cone tip, similar positive excess pore pressures were generated throughout the soil bed. These reached peak values at the end of cone penetration. Once the cone came to rest the excess pore pressures generated dissipated rapidly from throughout the bed, reducing to zero in 10 to 15 seconds. This behaviour is described by the characteristics set out below.

Penetration of the cone into the soil in these tests caused a rise in the surface of the soil bed. These movements were typically 1mm or 2mm and are recorded in the tables of this chapter as negative settlements.

t_1 - start of excess pore pressure generation
$\bar{u}_2, t_2$ - peak negative excess pore pressure generated
$\bar{u}_1, t_3$ - peak positive excess pore pressure generated
t_4 - full dissipation of excess pore pressure

<u>Characteristics of Class III(cone) tests, refer Figure 6.29</u>

The excess pore pressures recorded during test 75 are an example of those of a Class IV (cone) test. Figure 6.30 shows these excess pore pressures. As with Class III (cone) tests only partial cone penetration was achieved in these tests. The excess pore pressures recorded were complex and in some aspects similar to those recorded in Class III (cone) tests. Close to the final position of the cone tip negative excess pressures were generated as the instrument penetrated the soil bed. These dissipated to zero at the end of cone penetration. At depth, slight positive excess pore pressures were initially recorded at some points. These changed to slight negative excess pressures reaching maximum values after the end of cone penetration and before dissipating to zero. This behaviour is described by the characteristics set out below.

Surface movements observed in this class of test were generally zero or a 1mm to 2mm rise in bed level.

t_1 - start of excess pore pressure generation
$\bar{u}_1, t_2$ - peak positive excess pore pressure generated
$\bar{u}_2, t_3$ - peak negative excess pore pressure generated
t_4 - full dissipation of excess pore pressure

Characteristics of Class IV(cone) tests, refer Figure 6.30

6.4.2 Rate of cone penetration

The three suites of sand column tests carried out to examine the effect of cone penetration rate are described in section 5.6.1. Table 5.12 summarises the initial conditions in the tests. Results of these tests are summarised in Tables 6.17 to 6.20.

In two of the sand column tests, 69 and 70, the 60° cone was driven into very loose beds in a sequence of four steps, each of 200mm. In test 69 full excess pore pressure dissipation occurred before the next stage of cone penetration. The approximate depths and times of cone penetration in this test were as follows;

Stage of cone penetration	Depth of cone tip (m)	Elapsed time (seconds)
1	0.00 to 0.20	30 to 40
2	0.20 to 0.40	300 to 310
3	0.40 to 0.60	720 to 730
4	0.60 to 0.77	1200 to 1210

Only partial dissipation of excess pore pressures occurred between the stages of cone penetration in test 70 which were as follows;

Stage of cone penetration	Depth of cone tip (m)	Elapsed time (seconds)
1	0.00 to 0.20	30 to 40
2	0.20 to 0.40	100 to 110
3	0.40 to 0.60	210 to 220
4	0.60 to 0.77	370 to 380

Figures 6.31 and 6.32 show the excess pore pressures recorded during these tests. In both cases, Class I (cone) excess pore pressures were recorded for each stage of cone penetration.

6.4.3 Soil state

The seven tests carried out to determine the effect of soil state upon excess pore pressure response are described in section 5.6.2 The results of the tests are summarised in Tables 6.21 and 6.22. Table 5.13 summarises the initial conditions in the tests.

6.4.4. Cone geometry

The effect of cone geometry was examined by performing tests with three cones of different tip angles. These tests are described in section 5.6.3 of Chapter 5. Tables 5.13 and 5.14 summarise the initial conditions in these tests. The results of the tests performed with the 30° and 90° cones are presented in Tables 6.23 and 6.26. The results of the tests carried out with the 60° cone are presented separately in section 6.4.3 and summarised in Tables 6.21 and 6.22.

6.4.5 Piezocone filter position

Section 5.6.4 describes the three suites of tests performed to examine the effects of piezovane filter position upon the soil behaviour recorded, in particular the excess pore pressures recorded. Table 5.15 summarises the initial conditions in these tests. The results of individual tests are summarised in Table 6.27 to 6.33.

The results of several of the tests differ slightly from the definitive examples described in section 6.4.1. Figure 6.33 and 6.34 show two examples. These show a difference between the excess pore pressures recorded within the soil bed and those recorded by the piezocone. In each case the excess pressures recorded by the piezocone failed to dissipate to zero. In some cases these same excess pore pressures were non-zero before entering the soil bed. This is an error since on excess pore pressures could exist in the free water above the soil bed, or within the soil bed once full excess pore pressure dissipation had occurred.

The magnitude of the error ranged from 0.1kPa to 0.5kPa. The principal source of this error appeared to be the potentiometer based mechanism used to determine the vertical position of the cone in the sand column. This equipment is described in section 4.5.2. It was used to establish the change in static water pressure at the tip of the piezocone as it penetrated into the soil bed. These pressures were subtracted from the change in pore pressures measured by the piezocone to give excess pore pressure values. Clearly errors in the calculated position of the piezocone would give inaccurate excess pore pressure data. The main causes of such errors appears to have been slack in the cone driving mechanism, and the poor accuracy of the potentiometer based mechanism. Slack in the cable occurred when partial cone penetration was achieved with the result that the weight of the instrument was supported totally by the soil bed.

The values of excess pore pressure presented in Tables 6.27 to 6.33 for the piezocone tests are those recorded by the monitoring system, ie. no correction has been made for the above errors. Where appropriate values of this error are given as an apparent excess pore pressure in the comment column of each table.

CHAPTER 7 DISCUSSION

The results and observations of the laboratory research carried out by the author are discussed in this chapter. It concentrates upon the mechanics of liquefaction and the ability of in situ instruments to distinguish those soils capable of generating the large positive excess pore pressures necessary for liquefaction failure. The chapter discusses how the research might be used to improve the engineers ability to identify potentially hazardous sites.

The discussion is divided into five parts. The first of these, section 7.1, considers the basic or fundamental behaviour of the soil used in the majority of the tests. The results of conventional laboratory tests are used to derive a simple critical state soil mechanics model by defining the approximate position of the critical state line in stress space. Although this model is not sufficiently well defined for use in quantitative discussion, it is suitable as a conceptual model. As such, it is adopted in subsequent parts of the chapter to explain the various classes of soil behaviour observed. Section 7.1 also includes a discussion of the relationship between drained and undrained soil loading based upon the tests performed with the soil. Particular consideration is given to the generation of excess pore pressures by undrained loading.

Liquefaction is caused by the rapid increase in pore pressure which significantly reduces soil strength and stiffness. In Chapter 3 it is noted that in many cases failure at a particular location appears to result from the dissipation of excess pore pressures generated elsewhere in a soil structure or profile. The mechanics of excess pore pressure dissipation are therefore potentially an important factor in liquefaction failures. Two mechanisms of dissipation have been identified, consolidation and hindered settling (or resedimentation). These are considered in some detail in section 7.2.

The potential of a soil to generate excess pore pressures on rapid loading is a function of soil state, and in particular the position of this state relative to the critical state line. Soil state is defined by both specific volume and effective stress level. For soils typically associated with liquefaction, in situ testing is probably the most appropriate means of establishing soil state. This is because such a method can largely avoid sample disturbance and ensures testing at the correct, in situ, level of effective stress.

An in situ instrument can load soil in one of three basic ways; these are by applying principally shear stress (vanes), largely normal stress (expanding membrane probes), or a combination of shear and normal stresses (cones). The tests that were performed with examples of each of these instruments are discussed in section 7.3. It was established which, if any, of the instruments were able to determine soil state, and in particular, soil state relative to its critical state line. The section closes with a discussion of why a piezovane appears to be the best instrument for achieving these objectives.

Established theory and observations suggest that many factors can influence the excess pore pressures generated by an in situ instrument. These may have a significant effect upon the ability of an instrument to differentiate between soil states wet and dry of critical. Section 7.4 discusses the results of the tests carried out to establish whether specific factors are significant for the soils typically associated with liquefaction. Rate of loading, stress level, instrument geometry, piezo-filter position (ie. point at which pore pressures are monitored), and disturbance due to installation were considered. Other factors are noted and discussed further in Chapter 8.

The final part of the discussion, section 7.5, suggests how the findings of the research might be applied by an engineer when assessing the likelihood of liquefaction at a site. It is appreciated that further research and trials would be required before this could occur and this is considered in Chapter 8.

7.1 Basic soil properties

The soil used in sand column tests was a white fine very uniform very silty quartz sand. As such it was typical of the soils generally associated with liquefaction failure. The basic characteristics of the soil, derived from conventional laboratory testing, are discussed in Appendix A. This concludes that the soil behaviour may be explained by conventional soil mechanics theory, ie. the soil showed no special characteristics.

In this section, the results of drained direct shear tests are used to demonstrate that the behaviour of the soil was consistent with the simple critical state soil mechanics model introduced in Chapter 2. The level of instrumentation and the accuracy of recorded data were limited. This prevented the complete definition of the state boundary surface and the accurate plotting of stress paths for individual tests. However it is possible to use this conceptual model to discuss the results and observations of sand column tests in some detail. This is demonstrated by four examples in the last part of this section.

7.1.1 Dense and loose drained shear behaviours

In section 2.1 the concepts of peak and ultimate or critical soil states are introduced. As discussed in Appendix A these characteristics were observed in the drained direct shear tests performed with the soil. Figures A.2 and A.3 summarise the results of the tests. The stress paths of soil elements in these tests are shown in Figure 7.1. There is a significant scatter in this data and soil states would appear not to achieve a unique critical state line especially against axes of specific volume and effective normal stress. Reasons for this are introduced in section A.5 of Appendix A, and are discussed further in the sections that follow. These do not, however, prevent the results from being discussed further. The critical state angle of friction derived from these tests was 36°.

Relatively loose samples compressed during shearing to achieve a constant volume with continued deformation. At this point soil elements within the shear zone of the sample had reached a critical state. This corresponded with a gradual increase in shear stress which became constant once a critical state had been achieved. Initially dense samples showed a different response. In these tests samples compressed slightly before dilating strongly. Peak strengths were observed in these tests and tended to coincide with maximum rates of dilation. This behaviour corresponds with Taylor's model which states that peak strengths are a result of soil dilation, refer section 2.1.1. In drained direct shear box tests, the dilation of samples depends upon initial relative density and effective normal stresses. These factors combine to define the initial stress state of samples within stress space and therefore their proximity to the critical state line. Critical state soil mechanics theory suggests that the closer relatively dense samples lie to the critical state line, the smaller the ratio of peak and ultimate strengths (ie. the projection of the Hvorslev surface and the critical state line should converge as shown in Figure 2.2c). The results of the tests performed with the soil do not show this tendency, indeed Figure 7.1a suggests the ratio of peak and ultimate strengths increases slightly with effective normal stresses. There are two possible explanations for this recorded result. Firstly, that it is due to the poor quality of the direct shear test data at low effective stresses, and consequently is probably not due to a real soil behaviour. Secondly, if the result is real, it suggests a curved Hvorslev surface at low effective stresses. This possibility is supported by the work of Atkinson and Farrer (1985), and Crabb and Atkinson (1991).

From Figure 2.2 it is noted that samples subjected to similar effective normal stresses should achieve the same critical state under drained loading. Despite the quality of the test observations this would generally appear to have been the case, refer Figures A.2 and A.3.

7.1.2 Wet and dry states

Although the drained shear test data plotted in Figure 7.1a do not accurately define a unique critical state line, two groups of soil behaviour are apparent. One group contains the relatively loose samples which compress towards a critical state, the other, relatively dense samples which dilate strongly before achieving similar ultimate states. The principal reasons that a unique critical state line was not defined by these tests appear to be the non-uniform deformations that occur within direct shear samples and the crude nature of basic measurements, such as the initial state of a sample. However, a critical state line for the soil clearly exists between the two groups of soil behaviour which correspond with the wet and dry states as introduced in section 2.1.3.

In Figure 7.2 a series of undrained shear tests (sand column vane tests 100 to 104) are added to the data plotted in Figure 7.1. In two of the tests (100 and 102) relatively loose soil states generated large positive excess pore pressures as the soil was loaded rapidly. This caused a reduction in effective normal stresses as soil states moved towards the critical state line. In tests 104 and 101 negative excess pore pressures were generated. In these tests, effective normal stresses increased as soil states moved towards the critical state line.

These two different behaviours correspond to that described in section 2.1.3 for the undrained loading of wet and dry soil states respectively. Near zero excess pore pressures were generated in test 103 (refer Figure 6.15 and Table 6.7). The critical state line of the soil should therefore pass through or close to the initial soil state for this test as shown in Figure 7.2.

Although the exact position of the critical state line cannot be defined two points may be noted. Firstly, when the results of drained and undrained tests are plotted in specific volume - effective normal stress space, two groups of data can be identified. These correspond to wet and dry soil states and are separated by the soil's critical state line. Secondly, the geometry of a soil's critical state line is defined by λ when plotted against axes of specific volume and the logarithm of effective normal stress, Figure 7.3. Although λ cannot be defined accurately from these results it is clearly small ($\lambda \simeq 0.02$) since the critical state line is near to horizontal. This indicates an incompressible soil, as would be expected for a sand. Published values of λ for sand are not common. However values may be derived from previous work, eg. Sladen et al (1985) and Been et al (1986). These authors report the results of laboratory triaxial testing, and give an approximate range of λ-values from 0.02 to 0.20 (relatively high fines content in latter case). The value of λ derived from Figure 7.3 is consistent with this range. However it is noted that the axes of Figure 7.3 are different from those adopted for the interpretation of triaxial test data and conventionally used to define λ-values. The axes of Figure 7.3 are specific volume and effective normal stress acting on a surface or thin zone shearing at a critical state. Conversely specific volume and average effective stress are used when examining the results of triaxial tests. This prevents the direct comparison of values derived from the two types of plot, eg. λ-values.

7.1.3 Drained and undrained behaviours

In the previous section, the results of selected tests were used to demonstrate that a simplified critical state soil mechanics model may be defined for the soil used in sand column tests. The approximate position of the critical state line has been defined. This separates wet and dry of critical states and corresponding elements of the state boundary surface, ie. Roscoe and Hvorslev surfaces. The model is used in the remainder of this chapter to discuss the results of tests performed in the sand column.

In this section the results of four laboratory tests carried out by the author are discussed to illustrate how such a model may be used to describe and explain observed soil behaviours. Two of the tests considered were performed with soil elements wet of critical, one subjected to drained loading (drained direct shear, test 23.3) and the other undrained loading (sand column test 100). Similarly, sand column test 109 and drained direct shear test 23.9 are discussed as examples of undrained and drained loading respectively of soil states dry of critical. The effective stress paths followed by soil elements during these tests are shown in Figures 7.4 and 7.5. As noted previously the level of instrumentation used and the accuracy of the data derived from both direct shear and sand column tests were limited. The stress paths shown in these figures are therefore inferred from test results and observations, and are not a result of the direct measurement of total stresses (loads) and pore pressures.

The stress path of a relatively loose soil element in a drained direct shear test (Figure 7.1) would be A'B' in Figure 7.4. Normal stresses remain relatively constant throughout the test and shearing results in a gradual increase in shear stress and compression of the sample. This behaviour corresponds with that of a soil element wet of critical subjected to drained direct shear as described in section 2.1.3. Stress path A'B' therefore represents drained shearing as the soil element crosses the Roscoe surface. The sample appears to achieve a critical state at B' but this does not lie on the critical state line shown in Figure 7.1. It is suggested in section 7.1.2 that this was due principally to non-uniform deformations within the sample and the poor accuracy of test measurements, in particular the initial state of the sample. Only soil elements within the central deformation zone of a sample will achieve a critical state. The volume changes of these elements will be greater than the average values inferred from measurements at the boundary of a sample. The stress path of these elements would therefore be A'C' in Figure 7.4 where C' lies on the critical state line.

The stress path represented by E'F'G' in Figure 7.5 is that of a soil element in sand column test 100 which was performed with a vane (refer sections 5.4.3 and 6.2.4). Figure 7.6a shows the idealised excess pore pressure response for the test. The rotational loading applied during the test was relatively rapid, and may, at this stage be considered to be undrained, ie. the specific volume remained constant. Vane rotation results in the sudden generation of large positive excess pore pressures which are approximately 95% of the initial vertical effective stresses. The large magnitude of the positive excess pore pressures in this and similar tests is discussed in greater detail in section 7.4.1. The resistance to rotation and therefore the shear stresses acting adjacent to the vane were described as zero (Table 6.7). In reality small shear stresses will have been achieved as the stress path intersects the Roscoe surface at F' before traversing the surface (F'G' in Figure 7.5). The effective stresses acting within these soil elements reduce significantly from E' to G' as excess pore pressures increase.

The processes occurring during the four seconds of vane rotation were very rapid. Close examination of the excess pore pressures recorded suggests that excess pressures increased suddenly during the first two seconds of rotation and remained relatively constant during the remaining two seconds of shearing. At this point, G', the soil appears to have been shearing at a constant shear stress with constant pore pressures. A critical state would therefore appear to have been achieved at G'. This behaviour is consistent with that described in section 2.1.3 for undrained shearing of a wet of critical soil element. The remainder of the excess pore pressure response recorded in Test 100, G'H'I' in Figure 7.6a, corresponds to the period after vane rotation. Initially, excess pore pressures remain stable before dissipating to zero. This behaviour is considered in detail by section 7.2.2.

The effective stress path followed by a soil element in drained direct shear test 23.9 corresponds to J'K'L' in Figure 7.4. Prior to loading the soil is at J' under an initial effective stress, which remain relatively constant during the test, and zero shear stress. As the test sample is loaded shear stresses increase. After a small initial compression (J'K') the sample dilates strongly (K'L'). The point of maximum rate of dilation coincides with a peak shear strength, at K' on the Hvorslev surface. With further shearing the sample continues to dilate while shear stresses reduce, along K'L' in Figure 7.4. It is noted in section 7.1.1 that this behaviour corresponds with Taylor's model. At L' the sample is shearing at a constant shear stress. It would therefore appear to have achieved a critical state at this point. However, Figure 7.1 suggests this is not the case. As noted previously, the reasons for this discrepancy include the non-uniform nature of deformations imposed by a direct shear apparatus. Deformations are concentrated within a central zone of a sample. Average changes of specific volume calculated from measured movements at the sample boundary are therefore underestimates of that which occurred in the zone of shearing. Correcting the stress path for this effect would give the stress path J'M'N', where N' lies on the critical state line.

Sand column test 109 was a typical example of a rapid vane test performed with the soil in an initially dry of critical state. Figure 7.6b shows the idealised excess pore pressure response recorded during the test (Figure 6.17 shows the recorded excess pore pressure response and Table 6.8 summarises the observations made). Undrained loading in this type of test would produce the stress path P'Q'O' in Figure 7.5. Small positive excess pore pressures would be expected during the initial part of the loading (P'Q') before the stress path intersects the Hvorslev surface at Q' and the soil generates the large negative excess pore pressures necessary to achieve the critical state line at O'. However the stress path followed by soil elements in this and similar tests appears not to have been a straightforward undrained path. There is evidence to suggest that local drainage took place as the vane was rotated, resulting in some degree of volume change and excess pore pressure dissipation during loading. For example, a peak resistance to rotation was noted, and this was followed by a reduction in the negative excess pore pressures during the latter stages of vane movement. Local drainage will have resulted in an increased specific volume adjacent to the vane (ie. soil dilation) during loading. The effective stress path followed in test 109 would appear to have been P'Q'R' with peak shearing resistance coinciding with maximum negative excess pore pressures at R', on or close to the critical state line. The small positive excess pore pressures that would be anticipated during initial loading (corresponding to P'Q' in Figure 7.5) were not observed in test results. In the latter stages of vane rotation negative excess pore pressures dissipated. This is followed by a period of positive excess pore pressure generation and dissipation which is recorded after the end of vane rotation (S'T' in Figures 7.5 and 7.6b). It is suggested that these positive excess pore pressures are associated with the flow of free water away from the zone of soil loading. The free water exists as a result of the dilation that took place during vane rotation.

In section 2.1.3 of Chapter 2 the terms wet and dry of critical soil states are introduced. The theoretical relationship between drained and undrained loading of samples on either side of the critical state line is considered. This predicts that soil initially wet of critical will compress and expel water under drained loading. Undrained shearing of the same soil state generates positive excess pore pressure as the soil attempts to compress. Conversely drained shear loading of soil dry of critical causes dilation as the soil approaches the critical state line. A similar soil element subjected to undrained shear will generate negative excess pressures as it attempts to dilate. Drained tests and rapid, effectively undrained tests carried out with the soil are consistent with this theoretical relationship. Tests 23.3 and 100 were performed with the soil initially wet of critical. Drained loading (test 23.3) resulted in compression to achieve a critical state while undrained loading (test 100) generated large positive excess pore pressures. Tests conducted with the soil in an initially dry of critical state were 23.9 and 109. Drained loading in test 23.9 caused strong dilation while negative excess pore pressures were generated by rapid loading with a vane in test 109.

It is concluded that the soil showed a normal behaviour, and despite the poor quality of some of the test data, it is possible to define a basic critical state soil mechanics model for the soil. This relatively simple state boundary surface has been used to examine four different soil behaviours. These confirmed the relationship between drained and undrained loading of similar soil elements as derived from the theory introduced in Chapter 2.

7.2 Dissipation of excess pore pressures

It was suggested in Chapter 3 that liquefaction failure may result from the redistribution of excess pore pressures within a soil profile. The delay between the disturbance and observations of failure in many case histories suggests this is commonly the case. It is therefore important to understand the mechanics of excess pore pressure redistribution or dissipation from the point of generation. This was studied in the laboratory by monitoring pore pressure changes within sand column tests. Excess pore pressures were generated by soil perturbation or the application of a steady state water pressure at the base of model soil profiles.

Two potential mechanisms of excess pore pressure dissipation are identified in Chapter 2 (section 2.4): consolidation and hindered settling. Sand column test results demonstrate that both these mechanisms can act to control excess pore pressure redistribution within soil profiles. Hindered settling or resedimentation takes place when the excess pore pressures generated within a bed are equivalent to initial vertical effective stresses, ie. when effective stresses reduce to zero. When the excess pressures are less than this value dissipation occurs by consolidation.

Sand column tests were initially performed with simple uniform beds of the soil. A limited number of tests were also carried out with layered soil profiles to confirm that similar mechanisms act within layered profiles. The two mechanisms are discussed in detail in this section.

7.2.1 Consolidation

Sand column tests imposed essentially one-dimensional pore pressure movements with drainage from the top of the soil profile only. If excess pore pressure dissipation in any sand column test was by consolidation it should conform with the one-dimensional theory attributed to Terzaghi and outlined in section 2.4.1.

Redistribution of excess pore pressure by consolidation occurred in a number of different types of sand column tests. Examples include test 95 (Class IV, vane), 99 (Class Va, vane), 117 (Class II, vane) and 136 (Class II, expanding membrane probe). Figures 7.7 and 7.8 show the excess pore pressure dissipation recorded in two of these tests in the form of isochrones. The form of these plots is similar to that of a conventional one-dimensional consolidation test performed in an oedometer. This indicates that consolidation may be the mechanism of dissipation in these cases. It is confirmed by plotting test results against the axes of average degree of consolidation and the square root of time. Average degree of consolidation is normally derived from measurements of sample or soil bed thickness. This was not possible in sand column testing since no significant changes in bed thickness were observed. Average degree of consolidation values were therefore estimated from the ratio of areas enclosed by initial and subsequent isochrones. Figure 7.9 shows the results of three of the above tests plotted in this form. Figure 7.10 shows the same data plotted against linear time to demonstrate that results do not equally fit an alternative, linear mechanism. In Figure 7.9 the majority of the data for each test lies on a straight line, confirming the data is consistent with the Terzaghi model of one-dimensional consolidation.

Having identified that excess pore pressure dissipation is modelled by Terzaghi one-dimensional consolidation in these and other tests it is possible to determine values of the coefficient of consolidation (c_v) by adopting the theory introduced in Chapter 2 (section 2.4.1). Values calculated from Figure 7.9 range from $0.01m^2s^{-1}$ to $0.04m^2s^{-1}$ or $315x10^3m^2$ $year^{-1}$ to $1260x10^3m^2$ $year^{-1}$ respectively. Published values of the coefficient of consolidation for sand are uncommon. However these values may be compared with those for clays. Cherrill (1990) quotes a range of values for Kaolin, of the order of $1m^2$ $year^{-1}$ to $10m^2$ $year^{-1}$. The relatively large values derived for the soil used in sand column tests indicates rapid consolidation which is what would be anticipated for a fine silty sand.

7.2.2 Hindered settling

In tests such as test 42 (Class I), 56 (Class I, cone), 100 (Class I, vane) and 132 (Class I, expanding membrane probe) excess pore pressure dissipation did not appear to have occurred by consolidation. These tests are characterised by high excess pore pressures, relatively large settlements and movement between adjacent soil particles. Figure 7.11 plots surface settlements with time for each of the above tests. These appear to be linear with time. Isochrones of excess pore pressure for two of these tests are shown in Figures 7.12 and 7.13. It can be confirmed that excess pressures were not modelled by Terzaghi one-dimensional consolidation in these tests by plotting the average degree of consolidation against the square root of time. Figure 7.14 shows such a plot for these tests. In this case, unlike in section 7.2.1, it was possible to derive values of the average degree of consolidation from changes in bed thickness. If consolidation were the controlling mechanism in these tests the data plotted in this way would lie on straight lines. Figure 7.14 demonstrates this is not the case.

An alternative simple model for the dissipation of excess pore pressures in these tests is provided by Darcy's Law. For excess pore pressures to dissipate, an associated volume of pore water flows from the point of generation to a free surface. This model may be used to describe a column of soil moving downwards through a volume of free water generated at the base of the soil bed. The permeability of the soil in a loose state was 0.28×10^{-3}m s^{-1} (Table A.2) and the hydraulic gradient generated in these tests was approximately 1.0. The rate of relative pore water flow through soil beds would therefore have been 0.28mm s^{-1}. This compares with recorded rates of surface settlements of 0.04mm s^{-1} to 0.06mm s^{-1} derived from Figure 7.11. The difference in these values, together with the observations of soil behaviour described below suggests that, in these tests, this was not the mechanism of excess pore pressure dissipation.

During the period of excess pore pressure dissipation the soil bed was observed to divide into two layers; a lower solid layer and an upper fluidised layer. The interface between the layers progressed upwards at a relatively uniform rate from the base of the column. It started at the moment of soil perturbation and ceased when the interface reached the surface of the soil bed. No movement of soil particles was observed below the interface but above this level particles moved relative to each other and generally downwards. Rates of surface settlement derived from the typical tests shown in Figure 7.11 were 0.04mm s^{-1} to 0.06mm s^{-1}.

Yoshimi (1977) and Seed et al (1975) have attempted to describe this behaviour by adopting modified consolidation theory, refer section 3.2.5. However, Yoshimi (1977) noted that it was necessary to vary parameters significantly with effective stress levels accurately to model observed behaviour. This, together with the fact that during similar tests performed in the sand column the upper parts of the soil bed were seen to be in a fluidised state suggesting that the approach of adopting consolidation theory is inappropriate. However, observations and measurements made during sand column tests and those reported by Yoshimi (1977) are consistent with the theory presented in section 2.4.2 for the sedimentation of a heavy suspension. This mechanism is referred to in applied physics and hydraulics as hindered settling (Graf,1984). The process is basically one of resedimentation of soil particles at the base of a fluidised layer as water flows upwards from the zone of soil perturbation.

The theory is based upon modifications to Stokes Law for a single solid sphere falling vertically through a fluid. Graf (1984) presented the various corrections to the settling velocity derived from Stokes Law, refer section 2.4.2 of Chapter 2. By substituting appropriate values for the parameters in the equations for these corrections it may be demonstrated that in sand column tests, only the concentration of the soil particle/water fluid has a significant effect upon the average settling velocity of particles in a suspension.

Reynolds number (R_e) for a soil particle settling through a fluid is given by equation 7.1, and as discussed in section 2.4.2 this should be less than one for Stokes Law to hold.

$$R_e = \frac{\rho \, 2a \, v_s}{\mu} \qquad 7.1$$

(after Graf, 1984)

Taking typical values of a (particle radius, from $D_{50} = 0.08 \times 10^{-3}$m), μ (dynamic viscosity, 1.308×10^{-3} kg $m^{-1}s^{-1}$ at 10°C) and v_s (terminal settling velocity of a single sphere, approximately 1.1×10^{-3}m s^{-1} derived from equation 2.6 and Figure 7.11) then Reynolds number is 0.07. This is significantly less than one, hence Stokes Law may be used to describe the hindered settling of soil particles.

Table 7.1 presents values of theoretical settling velocity for a single sphere and corresponding hindered settling velocities for the soil used in the sand column. Values are shown for two particle sizes, D_{10} and D_{50}, derived from Figures A.1. These give hindered settling velocities of 0.06mm s^{-1} and 0.24mm s^{-1} respectively, and may be compared with observed surface settlements of 0.04mm s^{-1} to 0.06mm s^{-1} (Figure 7.11). Calculated values of hindered settling velocity derived for D_{10} are similar to those observed in testing. This result is not entirely surprising since Hazen (1892, refer Atkinson and Bransby, 1978) demonstrated that D_{10} can be considered a characteristic particle size for soil permeability, ie. the relative movement of water and soil.

7.2.3 Dissipation within a layered soil profile

A single, full scale sand column test (test 182-185) was performed to establish whether the mechanisms of consolidation and hindered settling also act within layered soil profiles. The test is described in section 5.3.3 and results are reported in section 6.1.6. The number of such tests was limited for two principal reasons. Firstly, the test was designed to confirm that excess pore pressures dissipated by processes similar to those observed in uniform beds. It was therefore not necessary to duplicate all of the tests performed previously. Secondly, the formation of impermeable layers from a clay slurry took some time and resulted in contamination of the sand used for testing. A large number of tests would have required excavation and refilling the sand column which would have been both cumbersome and time consuming. Small scale tests were carried out in a large glass beaker. These showed similar features, with a layer of free water beneath an impermeable layer and the formation of sand boil structures where this layer was weak.

During test 182-185 excess pore pressure dissipation within the basal sand layer was recorded on three occasions as shown in Figure 6.8. In two cases this appears to have occurred as hindered settling (20 to 400 second and 1540 to 2000 seconds). Figures 7.15 and 7.16 show isochrone plots of excess pore pressure for these periods. Figure 6.9 shows the surface settlement observed at the top of the basal sand layer for the initial period of dissipation. Movements of this interface were not recorded during the period from 1540 to 2000 seconds due to fluidised sand boiling through the ruptured clay layer. During both these periods maximum excess pore pressures increased with depth and were equivalent to the initial vertical effective stresses. The rate of settlement derived from Figure 6.9 was 0.04mm s^{-1} which is similar to the observed and calculated values for hindered settling discussed in the previous section. The form and rate of change of isochrones shown in Figures 7.15 and 7.16 are also similar to those described in section 7.2.2. These are characterised by vertical isochrones of excess pore pressure in the basal layer, inferring a distinct boundary between resedimented soil and a concentrated suspension above. This was associated with a relatively long period of excess pore pressure dissipation and large settlements within the basal layer.

In the introduction to section 7.2 it is suggested that dissipation by consolidation occurs when maximum excess pore pressures are less than initial vertical effective stresses. It is not clear whether this occurred during the third period of excess pore pressure dissipation recorded between 1475 and 1540 seconds. During this period, dissipation was rapid and no surface settlements were observed which is consistent with the behaviour described in section 7.2.1. However, it is unclear from Figure 7.17 whether the isochrones indicate dissipation by hindered settling or consolidation. This period of dissipation appears to be on the boundary between the two behaviours, with relatively large excess pressures redistributing rapidly and associated with very small or zero movements.

Although relatively few periods of excess pore pressure dissipation were monitored in sand column tests with layered soil profiles, these appear to confirm that excess pressures redistribute by the same mechanisms observed in uniform soil beds, ie. where excess pore pressures are less than initial vertical effective stresses consolidation occurs whilst in the remaining cases hindered settling takes place.

Several disturbances were required to cause the rupture of the impermeable layer in test 182-185. However, small scale testing demonstrated that where thin clay layers existed, rupture can occur some time after a single disturbance. This form of delayed failure took place after settlements within a basal layer of loose sand and the accumulation of free water beneath the overlying impermeable layer. It was accompanied by the progressive collapse of the clay layer from the base ultimately resulting in the rupture of the layer. Settlement within the basal layer, accumulation of free water and the progressive collapse of the impermeable layer were also observed in test 182-185. Rupture of the clay layer in this test may eventually have occurred without a second disturbance.

The principal factors controlling rupture would appear to be the thickness and stiffness of the clay layer, the thickness of the layer of free water, the rate of collapse of the clay layer and the permeability of the clay. Where the clay layer is thin and the layer of free water relatively thick, it is suggested that rupture will take place if progressive collapse occurs more rapidly than the flow of the free water through the clay layer. Clearly if shear stresses are acting within the soil profile these may significantly influence the behaviour.

7.3 Generation of excess pore pressures by in situ instruments

The excess pore pressures recorded in sand column tests with model instruments are discussed in this section. This is done by comparing recorded excess pore pressures with theoretical values from ideal undrained tests derived from the simple critical state soil mechanics model discussed in section 7.1. Three soil states are considered for each instrument: wet of critical, beneath the critical state line, and dry of critical. The discussion is used to assess which if any of the instruments is able to determine soil state, in particular to distinguish states wet and dry of critical.

The sand column tests produced a number of types of excess pore pressure response associated with a variety of soil behaviours. These are described in the previous chapter by defining various classes of soil behaviour performed with each type of instrument. Figures 7.18 to 7.20 are based upon the results presented in Chapter 6 and plot recorded excess pore pressures against elapsed time for each of the class of response defined. In Figures 7.21 to 7.23 characteristic excess pore pressures for individual tests are plotted against specific volume. These demonstrate that the classes of behaviour described in Chapter 6 are not isolated but form a spectrum of responses for each instrument type.

The discussion in this section is based upon assumed, simplified total and effective stress paths, as shown in Figures 7.24 to 7.26. These are derived from the excess pore pressures recorded in sand column tests and an understanding of the stresses applied by in situ instruments. Although the loading applied in tests was relatively rapid there is some evidence of local drainage during tests. In particular, local drainage would appear to be a major factor controlling the pore pressures recorded during Class I tests. This, and other factors, namely instrument geometry, piezofilter position, disturbance due to driving, and rate of loading are discussed in section 7.4.

In most tests the soil was loaded by a model instrument at the base of a soil bed. The specific volumes quoted in Chapter 5 and 6 are average values for the soil beds. A correction was therefore necessary to enable the specific volume adjacent to the instrument to be discussed. Figure 7.28 shows the method of correction that was adopted and summarises how it was derived from tests conducted to study variations in soil bed density with depth (section D.2 of Appendix D).

7.3.1 Instruments loading soil initially wet of critical

Assumed, simplified total and effective undrained stress paths of soil elements initially wet of critical and loaded by the three types of instruments are shown in Figure 7.24. With the exception of the vane, similar Class I excess pore pressure responses were recorded with each instrument. Class I and II (vane) behaviours were recorded in vane tests, the difference between these behaviours is discussed in section 7.4.1. At this stage it is noted that large positive excess pore pressures were recorded in all types of test. These were similar to initial vertical effective stresses in Class I tests, and significantly less than these values in Class II (vane) tests, refer section 6.2.1. Examples of the tests carried out in soil states wet of critical include tests 91 and 95 (vane), test 65 (cone) and test 132 (expanding membrane probe). At the start of all tests, total stresses are at A and effective stresses at A' in Figure 7.24. These are separated by the steady state water pressure (u_o).

Referring to Figure 7.24, the simplified total stress paths of the three instruments are AV (vane, predominantly shear stress), AC (cone, shear stress with a significant component of normal stress) and AE (expanding membrane probe, similar components of shear and normal stresses). In this discussion the effective stress paths are considered to be undrained. Since each test starts from the same initial effective stress (A'), a critical state must be reached at B' irrespective of the total stress path applied by an instrument. Figure 7.24 shows the theoretical excess pore pressures generated in the soil adjacent to each instrument. In all cases effective stresses are similar at the critical state (ie. at B'), the steady state water pressure is constant, and large positive excess pressures are generated. This agrees with the data recorded in sand column tests, and which is summarised in Figures 7.18 to 7.23.

Theoretically, the magnitude of excess pore pressures generated should vary between each instrument. This is because A', B' and u_o are constant while the total stress paths vary. The excess pore pressures generated at the critical state (B') must therefore vary. Examples of this behaviour can be seen by comparing the results of specific tests and referring to Figures 7.21 to 7.23. Consider the excess pore pressures generated at a specific volume of 1.82. Test results show a vane would generate excess pore pressures equivalent to 40% of initial vertical effective stresses (Class II) while cones and expanding membrane probes create excess pressures equivalent to initial vertical effective stresses (Class I). Although there is no difference between the cone and expanding membrane responses there is a clear distinction between these responses and that of the vane. This agrees with the theory presented in Chapter 2 and shown in Figure 7.24. The lack of a difference between the excess pore pressure response recorded in Class I tests, predicted in Chapter 2 and Figure 7.24, is discussed in detail in section 7.4.1. At this stage it is simply noted that the change from Class I to II responses occurs at different specific volumes for each type of instrument.

7.3.2 Instruments loading soil initially beneath the critical state line

Figure 7.25 shows the undrained total and effective stress paths for soil states initially directly beneath the critical state line and loaded by the various instruments. Examples of corresponding sand column tests are test 103 (vane, Class III), test 65 (cone, Class I) and test 133 (expanding membrane probe, Class II).

Before loading, soil elements adjacent to the various model instruments are at similar initial states; A (total stress) and A' (effective stress), separated by the steady state water pressure u_o. Undrained loading by any of the instruments must result in the critical state line being reached at B'. The effective stress path would therefore be A'B', and the total stress paths as shown in the figure. Anticipated excess pressures generated by the various instruments would be those shown on Figure 7.25.

It is assumed that the total stress path of a vane is vertical in shear stress - normal stress space. A' lies directly beneath the critical state line therefore no excess pore pressures should be generated by the total stress path AV (B'V equals A'A). Test 103 is an example of a Class III vane response (specific volume adjacent to the vane = 1.78). This appears to confirm the predicted behaviour with only very small positive excess pore pressures recorded during the period of vane rotation. Tables 5.6 and 6.7 present the details of this test.

In contrast, the arguments summarised in Figure 7.25 suggest that the loading applied by an expanding membrane or a cone would generate significant positive excess pore pressures, ie. B'E >> A'A and B'C > AA' respectively. The undrained stress paths shown in Figure 7.25 suggest that the expanding membrane probe would create the largest excess pressures. This is due to the greater component of normal stress in its stress path. However, test results show similar high positive excess pore pressures for both types of instrument. It is suggested that this is probably due to one or a combination of two factors. The pressures exerted by the membrane may not have been sufficient to achieve the critical state line, or some local drainage occurred during loading. There is evidence of local drainage in other tests despite the relatively rapid rate of loading. This is discussed further in section 7.4.1.

7.3.3 Instruments loading soils initially dry of critical

Figures 7.18 to 7.23 demonstrate that a wide range of excess pore pressure responses were recorded in tests where initially dry of critical soil was loaded. Class IV and V behaviours were recorded in vane tests, Classes I to IV in cone tests and Class II in expanding membrane probe tests.

In Figure 7.26, as in the previous sections, undrained loading by total stress paths AV, AC and AE results in the critical state line being achieved at B'. The other stress paths shown in this figure (WZ and X'Y') are not considered here but are discussed later in this section. With respect to effective stress path A'B' the soil will attempt to dilate as it approaches the critical state line with effective stress states traversing the Hvorslev surface. The excess pore pressures generated by each instrument as soil states reach the critical state line are shown in Figure 7.26.

For a vane the excess pore pressures generated should be negative in all cases, since if the total stress path (AV) is vertical B'V < A'A. The magnitude of the excess pressures generated by a vane should vary with the proximity of the initial effective stress state (A') to the critical state line, ie. for a given normal effective stress level or depth, excess pore pressures generated will vary with specific volume. Sand column test results confirm this behaviour; progressively larger negative excess pressures were generated with reducing specific volume through class IV, V and Va vane responses. Examples include test 95 (Class IV, vane), test 97 (Class V, vane) and test 98 (Class Va, vane). Theoretically this increase in negative excess pore pressures should be associated with an increase in the shear stress required to achieve the critical state line. Qualitative observations made during sand column tests confirm that the manual force required to rotate the vane increased with reduced specific volume through Class IV and V (vane) tests, to the point that insufficient force was available in Class Va (vane) tests. These observations and further details of the above tests are summarised in sections 5.4.2 and 6.2.3.

Total and effective stress paths of an expanding membrane probe loading initially dry of critical soil are shown in Figure 7.26. In this case, positive excess pressures are generated. These are a function of several factors including the maximum stresses the probe can apply, and the relative orientations of the critical state line and the total stress path applied to the adjacent soil. From Figure 7.26 it can be seen that negative excess pore pressures can only be generated if the critical state line and total stress paths converge, ie. B'E < A'A. Figures 7.19 and 7.22 demonstrate that positive excess pressures were generated in all the sand column tests performed with dry of critical soil. Examples include tests 133 and 134, both of which recorded Class II (ex. mem.) pore pressure responses. Table 6.16 presents further details of these and similar tests. Tests therefore appear to agree with the theory summarised by Figure 7.26. Further, since no negative excess pore pressures were recorded, it is suggested that the total stress path applied by the expanding probe was either parallel or diverged from the critical state line in shear stress-normal stress space. The stresses applied by the probe may not be sufficient to achieve the critical state line in all cases, in particular at small specific volumes where B'E is potentially very large. However, this would not change the sign of the excess pore pressures generated, simply the magnitude.

The total stress path of a cone might suggest a behaviour intermediate between that of a vane and an expanding membrane. However, sand column test results indicate a complex excess pore pressure response. As with the other types of instrument the excess pressures generated are a function of several factors. These include the available driving force, and the relative orientation of the total stress path applied by a cone and the critical state line of the soil. The latter point can be discussed by considering the undrained stress paths of two soil elements, A' and X' in Figure 7.26. The initial stresses on these elements are similar, but the specific volume of element X' is larger than that of A' and it is therefore closer to the critical state line. In the case of the effective stress path A'B' (total stress path AC) negative excess pore pressures are generated to achieve the critical state line at B', since B'C < A'A. However, in the case of effective stress path X'Y' (total stress path WZ) positive excess pressures are created because Y'Z > X'W. From this argument it would appear that a cone can generate positive, zero or negative excess pore pressures when loading dry of critical soil states. Figures 7.20 and 7.23 show that the sand column tests performed with cones confirm this argument. Large positive excess pore pressures were generated in Class I (cone) tests, eg. test 56 (Figure 6.24). Smaller positive excess pressures were recorded in Class II (cone) tests, eg. test 88 (Figure 6.28). Small negative excess pore pressures were recorded at the start of Class III (cone) tests increasing to large negative excess pore pressures throughout Class IV (cone) tests. Examples include test 81 (Figure 6.29) and test 75 (Figure 6.30) respectively. Although a zero excess pressure response was not recorded during any cone tests, a test of this type is theoretically possible and would be intermediate between Class II and III (cone) responses.

The partial cone penetration achieved in Class III and IV (cone) tests confirms that insufficient force was available to maintain penetration into the soil bed. As a result the critical state line was probably not achieved in these tests. The penetration achieved with the available force decreased with reduced specific volume. This is a result of the increased distance between the initial state, A', and the critical state line at B'. Driving forces were insufficient to achieve the critical state line during undrained loading, with large negative excess pore pressures generated. These then dissipated, thereby reducing effective stress levels enabling further slow cone penetration. This behaviour is discussed further in section 7.4.1.

7.3.4 Selection of a piezovane

Each of the instruments is able to distinguish soil states by the excess pore pressures generated which vary with specific volume. This is illustrated by Figures 7.21 to 7.23. In Chapter 2 it is suggested that liquefaction results from the large positive excess pore pressures generated by the shearing of wet of critical soil states. The most appropriate method of assessing liquefaction would therefore be that which is able to distinguish wet and dry soil states.

On the basis of the discussion in this section, only a piezovane shows a clear change in the excess pore pressures generated at the critical specific volume with a change from positive (wet of critical) to negative (dry of critical) values. This is a result of the orientation of the total stress path applied by a vane, ie. vertical or near vertical in stress space. Cones are capable of generating positive excess pore pressures in all wet, and a range of dry, soil states. Expanding membrane probes generate positive excess pore pressures in all soil states. Cones and expanding membrane probes are therefore less able to distinguish soil states relative to the critical state line. Again this is a consequence of the total stress applied by these instruments, ie. they contain a significant component of normal stress. Figure 7.27 summarises the results of the sand column tests performed with all three types of instrument. This enables a direct comparison of the excess pore pressures generated by each instrument. It confirms that a piezovane appears to be the best in situ method of distinguishing soil states relative to a soils critical state line.

This section has discussed the excess pore pressure generation and soil behaviours associated with three instruments by considering their undrained stress paths. In the introduction it is noted that other factors influence the excess pressures generated and might therefore alter the selection of a piezovane. These factors are discussed in detail in section 7.4. It is noted that although these factors influence the magnitude of the excess pore pressures generated they do not appear to influence the sign of the excess pressures. This is based upon the results of the sand column tests performed with a single soil (a fine very uniform very silty sand). Chapter 8 briefly considers the factors that have not been considered in these investigations and points to further areas of research.

7.4 Influence of test conditions on observed soil behaviour

The previous section of this chapter considers the behaviour of the soil when loaded rapidly by one of three instruments. This section discusses the results of tests designed to assess the significance of some of the principal factors associated with in situ testing. Factors considered are the rate of loading, stress level, instrument geometry, filter position, and installation disturbance.

Test results have shown that an expanding membrane probe generates positive excess pore pressures at all soil states. The reasons for this are discussed in section 7.3. Although the excess pore pressures generated by an expanding membrane probe vary with specific volume the lack of a change in sign makes it very difficult to establish accurately the soil state relative to the critical state line. This type of instrument is therefore not considered an appropriate method for investigating the liquefaction of soils. Consequently the tests discussed in this section were carried out with vanes and cones. The exception to this were the tests designed to study the effect of installation disturbance. These were only performed with vanes, not being appropriate for cones.

Each of the factors considered has been shown by previous workers significantly to influence soil behaviour and therefore excess pore pressure response. The work that has been conducted with cones and piezocones was summarised well by Meigh (1987). Unfortunately no similar references exists for in situ vane testing. In both cases the majority of the research that has been done has involved low permeability soils, ie. clays. This section includes a discussion of whether the findings of previous research are also applicable to tests in soils typically associated with liquefaction.

Rate of loading and stress level are discussed by considering idealised stress paths within the simplified critical state model defined in section 7.1. A different approach is used to assess instrument geometry, filter position, and installation disturbance. In these cases the discussion is based upon the comparison of excess pore pressure response on specific volume plots as used in the previous section. It is appreciated that other factors are likely significantly to influence the excess pore pressures monitored by in situ instruments. These would include other soils and alternative, more complex drainage paths. This is discussed further in Chapter 8.

As in the previous section most of the tests considered here involved soil loading by an instrument at the base of a soil bed. The specific volumes quoted in Chapters 5 and 6 are average values for the soil beds. A correction was therefore necessary to enable the specific volume adjacent to the probe to be discussed. Figure 7.28 shows the method of correction that was adopted and summarises how it was derived from tests conducted to study variations in soil bed density with depth (section D.2 of Appendix D).

7.4.1 Rate of loading and partial drainage

The rate at which a soil is loaded is recognised as being important in both field and laboratory tests. Atkinson and Richardson (1987) have demonstrated that local or partial drainage occurs when loading clays at a high rate. The degree of partial drainage is primarily a function of the rate of loading relative to soil permeability. It is suggested that if local drainage was significant in the tests performed by Atkinson and Richardson with a low permeability soil (reconstituted London clay, $k \simeq 1 \times 10^{-10} m\ s^{-1}$) then the rate of loading will be relevant in higher permeability soils such as that used in sand column tests. This is supported by observations made by others, eg. Michell and Dubin (1986).

In order to gain consistent results from tests, standard rates of loading have been proposed. For example the ISSMFE (Meigh,1987) has recommended a standard rate of penetration for cone penetration testing of 20mm s^{-1} with a tolerance of $\pm$ 5mm s^{-1}. Similarly BS1377 (1975) sets a rate of rotation for in situ vane testing in cohesive soils within the range $0.10°s^{-1}$ to $0.20°s^{-1}$ ($6°\ min^{-1}$ to $12°\ min^{-1}$).

Tests were performed in the laboratory to establish the effects of loading rate on excess pore pressure response. These are described in sections 5.4.1 and 5.6.1 with results presented in sections 6.2.2 and 6.4.2 for vanes and cones respectively. Test results are summarised in Figures 7.29 and 7.30 (cone), and 7.31 (vane). The tests were initially performed to establish what rates of loading were required to ensure undrained loading during subsequent test. The rates adopted were approximately 0.06 rev s^{-1} for vanes (ie. a 90° rotation in 4 seconds or $22.5°s^{-1}$) and 20mm s^{-1} for cones. These rates were derived from Figures 7.29 to 7.31 and were initially assumed to be sufficiently rapid to ensure undrained loading and therefore a maximum excess pore pressure response in subsequent tests. However, soil behaviour and excess pore pressures recorded during later tests suggest that local drainage occurred close to model instruments. Examples include tests which recorded a Class IV(vane) excess pore pressure response (section 6.2.1 and Figure 6.16). In these tests, negative excess pore pressures were recorded at the start of vane rotation, before dissipating and remaining close to zero during further rotation. Loading was therefore not undrained.

It is suggested that local drainage occurred during the majority of sand column tests. Soil behaviour was therefore more complex than the simple undrained case presented in Chapter 2 and assumed in previous sections of this chapter. Actual soil behaviour and the discrepancies between this behaviour and that predicted for undrained loading can be examined by considering the stress paths of soil elements loaded by instruments. Two cases are considered below:

Class III and IV cone tests are discussed to demonstrate the effect of local drainage in soil states dry of critical. Local drainage would appear to have a significant effect upon the excess pore pressures observed in soil states wet of critical. This is discussed by referring to behaviours recorded in Class I and II cone tests.

In Class III and IV cone tests (refer section 6.4.1) only partial cone penetration was achieved at the standardised rate. In many of these tests very slow cone penetration was observed for the remainder of the test. During this period zero or near zero excess pore pressures were recorded. Figure 7.32 shows the theoretical undrained total stress path (AC) and the effective stress path (A'B') for a cone. At a rate of penetration of 20mm s^{-1}, negative excess pore pressures were generated as the soil state moved towards the critical state line at B'. In these tests the driving force necessary to achieve B' was not available. When the cone stopped, the adjacent soil was at a state similar to D'. Negative excess pore pressures then dissipated and effective stresses reduced. It is suggested that if effective stresses reduced sufficiently the cone was able to continue penetration into the soil bed. This penetration was very slow and excess pore pressures were zero or near zero indicating that during this period, loading was essentially drained. The soil state would therefore move towards the critical state line at E' with an associated change in specific volume.

Class I excess pore pressure responses were similar for each of the three instruments. Examples are presented in sections 6.2 to 6.4. In each case large positive excess pressures were recorded over a relatively wide range of specific volumes corresponding to very loose and loose soils. The theory for undrained loading presented in Chapter 2 and discussed in section 7.3 predicts large positive excess pore pressures at these specific volumes with the magnitude of excess pore pressure generated reducing with initial specific volume. However, test results show that excess pore pressures were consistently equivalent to the initial vertical effective stress over a wide range of specific volume. Similar behaviours may be inferred from the observations of others, eg. Eckersley (1990) and Sladen et al (1985).

This behaviour appears to result from local drainage adjacent to an instrument. Figure 7.33 shows the suggested stress paths for soil elements adjacent to a cone in a Class I test. The loading of a wet of critical soil element at A' will result in a combination of positive excess pore pressures and a change in volume (compression). The amount of compression is a function of several factors including initial soil state and the rate of loading. Rapid, undrained loading would result in the effective stress path A'B' as discussed in section 7.3.1. Local drainage appears to have occurred during most tests. The critical state line would therefore be achieved at D' and not B', with an associated change in volume and an equivalent volume of free water generated. In Class I tests the volume change appears to be sufficient to fluidise the soil bed above, forming a heavy suspension as the soil particles settle through the volume of free water generated. This process is referred to as hindered settling, and is discussed in section 7.2.2. Excess pore pressures within the fluidised layer are equivalent to the initial vertical effective stress and effective stresses are reduced to zero. Soil elements adjacent to the instrument will therefore show a change in stress state from D' to H' if loading stops as excess pore pressures are generated, or D' to G' if loading continues. In the tests performed in the sand column it was not possible to differentiate between the excess pressures generated by the instrument and those due to the fluidised soil layer above.

Eckersley (1990) described similar mechanisms in model tests where flowslides were induced in instrumented stockpiles by slowly raising the water table. Eckersley was able to separate the components of excess pore pressure, concluding that high excess pore pressures were generated during rather than before movement, and liquefaction was therefore a result of shear failure rather than the cause. Sladen et al (1985) proposed that this mechanism can be described by defining a "collapse surface" in three-dimensional specific volume - shear stress - normal stress space. On the basis of sand column testing it is suggested that this mechanism is controlled by the volume of free water associated with local drainage during loading.

In Class II cone tests a similar soil behaviour appears to have occurred, although the volume change that is associated with the effective stress path A'D' is not sufficient to fluidise the soil bed above. The soil state adjacent to the instrument therefore remains at D' and excess pressures dissipate by the process of consolidation. This mechanism of dissipation is discussed in section 7.2.1.

In summary, the rate of loading applied by an instrument has a significant influence on the excess pore pressures generated, but it will not affect the sign of these excess pore pressures. Maximum positive or negative excess pore pressures are generated during undrained loading. It is suggested that in most sand column tests local drainage occurred adjacent to instruments. It would therefore appear difficult to achieve undrained loading with a piezovane in soils typically associated with liquefaction. A standardised rate(s) of loading would therefore appear to be the most appropriate solution.

7.4.2 Effective stress level

Three sand column tests were performed specifically to study the effect of stress level upon excess pore pressure response. Increased stress levels were achieved by applying a surface surcharge load to very loose soil beds. The tests are described in section 5.3.2 and results presented in section 6.1.5. It is noted in these sections that the tests were only a partial success. This was due to fluidised sand passing between the surcharge disc and the sides of the sand column. The two components became locked together with soil particles transferring the surcharge load from the soil bed to the walls of the sand column. Section 4.3.4 describes the attempts that were made to prevent this behaviour, although these met with only partial success. For this reason a full suite of tests was not performed at different specific volumes.

The results of test 180 are shown in Figure 7.34 which provides a comparison with other vane tests. Although not identical to other results the response was similar, with high positive excess pore pressures generated in soil wet of critical. Close examination of the data suggests that a maximum excess pressure may not have been achieved before the disc and sand column locked. Significant modifications to the surcharge load apparatus or a different system for achieving higher stress levels is needed to produce acceptable results. A simple method of extending the range of vertical effective stresses available would be to build a taller sand column. However, this would have obvious limitations in the laboratory.

Although these tests only provided limited results it is possible to discuss the effects of stress level further. From the theory presented in Chapter 2 it is suggested that soil behaviour at any stress level would be similar to that summarised in Figure 7.35. The testing that was performed showed that the change from positive to negative excess pore pressure is dependent upon the initial soil state and its position relative to the critical state line, ie. wet or dry soil states. Since the critical state of a soil varies with stress level, the change in sign of excess pore pressure would also be expected to alter with stress level. Two examples are shown in Figure 7.35. Although further testing is necessary to confirm these predictions, if they are correct a suitable in situ instrument would be able correctly to distinguish soil state relative to the critical state line. This would enable the correct prediction of soil behaviour including excess pore pressure generation and would therefore be valuable in assessing the risk due to liquefaction.

As a cone penetrates a soil bed it loads soil at increasing stress levels. However, interpretation of this data is difficult because the excess pore pressure response recorded high in a soil bed appears to be dominated by those generated deeper in the profile by further cone penetration. These data have therefore not been considered further in this dissertation.

7.4.3 Instrument geometry

Previous researchers have shown that the geometry of an in situ instrument can be a significant factor, eg. Meigh (1987) discussed the effect of different cone tip geometries. To eliminate this factor in site investigation work a standard cone geometry has been proposed by the ISSMFE (Meigh, 1987). Similarly field vane geometry has become standardised with a 2:1 ratio of blade height to diameter.

The majority of previous work to assess the influence of instrument geometry has been carried out with clays, ie. low permeability soils. Tests were therefore performed to establish whether the cone and vane geometries significantly influence the excess pore pressure response of the soils typically associated with liquefaction. Three cone angles of 30°, 60° and 90°, and three vane height to diameter ratios of 1:2, 1:1 and 2:1 were used. Tests are described in sections 5.4.3 and are reported in sections 6.2.4.

The results of these tests are summarised in Figure 7.34 for vanes and Figure 7.36 for cones. Tests with cones show similar curves indicating identical soil behaviour. This suggests that cone geometry is not a significant factor. Tests with vanes also show similar excess pore pressure responses, again inferring that instrument geometry is not a major factor. The greater scatter in vane test data, especially with negative excess pore pressure responses, is probably due to a number of factors including variations in the manual force applied to achieve vane rotation.

The tests performed in the sand column were relatively simple and they gave consistent results. This suggests that for both vanes and cones instrument geometry is not a significant factor. At first sight this appears to conflict with the results of previous work. However, it is suggested that this is not the case; rather that the relatively high permeability of soils associated with liquefaction, such as the soil used in sand column tests, result in an averaged value of excess pore pressure being recorded due to local drainage. The majority of tests performed by previous researchers have been based upon tests in clays. In these cases the combination of relatively low permeability and rapid loading causes undrained loading. The excess pore pressures recorded therefore vary significantly with instrument geometry and the point of pore pressure measurement.

7.4.4 Filter position

As with instrument geometry, previous workers have demonstrated that the point of pore pressure measurement is significant, eg. in the case of piezocones, De Ruiter (1982) and Meigh (1987). Sand column tests were performed with simple piezocones and piezovanes to establish whether filter position has a significant effect in soils typically associated with liquefaction. The tests are described in sections 5.4.5 and 5.6.4 with results presented in sections 6.2.6 and 6.4.5 for vanes and cones respectively.

Some problems were encountered during testing, in particular with the piezocone. The potentiometer used to measure cone penetration and correct measured excess pore pressures proved to be slightly non-linear. In tests where only partial cone penetration was achieved the cone driving mechanism became slack and consequently the system overestimated cone penetration into the soil bed. These effects produced errors in calculated initial vertical effective stress and generated excess pore pressure values. Limited corrections were made to the data in an attempt to minimise the effects of the errors. Two corrections were applied: where cone penetration was measured directly this was used to calculate initial vertical effective stress values in preference to that inferred by the potentiometer system. In the remaining tests where direct measurements were not made, inaccuracies in the potentiometer output and overestimation of cone penetration resulted in calculated excess pore pressures dissipating to a non-zero value. In these cases maximum excess pore pressure values measured by the probe were corrected by the non-zero value.

Despite the errors, results appear to be similar to those recorded in other tests. Figures 7.37 and 7.38 summarise the results and provide a comparison with the behaviour recorded in similar tests. These indicate that filter position has no significant effect upon the excess pore pressure response measured by a piezovane or piezocone. This would appear to disagree with the behaviour predicted by previous workers (Meigh, 1987) for piezocones and which might be expected to exist in some form for piezovanes. However, as in section 7.4.3, which considers the effect of geometry, it is suggested that this apparent discrepancy results from the relative rate of loading and soil permeability. It is suggested that the relatively high permeability of the soil resulted in local drainage during loading. Consequently an averaged excess pore pressure response was measured at points on the surface of instruments and in the adjacent soil.

Although test data show some scatter, both piezocones and piezovanes consistently show a change from a positive to a negative excess pressure at higher specific volumes than in other tests. The reason for this is not clear. It may be due to the fact that a monitoring position on an instrument is more sensitive to small negative excess pore pressures within a shearing zone. Elsewhere in the soil bed these may be masked by an averaged positive excess pressure response.

7.4.5 Disturbance due to installation

Tests to determine the influence of installation disturbance were only performed with a vane, since this is not appropriate for a cone. This was done by comparing the excess pore pressure response for vane rotation after driving into a soil bed, Figure 7.40, with the responses for tests in which soil beds were prepared around an instrument, Figure 7.34. Excess pore pressures and observed soil behaviour were also recorded during the installation of the vane by driving, Figure 7.39. This response is similar to that recorded during cone tests (refer Figure 7.36) suggesting that the same soil behaviour occurs during both vane and cone driving.

The excess pressures recorded during vane rotation after driving appear to be significantly different from those recorded in tests where soil beds were formed around the vane. In fact at first sight the response seems closer to that recorded during cone tests, refer Figure 7.40. This applies particularly to the point at which the response changes from positive to negative, indicating that driving a vane before rotation has a significant effect upon the ability to distinguish wet and dry soil states. However, the number of tests are limited and only partial vane penetration was achieved in tests 117, 115, 119 and 113. The effect of installation disturbance upon the excess pore pressure response can be explained by considering what happens to soil adjacent to the vane during driving. In soil states wet of critical, compression occurs close to the instrument as a result of local drainage during loading and excess pore pressure dissipation. Subsequent vane rotation therefore occurs in soil denser than its initial state. Consequently smaller positive excess pore pressures would be anticipated. This is not apparent from the test data which suggests that the volume change that occurred during rotation remained sufficient to fluidise the soil bed as discussed in section 7.3.1, ie. tests 111 and 121.

A similar but opposite behaviour would be anticipated in dry of critical soil beds. In this case the volume changes that occur during vane driving result in a loosening of the soil around the instrument. A reduced negative, or possibly a positive, excess pore pressure response would therefore be expected to be generated during vane rotation. This would appear to have been the case in test 117 where positive excess pressures were recorded after driving. In similar tests ie. similar initial soil states, where beds were prepared around the vane, small negative excess pressures were recorded, refer Figure 7.34.

To summarise, the test results presented in Figure 7.40 demonstrates that soil disturbance during vane driving had a significant effect upon its ability to distinguish wet and dry soil states in sand column tests. This observation differs from that made when initially interpreting test results (Atkinson and Jessett, 1990). A significant contribution to the disturbance observed in sand column tests would appear to be due to the geometry of the vane used. This had a relatively large shaft diameter when compared to the dimensions of the blades. It is suggested that further testing may demonstrate that the effect of disturbance can be reduced, for example by changing the geometry of the instrument. This is discussed further in Chapter 8.

7.5 Incorporating a piezovane into a new approach

In Chapter 3 it was argued that a new approach is required for the assessment of liquefaction failure at a site. This section discusses how the findings of the research undertaken by the author could form the basis of a new two stage approach.

The first stage would include a desk study followed by a conventional site investigation designed from the anticipated ground conditions and the proposed development. Boreholes, trial pits and other techniques such as continuous cone penetration testing (CPT) enable the soil profile and water pressures with depth to be established. In situ and laboratory testing confirm soil descriptions and provide geotechnical parameters. These would be used to assess whether any of the soils present in the soil profile are capable of generating the large positive excess pore pressures necessary for liquefaction. At this stage in the investigation the criteria would be based upon physical soil parameters, in particular soil grading and particle size uniformity. If uniform fine granular soils (eg. fine sands) are present, liquefaction would be considered a potential hazard requiring further investigation. If such soils do not exist within the profile then conventional designs could be followed.

Assuming uniform fine granular soils are present then it would be necessary to determine whether these are in a state capable of generating positive excess pore pressures sufficient to cause liquefaction failure. It is argued earlier in this dissertation that large positive excess pressures may only be generated in soils wet of critical. It is also argued that soil state can only be accurately determined with these soils by an in situ method. The results discussed in this chapter demonstrate that this is best achieved by a technique incorporating piezovane testing. Using such a technique it would be possible to determine the extent of any zones of potential large positive excess pore pressure generation within a profile.

Case histories and theory (Chapters 3 and 2 respectively) suggest that it is not sufficient to calculate the effective stresses within these zones and thereby infer the risk of liquefaction, ie. a coincident model of liquefaction. It is also necessary to consider whether failure can result from large positive excess pore pressures redistributing from the zone of generation to another more critical area, ie. a non-coincident model of liquefaction. It is proposed that this is better achieved using an appropriate numerical model rather than physical modelling. This is because although both methods would require detailed soil profile and parameter data, physical modelling would be cumbersome, time consuming and therefore expensive. Conversely, once a numerical model has been created this can be varied readily and the factors controlling the problem better understood. Such a numerical model should incorporate:

a) Comprehensive vertical and lateral soil profile data - provided by the site investigation.

b) A correct excess pore pressure generation model - this is gained by in situ testing with a piezovane which defines zones of potential large positive excess pore pressure within the soil profile.

c) A correct excess pore pressure redistribution model - the research has shown that excess pressures can dissipate by two mechanisms; consolidation and hindered settling. The model should incorporate both these mechanisms and be able to apply whichever is appropriate.

d) Details of changes in load due to the proposed development including foundation loads, earthworks and changes in water table. The importance of incorporating these factors was demonstrated by

Rollins and Seed (1990).

e) An appropriate model of soil failure for each soil present in the profile within the framework of critical state soil mechanics theory. However, this would require extensive laboratory testing to define state boundary surfaces.

To summarise, the research has identified a new in situ method which gives an accurate determination of in situ excess pore pressure generation. It has also identified the mechanisms of excess pore pressure dissipation and when these apply. These provide a new means for assessing the likelihood of liquefaction at a site. How this may be incorporated into a new approach is suggested above. Clearly further development of these and other areas, eg. an appropriate numerical modelling technique and field trials, is required before the approach can be adopted by practising engineers. This is discussed further in Chapter 8.

CHAPTER 8 SUMMARY, CONCLUSIONS AND THE NEED FOR FURTHER WORK

8.1 Summary of the research

8.1.1 Liquefaction

Liquefaction is defined here as a sudden reduction in soil strength and stiffness resulting from a rapid increase in pore pressures. Liquefaction failures occur when the reduction in soil strength or stiffness is sufficient to cause unacceptable soil or structural movements, eg. settlement, rotation, flotation, or lateral displacements. Field observations and numerical modelling have demonstrated that the location of soil failure may be remote from the zone of excess pore pressure generation, section 3.1.4. This form of failure is referred to as a non-coincident model of liquefaction. The term coincident liquefaction is used to describe those cases where soil failure occurs at the point of excess pore pressure generation.

8.1.2 Existing methods

Various theoretical, laboratory and field based approaches have been proposed and adopted in the past and these have been studied, section 3.2. The majority are empirical and fail to consider excess pore pressure redistribution as a potential contributing factor. Because the correct theory is not incorporated into these methods they can be conservative, resulting in uneconomic, or conversely, unsafe design.

The need for a new approach was identified in section 3.3. This should be based upon the controlling factors of excess pore pressure generation and dissipation within real soil profiles or structures. It is suggested that a means of establishing excess pore pressure generation characteristics should be based upon an in situ method for determining soil state relative to its critical state.

Liquefaction failures resulting from rapid single increment soil loading have been discussed in detail by this dissertation. Those caused by cyclic loading have also been considered.

8.1.3 Equipment

The research was laboratory based. A principal component of the equipment was the soil selected. This was described as a white fine very uniform very silty quartz sand (Figure A.1 shows the particle size distribution curve for the soil). As such its physical characteristics were similar to soils typically associated with liquefaction. These included permeability, which was relatively low for a sand. It was relatively easy to prepare test beds of the soil in a wide range of states.

Various new pieces of equipment were developed. These included a rapid method for preparing uniform beds of soil (the sand column) and a computer controlled data logging system. The equipment generally worked well and to an acceptable level of accuracy, refer Appendix C. Computer based data handling enabled rapid logging, together with the analysis and preliminary plotting of a large amount of detailed data.

Models of three types of in situ instrument were constructed. These were vanes, cones and an expanding membrane probe. The models were used to establish which, if any, of the instruments were able to determine in situ soil state relative to the critical state line of a soil, and study the influence of various factors such as geometry and rate of loading. The model instruments were relatively simple, and each proved robust and straightforward to modify.

8.1.4 Critical state model and excess pore pressure generation

Conventional laboratory tests demonstrated that the behaviour of the soil was consistent with modern soil mechanics theory in that the behaviour of the soil, and its strength, depend on the current volume as well as on the current effective stress, section 7.1. A simplified critical state soil model has been defined by the approximate position of the critical state line in stress space. This model has been used to discuss the results of tests, including the relationship between drained direct shear and relatively rapid, effectively undrained soil behaviours. Examples of shear box and sand column tests were used to confirm that the behaviour of the soil was consistent with basic theory. The model has also been used to compare theoretical and observed behaviours, in particular excess pore pressure generation during undrained loading.

8.1.5 Sand column tests

A standardised general test procedure was developed for the large number of tests performed in the sand column, refer section 5.2. The general procedure and deviations from it for specific tests are described. This approach to testing appears to have worked well with reproducible results achieved despite relatively crude equipment and methods.

Many of the tests performed resulted in similar excess pore pressure responses. To avoid unnecessary repetition in description and discussion, results are classified into similar responses for each type of test, sections 6.1.1, 6.2.1, 6.3.1 and 6.4.1. Each class of excess pore pressure response recorded in tests with model in situ instruments has been studied. This was done by considering the simplified stress paths applied by the instruments relative to the basic critical state soil model defined previously, refer section 7.3. Excess pore pressure generation and soil behaviour were consistent with modern soil mechanics theory in each case. The classes of response defined were not isolated but form part of a continuous spectrum of behaviour for each type of instrument. The approach of defining classes of response was adopted only for convenience of presentation and discussion.

8.2 Principal conclusions

8.2.1 Mechanics of liquefaction

Liquefaction is an expression of the principle of effective stress and is not a special soil behaviour. Failure by liquefaction occurs when positive excess pore pressures significantly reduce soil stiffness or strength. Excess pore pressures may be generated at the point at which liquefaction is observed (coincident model), or elsewhere in the soil profile before redistributing to cause failure (non-coincident model).

There is strong evidence to suggest that many liquefaction failures result from excess pore pressure redistribution, section 3.1.4. The mechanisms of redistribution or dissipation are therefore significant. The research has shown that two mechanisms may act; consolidation and hindered settling (resedimentation).

The research indicated that consolidation occurs if the hydraulic gradients generated are less than critical, section 7.2.1. In the sand column tests in which the hydraulic gradients were less than unity the process of excess pore pressure dissipation was consistent with Terzaghi's one-dimensional consolidation theory. This mechanism was associated with small surface settlements, relatively rapid dissipation and no visible movements between adjacent soil particles. A range of values of the coefficient of consolidation for the soil were derived.

The research indicated that hindered settling takes place if a critical hydraulic gradient is created, section 7.2.2. The soil bed fluidises and acts as a heavy suspension with resedimentation at the base to form a new soil bed. This behaviour is associated with large surface settlements, and relative movement between adjacent soil particles visible within the fluidised, upper part of the soil bed. A theory for hindered settling is provided by applied physics. It is based upon Stokes Law with various modifications to settling velocities including one for the concentration of the suspension.

There is evidence of local drainage and therefore volume change during soil loading in many of the sand column tests preformed, section 7.4.1. The associated volume of free water appears to be a significant factor in the hydraulic gradient generated and therefore the subsequent mechanism of excess pressure dissipation.

Hindered settling appears to have been observed and modelled by previous workers. However in many cases they have attempted to describe the mechanism by applying significant modifications to consolidation theory, refer sections 3.2.5 and 3.3. It is suggested that this approach is incorrect. Hindered settling appears to be a possible controlling mechanism in liquefaction failures and should therefore be incorporated, together with consolidation theory (where appropriate), into a correct model.

8.2.2 Best in situ test

On the basis of sand column tests in which soil beds were created around model instruments a piezovane appears to be the best in situ instrument for determining soil state relative to the critical state line, section 7.3.4. This is due to the relatively small changes of normal stresses and the relatively large changes of shear stress applied by the instrument. This results in a clear change from positive to negative excess pore pressures as initial soil states pass from wet to dry of critical. It is less able to determine how far an initial soil state is from the critical state line. At present it is not clear whether this is significant. For example, it may be sufficient to identify which parts of a soil profile are capable of generating large excess pore pressures. The results of sand column tests suggest that this would be all wet of critical soil states. However, there is evidence in the research to indicate that the volume of free water associated with the positive excess pore pressures may also be a relevant factor (section 7.4.1), eg. in controlling the mechanism of excess pore pressure dissipation. The volume of free water that can be generated is proportional to the distance between an initial soil state and the critical state line. The ability to determine quantitively the state of a soil relative to the critical state line may therefore be relevant.

Cones and expanding membrane probes are less able to establish soil state. This is principally a consequence of the relatively large changes of normal stress applied by these instruments.

8.2.3 Factors influencing excess pore pressure generation by model instruments

Previous workers have demonstrated that many factors influence the behaviour of soil adjacent to an in situ instrument. Some of these have been considered to establish whether they significantly affect the ability of the test to determine soil state. This was only done for piezocones and piezovanes, the use of an expanding membrane probe having previously been discounted on the basis of the stress path applied during loading.

Rate of loading can have a significant effect upon the magnitude of the excess pore pressures recorded, section 7.4.1. However, it does not alter the sign of the response, and therefore the ability of an instrument to distinguish soil states. The relatively high permeability of soils associated with liquefaction makes undrained loading to achieve maximum excess pore pressures difficult. It is therefore suggested that a standard rate of loading should be adopted. Local drainage during loading has a major effect upon the excess pressures generated and the subsequent mechanism of redistribution.

Tests at different stress levels were only partially successful, refer section 7.4.2. The results of the most successful test were consistent with established theory. This predicts a similar but displaced excess pore pressure response in stress space, with soil behaviour controlled by the geometry of the critical state line. Although further work is required, stress level is not anticipated to be a significant factor.

Previous research with piezocones suggests that both instrument geometry and piezofilter position significantly affect measured pore pressures. Similar research does not appear to have been carried out with piezovanes. Sand column tests indicate that geometry and filter position are generally not significant factors in the excess pore pressures recorded, sections 7.4.3 and 7.4.4. The explanation for this discrepancy with observations of previous researchers is provided by the permeability of the soils used. The majority of earlier work has been carried out with low permeability soils where local drainage is less significant. In this case the excess pore pressures recorded around instruments vary with geometry and filter position. In higher permeability soils local drainage during loading results in averaged excess pore pressures being recorded around an instrument. It may be concluded that filter position and instrument geometry do not appear to be a major factor when testing soil types typically associated with liquefaction.

Installation disturbance was only considered for vanes. It appears significantly to influence the ability of a piezovane to establish soil state relative to the critical state line, section 7.4.5. The reasons for this can be understood by examining the changes in soil state that occurred during installation. The geometry of the model instruments used is likely to have contributed to this effect. Vanes had a relatively large shaft diameter, especially when compared to the dimensions of the instruments' blades. Ways in which this effect might be minimised are proposed in section 8.3.3.

Of the factors considered, only installation disturbance would appear significantly to affect the ability of a piezovane to determine soil state relative to its critical state line.

8.2.4 Proposed new approach

The findings of the research have been used to propose a new two stage approach for assessing the risk of liquefaction failure at a site, section 7.5. The first stage would include a conventional site investigation to identify the extent and characteristics of the soils present. If uniform, relatively fine grained granular soils are present then liquefaction would be considered a potential hazard requiring the second stage of investigation. If such soils do not exist then a conventional approach to design would be adopted.

The second stage would involve determining the in situ state of these soils and therefore their ability to generate the large positive excess pore pressures necessary for liquefaction. The research has shown that this could be achieved by using a technique incorporating in situ testing with a piezovane. Having identified the zones of positive excess pore pressure generation within a soil profile or structure it would be necessary for the new approach to establish whether these are sufficient to cause failure, at the point of generation (coincident model) or elsewhere in the profile (non-coincident model). Numerical modelling is proposed as the most suitable method of making this assessment, provided it incorporates the correct mechanisms. For example, the two mechanisms of excess pore pressure redistribution identified in the research; consolidation and hindered settling.

8.3 Limitations of present work and recommendations for further work

8.3.1 Limitations of equipment and methods

The principal limitations of the equipment were as follows. The inability to drive cones and vanes to the base of relatively dense soil beds made the comparison of soil behaviour at states dry and wet of critical difficult. However it is noted that if an instrument cannot be driven into a soil bed easily then the soil will be in a dense state. Consequently, it is unlikely that the soil will be able to generate the large positive excess pore pressures necessary for liquefaction.

The tests carried out at increased stress levels were only a partial success due to the poor performance of the surcharge apparatus. Consequently the detailed findings of the research are based upon the results of tests at one stress level. The low level of accuracy of the system used to monitor the penetration of piezovanes and piezocones made it necessary to correct calculated excess pore pressure values derived from tests where these instruments were driven into soil beds.

The geometry of the sand column had two effects, both of which relate to the internal diameter of the column which was relatively small. Any edge effects due to the rigid sand column were ignored in the research. The work of others, eg. Schnaid and Houlsby (1991), suggests that these may have been significant, especially in dense soil beds. Excess pore pressure dissipation within the sand column was essentially one-dimensional. This is not always the case in a soil profile during a potential liquefaction failure or adjacent to an in situ instrument. In these cases drainage and therefore excess pore pressure dissipation is more likely to be two or three-dimensional.

A single soil was used to create uniform beds in the majority of sand column tests. Tests with other soils and more complex soil profiles are needed to confirm the findings of the research. The methods used to define a critical state model for the soil used were basic. Consequently, the model produced was relatively simple, which limited the interpretation and discussion of results.

8.3.2 Limitations of the present piezovane

The research has demonstrated that a piezovane was able to distinguish between soil states wet and dry of critical when beds were created around model instruments. However, installation disturbance would appear to have an effect upon this ability. This is a result of the changes in soil state that occur adjacent to the instrument as it is driven into a soil bed, section 7.4.5. This is particularly relevant in relatively high permeability soil because significant local drainage can take place during loading. It has been noted that the ratio of vane blade to shaft diameter was relatively large and that this would be expected to cause significant disturbance during installation. Further testing with modified vane geometries will enable this effect to be minimised. Additional alterations that could be considered include; reducing the instruments' shaft diameter, reducing the number of blades, or developing an instrument with retractable blades (partial or complete).

Other limitations, such as difficulty in driving the piezovane into relatively dense beds relate to the associated equipment and not the instrument itself. These have been discussed above.

8.3.3 Recommendations for further work

Recommended further work may be considered under four headings. These are the continued development of the equipment, modifications to the piezovane, the development of the new approach (including field or large scale laboratory testing, and the numerical modelling of excess pore pressure dissipation), and a comparison of rapid single increment loading and cyclic loading cases.

Although the equipment and methods used generally worked well a number of limitations have been noted. Modifications to overcome these would be of value. Of significance would be the ability to drive model instruments into relatively dense as well as loose soil beds and the construction of a larger sand column or testing tank. The use of such a testing chamber would reduce edge effects and enable two and three-dimensional excess pore pressure dissipation to be studied. A more accurate means of monitoring the penetration of model instruments into soil beds would also be of value. Testing at increased stress levels should be included in any further work. This would require the use of a better means of creating higher stress levels. It is recommended that testing is extended to other soils to determine whether the proposed approach is generally applicable.

The principal constraint upon the use of a piezovane would appear to be the disturbance caused during installation of the instrument. Several options have been suggested in the previous section to minimise this effect. Development of the instrument in this way should form an important part of the further work. Tests in which excess pore pressures can dissipate in two and three-dimensions should be performed with the piezovane. This will enable the effect of different drainage paths upon the ability of the instrument to determine soil states to be established. Clearly, as noted in the introduction to this dissertation, field trials would be necessary to achieve a practical in situ method. However, it is noted that considerable practical expertise exists from previous work with piezocones by both commercial and research organisations. It is understood that Fugro McClelland are now able to perform vane tests with their standardised truck mounted penetration equipment. At this stage tests are limited to the more conventional application of determining the undrained shear strength of soft clays and silts.

For the proposed new approach for assessing the risk of liquefaction failure to be viable it will be necessary to develop the analytical method. In particular, a numerical method to enable the correct modelling of excess pore pressure distribution and dissipation within real soil profiles is required. Such a method should enable both simple and complex soil profiles to be modelled. To ensure the method works correctly, it will be necessary to compare observed or recorded behaviour with numerical predictions. Observations might be based upon case histories, although base data from before these events is often limited. It would be more appropriate to use instrumented model tests carried out in a sand column or a centrifuge.

The research presented in this dissertation has concentrated upon liquefaction due to rapid single increment loading. However, many failures have been associated with cyclic loading environments. The mechanisms of soil failure and potential excess pore pressure redistribution are similar in both cases although different loading cases generate the excess pore pressures. The research has confirmed that a principal factor controlling liquefaction is the generation of large positive excess pore pressures and the associated volume of free water created. In the single increment loading case these can only be generated by soils wet of critical. There is some evidence that these may also be created in soils just dry of critical by cyclic loading. This area requires further work. If this is correct an in situ technique will need to establish soil states relative to different limit values (ie. other than critical state values) for various forms of cyclic loading. A similar approach could then be used to assess the potential risk of liquefaction failure by correct modelling of excess pore pressure dissipation and failure mechanisms.

APPENDIX A ROUTINE TESTS TO SELECT A SOIL

The results of the routine soil tests described in this appendix were used to select a soil for subsequent sand column testing. The characteristics required of the soil are defined in section 4.1.

Initially, thirty soils were selected from a variety of natural and industrial sources. Classification tests were used to form a short list of eight uniformly graded fine sands which are listed in Figure A.1. The tests described below were carried out on these eight soils to enable the final selection to be made.

Permeability and density tests were carried out simultaneously to determine the coefficient of permeability and its relationship with soil state for each of the eight soils. Relative density tests were performed with the soil finally selected for sand column tests. This was done to obtain an estimate of its loosest and densest states.

The excess pore pressure response of a soil subjected to rapid loading may be measured directly during undrained testing, or inferred from the results of drained tests. The relationship between the excess pore pressures generated in undrained loading and the volume changes that occur in drained testing is discussed in section 2.1.3. Drained direct shear testing was used in the selection of a suitable soil because sample preparation is straightforward and the test procedure is relatively simple and quick to perform. These were considered relevant factors because of the large number of tests carried out.

To summarise, drained direct shear tests were used to identify a soil that exhibited a tendency to compress when loaded in a loose state and a similar trend to dilate when dense.

A.1 Classification tests

Grading and specific gravity tests were conducted in accordance with BS1377 (1975) Test 7(B) and Test 6(B) respectively. Grain shape was determined by examining each soil under an optical microscope to establish sphericity and roundness. Results of these tests and observations are summarised in Table A.1 and Figure A.1.

A.2 Permeability and density tests

A constant head permeameter was used to establish the permeability of each soil in various states. The unit weight of each sample was also determined in order to relate soil state and permeability. The test procedure adopted was similar to that described by Head (1982). Samples were prepared by the following methods: loose samples were produced by pluvation through water; dense samples were formed by prolonged vibration of loose samples. Vibration was caused by lightly striking the permeameter with a wooden block at all levels and from all directions. Vibration ceased when no further surface settlements were observed. The results of these tests are set out in Table A.2 with density values presented as dry unit weight, bulk unit weight and specific volume.

A.3 Relative density tests

Maximum and minimum density tests were only carried out with soil 23. The procedure used was generally that outlined by ASTM D2049-69 (1969). Deviations from the ASTM method were as follows: a Proctor compaction mould was used in place of the standard mould, dense samples were produced by prolonged shock loading, and no surcharge load was applied during maximum density tests. The minimum density value was determined by both the dry and wet methods, ie. pluvation through air and pluvation through water. The maximum density value was established by shock loading dry and water saturated samples. Table A.3 presents a summary of results for these tests. Maximum and minimum dry densities as defined by the ASTM were 1610kg m^{-3} (specific volume = 1.65) and 1230kg m^{-3} (specific volume = 2.16) respectively.

A.4 Direct shear tests

Eight shear box tests were generally conducted with each soil. Five of these were with relatively loose samples and the remainder with relatively dense samples. The normal stress applied ranged from 5kN m^{-2} to 55kN m^{-2}. The tests were carried out by the author and M. O'Conner (1983).

A.4.1 Equipment

Two Wykeham Farrance 25000 direct shear boxes were used. These were similar in design and operation to those described by Head (1982). Samples were 60mm square and approximately 20mm thick.

A.4.2 Sample preparation

To ensure that consistent loose and dense samples were produced standard preparatation methods were adopted. Samples were formed with the shear box in place on the test rig in order to minimise sample disturbance. Soils were boiled in deaired water before sample preparation to avoid entrapped air.

Loose samples were formed by pluvation through water with care taken to produce a level upper surface. Dense samples were created by tamping each of five layers twenty five times. A steel tamper of square section (19mm by 19mm) and a mass of 1kg was used. The mass of soil forming each sample was recorded. The thickness of a sample was established in the following manner. Before preparing the sample the depth of the split box was measured at each of its four corners. The average for these values was noted as the depth of the box. Once the sample had been formed, the upper perforated plate was carefully lowered on to the soil. Measurements were repeated at each corner of the box. The average of these values plus the thickness of the perforated plate were deducted from the initial depth of the shear box to give an average sample thickness. The normal load was applied to the sample and any settlement noted. These were deducted from the initial thickness of the sample to give the actual thickness at the start of shearing.

A.4.3 Test procedure

Samples were sheared at a constant rate, typically 0.061mm/minute. Horizontal displacements, vertical displacement and shear force were monitored throughout tests. The end of a test occurred when a sample was judged to have achieved an ultimate or critical state (ie. shearing continued at a constant volume under a constant shear stress), or the split box reached the limit of its travel.

A.4.4 Results of direct shear tests

Initially the test data was plotted against axes of shear stress - horizontal displacement and vertical displacement - horizontal displacement. Figure A.2 show these plots for the tests carried out with soil 23. Where appropriate, these were used to define peak and ultimate stress states. Results were summarised by plotting peak and ultimate shear strength against axes of shear stress and effective normal stress for each soil. These plots are shown in Figure A.3a for soil 23.

The tests were performed to assess the compression and dilation characteristics of the soils and in each case establish the influence of the effective stress level and the initial soil state. There are two basic methods of studying this behaviour. The first of these involves plotting the maximum change in specific volume observed during a test against the corresponding effective normal stress. The second method requires the maximum rate of dilation to be plotted against the same horizontal axis. Both of these types of plots are shown in Figure A.3 for soil 23.

A.5 Discussion and soil selected

The initial group of thirty soils was reduced to eight by studying their physical properties. This section discusses the final selection of a soil for sand column testing. The selection was based upon routine laboratory tests.

Soil 23 was selected as fulfilling the requirements stipulated in section 4.1. It was the least permeable, finest and most uniformly graded soil tested and was easily prepared in a wide range of states. Drained direct shear testing demonstrated that soil 23 would exhibit the required undrained behaviour, ie. a strong tendency to generate high positive excess pore pressures when loaded rapidly in a loose state and a similar negative response when dense. Relative density tests confirmed that the soil could be prepared in a wide range of states.

The eight soils tested ranged from a sandy silt (soil 21) to medium sands (soil 24, 25 and 26). Each soil exhibited a uniform grading and consisted principally of quartz grains although soils 6, 11 and 21 contained other minerals, primarily glauconite. Specific gravity values ranged from 2.65 to 2.67 which is typical of predominantly quartz grained soils.

The sphericity and roundness of soil grains varied considerably for each material. In general the natural soils (6, 11 and 21) showed higher values of sphericity, reflecting the high percentage of quartz present. The wider range of sphericity of the remaining soils (23, 24, 25, 26 and 28) was due to the crushing of larger quartz particles during industrial production.

Permeability values varied over a wide range. The results show clearly that this was principally due to two factors, grain size and soil state. Permeability increased with grain size eg. 0.28×10^{-3}m s^{-1} for D_{50} = 0.08mm (soil 23) to 7.9×10^{-3}m s^{-1} for D_{50} = 0.28mm (soil 25). These values may be compared with estimated values for clean sand derived from Hazen's formula. This gives values of 0.02×10^{-3}m s^{-1} and 0.3×10^{-3}m s^{-1} for D_{10} of 0.04mm (soil 23) and 0.18mm (soil 25). Although calculated and measured values are not identical, they are of a similar order of magnitude and exhibit the same trend of increased permeability with larger grain size. The results shown in Table A.2 also demonstrate the relationship of increased permeability with increased specific volume. The permeability of loose samples was typically twice that of dense samples.

The specific volume of loose and dense samples prepared in the permeameter ranged from 1.57 (soil 26, dense) to 2.02 (soil 23, loose). These represent a typical range for uniform cohesionless soils (Atkinson and Bransby, 1978). There appears to be no clear relationship between the range of specific volume exhibited by a soil and its physical properties such as size and shape. Relative density tests performed with soil 23 gave maximum and minimum specific volume values of 2.16 and 1.65. Consequently the relative density of the sample two samples of soil 23 prepared in the permeameter was 27% (loose, υ = 2.02) and 78% (dense, υ = 1.76).

Drained direct shear tests successfully demonstrated the shear characteristics of the soils. Two types of data plot were used to study the behaviour of each soil, these are shown in Figure A.3 for soil 23. Maximum change in specific volume - effective normal stress enabled the relationship between volume change and soil state to be examined. Similarly the relationship between the maximum rate of dilation and soil state could be studied by referring to the plot of maximum rate of dilation - effective normal stress.

Each of the soils exhibited a strong tendency to dilate when sheared in a dense state and a similar, less strong, trend to compress when loose. Soils 25 and 26 showed the largest difference between maximum volume change for loose and dense samples. This suggests a wide potential range of volume change in these soils. Similarly soils 23 and 11 showed the least difference in these values. In these cases a relatively narrow range of volume change might be expected. A correlation between the volume changes observed in direct shear tests and the range of specific volume noted in the parameter and relative density tests might be anticipated. Test results suggest that this was not the case. However there is a broad correlation between the physical properties of each soil, in particular grain size, and the behaviour observed in direct shear tests. The widest range of volume change is associated with the coarser soils (soils 25 and 26), while the finer soils (soils 23 and 11) exhibited a narrow range of volume change. It is suggested that these observations result from the non-uniform shearing that takes place in test samples. Deformation in direct shear tests is concentrated within a shear zone through the centre of a sample, the dimensions of which appear to be a function of grain size. To conclude, the volume change observed in drained direct shear tests appears to be proportional to soil grain size.

The dilation of dense samples results in a positive value of the rate of dilation, while the compression of loose samples gives negative values. These are shown in Figures A.3c for soil 23. It might be expected that the difference between the rate of dilation of loose and dense samples of a given soil is related to the difference in volume change discussed above. In general this appears to be the case, with the exception of soil 11. This showed the least difference in volume change but the greatest difference in the rate of dilation values.

By referring to the theory introduced in section 2.1.3 it is suggested that each of the eight soils tested would produce positive excess pore pressures when subjected to undrained loading if loose, and a negative response if loaded in a similar manner when dense. It is difficult to place the soils in a rank order, since grain size appears to significantly influence the volume change and rate of dilation observed in drained direct shear tests.

Angles of friction (ultimate state) derived from the direct shear tests are presented in Table A.1. Typically ultimate state angles of friction for sand range from 30° to 37° (after Bolton, 1986). The majority of soils tested fell within this range, the exception being soil 28, which appeared to show a low value of 24°. This, together with the fact that in several cases the soil was still compressed during the latter stages of testing, suggests that loose samples had not achieved an ultimate state. The value of 24° is therefore probably not a true ultimate state angle of friction.

APPENDIX B COMPUTER SOFTWARE

The software package described in Appendix B formed an important part of the computer controlled data logging system. It consisted of four types of program. These enabled continuous logging, data logging during a test, analysis, and the plotting of data to take place. The use of each type of program is discussed in section 5.2.

The programs were written by the author in BBC BASIC. Examples of each type of program are presented in this appendix by way of listings. The operation of the programs is demonstrated by flow charts and examples of printed output, where appropriate.

B.1 Continuous logging programs

Two similar continuous logging programs were developed, CONLOG and PEN1. Their primary function was to enable the calibration of the logging system before and after a sand column test. CONLOG enabled the continuous logging of six interface channels at one second intervals. Figure B.1 and B.2 present a flow chart and listing of the program. Once in operation the program displayed the digital output of the interface on the monitor screen. This was continuously updated and presented in a tabular format comprising six columns of data. The left hand column represented the supply voltage to the instrumentation, while the remaining five columns corresponded to the millivolt output of the miniature pore pressure transducers.

PEN1 was developed from CONLOG to perform a similar task with seven interface channels, for use in piezocone tests. The additional channel of data represented the output of the cone displacement potentiometer. This was displayed as a seventh column of data as above.

Line 300 to line 580 of CONLOG (refer Figure B.2) and similar parts of PEN1 and the logging programs described below were provided with the logging interface for use with a BBC computer. This section of the programs enabled the rapid logging of data and its transfer from the interface to the computer.

B.2 Test logging programs

UDISLO5 and PEN2 enabled the logging, display and storage of the unprocessed digital data generated during a sand column test. UDISLO5 (derived from; excess pore pressure, ū, dissipation logging program, 5 channels) permitted the output of five miniature pore pressure transducers and the supply voltage to the instrumentation to be logged. Data was recorded throughout a test, typically a period of 500 seconds, at 1.25 second intervals. Figure B.3 shows a flow chart for the program and Figure B.4 lists the program.

PEN2 performed a similar function to UDISLO5 and therefore had a similar flow chart. The program was developed for piezocone testing with the output of the cone driving potentiometer recorded as an additional channel of data. This information was used to correct for the increasing static pore pressure acting at the level of the piezocone tip as it penetrated a soil bed. The logging of this extra channel resulted in a slightly slower interval between readings of 1.4 seconds.

A sand column test commenced with the start of the logging sequence. Throughout the monitoring period the unprocessed data was displayed via the monitor as a series of columns. At the end of a test the unprocessed data was automatically transferred to a designated data file on floppy disc.

B.3 Programs to analyse test data

UDISAN5 and PEN3.1 were developed to enable the analysis and presentation of the unprocessed test data. UDISAN5 (derived from; excess pore pressure, ū, dissipation analysis program, 5 channels) analyzed data recorded by UDISLO5. PEN3.1 performed a similar task for data recorded during tests with piezocones. In order to perform the necessary calculations, calibration constants were required for the supply voltage, each miniature pore pressure transducer, and where appropriate the cone driving potentiometer. These were determined during the sand column testing procedure described in section 5.2. Figure B.5 shows the flow chart for the programs. Figures B.6 and B.7 list the contents of UDISAN5.

The two programs ran in a similar manner. Once loaded, the data file to be analyzed was requested. When this had been supplied a list of options was presented, refer Figure B.5. By selecting an option between 1 and 4 the appropriate function was performed before the program returned to the list of options. Each of the options is described below.

Option 1 (Analysis of test data) started with a request for the calibration values required for analysis. These supplied, the program proceeded to calculate the supply voltage, excess pore pressures monitored by each transducer and where appropriate the penetration of the model instruments into the soil bed (piezocone tests). The analyzed data was returned to the computers memory in place of the unprocessed data file. In order to view the test data on the monitor screen option 2 was selected. Selecting this option before option 1 resulted in the unprocessed data being presented, otherwise the analyzed values were shown. Data was displayed as a series of columns in an annotated table. The columns read, from left to right, elapsed time (seconds), supply voltage (volts) and the excess pore pressures monitored by each of the miniature transducers (kPa). When appropriate, the position of the piezocone tip (metres above the basal filter of the sand column) was shown in a further column.

To produce a permanent or hard copy of the analyzed data option 3 was selected. This printed the data file onto paper together with the appropriate calibration constants. Figure B.8 shows an example of the output produced by this option. By selecting option 4 the analyzed data was transferred to a floppy disc file. Option 5 simply closed the program, while option 6 terminated the program by loading and running the appropriate plotting routine.

B.4 Data plotting programs

Two types of plotting program were developed: one made a preliminary plot of the data and the other accurately plotted test data against scaled axes. Both programs presented the plotted data on the monitor screen before transferring the image to paper using the printer.

UDISPR5 and PEN4 were the preliminary plotting routines. UDISPR5 (derived from excess pore pressure, u, dissipation printing program, 5 channels) was used in the majority of cases, while PEN4 enabled the presentation of piezocone test data. Figures B.9 and B.10 show a flow chart for the programs and a listing of UDISPR5 respectively. The two programs operated in a similar manner. Once loaded the data file to be plotted was requested. With this supplied, the program requested the appropriate calibration constants needed to analyse the unprocessed test data. This done the excess pore pressures monitored by each transducer were calculated and plotted against axes of excess pressure and time. With plotting complete the image was printed on paper. Figure B.11 shows an example of this output.

Accurate plotting of test data was performed by a modified version of the software package DOODLE/PLOT, developed by Clinton (1986) initially for use with triaxial test data. The modification made to the program permitted the precise plotting of excess pore pressure against time for each transducer. The output from this software was used to prepare the figures presented in Chapter 6.

APPENDIX C   ASSESSMENTS OF THE INSTRUMENTATION AND LOGGING SYSTEM

The system developed to monitor the generation and dissipation of excess pore pressures inside the sand column is described in section 4.4. The tests carried out to establish whether this equipment performed reliably and to an acceptable degree of accuracy are presented in this appendix. The accuracy required of the system has been defined as less than or equal to 0.1kPa (section 4.1), ie. the maximum difference between actual and recorded values of excess pore pressure should not exceed 0.1kPa.

Before determining the characteristics of the combined system, it was necessary to assess the reliability of the individual components. These consisted of the analogue to digital interference and the electrical pore pressure transducers. This is discussed in the first two sections of the appendix. The third and final section considers the reliability and accuracy of the assembled system for the range of output anticipated during sand column tests.

C.1   Interface reliability

Three tests were devised to establish the suitability of the interface. The first assessed the stability of the supply voltage to the instrumentation via the interface. The second determined the stability of the interface with time, while the third test examined inter-channel interference.

An accurate digital volt meter was used in the first test to monitor the output voltage from the interface. Readings were recorded at regular intervals over one and twelve hour periods. In both instances the voltage remained effectively constant, ie. a maximum drift or deviation of less than 0.1% of the initial voltage was recorded.

In the remaining two tests displacement transducers of an appropriate output range were connected to six of the interface's logging channels. These were supplied with the constant voltage as established in the first test. The transducers had previously been tested on other equipment and were known to be stable. The second test involved clamping each of the six transducers in a mid-range position. The program CONLOG was used to present the interface output on the screen of the monitor. Readings were recorded over one and twelve hour periods. Each of the six channels was found to be relatively stable over both periods, ie. a maximum drift or deviation in the digital output (millivolts) presented of less than 0.5% of full range values.

The third test involved clamping five of the transducers in a mid-range position and varying the displacement of the sixth. The output of the transducers was displayed on the monitor as above. If there is no interference within a unit the output will only show a change in the date appropriate to the sixth channel. The procedure was adopted for each of the six interface channels under test. In each case no interference was observed, provided the output of the transducer remained within the range of the associated logging channel. Beyond this range significant interference occurred.

It was concluded that the above characteristics made the interface suitable for its intended use provided the transducer outputs did not exceed the range of their associated interface logging channel.

C.2 Instrumentation

The specifications of the miniature electrical pore pressure transducers used in sand column tests are summarised in Table 4.2. Each transducer was calibrated and its sensitivity to temperature change determined. This type of transducer, unlike many others is not temperature compensated. Other characteristics such as stability, linearity, drift and noise are discussed for the combined system in section C.3.

Transducers were calibrated by applying a range of static water heads or pressures. These were varied in increments of 100mm with the temperature of the water constant. The digital output of the interface (millivolts) was recorded for each transducer and plotted against the applied static water head (millimetres). An example of this type of plot is shown in Figure 5.1. Calibration constants were determined for each transducer by drawing a straight line through the appropriate data. Typical constants for the transducers used are presented in Table C.1. Specific values were determined by conducting the calibration procedure before and after individual sand column tests. Variations in values between tests are discussed in section C.3.

Temperature sensitivity was examined by placing the transducers under a constant static head of water and slowly increasing the water temperature from 12°C to 30°C. Over this range the output of the instrumentation varied linearly with temperature. Temperature calibrations are presented in Table C.1 in terms of equivalent units of pressure (kPa).

C.3 Characteristics and accuracy of the combined logging system

The following terms may be used to describe the characteristics of the combined logging system.

C.3.1 Resolution

The processes of digitising and storing a continuous analogue signal reduces data into an incremental form. The magnitude of the increments in the recorded data defines the resolution of the system. Discrepancies can be introduced between actual and recorded values at two points in the system: firstly during the analogue to digital conversion, and secondly as the computer stores the digital data.

In reducing an analogue signal to an incremental digital signal, values are either truncated or rounded off. In electronics the error produced in this way is known as quantisation noise.

The resolution of stored data can be reduced further if the computer used has insufficient memory capacity. This is a function of the bit capacity of the machine used. If the capacity is too small to record the complete digital signal, the latter part of each value is effectively lost.

The combined effect of these processes on the accuracy of recorded data can be assessed by independently establishing the characteristics of the analogue to digital converter and the computer's memory. This option was not available in this cases because the characteristics of the analogue to digital converter were not known. The resolution of a system may also be determined by establishing the minimum increment in recorded data, this is equivalent to the combined resolution error. Table C.2 presents values of resolution error derived from recorded test data.

C.3.2 Random noise and drift

Random noise is defined as the unwanted components in a system's output. In a system with constant input signal this is characterised by randomness in the output about a mean value. During the calibration procedure carried out before and after each sand column test it was possible to observe such random noise. This appeared as fluctuations in the stored data set for periods of known constant transducer conditions. Table C.2 summarises the maximum excursions observed during these periods, and therefore quantifies the level of random noise of each channel-transducer combination.

A gradual shift in the output of a system over a period of time due to change or ageing of components when input is constant is defined as drift. By comparing the pre and post sand column test calibration data it was possible to make an assessment of the drift that might occur during a sand column test. Worst case examples of observed drift are set out in Table C.2. The period of time between calibrations was typically of the order of two hours. As indicated above, drift is associated with long term ageing effects on the components of a system. By calibrating immediately before and after each test, drift effects will have been largely eliminated. The drift observed during this time may well have been due to temperature changes in the sand column over this period.

C.3.3 Linearity and stability

If a system behaves linearly then calibration values will be constant, ie. a plot of applied pressure against the recorded digital output would be linear. Plots of this type were used to determine calibration constants for each sand column test. An example is shown in Figure 5.1. Although these plots show some scatter in the data, this appears to be due to noise and not non-linearity. Over the range of pressure considered errors due to non-linearity therefore appear to be less than the resolution of the system.

Temperature stability is considered separately in section C.2. Instability with time can either be a result of one or a combination of two factors; changes in initial "zero" values due to drift and changes in calibration constants over time. Drift is discussed above in section C.3.2. Values of calibration constants derived from before and after sand column tests suggest that the instrumentation remained stable during tests. However, slight variations in calibration constant values were observed over the longer periods between tests.

C.3.4 Accuracy

The accuracy of a logging system describes the maximum difference between actual and measured values of a parameter, in this case pore pressures. Each of the factors considered above can affect the accuracy of the recorded data.

By calibrating the system before and after each sand column test it was possible to ensure it remained stable during the recording period. The linearity of the system has been shown to be better than its resolution. Although a small amount of drift was observed between these calibrations, it is thought that this was a result of temperature changes inside the sand column. The period between calibrations was typically of the order of two hours. This compares with a typical test duration of five hundred seconds. Drift is therefore not considered to be a significant factor during the relatively short period of a test.

The accuracy of the monitoring system is the sum of the maximum errors due to resolution, drift, random noise, instability and non-linearity. Instability and drift during a test period have been shown to be insignificant. Linearity appears to have been better than the resolution of the system. Therefore accuracy can be assumed to be given by the equation;

$$\text{Accuracy} = \text{Resolution Error} + \text{Random Noise} \qquad \text{C.1}$$

Table C.2 presents values of accuracy calculated by adopting the data for resolution and noise given in the same table. These are within the value of 0.1kPa stipulated in section 4.1 as the required level of accuracy. The logging system was therefore considered to be sufficiently accurate for its intended use.

APPENDIX D TEST TO ASSESS SAND COLUMN PROCEDURES

Two types of tests were performed to establish whether the procedures outlined in section 5.2 created uniform beds of soil in the sand column. The first was designed to study differential grading within soil beds, and the second variations in soil density with depth. The tests were carried out with medium dense and dense soil beds. Loose soil beds were not used because these would have been very susceptible to disturbance.

D.1 Differential grading within test beds

No tests were performed with soil 23. However a test carried out with soil 26 is described in this section. This demonstrates that although differential grading did occur in the sand column, the majority of a soil bed was relatively homogeneous.

A one metre thick bed of soil 26 was prepared by the methods set out in section 5.2. The bed was then excavated in fourteen layers by syphoning. Samples were taken from each layer and their particle size distribution determined by sieving in accordance with BS 1377 (1975), Test 7(B). The grading curves of selected samples are shown in Figure D.1. This illustrates a trend from very uniform fine sand at the top of the bed (sample 1) to less uniform medium sand at the base (sample 14). The majority of the bed, from 0.05m below the surface to the base, fell within the narrow grading envelope delineated by samples 4 and 14.

The differential grading shown by Figure D.1 is a result of the sedimentation process that formed the initial very loose soil bed. Once the upward flow of water through the fluidised bed stopped larger, heavier particles tend to settle most rapidly forming a coarser basal layer. Similarly, smaller particles remain in suspension for the longest period before settling to form a surface layer of finer particles.

D.2 Variations in soil density within a test bed

Soil 23 was used to form beds by the procedures described in section 5.2. Soil layers of measured thickness were then excavated by syphoning. The soil forming each layer was oven dried and weighed.

This procedure was repeated three times, twice with dense soil beds and once with a medium dense soil bed.

Table D.1 presents the density values for the individual soil layers. Figure D.2 summarises the data for the three tests with specific volume plotted against depth. The data plots as a series of parallel curves with specific volume reducing with depth in each case. The two beds prepared at greater energy levels (ie. the dense soil beds) show lower specific volumes as would be expected. The results of these tests were used to construct the correction shown in Figure 7.28.

REFERENCES

ASTM D2049-69 (1969), Standard Method of Test for Relative Density of Cohesionless Soils, American Soc. for Testing and Materials, Philadelphia.

Ambraseys, N. and Sarma, S. (1969), Liquefaction of Soil Induced by Earthquakes, Bulletin of the Seismological Society of America, Vol.59(2) : 651-664.

Arulanandan, K. and Muraleetharan, K.K. (1988a), Level ground soil-liquefaction analysis using in situ properties : I, Journal of Geotechnical Engineering, American Soc. of Civil Engineering, Vol.114(7) :753-770.

Arulanandan, K. and Muraleetharan, K.K. (1988b), Level ground soil-liquefaction analysis using in situ properties : II, Journal of Geotechnical Engineering, American Soc. of Civil Engineering, Vol.114(7) :771-790.

Arulmoli, K., Arulanandan, K. and Seed, H.B. (1981), A New Method for Evaluating Liquefaction Potential In Situ, In: In Situ Testing to Evaluate Liquefaction Susceptibility, American Soc. of Civil Engineers, Conference, 1981, Preprint (81-544).

Arulmoli, K., Arulanandan, K., and Seed, H.B. (1985), New Method of Evaluating Liquefaction Potential, Journal of Geotechnical Engineering, American Soc. of Civil Engineering, Vol.111(1) : 95-114.

Atkinson, J.H. and Bransby, P.L. (1978), The Mechanics of Critical State Soil Mechanics. (London : McGraw-Hill).

Atkinson, J.H. and Farrer, D.M. (1985), Stress path tests to measure soil strength parameters for shallow landslips, In: International Conference on Soil Mechanics and Foundation Engineering, Eleventh, San Francisco, 1985, Proceedings : 983-987.

Atkinson, J.H. and Jessett, C.A. (1988), Measurement of relative density of saturated sands using a piezovane, In: Field Testing in Engineering Geology, Sunderland, 1988, Proceedings, (London : Geological Soc., Engng. Geology Special Publication No.6) : 229-233.

Atkinson, J.H. and Richardson, D. (1987), Effects of Local Drainage in Shear Zones on the Undrained Shear Strength of Overconsolidated Clay, Geotechnique, Vol.37(3) : 393-403.

BS 1377, (1975), Methods of test for soils for civil engineering purposes, British Standards Institute, London.

Been, K., Crooks, J.H.A., Becker, D.E. and Jefferies, M.G. (1986), The cone penetration test in sands : part 1, state parameter interpretation, Geotechnique, Vol.36(1) : 239-249.

Bolton, M.D. (1986), The strength and dilatancy of sands, Geotechnique, Vol.36(1) : 65-78.

Bjerrum, L. (1973), Geotechnical problems of structures in the North Sea, Geotechnique, Vol.23(3) : 319-358.

Casagrande, A. (1936), Characteristics of Cohesionless Soils Affecting the Stability of Earth Fills, Journal of the Boston Soc. of Civil Engineers, Vol.23(1) : 13-32.

Casagrande, A. (1975), Liquefaction and Cyclic Deformation of Sands. A critical review, Pan American Conference on Soil Mechanics and Foundation Engineering, Fifth, Buenos Aires, 1975 : 80-133.

Castro, G. (1969), Liquefaction of sands, PhD thesis, Harvard University, Division of Engineering and Applied Physics.

Castro, G. (1975), Liquefaction and Cyclic Mobility of Saturated Sands, Journal of the Geotechnical Engineering Division, American Soc. of Civil Engineers, Vol.101(6) : 551-569.

Castro, G., Seed, R.B., Keller, T.O. and Seed, H.B. (1992), Steady-state strength analysis of Lower San Fernando dam slide, Journal of Geotechnical Engineering, American Soc. of Civil Engineers, Vol.118(3) : 406-427.

Charlie, W.A., Jacobs, P.J. and Doehring, D.O. (1992), Blast-induced liquefaction of an alluvial sand deposit, Geotechnical Testing Journal, American Soc. of Testing and Materials, Vol.15(1) : 14-23.

Cherrill, H.E. (1990), The influence of loading rate on excess pore pressures in triaxial tests, PhD thesis, Geotechnical Engineering Research Centre, The City University, London.

Clinton, D (1986), Programs for data analysis on the BBC microcomputer, Geotechnical Engineering Research Centre, The City University, London, Research Report GE/86/2.

Crabb, G.I. and Atkinson, J.H. (1991), Determination of soil strength parameters for the analysis of highway slope failures, In: International Conference on Slope Stability Engineering - Developments and Applications, London, 1991, Proceedings : 13-18.

Craig, R.F. (1987), Soil mechanics (London : Van Nostrand Reinhold)

Deltf Soil Mechanics Laboratory (1984, technical trade literature), Density Measurement In situ and critical density.

De Ruiter, J. (1982), The static cone penetration test, State of the art report, In: Second European Symposium on Penetration Testing, Amsterdam, 1982, Proceedings, Vol.2 : 389-405.

Dobry, R., Stokes, K.H., Ladd, R.S. and Youd, T.L. (1981), Liquefaction Susceptibility from S-wave Velocity, In: In Situ Testing to Evaluate Liquefaction Susceptibility, American Soc. of Civil Engineers, Conference, 1981, Preprint (81-544).

Dwyer, E.S. (1986), Dissipation of excess pore pressure in a readily liquefiable soil, Final year undergraduate report, Department of Civil Engineering, The City University, London.

Eckersley, J.D. (1990), Instrumented laboratory flowslides, Geotechnique, Vol.40(3) : 489-502.

Finn, W.D.L., Siddharthan, R. and Martin, G.R. (1983), Response of Seafloor to Ocean Waves, Journal of Geotechnical Engineering, American Soc. of Civil Engineers, Vol.109(4) : 556-572.

Florin, V.A. and Ivanov, P.L. (1969), Liquefaction of Saturated Sandy Soils, In: International Conference on Soil Mechanics and Foundation Engineering, Fifth, Paris, 1969, Proceedings, Vol.1 : 107-111.

Gilbert, P.A. and Marcuson, W.F. (1988), Density variation in specimens subjected to cyclic and monotonic loads, Journal of Geotechnical Engineering, American Soc. of Civil Engineers, Vol.114(1) : 1-20.

Graf, W.H. (1984), Hydraulics of Sediment Transport (Littleton, Colorado : Water Resources Publications).

Head, K.H. (1982), Manual of Soil Laboratory Testing, Volume 2, Permeability, Shear strength and Compressibility Tests (London : Pentech Press).

Hughes, J.M.O., Wroth, C.P. and Windle, D. (1977), Pressuremeter tests in sands, Geotechnique, Vol.27(4) : 455-477.

Ishihara, K. and Perlea, V. (1984), Liquefaction associated Ground Damage during the Vrance Earthquake of March, 1977, Soils and Foundations, Vol.24(1) : 90-112.

Ishihara, K. and Yamada, Y. (1981), Liquefaction Tests Using a True Triaxial Apparatus, In: International Conference on Soil Mechanics and Foundation Engineering, Tenth, Stockholm, 1981. Proceedings, Vol.3 : 235-238.

Ishihara, K. and Yasuda, S. (1975), Soil Liquefaction in Hollow Cylinder Torsion Under Irregular Excitation, Soils and Foundations, Vol.15(1) : 45-59.

Ivanov, P.L. and Sinitsyn, A.P. (1977), Soil Liquefaction and Stability of Foundations, In: International Conference on Soil Mechanics and Foundation Engineering, Tokyo, 1977. Proceedings, Vol.2 : 265-268.

Japanese Society of Soil Mechanics and Foundation Engineering, (1966), various papers describing damage caused by the 1964 Niigata Earthquake, Soils and Foundations, Vol.6(1) : 1-112.

Kummeneje, O. and Eide, O. (1961), Investigation of Loose Sand Deposits by Blasting, In: International Conference on Soil Mechanics and Foundation Engineering, Fifth, Paris, 1969. Proceedings, Vol.1 : 491-497.

Law, K.T., Cao, Y.L. and He, G.N. (1990), An energy approach for assessing seismic liquefaction potential, Canadian Geotechnical Journal, Vol.27 : 320-329.

Lee, F.H. and Schofield, A.N. (1984), Centrifuge Modelling of Artificial Sand Islands in Earthquakes, Research report, Cambridge University, Engineering Department, No CUED/D-Soils TR160.

Lee, F.H. and Schofield, A.N. (1988), Centrifuge Modelling of Artificial Sand Islands in Earthquakes, Geotechnique, Vol.38(1) : 45-58.

Lee, K.L. and Focht, J.A. (1975), Liquefaction Potential at Ekofisk Tank in North Sea, Journal of the Geotechnical Engineering Division, American Soc. of Civil Engineers, Vol.101(1) : 1-18.

Lindenberg, J. and Koning, H.L. (1981), Critical density of sands, Geotechnique, Vol.31(2) : 231-245.

Marsal, R.J. (1961), Behaviour of Sandy Uniform Soil during the Jaltipan Earthquake, Mexico, In: International Conference on Soil Mechanics and Foundation Engineering, Fifth, Paris, 1961. Proceedings, Vol.1 : 229-233.

Martin, G.R., Lam, I. and Tsai, C.F. (1980), Pore-Pressure Dissipation During Offshore Cyclic Loading, Journal of the Geotechnical Engineering Division, American Soc. of Civil Engineers, Vol.106(9) : 981-996.

Martin, G.R., Finn, W.D.L. and Seed, H.B. (1975), Fundamentals of Liquefaction under Cyclic Loading, Journal of the Geotechnical Engineering Division, American Soc. of Civil Engineers, Vol.101(5) : 423-438.

Maude, A.D. and Whitmore, R.L. (1958), A generalised theory of sedimentation, British Journal of Applied Physics, Vol.9 : 477-482.

Meigh, A.C. (1987), Cone penetration testing : methods and interpretation. Construction Industry Research and Information Association, Ground Engineering Report: In-situ Testing (London : Butterworths).

Michell, R.J. and Dubin, B.I. (1986), Pore pressure generation and dissipation in dense sands under cyclic loading, Canadian Geotechnical Journal, Vol.23 : 393-398.

Morris, D.V. (1983), A note on earthquake-induced liquefaction, Geotechnique, Vol.33(4) : 451-454.

O'Conner, M. (1984), Dissipation of Excess Pore Pressure in a readily Liquefiable Soil. Final year undergraduate dissertation, Department of Civil Engineering, The City University, London.

Poulos, S.J., Castro, G. and France, J.W. (1985), Liquefaction evaluation procedure, Journal of Geotechnical Engineering, American Soc. of Civil Engineers, Vol.111(6) : 772-792.

Prakash, S. (1981), Liquefaction of Soils, In: Soil Dynamics, (New York : McGraw-Hill) : 274-339.

Robertson, P.K. and Campenella, R.G. (1985), Liquefaction Potential of Sands Using the CPT, Journal of Geotechnical Engineering, American Soc. of Civil Engineers, Vol.111(3) : 384-403.

Rollins, K.M. and Seed, H.B. (1990), Influence of buildings on potential liquefaction damage, Journal of Geotechnical Engineering, American Soc. of Civil Engineers, Vol.116(2) : 165-185.

Schnaid, F. and Houlsby, G.T. (1991), An assessment of chamber size effects in the calibration of in situ tests in sand, Geotechnique, Vol.41(3) : 437-445.

Schofield, A.N. (1981), Dynamic and Earthquake Geotechnical Centrifuge Modelling, Research report, Cambridge University, Engineering Department, No CUED/D-Soils TR104.

Seed, H.B. (1970), Soil Problems and Soil Behaviour (chapter 10), and Earth Slope Stability during Earthquakes (Chapter 15), In: Earthquake Engineering, Ed. by Wiegel, R.L. (London : Prentice-Hall).

Seed, H.B. (1979a), Soil Liquefaction and Cyclic Mobility Evaluation for Level Ground during Earthquakes, Journal of the Geotechnical Engineering Division, American Soc. of Civil Engineers, Vol.105(2) : 201-255.

Seed, H.B. (1979b), Considerations in the earthquake-resistant design of earth and rock fill dams, Geotechnique, Vol.29(3) : 215-263.

Seed, H.B. (1987), Design problems in soil liquefaction, Journal of Geotechnical Engineering, American Soc. of Civil Engineers, Vol.113(8) : 827-845.

Seed, H.B. and Idriss, I.M. (1967), Analysis of Soil Liquefaction : Niigata Earthquake, Journal of the Soil Mechanics and Foundations Division, American Soc. of Civil Engineers, Vol.93(3) : 83-108.

Seed, H.B., Irango, I., Chan, C.H., Gomez-Masso, A. and Ascoli, R.G. (1981), Earthquake-Induced Liquefaction near Lake Amatitlan, Guatemala, Journal of the Geotechnical Engineering Division, American Soc. of Civil Engineers, Vol.107(4) : 501-518.

Seed, H.B., Idriss, I.M. and Arango, I. (1983), Evaluation of Liquefaction Potential Using Field Performance Data, Journal of Geotechnical Engineering, American Soc. of Civil Engineers, Vol.109(3) : 458-482.

Seed, H.B., Martin, P.P. and Lysmer, J. (1975), The Generation and Dissipation of Pore Water Pressures during Soil Liquefaction, Research report, University of California, Earthquake Engineering Research Centre, No. EERC 75-26.

Seed, H.B., Tokimatsu, K., Harder,L.F. and Chung, R.M. (1985), Influence of SPT procedures in soil liquefaction resistance evaluations, Journal of Geotechnical Engineering, American Soc. of Civil Engineers, Vol.111(12) : 1425-1445.

Skempton, A.W. (1986), Standard penetration test procedures and the effects in sands of overburden pressure, relative density, partial size, ageing and over consolidation, Geotechnique, Vol.36(3) :425-447.

Sladen, J.A., D'Hollander, R.D. and Krahn, J. (1985), The liquefaction of sands, a collapse surface approach, Canadian Geotechnical Journal, Vol.23 : 564-578.

Vaid, Y.P., Byrne, P.M. and Hughes, J.M.O. (1981), Dilation Angle and Liquefaction Potential, Journal of the Geotechnical Engineering Division, American Soc. of Civil Engineers, Vol.107(7) : 1003-1008.

Yoshimi, Y. (1977), Liquefaction and Cyclic Deformation of Soils Under Undrained Conditions, In: International Conference on Soil Mechanics and Foundation Engineering, Ninth, Tokyo, 1977. Proceedings, Vol.2 : 613-623.

Yoshimi, Y. and Kuwabara, F. (1973), Effects of Subsurface Liquefaction on the Strength of Surface Soil, Soils and Foundations, Vol.13(2) : 68-81.

Youd, T.L. and Bennett, M.J. (1983), Liquefaction Sites, Imperial Valley, California, Journal of Geotechnical Engineering, American Soc. of Civil Engineers, Vol.109(3) : 440-457.

Approach				Techniques Adopted
Theoretical	-	critical void ratio and critical state soil mechanics (section 3.2.1)	-	laboratory triaxial testing and in situ density by electrical resistivity
	-	Equivalent stress path (section 3.2.2)	-	uniform cyclic triaxial testing
			-	complex stress paths (true triaxial and hollow cylinder)
	-	Critical strain (section 3.2.3)	-	Shear wave velocity
Modelling	-	Physical modelling (section 3.2.4)	-	Vibrating table tests
			-	Centrifuge modelling
	-	Numerical modelling (section 3.2.5)	-	Excess pore pressure generation
			-	Dissipation of excess pore pressures
			-	Coupled excess pore pressure generation and dissipation
Empirical	-	Field methods (section 3.2.6)	-	Penetration tests (SPT and CPT)
			-	Self-boring pressuremeter
			-	Electrical resistivity
	-	Field simulation (section 3.2.7)	-	Blasting techniques

Table 3.1 Methods of investigating liquefaction behaviour

	Computed		Observed
0-50 sec.	Earthquake	0-50 sec.	Earthquake
20-50 sec.	Liquefaction between depths of 15 and 40 ft.	0-50 sec.	Liquefaction at some depth below ground surface.
1-4 min.	Development of essentially liquefied condition between depths of 3 and 15 ft.		
≈ 5 min.	At depth of 3 ft water pressure becomes equal to overburden pressure. Cracks likely to develop in top 3 ft of soil with water boiling up through cracks and cavities.	≈ 3 min.	Ground cracking and some eruptions of water near school building.
≈ 12 min.	Water table rises to ground surface. Water emerges generally from ground surface. Surface becomes 'quick'.	≈ 8 min.	Sudden upward flow of water in cracked area.
		≈ 13 min.	Heavy water flow at surface to heights of above 3 ft.
≈ 17 min.	Pore pressures begin to drop at ground surface - surface begins to stabilise but water continues to flow at surface.	≈ 14 min.	Several inches of water accumulated on ground surface.
		≈ 28 min.	Water still flowing at ground surface.
≈ 60 min.	Pore pressure ratio in all layers has dropped to 0.1 to 0.3. All soils stabilised but small flow of water continues at surface.		

Table 3.2 Comparison of computed rate of pore pressure development and obsevations of surface phenomena at Niigata, 1964 (after Seed et al, 1975)

Time, elapse (seconds)	Observation
0	Start of main shock of earthquake
≈14	Strong motion completed - slight tilting of dam crest
≈40	Start of slide movements at crest of dam
≈56-57	Aftershock 2
≈62-63	Aftershock 3
≈72-73	Aftershock 4
≈75-76	Aftershock 5
≈90	End of main slide movement - instrument tilted about 26°
>90	Further tilting to about 37° after 10 days

Table 3.3 Sequence of events observed during the partial collapse of the lower San Fernando Dam (after Seed, 1979b)

Grading Parameters (from Figure A.1)	
D_{10}(mm)	0.04
D_{50}(mm)	0.08
U	1.4
Average specific gravity of particles	2.65
Maximum specific volume	2.16
Minimum specific volume	1.65
Permeability (m s^{-1})	
Loose state (specific volume 2.02)	2.8×10^{-4}
Dense state (specific volume 1.76)	2.1×10^{-4}
Ultimate or critical state angle of friction	36°

Table 4.1 The basic properties of soil 23

Notes

1. Maximum and minimum specific volumes are defined in Appendix A.

Manufacturer :	Druck (UK) Ltd	
Type :	Miniature electrical resistance pore pressure transducers, reference PDCR 81	
Range :	350mbar (35kPa)	1 bar(100kPa)
Maximum supply voltage :	10 volts	5 volts
Serial numbers :	2756, 2757	2930, 2941, 2943, 3201

Table 4.2 Specification of miniature pore pressure transducers

PURPOSE OF TEST	TYPE OF TEST	PARAMETER/CHARACTERISTIC STUDIED	RESULTS (SECTION OF CHAPTER SIX)
Tests to study processes of liquefaction (section 5.3)	Distribution and dissipation of excess pore pressures within a uniform soil profile (section 5.3.1).	Magnitude of initial excess pore pressure	6.1.1
		Period of excess pore pressure generation	
		Soil state	
	Surface surcharge load (section 5.3.2).	Excess pore pressure generation and at increased effective stress levels	6.1.2
	Distribution and dissipation of excess pore pressures within a layered soil profile (section 5.3.3).	Influence of an impermeable near surface layer upon excess pore pressure dissipation	6.1.3
Tests to assess and develop prototype instruments	Vane and piezovane (section 5.4).	Vane rotation rate (section 5.4.1)	6.2.2
		Soil state (section 5.4.2)	6.2.3
		Vane geometry (section 5.4.3)	6.2.4
		Installation disturbance (section 5.4.4)	6.2.5
		Piezovane filter position (section 5.4.5)	6.2.6
	Expanding membrane probe (section 5.5)	Membrane pressure (section 5.5.1)	6.3.2
		Soil state (section 5.5.2)	6.3.3
	Cone and piezocone (section 5.6)	Cone penetration rate (section 5.6.1)	6.4.2
		Soil state (section 5.6.2)	6.4.3
		Cone geometry (section 5.6.3)	6.4.4
		Piezovane filter position (section 5.6.4)	6.4.5

Table 5.1 Schedule of sand column tests

Test (No)	Hydraulic gradient, i	Time for which hydraulic gradient applied, t (seconds)	Soil state (average specific volume)
A	1.0	1	2.02
D	1.0	9	2.02
F	0.5	3	2.02
I	1.5	3	2.02
L	0.25	3	2.02
O	1.0	3	1.65
42	1.0	3	2.02
43	1.0	3	1.85
44	1.0	4	1.91

Table 5.2 Tests to study the distribution and dissipation of excess pore pressures in a uniform soil profile

Test (No)	Soil state, average specific volume,	Method of excess pore pressure generation
180	1.96	3 rapid clockwise-anticlockwise movements of 1:1 piezovane
181	1.92	3 rapid clockwise-anticlockwise movements of 1:1 piezovane
186	<1.92	Shock loading at base of column for approximately 3 seconds

Table 5.3 Tests performed with a surface surcharge

Notes

1. Tests 181 and 186 were performed during the same logging sequence. The shock loading of test 181 took place at 330 seconds, after the complete dissipation of the excess pore pressures generated in test 181.

Test (No)	Soil state, average specific volume	Rate of 90° clockwise rotation (rev/sec)	Initial bed thickness (m)
89	2.02	0.51	0.794
90	2.02	0.17	0.794
91	2.02	0.06	0.794
92	2.02	0.01	0.792
93	2.02	0.004	0.794

Table 5.4 Tests to determine the influence of vane rotation rate

Test (No)	Soil state, average specific volume	Rate of 90° clockwise rotation (rev/sec)	Initial bed thickness (m)
91	2.02	0.06	0.794
94	1.84	0.06	0.721
95	1.89	0.06	0.739
96	1.94	0.06	0.760
97	1.78	0.06	0.697
98	1.64	0.06	0.641
99	1.68	0.06	0.659

Table 5.5 Tests to determine the soil state - excess pore pressure relationship for a 1:1 ratio vane

Test (No)	Soil state, average specific volume	Rate of 90° rotation (rev/sec)	Vane geometry (height: diameter)	Initial bed thickness (m)
100	2.02	0.06	2:1	0.790
101	1.77	0.06	2:1	0.692
102	1.93	0.06	2:1	0.754
103	1.88	0.06	2:1	0.734
104	1.85	0.06	2:1	0.721
105	2.02	0.06	1:2	0.790
106	1.84	0.06	1:2	0.720
107	1.93	0.06	1:2	0.753
108	1.87	0.06	1:2	0.729
109	1.77	0.06	1:2	0.693

Table 5.6 Tests to assess the influence of vane geometry (refer to Table 5.5)

Test (No)	Soil state, average specific volume	Approximate rate of penetration (mm/sec)	Initial thickness of bed (m)
110	2.02	20	0.783
112	1.79	20	0.694
114	1.85	20	0.717
116	1.88	20	0.730
118	1.83	20	0.708
120	1.92	20	0.746

Table 5.7 Tests in which a 1:1 ratio vane was driven into a soil bed before rotation
(refer to Table 5.8)

Test (No)	Soil state, average specific volume	Rate of vane rotation (rev/sec)	Elevation of vane tip above basal filter (m)
111	2.02	0.06	0.101
113	1.79	0.06	0.600
115	1.85	0.06	0.506
117	1.88	0.06	0.093
119	1.83	0.06	0.608
121	1.92	0.06	0.080

Table 5.8 Tests in which a 1:1 ratio vane was rotated following driving into a soil bed
(refer to Table 5.7)

Test (No)	Soil state, average specific volume	Rate of vane rotation (rev/sec)	Filter position	Initial thickness of bed (m)
140	2.02	0.06	shaft	0.816
141	1.96	0.06	shaft	0.790
142	1.88	0.06	shaft	0.756
143	1.88	0.06	shaft	0.756
144	1.92	0.06	shaft	0.773
145	1.85	0.06	shaft	0.746
146	1.81	0.06	shaft	0.729
147	1.77	0.06	shaft	0.712
148	2.02	0.06	blade edge	0.814
149	1.77	0.06	blade edge	0.712
151	1.92	0.06	blade edge	0.772
152	1.93	0.06	blade edge	0.778
154	1.97	0.06	blade edge	0.793
155	1.92	0.06	blade edge	0.774
156	1.84	0.06	blade edge	0.741

Table 5.9 Tests to assess the influence of the filter position on a 1:1 ratio piezovane

Test (No)	Soil state, average specific volume	Initial chamber pressure (kPa)	Initial bed thickness (m)
122	2.02	27.6	0.788
124	2.02	13.8	0.789
125	2.02	41.4	0.789
127	2.02	55.2	0.789
129	2.02	20.7	0.788

Table 5.10 Tests to demonstrate the effect of membrane pressure

Test (No)	Soil state, average specific volume	Initial chamber pressure (kPa)	Initial bed thickness (m)
132	2.02	34.5	0.828
133	1.79	34.5	0.733
134	1.71	34.5	0.698
135	1.84	34.5	0.750
136	1.89	34.5	0.774

Table 5.11 Tests to determine the soil state - excess pore pressure relationship for an expanding membrane probe

Test (No)	Soil state, average specific volume	Rate of cone penetration (mm/sec)	Nature of penetration	Initial bed thickness (m)
54	2.02	26	continuous	0.795
55	2.02	80	continuous	0.792
56	2.02	300	continuous	0.791
57	2.02	7	continuous	0.793
67	2.02	2	continuous	0.791
69	2.02	20	200mm steps	0.791
70	2.02	20	200mm steps	0.787
63	1.85	22	continuous	0.729
85	1.85	81	continuous	0.721
86	1.84	10	continuous	0.720
87	1.84	2.5	continuous	0.719
88	1.84	4	continuous	0.719

Table 5.12 Tests to determine the influence of cone penetration rate

Test (No)	Soil state, average specific volume	Approximate rate of continuous penetration (mm/sec)	Initial bed thickness (mm)
54	2.02	20	0.795
62	1.62	20	0.639
63	1.85	20	0.729
64	1.99	20	0.782
65	1.94	20	0.762
66	1.71	20	0.672
81	1.80	20	0.703

Table 5.13 Tests to determine the soil state - excess pore pressure relationship for a 60° cone

Test (No)	Soil state, average specific volume	Approximate rate of continuous penetration (mm/sec)	Cone geometry, tip angle (degrees)	Initial bed thickness (m)
71	2.02	20	30	0.789
72	1.85	20	30	0.724
73	1.92	20	30	0.750
74	1.81	20	30	0.707
75	1.76	20	30	0.688
76	1.63	20	30	0.638
77	2.02	20	90	0.789
78	1.64	20	90	0.639
79	1.80	20	90	0.704
82	1.92	20	90	0.749
83	1.85	20	90	0.723
84	1.74	20	90	0.680

Table 5.14 Tests to assess the influence of cone geometry (refer to Table 5.13)

Test (No)	Soil state, average specific volume	Approximate rate of continuous penetration (mm/sec)	Filter position	Initial bed thickness (m)
159	2.02	20	shaft(2)	0.808
160	1.84	20	shaft(2)	0.737
161	1.88	20	shaft(2)	0.751
162	1.84	20	shaft(2)	0.732
163	1.80	20	shaft(2)	0.718
164	1.78	20	shaft(2)	0.712
165	2.02	20	face	0.808
166	1.78	20	face	0.710
167	1.81	20	face	0.723
168	1.79	20	face	0.714
169	1.83	20	face	0.733
170	1.88	20	face	0.751
171	1.92	20	face	0.770
173	2.02	20	sholder	0.808
174	1.90	20	sholder	0.760
175	1.84	20	sholder	0.732
177	1.80	20	sholder	0.719
178	1.82	20	sholder	0.728
179	1.85	20	sholder	0.738

Table 5.15 Tests to assess the influence of filter position on a 60° piezocone

Test No	Transducer No	Initial depth (m)	Class of response	Elapsed times (sec) t_1	t_2	t_3	t_4	Excess pore pressure (kN/m^2) $\bar{u}_1$	Comments
F	T2943	0.181	II	30.0	31.3	33.8	88.0	0.93	Surface settlement 0.001m.
	T2941	0.281		30.0	31.3	33.8	95.0	1.42	
	T2930	0.381		30.0	31.3	33.8	88.0	1.87	
	T2757	0.581		30.0	31.3	33.8	100.0	2.90	
	T2756	0.681		30.0	31.3	33.8	100.0	3.31	
I	T2943	0.180	I	30.0	31.3	410.0	580	1.31	Elapsed times in excess of 500 seconds estimated by extrapolation. Surface settlement 0.027m.
	T2941	0.280		30.0	32.5	345.0	580	2.10	
	T2930	0.380		30.0	32.5	275.0	580	2.90	
	T2757	0.580		30.0	32.5	150.0	580	4.68	
	T2756	0.680		30.0	32.5	90.0	580	5.46	
L	T2943	0.180	II	27.5	32.5	33.8	60.0	0.47	Surface settlement 0.001m.
	T2941	0.280		27.5	32.5	33.8	67.5	0.73	
	T2930	0.380		27.5	32.5	33.8	65.0	1.01	
	T2757	0.580		27.5	32.5	33.8	67.5	1.53	
	T2756	0.680		27.5	32.5	35.0	70.0	1.92	
42	T2756	0.030	I	31.3	32.5	640.0	640	0.20	Elapsed times in excess of 500 seconds estimated by extrapolation. Surface settlement 0.025m.
	T2757	0.180		31.3	33.8	390.0	640	1.34	
	T2930	0.380		31.3	33.8	241.2	640	2.98	
	T2941	0.580		31.3	33.8	138.8	640	4.55	
	T2943	0.780		31.3	33.8	40.0	640	6.14	

Table 6.1 Results of tests performed to assess influence of excess pore pressure magnitude

Test No	Transducer No	Initial depth (m)	Class of response	Elapsed times (sec) t_1	t_2	t_3	t_4	Excess pore pressure (kN/m^2) $\bar{u}_1$	Comments
A	T2756	0.282	I	33.8	36.3	175.5	395.0	2.10	Surface settlement 0.013m.
	T2757	0.382		33.8	35.0	95.0	435.0	2.97	
	T2930	0.482		33.8	35.0	76.3	437.8	3.76	
	T2941	0.582		33.8	35.0	55.0	406.3	4.64	
	T2943	0.682		33.8	35.0	37.5	406.3	5.27	
D	T2943	0.181	I	31.3	36.3	405.0	660	1.36	Elapsed times in excess of 500
	T2941	0.281		31.3	33.8	340.0	660	2.13	seconds estimated by extrapolation.
	T2930	0.381		31.3	33.8	280.0	660	2.94	Surface settlement 0.022m.
	T2757	0.581		31.8	33.8	151.3	660	4.71	
	T2756	0.681		31.8	33.8	96.3	660	5.43	
42	T2756	0.030	I	31.3	32.5	640.0	640	0.20	Elapsed times in excess of 500
	T2757	0.180		31.3	33.8	390.0	640	1.34	seconds estimated by extrapolation.
	T2930	0.380		31.3	33.8	241.2	640	2.98	ation. Surface settlement 0.025m.
	T2941	0.580		31.3	33.8	138.8	640	4.55	
	T2943	0.780		31.3	33.8	40.0	640	6.14	

Table 6.2 Results of tests performed to assess significance of period of excess pore pressure generation

Test No	Transducer No	Initial depth (m)	Class of response	Elapsed times (sec) t_1	t_2	t_3	t_4	Excess pore pressure (kN/m^2) $\bar{u}_1$	Comments
0	T2943	0.120	II	30.0	31.0	33.8	48.8	1.35	Surface settlement zero.
	T2941	0.220		30.0	32.5	33.8	47.5	2.67	
	T2930	0.320		30.0	32.5	33.8	51.3	3.91	
	T2757	0.420		30.0	32.5	33.8	52.5	5.06	
	T2756	0.520		30.0	32.5	35.0	50.0	6.26	
42	T2756	0.030	I	31.3	32.5	640.0	640	0.20	Elapsed times in excess of 500
	T2757	0.180		31.3	33.8	390.0	640	1.34	seconds estimated by extrapolation
	T2930	0.380		31.3	33.8	241.2	640	2.98	Surface settlement 0.025m.
	T2941	0.580		31.3	33.8	138.8	640	4.55	
	T2943	0.780		31.3	33.8	40.0	640	6.14	
43	T2756	0.013	II	32.5	33.8	53.8	66.3	0.08	Class of response intermediate
	T2757	0.113	(I/II)	31.3	33.8	41.3	62.5	0.94	between I and II. The response has
	T2930	0.313		31.3	32.5	35.0	73.8	2.81	been classified as class II for
	T2941	0.513		31.3	32.5	35.0	75.0	5.12	detailed description. Surface
	T2943	0.713		31.3	32.5	35.0	77.5	7.38	settlement zero.
44	T2756	0.010	I	36.3	43.8			0.11	Dissipation at pore pressures
	T2757	0.135		36.3	40.0	150.0	274.5	1.08	monitored by T2756 difficult to
	T2930	0.335		36.3	40.0	110.0	247.5	2.80	describe with times t_3 and t_4.
	T2941	0.535		36.3	37.5	92.5	247.5	4.69	Surface settlement 0.005m.
	T2943	0.735		36.3	37.5	41.3	280.0	6.57	

Table 6.3 Results of tests performed to assess influence of soil state

Test No	Transducer No	Initial depth (m)	Class of response	Elapsed times (sec) t_1	t_2	t_3	t_4	t_5	t_6	t_7	t_8	Excess pore pressure (kN/m^2) $\bar{u}_1$	$\bar{u}_2$	$\bar{u}_3$	Comments
89	T2943	0.078	I	33.8	35.0	630	710					0.52			Elapsed times in excess of 500
	T2756	0.278	(vane)	35.0	36.3	355.0	710					2.01			seconds estimated by extrapolation.
	T2941	0.478		33.8	36.3	185.0	710					3.59			Surface settlement 0.026m. No
	T2757	0.628		35.0	36.3	85.0	710					4.91			resistance to rotation.
	T2930	0.778		33.8	36.3	36.3	710					5.56			
90	T2943	0.078	II	28.8	32.5	460.0	580					0.55			Elapsed times in excess of 500
	T2756	0.278	(vane)	30.0	32.5	240.0	580					2.01			seconds estimated by extrapolation.
	T2941	0.478		30.0	32.5	100.0	580					3.62			Surface settlement 0.021. No
	T2757	0.628		30.0	32.5	45.0	580					4.85			resistance to rotation.
	T2930	0.778		30.0	32.5	32.5	580					5.06			
91	T2756	0.078	I	28.8	33.8	440.0	620					0.51			Elapsed times in excess of 500
	T2943	0.278	(vane)	28.8	33.8	215.0	620					2.05			seconds estimated by extrapolation.
	T2757	0.478		28.8	35.0	90.0	620					3.75			Surface settlement 0.020m. No
	T2941	0.628		28.8	33.8	33.8	620					4.68			resistance to rotation.
	T2930	0.778		28.8	33.8	33.8	620					5.00			
92	T2756	0.076	Ia	30.0	38.8	450.0	600					0.51			Elapsed times in excess of 500 seco-
	T2943	0.276	(vane)	28.8	38.8	227.5	600					2.02			nds estimated by extrapolation. Re-
	T2757	0.476		30.0	38.8	100.0	600					3.72			sults difficult to interpret for
	T2941	0.626		28.8	33.8		600	52.5	53.8	53.8	87.5	4.38	4.65	3.75	T2941 and T2930. Surface settlement
	T2930	0.776		30.0	33.8		600	52.5	53.8	53.8	87.5	4.50	4.94	3.75	0.021m. No resistance to rotation.
93	T2756	0.078	Ia	30.0	40.0	490.0	600					0.51			Elapsed time in excess of 500
	T2943	0.278	(vane)	28.8	38.8	240.0	600					2.02			seconds estimated by extrapolation.
	T2757	0.478		30.0	40.0	75.0	600	93.8	96.3	106.3	165	3.75	3.75	2.9	Surface settlement 0.021m. No
	T2941	0.628		30.0	36.3	38.8	600	93.8	96.3	96.3	165	4.35	4.32	2.9	resistance to rotation.
	T2930	0.778		30.0	36.3	38.8	600	93.8	96.3	96.3	165	4.47	4.50	2.9	

Table 6.4 Results of tests performed to assess influence of vane rotation rate

Test No	Transducer No	Initial depth (m)	Class of response	Elapsed times (sec) t_1	t_2	t_3	t_4	t_5	t_6	Excess pore pressure (kN/m^2) $\bar{u}_1$	$\bar{u}_2$	Comments
91	T2756	0.078	I	28.8	33.8	440.0	620			0.51		Elapsed times in excess of 500
	T2943	0.278	(vane)	28.8	33.8	215.0	620			2.05		seconds estimated by extrapolation.
	T2757	0.478		28.8	35.0	90.0	620			3.75		Surface settlement 0.021m. No
	T2941	0.628		28.8	33.8	33.8	620			4.68		resistance to rotation.
	T2930	0.778		28.8	33.8	33.8	620			5.00		
94	T2756	0.055	V	31.3	32.5	35.0	36.3	42.5		0.08	-0.11	Surface settlement zero. Slight
	T2943	0.205	(vane)	30.0	32.5	35.0	36.3	41.3		0.18	-0.33	resistance to rotation.
	T2757	0.405		30.0	32.5	35.0	36.3	42.5		0.27	-0.60	
	T2941	0.555		30.0	32.5	35.0	36.3	42.5		0.53	-1.28	
	T2930	0.705		30.0	32.5	35.0	36.3	40.0		0.41	-1.17	
95	T2943	0.073	IV	28.8	31.3	32.5	33.8	37.5	53.8	0.27	-0.06	Surface settlement zero. Moderate
	T2756	0.223	(vane)	30.0	31.3	32.5	33.8	37.5	62.5	0.67	-0.11	resistance to rotation.
	T2941	0.423		28.8	31.3	32.5	33.8	36.3	57.5	1.31	-0.12	
	T2757	0.573		28.8	31.3	32.5	33.8	36.3	65.0	1.77	-0.60	
	T2930	0.723		30.0	31.3	32.5	33.8	36.3	71.3	1.92	-0.09	
96	T2943	0.045	I	28.8	35.0	188.7	242.5			0.33		Surface settlement 0.005m. No
	T2756	0.245	(vane)	28.8	47.5	112.5	265.0			1.87		resistance to rotation.
	T2941	0.445		28.8	52.5	72.5	267.5			3.53		
	T2757	0.595		28.8	41.3	43.8	265.0			4.72		
	T2930	0.745		28.8	36.3	36.3	266.3			4.85		

Table 6.5 Results of tests performed with a 1:1 vane to examine the effect of soil state (continued in Table 6.6)

Test No	Transducer No	Initial depth (m)	Class of response	Elapsed times (sec) t_1	t_2	t_3	t_4	t_5	Excess pore pressure (kN/m^2) $\bar{u}_1$	$\bar{u}_2$	Comments
97	T2943	0.031	V	28.9	31.3	33.5	35.0	36.3	0.03	-0.21	Surface settlement zero. Slight
	T2756	0.181	(vane)	30.0	32.5	34.5	35.0	41.3	0.29	-1.04	resistance to rotation.
	T2941	0.381		28.8	31.3	33.5	35.0	41.3	0.32	-1.66	
	T2930	0.681		30.0	31.3	34.0	35.0	41.3	0.50	-2.34	
98	T2943	0.025	Va	30.0	31.3	35.0	36.3	38.8	0.03	-0.28	Surface settlement zero. Very large
	T2756	0.175	(vane)	30.0	32.5	35.0	37.5	48.8	0.43	-1.84	resistance to rotation. 30° to 40°
	T2941	0.325		28.8	32.5	35.0	36.3	46.3	0.77	-2.79	rotation achieved with a 20° recoil
	T2757	0.475		30.0	32.5	35.0	36.3	46.3	1.06	-4.24	observed on release.
	T2930	0.625		30.0	32.5	35.0	36.3	46.3	1.13	-3.84	
99	T2943	0.043	Va	28.8	31.3	34.2	35.0	40.0	0.21	-0.70	Surface settlement zero. Initial
	T2756	0.193	(vane)	30.0	31.3	34.8	36.3	45.0	0.81	-2.30	resistance large, but reduced
	T2941	0.343		28.8	31.3	34.5	35.0	45.0	1.62	-3.91	with rotation.
	T2757	0.493		28.8	31.3	34.5	35.0	43.8	2.07	-7.30	
	T2930	0.643		28.8	31.3	34.5	35.0	45.0	2.14	-5.61	

Table 6.6 Results of tests performed with a 1:1 vane to examine the effect of soil state (continued from Table 6.5)

Test No	Transducer No	Initial depth (m)	Class of response	Elapsed times (sec) t_1	t_2	t_3	t_4	t_5	t_6	Excess pore pressure (kN/m^2) $\bar{u}_1$	$\bar{u}_2$	Comments
100	T2756	0.054	I	28.8	32.5	500	640			0.49		Elapsed times in excess of 500
	T2943	0.254	(vane)	28.8	32.5	225.0	640			0.26		seconds estimated by extrapolation.
	T2930	0.454		28.8	32.5	90.0	640			3.65		Surface settlement 0.020m. No
	T2941	0.593		28.8	33.8	33.8	640			4.61		resistance to rotation.
101	T2756	0.026	V	30.0	32.5	34.9	36.3	38.8		0.03	-0.23	Surface settlement zero. Large
	T2943	0.176	(vane)	28.8	31.3	34.8	36.3	40.0		0.19	-0.79	resistance to rotation. 85°
	T2930	0.376		28.8	32.5	34.8	36.3	41.3		0.35	-1.73	rotation achieved with a 5° recoil
	T2941	0.507		28.8	31.3	34.8	36.3	40.0		0.46	-2.82	observed on release.
102	T2756	0.040	II	30.0	36.3	113.8	178.7			0.30		Surface settlement 0.002m. No
	T2943	0.240	(vane)	28.8	50.0	78.8	182.5			1.87		resistance to rotation.
	T2930	0.440		28.8	50.0	63.8	185.0			3.54		
	T2941	0.579		28.8	37.5	40.0	185.0			4.36		
103	T2756	0.068	III	30.0	33.8	36.3	73.8			0.20		Surface settlement zero. Slight
	T2943	0.218	(vane)	28.8	33.8	36.3	53.8			0.52		resistance to rotation.
	T2930	0.418		30.0	32.5	36.3	67.5			0.96		
	T2941	0.577		28.8	32.5	35.0	63.8			1.25		
104	T2756	0.055	IV	28.8	31.3	32.5	33.8	35.0	40.0	0.10	-0.07	Surface settlement zero. Slight
	T2943	0.205	(vane)	28.8	30.0	32.5	33.8	35.0	42.5	0.19	-0.26	resistance to rotation.
	T2930	0.405		28.8	30.0	32.5	33.8	35.0	47.5	0.38	-0.42	
	T2941	0.544		28.8	30.0	32.5	33.8	35.0	48.8	0.58	-1.30	

Table 6.7 Results of tests performed to assess influence of vane geometry (2:1 ratio vane) (continued in Table 6.8)

Test No	Transducer No	Initial depth (m)	Class of response	Elapsed times (sec) t_1	t_2	t_3	t_4	t_5	t_6	Excess pore pressure (kN/m^2) $\bar{u}_1$	$\bar{u}_2$	Comments
105	T2756	0.076	I	28.8	32.5	560	680			0.49		Elapsed times in excess of 500
	T2943	0.276	(vane)	28.8	32.5	297.5	680			2.04		seconds estimated by extrapolation.
	T2930	0.476		28.8	33.8	112.5	680			3.62		Surface settlement 0.002m. No
	T2941	0.638		28.8	33.8	43.7	680			5.05		resistance to rotation.
106	T2756	0.066	IV	30.0	31.3	35.0	35.0	36.3	38.8	0.03	-0.13	Surface settlement zero. Moderate
	T2943	0.204	(vane)	28.8	31.3	32.5	33.8	35.0	40.0	0.11	-0.30	resistance to rotation.
	T2930	0.404		30.0	31.3	33.8	33.8	36.3	42.5	0.27	-0.57	
	T2941	0.566		28.8	31.3	32.5	32.5	35.0	56.3	0.54	-1.19	
107	T2756	0.037	I	28.8	35.0	242.5	202.5			0.23		Surface settlement 0.003m. Slight
	T2943	0.237	(vane)	28.8	35.0	102.5	231.3			1.85		resistance to movement.
	T2930	0.437		28.8	35.0	87.5	232.5			3.47		
	T2941	0.599		28.8	35.0	55.0	263.8			4.83		
108	T2756	0.063	IV	28.8	31.3	32.5	35.0	37.5	46.3	0.13	-0.07	Surface settlement zero. Moderate
	T2943	0.213	(vane)	28.8	30.0	32.5	33.8	36.3	51.3	0.33	-0.26	resistance to rotation. 90° rotation
	T2930	0.413		28.8	30.0	32.5	32.5	36.3	51.3	0.65	-0.39	achieved with a small recoil observed
	T2941	0.575		28.8	30.0	32.5	33.8	35.0	55.0	1.01	-1.69	on release.
109	T2756	0.027	V	28.8	32.5	34.5	35.0	50.0		0.07	-0.20	Surface settlement zero. Large
	T2943	0.177	(vane)	28.8	31.3	33.5	35.0	38.8		0.18	-0.84	resistance to rotation. Resistance
	T2930	0.377		28.8	32.5	34.5	35.0	41.3		0.46	-1.81	to rotation reduced after initial
	T2941	0.539		28.8	31.3	33.8	35.0	41.3		0.56	-3.39	peak value.

Table 6.8 Results of tests performed to assess influence of vane geometry (1:2 ratio vane) (continued from Table 6.7)

Test No	Transducer No	Initial depth (m)	Class of response	Elapsed times (sec) t_1	t_2	t_3	t_4	Excess pore pressure (kN/m^2) $\bar{u}_1$	$\bar{u}_2$	Comments
110	T2756	0.067	I	27.5	32.5	670	720	0.59		Elapsed times in excess of 500
	T2943	0.267	(cone)	27.5	40.0	466.3	720	2.09		seconds estimated by extrapolation.
	T2930	0.467		27.5	47.5	232.5	720	3.74		Surface settlement 0.023m.
	T2941	0.617		27.5	52.5	82.5	720	4.93		Penetration into bed 0.682m.
112	T2756	0.029	IV	28.8		32.5	85.0		-0.85	Surface settlement -0.001m. Partial
	T2943	0.179	(cone)	28.8	30.0	33.8	85.0	0.18	-0.48	penetration of 0.094m achieved.
	T2930	0.379		28.8	32.5	36.3	85.0	0.42	-0.38	
	T2941	0.529		28.8	32.5	36.3	85.0	0.43	-0.36	
114	T2756	0.051	III	30.0		47.5	102.5	0.33	-0.07	Surface settlement -0.001m. Partial
	T2943	0.201	(cone)	31.3	32.5	36.3	110.0	1.15		penetration of 0.211m achieved.
	T2930	0.401		30.0		37.5	105.0	1.19		
	T2941	0.551		30.0		37.5	110.0	2.18		
116	T2756	0.064	I	30.0	36.3	73.8	430.0	0.56		Surface settlement 0.003m.
	T2943	0.214	(cone)	30.0	45.0	245.0	430.0	1.85		Penetration into bed 0.637m.
	T2930	0.414		30.0	50.0	220.0	455.0	3.62		
	T2941	0.564		30.0	52.5	315.0	452.5	4.86		
118	T2756	0.041	III	32.5	36.3		41.3		-0.39	Surface settlement -0.001m. Partial
	T2943	0.190	(cone)	31.3		35.0	43.8	0.89		penetration of 0.100m achieved.
	T2930	0.390		32.5		36.3	53.8	1.14		
	T2941	0.540		31.3		36.3	68.8	1.32		
120	T2756	0.080	I	37.5	52.5	122.5	640	0.65		Elapsed times in excess of 500
	T2943	0.230	(cone)	36.3	52.5	268.8	640	2.00		seconds estimated by extrapolation.
	T2930	0.430		37.5	61.3	365.0	640	3.70		Surface settlement 0.009m.
	T2941	0.580		37.5	61.3	491.3	640	4.96		Penetration into bed 0.666m.

Table 6.9 Results of tests in which 1:1 ratio vane driven into a soil bed prior to rotation

Test No	Transducer No	Initial depth (m)	Class of response	Elapsed times (sec) t_1	t_2	t_3	t_4	t_5	Excess pore pressure (kN/m^2) $\bar{u}_1$	$\bar{u}_2$	Comments
111	T2756	0.064	I	30.0	31.3	277.5	352.5		0.26		Surface settlement 0.009m. Slight
	T2943	0.264	(vane)	28.8	41.3	133.8	386.3		1.87		resistance to rotation.
	T2930	0.464		28.8	48.8	82.5	386.3		3.55		
	T2941	0.614		28.8	46.3	50.0	370.0		4.75		
113	T2756	0.030	V	30.0	31.3	34.5	37.5	53.8	0.13	-0.53	Surface settlement zero. Slight/
	T2943	0.180	(vane)	28.8	31.3	34.5	36.3	66.3	0.15	-1.15	moderate resistance to rotation.
	T2930	0.380		30.0	32.5	35.0	37.5	52.5	0.15	-0.72	
	T2941	0.053		30.0	32.5	35.0	37.0	66.3	0.14	-0.68	
115	T2756	0.052	III	35.0	37.5	41.3	77.5		0.36		Surface settlement 0.001m. Moderate
	T2943	0.202	(vane)	33.8	37.5	40.0	71.3		1.04	-0.15	resistance to rotation.
	T2930	0.402		35.0	37.5	41.3	83.8		0.91	-0.04	
	T2941	0.552		35.0	37.5	41.3	80.0		0.89		
117	T2756	0.061	II	30.0	37.5	43.8	103.8		0.43		Surface settlement 0.001m. Slight
	T2943	0.211	(vane)	28.8	38.8	42.5	118.8		1.48		resistance to rotation.
	T2930	0.411		28.8	37.5	41.3	112.5		2.74		
	T2941	0.561		28.8	36.3	38.8	118.8		3.61		
119	T2756	0.042	V	30.0	31.3	34.5	36.3	72.5	0.20	-0.95	Surface settlement zero. Slight
	T2943	0.191	(vane)	28.8	31.3	34.5	37.5	60.0	0.26	-0.85	resistance to rotation.
	T2930	0.391		28.8	31.3	35.7	37.5	62.5	0.23	-0.72	
	T2941	0.541		28.8	31.3	35.7	37.5	62.5	0.21	-0.68	
121	T2756	0.079	I	60.0	62.5	266.3	380.0		0.55		Surface settlement 0.006m. Slight
	T2943	0.221	(vane)	58.8	62.5	196.2	392.5		1.82		resistance to rotation.
	T2930	0.421		58.8	62.5	167.5	380		3.47		
	T2941	0.579		58.8	62.5	107.5	380		4.79		

Table 6.10 Results of tests in which 1:1 ratio vane rotated following driving into a soil bed

Test No	Transducer No	Initial depth (m)	Class of response	Elapsed times (sec) t_1	t_2	t_3	t_4	t_5	t_6	Excess pore pressure (kN/m^2) $\bar{u}_1$	$\bar{u}_2$	Comments
140	T2756	0.100	I	30.0	32.5	170.0	315.0			0.69		Surface settlement 0.011m. No
	T2943	0.250	(vane)	28.8	31.3	82.5	315.0			1.85		resistance to rotation.
	T2930	0.400		30.0	32.5	40.0	295.0			2.87		
	T2941	0.438		28.8	31.3	35.0	300.0			3.10		
	T3201	0.438		30.0	33.8	40.0	282.5			3.21		
141	T2756	0.074	I	30.0	33.8	75.0	137.5			0.53		Surface settlement 0.002m. Slight
	T2943	0.224	(vane)	28.8	33.8	60.0	136.3			1.70		resistance to rotation.
	T2930	0.374		28.8	35.0	43.8	150.0			2.82		
	T2941	0.412		28.8	33.8	38.8	150.0			3.09		
	T3201	0.412		28.8	33.8	45.0	131.3			2.91		
142	T2756	0.040	IV	30.0	31.3	33.0	33.0	37.5	46.3	0.10	-0.07	Surface settlement zero. Moderate
	T2943	0.190	(vane)	28.8	31.3	32.5	32.5	36.3	48.8	0.48	-0.19	resistance to rotation. A recoil
	T2930	0.340		30.0	31.3	33.0	33.0	36.3	53.8	0.91	-0.69	of less than 5° was observed on
	T2941	0.378		28.8	31.3	32.5	32.5	36.3	52.5	1.01	-0.83	release.
	T3201	0.378		30.0	31.3	33.3	33.6	36.3	47.5	0.95	-1.29	
143	T2756	0.040	IV	30.0	31.3	33.8	37.5	38.9	43.8	0.07	-0.07	Surface settlement zero. Moderate
	T2943	0.190	(vane)	28.8	30.0	32.5	36.3	37.5	53.8	0.37	-0.15	resistance to rotation.
	T2930	0.340		28.8	31.3	32.5	36.3	38.8	55.0	0.69	-0.46	
	T2941	0.378		28.8	30.0	32.5	36.3	38.8	53.8	0.83	-0.50	
	T3201	0.378		28.8	31.3	32.5	35.0	38.8	55.0	0.84	-0.95	

Table 6.11 Results of tests performed with pore pressure monitoring on the shaft of the 1:1 ratio piezovane (continued in Table 6.12)

Test No	Transducer No	Initial depth (m)	Class of response	Elapsed times (sec) t_1	t_2	t_3	t_4	t_5	t_6	Excess pore pressure (kN/m^2) $\bar{u}_1$	$\bar{u}_2$	Comments
144	T2756	0.057	IV	28.8	30.0	31.3	32.5	36.3	62.5	0.23	-0.03	Surface settlement zero. Slight/
	T2943	0.207	(vane)	28.8	30.0	31.3	32.5	35.0	62.5	0.78	-0.11	moderate resistance to rotation.
	T2930	0.357		28.8	30.0	31.3	32.5	35.0	62.5	1.33	-0.38	
	T2941	0.395		28.8	30.0	31.3	32.5	35.0	66.3	1.51	-0.68	
	T3201	0.395		28.8	30.0	32.0	32.0	35.0	67.5	1.57	-1.18	
145	T2756	0.030	IV	30.0	31.3	32.5	33.0	35.0	37.5	0.03	-0.17	Surface settlement zero. Initial
	T2943	0.187	(vane)	28.8	30.0	32.5	32.5	35.0	41.3	0.15	-0.41	resistance to rotation large, but
	T2930	0.337		28.8	31.3	32.5	33.8	35.0	41.3	0.42	-1.14	reduced with further rotation.
	T2941	0.368		28.8	30.0	32.5	33.8	35.0	42.5	0.36	-1.04	
	T3201	0.358		28.8	31.3	32.5	33.8	35.0	42.5	0.67	-2.07	
146	T2756	0.063	IV	28.8	31.3	32.5	33.8	35.0	38.8	0.10	-0.40	Surface settlement zero. Large
	T2943	0.163	(vane)	28.8	30.0	32.5	33.8	35.0	40.0	0.22	-1.07	resistance to rotation. A 5° to
	T2930	0.313		28.8	30.0	32.5	33.8	35.0	41.3	0.57	-2.51	10° recoil was observed on release.
	T2941	0.351		28.8	30.0	32.5	33.8	35.0	41.3	0.47	-3.48	
	T3201	0.351		28.8	30.0	33.8	33.8	35.0	41.3	1.18	-3.48	
147	T2756	0.046	V	30.0	33.8	37.2	37.5	41.3		0.07	-0.80	Surface settlement zero. Initial
	T2943	0.146	(vane)	28.8	32.5	35.8	36.3	40.0		0.26	-2.20	resistance to rotation very large,
	T2930	0.296		28.8	32.5	36.5	37.5	42.5		0.26	-4.22	but reduced with further rotation.
	T2941	0.334		28.8	32.5	35.8	36.3	41.3		0.43	-5.04	
	T3201	0.334		28.8	32.5	37.0	37.5	42.5		0.40	-4.26	

Table 6.12 Results of tests performed with pore pressure monitoring on the shaft of the 1:1 ratio piezovane (continued from Table 6.11)

Test No	Transducer No	Initial depth (m)	Class of response	Elapsed times (sec) t_1	t_2	t_3	t_4	t_5	t_6	Excess pore pressure (kN/m^2) $\bar{u}_1$	$\bar{u}_2$	Comments
148	T2756	0.096	I	30.0	32.5	175.8	333.8			0.65		Surface settlement 0.012m. No resistance to rotation.
	T2943	0.296	(vane)	28.8	31.3	66.3	340.0			2.20		
	T2930	0.396		30.0	32.5	38.8	351.3			2.96		
	T2941	0.434		28.8	31.3	37.5	351.3			3.13		
	T3201	0.434		30.0	33.8	40.0	326.3			3.12		
149	T2756	0.046	V	30.0	33.8	40.0	40.0	43.8		0.13	-0.65	Surface settlement zero. Initial resistance very large, reduced with further rotation. A 5° to 10° recoil was observed on release.
	T2943	0.196	(vane)	28.8	32.5	38.8	38.8	47.5		0.48	-2.27	
	T2930	0.296		28.8	32.5	40.0	40.0	47.5		0.39	-2.96	
	T2941	0.334		28.8	32.5	38.8	38.8	46.3		0.58	-3.89	
	T3201	0.334		28.8	33.8	40.0	40.0	47.5		0.52	-3.35	
151	T2756	0.056	IV	30.0	31.3	33.8	33.8	36.3	50.0	0.23	-0.07	Surface settlement zero. Slight/moderate resistance to rotation.
	T2943	0.256	(vane)	28.8	30.0	32.5	32.5	35.0	53.8	0.92	-0.11	
	T2930	0.356		30.0	31.3	33.8	33.8	35.0	55.0	1.31	-0.12	
	T2941	0.394		30.0	31.3	32.5	32.5	35.0	53.8	1.48	-0.07	
	T3201	0.394		30.0	31.3	33.8	33.8	36.3	50.0	1.39	-0.46	
152	T2756	0.062	IV	28.8	30.0	31.3	32.5	37.5	68.8	0.29	-0.03	Surface settlement zero. Slight/moderate resistance to rotation. A recoil of less than 5° was observed on release.
	T2943	0.262	(vane)	28.8	30.0	31.3	31.3	35.0	73.8	1.07	-0.04	
	T2930	0.362		28.8	30.0	31.3	32.5	35.0	60.0	1.41	-0.27	
	T2941	0.400		28.8	30.0	30.8	30.8	35.0	73.8	1.62	-0.22	
	T3201	0.400		28.8	30.0	31.3	31.3	36.3	56.3	1.49	-0.61	

Table 6.13 Results of tests performed with pore pressure monitoring on the blade of the 1:1 ratio piezovane (continued in Table 6.14)

Test No	Transducer No	Initial depth (m)	Class of response	Elapsed times (sec) t_1	t_2	t_3	t_4	t_5	t_6	Excess pore pressure (kN/m^2) $\bar{u}_1$	$\bar{u}_2$	Comments
154	T2756	0.077	I	30.0	33.8	120.0	200.0			0.56		Surface settlement 0.004m. No
	T2943	0.277	(vane)	28.8	33.8	62.5	198.7			2.15		resistance to rotation.
	T2930	0.377		30.0	33.8	47.5	197.5			2.90		
	T2941	0.415		28.8	33.8	37.5	206.2			3.13		
	T3201	0.415		30.0	33.8	50.0	200.0			2.93		
155	T2756	0.058	IV	30.0	31.3	32.5	33.8	37.5	56.3	0.26	-0.03	Surface settlement zero. Slight/
	T2943	0.258	(vane)	30.0	31.3	32.5	33.8	36.3	55.0	1.04	-0.15	moderate resistance to rotation.
	T2930	0.358		30.0	31.3	32.5	33.8	36.3	58.8	1.45	-0.34	
	T2941	0.396		30.0	31.3	32.5	33.8	36.3	55.0	1.62	-0.54	
	T3201	0.396		30.0	31.3	32.5	33.5	37.5	60.0	1.65	-1.08	
156	T2756	0.075	V	28.8	31.3	32.8	35.0	37.5		0.10	-0.33	Surface settlement zero. Moderate
	T2943	0.225	(vane)	28.8	30.0	32.0	33.8	40.0		0.37	-1.04	resistance to rotation. A recoil of
	T2930	0.325		28.8	30.0	32.5	33.8	42.5		0.61	-1.56	less than 5° was observed on release.
	T2941	0.363		28.8	30.0	32.2	33.8	40.0		0.83	-3.03	
	T3201	0.363		28.8	31.3	33.0	33.8	40.0		0.34	-1.31	

Table 6.14 Results of tests performed with pore pressure monitoring on the blade of 1:1 ratio piezovane (continued from Table 6.13)

Test No	Transducer No	Initial depth (m)	Class of response	Elapsed times (sec) t_1	t_2	t_3	t_4	Excess pore pressure (kN/m^2) $\bar{u}_1$	Comments
122	T2756	0.122	II	30.0	31.3	111.3		0.72	Surface settlement 0.001m. Membrane pressure 22.8kN/m^2.
	T2943	0.322	(ex.mem)	28.8	30.0	102.5		1.81	
	T2930	0.522		28.8	31.3	101.3		2.59	
	T2941	0.622		28.8	30.0	102.5		4.25	
124	T2756	0.123	III						Surface settlement zero. Membrane pressure 11.7kN/m^2.
	T2943	0.323	(ex.mem)						
	T2930	0.523							
	T2941	0.623							
125	T2756	0.123	I	30.0	31.3	330.0	580	0.836	Elapsed times in excess of 500 seconds are as estimated by extrapolation of plotted data. Surface settlement 0.017m. Membrane pressure 25.5kN/m^2.
	T2943	0.323	(ex.mem)	28.8	30.0	136.3	580	2.46	
	T2930	0.523		28.8	30.0	45.0	580	4.08	
	T2941	0.623		28.8	30.0	41.3	580	4.89	
127	T2756	0.123	I	30.0	31.3	478.8	640	0.836	Elapsed times in excess of 500 seconds are as estimated by extrapolation of plotted data. Surface settlement 0.023m. Membrane pressure 25.5kN/m^2.
	T2943	0.323	(ex.mem)	28.8	30.0	162.5	640	2.46	
	T2930	0.523		28.8	31.3	85.0	640	4.04	
	T2941	0.623		28.8	30.0	46.3	640	4.92	
129	T2756	0.122	III						Surface settlement zero. Membrane pressure 19.3kN/m^2.
	T2943	0.322	(ex.mem)						
	T2930	0.522							
	T2941	0.622							

Table 6.15 Results of tests performed to assess the effect of expanding membrane pressure

Test No	Transducer No	Initial depth (m)	Class of response	Elapsed times (sec) t_1	t_2	t_3	t_4	Excess pore pressure (kN/m^2) $\bar{u}_1$	Comments
132	T2756	0.062	I	30.0	31.3	442.5	580	0.43	Elapsed times in excess of 500 seconds are as estimated by extrapolation of plotted data. Surface settlement 0.018m. Membrane pressure 29.0kN/m^2.
	T2943	0.362	(ex.mem)	28.8	31.3	140.0	580	2.73	
	T2930	0.562		30.0	31.3	31.3	580	4.30	
	T2941	0.662		28.8	30.0	30.0	580	5.20	
133	T2756	0.067	II	30.0	31.3	37.5		0.13	Surface settlement zero. Membrane pressure 31.7kN/m^2.
	T2943	0.267	(ex.mem)	28.8	31.3	36.3		0.36	
	T2930	0.467		30.0	31.3	37.5		0.67	
	T2941	0.567		28.8	31.3	40.0		0.74	
134	T2756	0.032	II	31.3	32.5	36.3		0.07	Surface settlement zero. Membrane pressure 32.4kN/m^2.
	T2943	0.232	(ex.mem)	30.0	31.3	40.0		0.29	
	T2930	0.432		30.0	32.5	40.0		0.41	
	T2941	0.532		30.0	32.5	38.8		0.39	
135	T2756	0.084	II	30.0	31.3	43.8		0.26	Surface settlement zero. Membrane pressure 31.7kN/m^2.
	T2943	0.284	(ex.mem)	28.8	30.0	45.0		0.91	
	T2930	0.484		28.8	30.0	45.0		1.06	
	T2941	0.584		28.8	30.0	45.0		1.96	
136	T2756	0.108	II	30.0	31.3	56.3		0.81	Surface settlement zero. Membrane pressure 29.0kN/m^2.
	T2943	0.308	(ex.mem)	28.8	30.0	61.3		2.43	
	T2930	0.508		30.0	31.3	57.5		3.96	
	T2941	0.608		28.8	30.0	60.0		4.78	

Table 6.16 Results of tests performed with an expanding membrane probe to examine the effect of soil state

Test No	Transducer No	Initial depth (m)	Class of response	Elapsed times (sec) t_1	t_2	t_3	t_4	Excess pore pressure (kN/m^2) $\bar{u}_1$	Comments
54	T2930	0.079	I	43.8	47.5	590	700	0.58	Cone entered bed at 45 seconds and came to rest at 75 seconds. Elapsed times in excess of 500 seconds are estimated by extrapolation of plotted data. Penetration into bed 0.770m. Surface settlement 0.026m.
	T2757	0.179	(cone)	43.8	52.5	457.5	700	1.37	
	T2941	0.279		43.8	57.5	373.8	700	2.15	
	T2756	0.479		43.8	67.5	202.5	700	3.85	
	T2943	0.679		43.8	71.3	86.3	700	5.50	
55	T2930	0.076	I	45.0	47.5	620	670	0.55	Cone entered bed at 47 seconds and came to rest at 54.5 seconds. Elapsed times in excess of 500 sec. are estimated by extrapolation of plotted data. Penetration into bed 0.600m. Surface settlement 0.030m.
	T2757	0.176	(cone)	45.0	48.8	515	670	1.34	
	T2941	0.276		45.0	51.3	412.5	670	2.15	
	T2756	0.476		45.0	53.8	230.0	670	3.79	
	T2943	0.676		45.0	55.0	78.8	670	5.41	
56	T2930	0.075	I	30.0	31.3	570	620	0.56	Cone entered bed at 33 seconds and came to rest at 36 seconds. Elapsed times in excess of 500 seconds are estimated by extrapolation of plotted data. Penetration into bed 0.600m. Surface settlement 0.033m.
	T2757	0.175	(cone)	30.0	31.3	471.3	620	1.33	
	T2941	0.275		28.8	33.8	380.0	620	2.17	
	T2756	0.475		30.0	35.0	220.0	620	3.72	
	T2943	0.675		28.8	36.3	78.8	620	5.49	
57	T2930	0.060	I	32.5	37.5	491.3	580	0.58	Cone entered bed at 32.5 seconds and came to rest at 145 seconds. Elapsed times in excess of 500 seconds are estimated by extrapolation of plotted data. Penetration into bed 0.750m. Surface settlement 0.020m.
	T2757	0.160	(cone)	32.5	46.3	373.8	580	1.30	
	T2941	0.260		32.5	71.3	320.0	580	2.14	
	T2756	0.460		32.5	106.3	212.5	580	3.78	
	T2943	0.660		32.5	142.5	153.8	580	5.46	

Table 6.17 Results of tests performed in very loose soil to assess the influence of cone penetration rate (continued in Table 6.18)

Test No	Transducer No	Initial depth (m)	Class of response	Elapsed times (sec) t_1	t_2	t_3	t_4	Excess pore pressure (kN/m^2) $\bar{u}_1$	Comments
67	T2930	0.075	II	37.5	75	480	502.5	0.45	Cone entered bed at 37 seconds and came to rest at 480 seconds. Elapsed times and $\bar{u}$ values are taken from a simplified plot of test data, refer Figure 6.27. Penetration into bed 0.770m. Surface settlement 0.010m.
	T2757	0.175	(cone)	37.5	140	480	517.5	1.00	
	T2941	0.275		37.5	180	480	528.7	1.40	
	T2756	0.475		37.5	265	480	521.2	2.20	
	T2943	0.675		37.5	306	480	528.7	2.50	
69	T2930	0.180	I	1200	1204	1481	1560	0.38	Data presented is for the final stage of penetration (0.60-0.77m) 1200-1210 seconds. Elapsed times in excess of 1500 seconds estimated by extrapolation of plotted data. Total penetration into bed 0.770m. Surface settlement 0.030m.
	T2757	0.280	(cone)	1196	1204	1414	1560	1.17	
	T2941	0.380		1196	1200	1380	1560	2.07	
	T2756	0.580		1196	1204	1290	1560	3.77	
	T2943	0.680		1196	1207	1219	1560	5.52	
70	T2930	0.071	I		375	754	870	0.42	Data presented is for the final stage of penetration (0.60-0.77m) 370-380 seconds. t_1 is not presented because excess pore pressures were not initially zero, refer Fig. 6.32. Total penetration into bed 0.770m. Surface settlement 0.027m.
	T2757	0.171	(cone)		379	679	870	1.23	
	T2941	0.271			375	611	870	2.02	
	T2756	0.471			375	480	870	3.74	
	T2943	0.671			379	394	870	5.40	

Table 6.18 Results of tests performed in very loose soil to assess the influence of cone penetration rate (continued from Table 6.17)

Test No	Transducer No	Initial depth (m)	Class of response	Elapsed times (sec) t_1	t_2	t_3	t_4	t_5	Excess pore pressure (kN/m^2) $\bar{u}_1$	$\bar{u}_2$	Comments
63	T2930	0.013	Ia	32.5	37.5	170.0	250	70.0	0.13	0.13	Cone entered bed at 33 seconds and
	T2757	0.113	(cone)	32.5	43.8	153.8	250	70.0	0.91	0.94	came to rest at 70 seconds.
	T2941	0.313		32.5	55.0	113.8	250	70.0	2.78	2.63	Penetration into bed 0.710m.
	T2756	0.513		32.5	60.0	86.3	250	72.5	5.27	4.40	Surface settlement 0.008m.
	T2943	0.713		32.5	67.5	70.0	250	70.0	6.86	5.76	
85	T2930	0.055	Ia	30.0	38.8	243.7	340	40.0	0.50	0.47	Cone entered bed at 31 seconds and
	T2757	0.155	(cone)	30.0	38.8	186.2	340	40.0	1.49	1.30	came to rest at 40 seconds.
	T2941	0.305		30.0	35.0	140.0	340	40.0	3.44	2.58	Penetration into bed 0.688m.
	T2956	0.505		30.0	38.8	82.5	340	40.0	6.57	4.38	Surface settlement 0.005m.
	T2943	0.705		30.0	37.5	42.5	340	40.0	7.49	5.88	
86	T2930	0.054	Ia	31.3	68.8	172.5	250	97.5	0.44	0.47	Cone entered bed at 30 seconds and
	T2757	0.154	(cone)	31.3	66.3	138.8	250	97.5	1.30	1.33	came to rest at 96 seconds.
	T2941	0.304		31.3	72.5	115.0	250	97.5	2.82	2.61	Penetration into bed 0.688m.
	T2956	0.504		31.3	86.3	98.8	250	97.5	5.54	4.57	Surface settlement 0.004m.
	T2943	0.704		31.3	96.3	98.8	250	97.5	7.09	5.09	

Table 6.19 Results of tests performed in medium dense soil to assess the influence of cone penetration rate (continued in Table 6.20)

Test No	Transducer No	Initial depth (m)	Class of response	Elapsed times (sec) t_1	t_2	t_3	t_4	t_5	Excess pore pressure (kN/m^2) $\bar{u}_1$	$\bar{u}_2$	Comments
87	T2930	0.053	II	30.0	72.5	115.0	130		0.22		Cone entered bed at 30 seconds, driving cable became slack at 120 seconds with further very slow penetration continuing beyond end of test. Partial penetration of 0.140m achieved. Surface settlement zero.
	T2757	0.153	(cone)	30.0	85.0	115.0	130		0.61		
	T2941	0.303		30.0	103.8	115.0	130		0.94		
	T2956	0.503		30.0	103.8	115.0	130		0.99		
	T2943	0.703		30.0	103.8	115.0	130		1.03		
88	T2930	0.053	II	42.5	82.5	98.8	130		0.41		Cone entered bed at 32 seconds, driving cable became slack at 95 seconds with further very slow penetration continuing beyond end of test. Partial penetration of 0.265m achieved. Surface settlement zero.
	T2757	0.153	(cone)	42.5	77.5	95.0	130		0.91		
	T2941	0.303		42.5	87.5	92.5	130		1.50		
	T2956	0.503		42.5	92.5	92.5	130		1.83		
	T2943	0.703		42.5	87.5	93.8	130		1.76		

Table 6.20 Results of tests performed in medium dense soil to assess the influence of cone penetration rate (continued from Table 6.19)

Test No	Transducer No	Initial depth (m)	Class of response	Elapsed times (sec) t_1	t_2	t_3	t_4	t_5	Excess pore pressure (kN/m^2) $\bar{u}_1$	$\bar{u}_2$	Comments
54	T2930	0.079	I	43.8	47.5	590	700		0.58		Cone entered bed at 45 seconds and came to rest at 75 seconds. Elapsed times in excess of 500 seconds are estimated by extrapolation of plotted data. Penetration into bed 0.770m. Surface settlement 0.026m.
	T2757	0.179	(cone)	43.8	52.5	457.5	700		1.37		
	T2941	0.279		43.8	57.5	373.8	700		2.15		
	T2756	0.479		43.8	67.5	202.5	700		3.85		
	T2943	0.679		43.8	71.3	86.3	700		5.50		
62	T2930	0.023	IV	31.3	32.5	35.0	138.8		0.19	-1.20	Cone entered bed at approximately 31 seconds with driving cable becoming slack at approximately 38 seconds. Exact cone penetration not recorded, approximately 100mm. Surface settlement zero.
	T2757	0.123	(cone)	32.5		36.3	131.3			-1.41	
	T2941	0.273		31.3	32.5	36.3	141.3		0.06	-1.18	
	T2956	0.423		33.8		37.5	167.5			-1.14	
	T2943	0.623		31.3	32.5	37.5	141.3		0.06	-1.04	
63	T2930	0.013	Ia	32.5	37.5	170.0	250	70.0	0.13	0.13	Cone entered bed at 33 seconds and came to rest at 70 seconds. Penetration into bed 0.710m. Surface settlement 0.008m.
	T2757	0.113	(cone)	32.5	43.8	153.8	250	70.0	0.91	0.94	
	T2941	0.313		32.5	55.0	113.8	250	70.0	2.78	2.63	
	T2956	0.513		32.5	60.0	86.3	250	72.5	5.27	4.40	
	T2943	0.713		32.5	67.5	70.0	250	70.0	6.86	5.76	
64	T2930	0.066	I	30.0	33.8	461.3	640		0.50		Cone entered bed at 30 seconds and came to rest at 73 seconds. Elapsed times in excess of 500 seconds estimated by extrapolation of plotted data. Penetration into bed 0.710m. Surface settlement 0.014m.
	T2757	0.166	(cone)	31.3	40.0	337.5	640		1.28		
	T2941	0.366		30.0	52.5	201.2	640		1.91		
	T2956	0.566		31.3	66.3	87.5	640		4.55		
	T2943	0.766		30.0	72.5	73.8	640		5.92		

Table 6.21 Results of tests performed to assess influence of soil state for a 60° cone (continued in Table 6.22)

Test No	Transducer No	Initial depth (m)	Class of response	Elapsed times (sec) t_1	t_2	t_3	t_4	Excess pore pressure (kN/m^2) $\bar{u}_1$	$\bar{u}_2$	Comments
65	T2930	0.046	I	30.0	40.0	347.5	440	0.35		Cone entered bed at 30 seconds and
	T2757	0.146	(cone)	30.0	42.5	262.5	440	1.13		came to rest at 75 seconds.
	T2941	0.346		30.0	55.0	190.0	440	2.87		Penetration into bed 0.710m. Surface
	T2756	0.546		31.3	67.5	87.5	440	4.60		settlement 0.010m.
	T2943	0.746		30.0	76.3	77.5	440	5.95		
66	T2756	0.055	IV	28.8		32.5	142.5		-1.86	Cone entered bed at 30 seconds
	T2757	0.205	(cone)	28.8		33.8	120.0		-1.40	driving cable slack at 35 seconds
	T2930	0.355		28.8		33.8	133.8		-1.28	with further very slow penetration
	T2941	0.505		30.0		35.0	155.0		-1.25	until 210 seconds. Partial penetr-
	T2943	0.655		28.8		35.0	135.0		-1.22	ation of 0.105m achieved. Surface
										settlement zero.
81	T2930	0.037	III	28.8	31.3	38.8	58.8	0.25	-0.69	Cone entered bed at 29 seconds,
	T2757	0.137	(cone)	28.8	31.3	36.3	68.8	1.27	-0.42	driving cable slack at 36 seconds
	T2941	0.287		28.8	31.3	36.6	60.0	2.40	-0.06	with further very slow penetration
	T2756	0.487		30.0		37.5	68.8	2.71		continuing to end of test (500
	T2943	0.687		28.8		36.3	65.0	2.78		seconds). Partial penetration of
										0.200m achieved. Surface settlement
										-0.001m.

Table 6.22 Results of tests performed to assess influence of soil state for a 60° cone (continued from Table 6.21)

Test No	Transducer No	Initial depth (m)	Class of response	Elapsed times (sec) t_1	t_2	t_3	t_4	t_5	Excess pore pressure (kN/m^2) $\bar{u}_1$	$\bar{u}_2$	Comments
71	T2930	0.073	I	30.0	36.3	560	700		0.54		Cone entered bed at 30 seconds and
	T2757	0.223	(cone)	30.0	41.3	332.5	700		1.70		came to rest at 64 seconds. Elapsed
	T2941	0.373		30.0	47.5	235.0	700		2.84		times in excess of 500 seconds are
	T2756	0.573		30.0	57.5	70.0	700		4.52		estimated by extrapolation of plotted
	T2943	0.773		30.0	62.5	63.8	700		5.74		data. Penetration into bed 0.780m.
											Surface settlement 0.023m.
72	T2930	0.058	Ia	32.5	37.5	198.7	300		0.60	1.80	Cone entered bed at 32 seconds and
	T2757	0.208	(cone)	32.5	46.3	145.0	300	62.5	1.97	2.63	came to rest at 60 seconds.
	T2941	0.308		32.5	47.5	123.8	300	62.5	2.87	4.41	Penetration into bed 0.720m. Surface
	T2756	0.508		32.5	52.5	83.8	300	62.5	5.35	5.65	settlement 0.004m.
	T2943	0.708		32.5	58.8	61.3	300	61.3	6.63		
73	T2930	0.034	Ia	30.0	36.3	320.0	420		0.32		Cone entered bed at 30 seconds and
	T2757	0.184	(cone)	31.3	45.0	218.7	420		1.55		came to rest at 62 seconds.
	T2941	0.334		30.0	48.8	162.5	420	62.5	2.83	2.81	Penetration into bed 0.750m. Surface
	T2756	0.534		31.3	55.0	87.5	420	62.5	4.65	4.54	settlement 0.009m.
	T2943	0.734		30.0	60.0	62.5	420	62.5	5.74	5.59	

Table 6.23 Results of tests performed with 30° cone to examine effect of cone geometry (continued in Table 6.24)

Test No	Transducer No	Initial depth (m)	Class of response	Elapsed times (sec) t_1	t_2	t_3	t_4	t_5	Excess pore pressure (kN/m^2) $\bar{u}_1$	$\bar{u}_2$	Comments
74	T2930	0.043	III	30.0	32.5	41.3	80.0		0.32	-0.60	Cone entered bed at 30 seconds and
	T2757	0.143	(cone)	30.0	31.3	40.0	82.5		1.21	-0.12	came to rest at 42 seconds. Partial
	T2941	0.293		30.0		38.8	88.8		2.51		penetration of 0.220m achieved.
	T2756	0.493		30.0		40.0	82.5		2.89		Surface settlement -0.001m.
	T2943	0.693		30.0		38.8	92.5		2.99		
75	T2930	0.022	IV	31.3		33.8	67.5			-1.66	Cone entered bed at 31 seconds,
	T2757	0.172	(cone)	32.5		35.0	77.5			-0.87	driving cable slack by 35-40
	T2941	0.372		32.5		36.3	76.3			-0.51	seconds and came to rest by 90-120
	T2756	0.572		31.3	32.5	36.3	75.0		0.33	-0.46	seconds. Partial penetration of
	T2943	0.672		31.3	32.5	36.3	76.3		0.06	-0.49	0.220m achieved. Surface settlement
											-0.001m.
76	T2930	0.022	IV	30.0		32.5	146.3			-1.57	Cone entered bed at 30 seconds,
	T2757	0.122	(cone)	30.0	31.3	32.5	146.3		0.06	-1.65	driving cable slack by 34 seconds,
	T2941	0.222		30.0		32.5	137.5			-1.25	cone continued to move very slowly
	T2756	0.422		30.0	31.3	35.0	125.0		0.03	-1.17	for further 150 seconds. Partial
	T2943	0.622		30.0		33.8	158.8			-1.16	penetration into bed 0.780m. Surface
											settlement zero.

Table 6.24 Results of tests performed with 30° cone to examine effect of cone geometry (continued from Table 6.23)

Test No	Transducer No	Initial depth (m)	Class of response	Elapsed times (sec) t_1	t_2	t_3	t_4	t_5	Excess pore pressure (kN/m^2) $\bar{u}_1$	$\bar{u}_2$	Comments
77	T2930	0.073	I	33.0	37.5	590	660		0.53		Cone entered bed at 33 seconds, came
	T2757	0.273	(cone)	33.0	46.3	348.8	660		2.09		to rest at 67 seconds. Elapsed times
	T2941	0.473		33.0	55.0	206.2	660		3.75		in excess of 500 seconds are
	T2756	0.673		33.0	66.3	71.3	660		5.34		estimated by extrapolation of plotted
	T2943	0.773		33.0	67.5	68.8	660		6.05		data. Penetration into bed 0.755m.
											Surface settlement 0.026m.
78	T2930	0.023	IV	28.8		31.3	76.3			-1.41	Cone entered bed at 30 seconds,
	T2757	0.123	(cone)	28.8		31.3	72.5			-1.36	driving cable slack by 32-33 seconds
	T2941	0.223		28.8		31.3	72.5			-1.11	with very slow movement continuing
	T2756	0.423		28.8	30.0	33.8	72.5		0.16	-1.05	to 120 seconds. Partial penetration
	T2943	0.623		28.8	30.0	32.5	72.5		0.00	-1.04	of 0.054m achieved. Surface
											settlement zero.
79	T2930	0.038	III	30.0	31.3	38.8	57.5		0.22	-0.82	Cone entered bed at 30 seconds,
	T2757	0.138	(cone)	30.0	31.3	37.5	57.5		0.85	-0.30	driving cable slack by 37 seconds
	T2941	0.258		30.0	31.3	37.5	65.0		1.74	-0.18	with very slow movement continuing
	T2756	0.488		30.0	32.5	37.5	57.5		2.04	-0.08	to 120 seconds. Partial penetration
	T2943	0.688		30.0	31.3	37.5	65.0		2.14	-0.09	of 0.171m achieved. Surface
											settlement zero.

Table 6.25 Results of tests performed with 90° cone to examine effect of cone geometry (continued in Table 6.26)

Test No	Transducer No	Initial depth (m)	Class of response	Elapsed times (sec) t_1	t_2	t_3	t_4	t_5	Excess pore pressure (kN/m^2) $\bar{u}_1$	$\bar{u}_2$	Comments
82	T2930	0.085	Ia	28.8	33.8	315.0	460	67.5	0.66	0.66	Cone entered bed at 30 seconds and
	T2757	0.183	(cone)	28.8	38.8	242.5	460	67.5	1.58	1.58	came to rest at 67 seconds.
	T2941	0.333		28.8	48.8	188.7	460	67.5	2.78	2.78	Penetration into bed 0.720m. Surface
	T2756	0.533		30.0	57.5	107.5	460	67.5	4.56	4.56	settlement 0.009m.
	T2943	0.733		28.8	66.3	67.5	460	67.5	5.91	5.79	
83	T2930	0.057	Ia	30.0	36.3	198.7	278.8	75.0	0.50	0.50	Cone entered bed at 31 seconds and
	T2757	0.207	(cone)	30.0	47.5	145.0	285	75.0	1.92	1.82	came to rest at 73 seconds.
	T2941	0.307		30.0	52.5	125.0	285	75.0	2.75	2.63	Penetration into bed 0.694m. Surface
	T2756	0.507		31.3	63.8	92.5	285	75.0	5.02	4.386	settlement 0.004m.
	T2943	0.707		30.0	71.3	75.0	296.3	75.0	6.67	5.76	
84	T2930	0.014	IV	28.8		31.3	62.5			-0.69	Cone entered bed at 30 seconds,
	T2757	0.164	(cone)	28.8	30.0	33.8	86.3		0.09	-1.17	driving cable slack at 34 seconds,
	T2941	0.464		28.8	30.0	33.8	86.3		0.27	-0.83	with very slow movement continuing
	T2756	0.564		30.0		35.0	85.0			-0.78	to the end of the tests. Partial
	T2943	0.664		28.8	30.0	33.8	86.3		0.27	-0.76	penetration of 0.110m achieved.
											Surface settlement -0.001m.

Table 6.26 Results of tests performed with 90° cone to examine effect of cone geometry (continued from Table 6.25)

Test No	Transducer No	Initial depth (m)	Class of response	Elapsed times (sec) t_1	t_2	t_3	t_4	t_5	Excess pore pressure (kN/m^2) $\bar{u}_1$	$\bar{u}_2$	Comments
159	T2930	0.044	I	28.0	32.2	496.6	552.6		0.31		Cone entered bed at 29 seconds and
	T2941	0.194	(cone)	28.0	43.3	311.8	560.0		1.44		came to rest at 115 seconds. An
	T2943	0.394		28.0	57.3	178.8	560.0		3.04		apparent $\bar{u}$ of 0.55kPa was recorded at
	T2756	0.594		29.4	72.7	74.1	560.0		4.66		the end of dissipation with the pie-
	T3201			29.4	74.1	74.1			5.32		zocone (T3201). Penetration into bed
											0.704m. Surface settlement 0.021m.
160	T2930	0.071	III	26.6	28.0	37.7	89.4		0.57	-0.19	Cone entered bed at 27 seconds,
	T2941	0.171	(cone)	26.6	28.0	36.3	89.4		1.22	-0.07	driving cable slack by 39 seconds.
	T2943	0.321		26.6	28.0	36.3	76.8		2.00	-0.04	An apparent $\bar{u}$ of 0.09kPa was recorded
	T2756	0.521		26.6	29.4	37.7	89.4		2.43	-0.10	at the end of dissipation with the
	T3201			26.6	28.0	37.7			1.19	-0.10	piezocone (T3201). Partial penetr-
											ation of 0.356m achieved. Surface
											settlement -0.001m.
161	T2930	0.035	Ia	25.2	29.4	178.8	219.5	60.1	0.23	0.23	Cone entered bed at 25 seconds, and
	T2941	0.135	(cone)	25.2	36.3	135.5	236.3	60.1	1.08	1.08	came to rest at 60 seconds. An
	T2943	0.335		25.2	47.5	97.8	247.5	60.1	2.85	2.85	apparent $\bar{u}$ of 0.45kPa was recorded at
	T2756	0.535		25.2	58.7	64.3	255.9	60.1	4.72	4.62	the end of dissipation with the pie-
	T3201			25.2	58.7	69.9		60.1	5.40	5.17	zocone (T3201). Penetration into bed
											0.707m. Surface settlement 0.004m.

Table 6.27 Results of tests performed with 60° piezocone (shaft) to examine effect of filter position (continued in Table 6.28)

Test No	Transducer No	Initial depth (m)	Class of response	Elapsed times (sec) t_1	t_2	t_3	t_4	t_5	Excess pore pressure (kN/m^2) $\bar{u}_1$	$\bar{u}_2$	Comments
162	T2930	0.066	III	23.8	26.6	34.9	72.6		0.50	-0.34	Cone entered bed at 24 seconds,
	T2941	0.166	(cone)	23.8	25.2	33.5	64.3		1.22	-0.14	driving cable slack by 37 seconds.
	T2943	0.266		23.8	25.2	34.9	71.2		2.00	-0.04	An apparent $\bar{u}$ of -0.10kPa was
	T2756	0.416		23.8	26.6	34.9	85.2		2.60	-0.03	recorded at the end of dissipation
	T3201			23.8	25.2	34.9			0.93	-0.17	with the piezocone (T3201). Partial
											penetration of 0.369m achieved.
											Surface settlement -0.002m.
163	T2930	0.022	IV	26.6		28.0	44.7			-1.18	Cone entered bed at 27 seconds,
	T2941	0.122	(cone)	26.6		28.0	60.9			-0.84	driving cable slack by 32-33 seconds.
	T2943	0.252		26.6	30.8	28.0	60.9		0.11	-0.55	An apparent $\bar{u}$ of -0.06kPa was
	T2756	0.402		26.6	32.1	29.4	60.9		0.20	-0.43	recorded at the end of dissipation
	T3201			26.6		34.9				-0.16	with the piezocone (T3201). Partial
											penetration of 0.265m achieved.
											Surface settlement -0.001m.
164	T2930	0.016	IV	23.8		25.2	46.1			-1.30	Cone entered bed at 24 seconds,
	T2941	0.116	(cone)	23.8		25.2	72.7			-1.31	driving cable slack by 29 seconds.
	T2943	0.246		23.8		25.2	72.7			-0.78	An apparent $\bar{u}$ of -0.13kPa was
	T2756	0.396		25.2		29.4	75.5			-0.50	recorded at the end of dissipation
	T3201			23.8		39.1				-0.26	with the piezocone (T3201). Partial
											penetration of 0.271m achieved.
											Surface settlement -0.001m.

Table 6.28 Results of tests performed with 60° piezocone (shaft) to examine effect of filter position (continued from Table 6.27)

Test No	Transducer No	Initial depth (m)	Class of response	Elapsed times (sec) t_1	t_2	t_3	t_4	Excess pore pressure (kN/m^2) $\bar{u}_1$	$\bar{u}_2$	Comments
165	T2930	0.043	I	29.4	32.1	454.4	508.9	0.27		Cone entered bed at 29 seconds and came to rest at 67 seconds. An apparent $\bar{u}$ of 0.46kPa was recorded at the end of dissipation with the piezocone (T3201). Penetration into bed 0.713m. Surface settlement 0.020m.
	T2941	0.193	(cone)	28.0	37.7	286.5	534.1	1.40		
	T2943	0.393		28.0	54.5	153.6	560	3.04		
	T2756	0.593		29.4	67.1	68.5	560	4.73		
	T3201			29.4	68.5	69.9		5.58		
166	T2930	0.014	IV	29.4		30.8	58.7		-0.69	Cone entered bed at 29 seconds, driving cable slack by 36 seconds and very slow movement continuing to 300-350 seconds. An apparent $\bar{u}$ of 0.52kPa was recorded at the end of dissipation with the piezocone (T3201). Partial penetration of 0.110m achieved. Surface settlement -0.001m.
	T2941	0.114	(cone)	29.4		33.5	81.0		-0.94	
	T2943	0.244		29.4		30.8	75.4		-0.55	
	T2756	0.394		29.4		36.4	79.6		-0.50	
	T3201			29.4		30.8	60.1		-0.19	
167	T2930	0.027	III	26.6	29.4		36.3		-0.81	Cone entered bed at 28 seconds, with driving cable slack by 36 seconds and very slow movement continuing to end of test. An apparent $\bar{u}$ of -0.09kPa was recorded at the end of dissipation with the piezocone (T3201). Partial penetration of 0.138m achieved. Surface settlement -0.001m.
	T2941	0.127	(cone)	26.6	29.4	33.5	48.9	0.07	-0.40	
	T2943	0.257		26.6	29.4	33.5	69.8	0.70	-0.15	
	T2756	0.407		28.0	29.4	33.5	55.9	0.84	-0.13	
	T3201			26.6	29.4				-0.56	

Table 6.29 Results of tests performed with 60° piezocone (face) to examine effect of filter position (continued in Tables 6.30 and 6.31)

Test No	Transducer No	Initial depth (m)	Class of response	Elapsed times (sec) t_1	t_2	t_3	t_4	Excess pore pressure (kN/m^2) $\bar{u}_1$	$\bar{u}_2$	Comments
168	T2930	0.018	IV	28.0		29.4	55.9	0.50	-0.72	Cone entered bed at 28 seconds with driving cable slack by 35 seconds, very slow movement continued to beyond 200 seconds. An apparent $\bar{u}$ of -0.23kPa was recorded at the end of dissipation with the piezocone T3201). Partial penetration of 0.112m achieved. Surface settlement -0.001m.
	T2941	0.118	(cone)	28.0		32.1	60.1	1.22	-0.68	
	T2943	0.248		28.0		30.8	62.9	2.00	-0.52	
	T2756	0.398		28.0		30.8	58.7	2.60	-0.47	
	T3201			28.0		29.4		0.93	-0.90	
169	T2930	0.067	III	29.4	30.8	41.9	69.8	0.42	-0.31	Cone entered bed at 30 seconds with driving cable slack by 43 seconds and very slow movement continuing beyond 120 seconds. An apparent $\bar{u}$ of -0.21kPa was recorded at the end of dissipation with the piezocone (T3201). Partial penetration of 0.218m achieved. Surface settlement -0.001m.
	T2941	0.167	(cone)	29.4	30.8	39.1	65.7	0.97	-0.18	
	T2943	0.267		29.4	30.8	40.5	65.7	1.56	-0.19	
	T2756	0.417		30.8	32.2	41.9	72.6	1.96	-0.00	
	T3201			29.4	30.8	41.9		0.63	-0.68	

Table 6.30 Results of tests performed with 60° piezocone (face) to examine effect of filter position (continued in Tables 6.29 and 6.31)

Test No	Transducer No	Initial depth (m)	Class of response	Elapsed times (sec) t_1	t_2	t_3	t_4	t_5	Excess pore pressure (kN/m^2) $\bar{u}_1$	$\bar{u}_2$	Comments
170	T2930	0.035	Ia	32.2	37.7	180.1	240	74.0	0.31	0.31	Cone entered bed at 31 seconds and coming to rest at 72 seconds. An apparent $\bar{u}$ of -0.26kPa was recorded at the end of dissipation with the piezocone (T2301). Penetration into bed 0.616m. Surface settlement 0.015m.
	T2941	0.235	(cone)	30.8	54.5	118.7	240	74.0	2.02	1.94	
	T2943	0.435		30.8	64.3	86.6	240	74.0	3.85	3.70	
	T2756	0.635		30.8	72.6	74.0	240	74.0	5.12	5.02	
	T3201			30.8	72.6	74.0		74.0	4.95	4.91	
171	T2930	0.054	I	29.4	39.1	230.5	296.3		0.42		Cone entered bed at 30 seconds, and came to rest at 74 seconds. An apparent $\bar{u}$ of 0.56kPa was recorded at the end of dissipation with the piezocone (T3201). Penetration into bed 0.628m. Surface settlement 0.006m.
	T2941	0.254	(cone)	29.4	48.9	149.4	304.7		2.12		
	T2943	0.454		29.4	64.3	101.9	292.1		3.81		
	T2756	0.654		30.8	74.0	75.4	296.3		5.25		
	T3201			30.8	74.0	76.8			5.44		

Table 6.31 Results of tests performed with 60° piezocone (face) to examine effect of filter position (continued from Tables 6.29 and 6.30)

Test No	Transducer No	Initial depth (m)	Class of response	Elapsed times (sec) t_1	t_2	t_3	t_4	Excess pore pressure (kN/m^2) $\bar{u}_1$	$\bar{u}_2$	Comments
173	T2930	0.042	I	28.0	29.4	391.7	457.5	0.31		Cone entered bed at 28 seconds and
	T2941	0.192	(cone)	28.0	39.1	250.2	479.9	1.43		came to rest at 70 seconds.
	T2943	0.392		28.0	54.5	143.9	451.9	3.02		Penetration into bed 0.735m. Surface
	T2756	0.592		28.0	69.9	71.3	460	4.63		settlement 0.020m.
	T3201			28.0	71.3	72.7	460	4.65		
174	T2930	0.044	I	28.0	33.5	174.6	229.2	0.35		Cone entered bed at 28 seconds and
	T2941	0.244	(cone)	28.0	43.3	122.9	232.0	2.02		came to rest at 65 seconds.
	T2943	0.444		28.0	55.9	83.8	232.0	3.81		Penetration into bed 0.736m. Surface
	T2756	0.644		28.0	64.3	65.7	269.8	5.27		settlement 0.005m.
	T3201			28.0	65.7	81.0	254.4	4.60		
176	T2930	0.066	III	30.7	32.1	44.7	67.0	0.39	-0.23	Cone entered bed at 30 seconds, with
	T2941	0.166	(cone)	29.3	32.1	44.7	69.8	0.95	-0.11	driving cable slack by 47 seconds,
	T2943	0.266		29.3	32.1	44.7	69.8	1.42	-0.08	and continued very slow movement to
	T2756	0.416		30.7	32.1	46.1	74.0	1.69	-0.07	past 180 seconds. At end of dissi-
	T3201			30.7	33.5	46.1		0.54	-0.18	pation piezocone (T3201) recorded an
										apparent $\bar{u}$ of -0.21kPa. Penetration
										into bed 0.735m. Surface settlement
										0.020m.

Table 6.32 Results of tests performed with 60° piezocone (shoulder) to examine effect of filter position (continued in Table 6.33)

Test No	Transducer No	Initial depth (m)	Class of response	Elapsed times (sec) t_1	t_2	t_3	t_4	Excess pore pressure (kN/m^2) $\bar{u}_1$	$\bar{u}_2$	Comments
177	T2930	0.023	IV	33.5		36.3	61.5		-0.58	Cone entered bed at 34 seconds with driving cable slack by 44 seconds, and continued very slow movement to beyond 300 seconds. At end of dissipation piezocone (T3201) recorded an apparent $\bar{u}$ of -0.11kPa. Penetration into bed 0.736m. Surface settlement 0.005m.
	T2941	0.123	(cone)	33.5		37.7	60.1		-0.51	
	T2943	0.253		33.5		36.3	62.9		-0.41	
	T2756	0.403		34.9		46.1	62.9		-0.14	
	T3201			34.9		43.3	62.9		-0.29	
178	T2930	0.032	III	29.4	32.2	43.3	53.1	0.19	-0.35	Cone entered bed at 30 seconds with driving cable slack by 44 seconds and continued very slow movement to beyond 300 seconds. At end of dissipation piezocone (T3201) recorded an apparent $\bar{u}$ of -0.39kPa. Partial penetration of 0.234m achieved. Surface settlement -0.002m.
	T2941	0.132	(cone)	29.4	32.2	41.9	53.1	0.62	-0.18	
	T2943	0.262		29.4	30.8	40.5	53.1	1.12	-0.11	
	T2756	0.412		29.4	32.2	41.9	53.1	1.35	-0.14	
	T3201			29.4	32.2	41.9	53.1	0.27	-0.23	
179	T2930	0.042	III	29.4	32.2	46.1	96.4	0.35	-0.23	Cone entered bed at 31 seconds with driving cable slack by 54 seconds and continued very slow movement to 120 seconds. At end of dissipation piezocone (T3201) recorded an apparent $\bar{u}$ of -0.18kPa. Partial penetration of 0.128m achieved. Surface settlement -0.001m.
	T2941	0.222	(cone)	29.4	32.2	48.9	96.4	1.69	-0.07	
	T2943	0.422		29.4	32.2	50.3	99.2	2.88	-0.08	
	T2756	0.622		30.8	32.2	51.7	120.1	3.25	-0.03	
	T3201			30.8	32.2	50.3	118.7	1.62	-0.16	

Table 6.33 Results of tests performed with 60° piezocone (shoulder) to examine effect of filter position (continued from Table 6.32)

	Particle diameter ($\times 10^{-3}$m)	Particle radius, a ($\times 10^{-3}$m)	Terminal velocity single sphere, v_s (m s^{-1})	Hindered settling velocity, v_{hs} (m s^{-1})
Values derived from Figure A.1				
D_{10}	0.04	0.02	1.3×10^{-3}	0.06×10^{-3}
D_{50}	0.08	0.04	5.2×10^{-3}	0.24×10^{-3}

Table 7.1 Theoretical values of settling velocity for a single sphere and concentrated suspension

Notes 1. $v_s = \frac{2}{9} a^2 g \frac{\rho_s - \rho_w}{\mu}$ equation 2.5

where; a = as above, $g = 9.81$ m s^{-1}, $\rho_s = 2650$ kg m^{-3}, and μ = variable, assume 1.1×10^{-3} kg $m^{-1}s^{-1}$

2. $v_{hs} = K(v_s)$ equation 2.6

where $K = (1-C)^m$ equation 2.7

and $C = 1/\upsilon$ (assume $\upsilon = 2.02$), $m = 4.5$ (after Graf, 1984)

Soil	D_{50} (mm)	U	G_s	Sphericity	Roundness	Mineralogy	ϕ_{cs} (degrees)
6	0.16	1.3	2.65	0.9-0.5	0.7-0.3	quartz + glauconite	38
11	0.17	1.2	2.66	0.9-0.6	0.7-0.3	quartz + glauconite	33
21		*	2.67	1.0-0.5	0.7-0.1	quartz + ore mineral	37
23	0.08	1.4	2.65	0.9-0.2	1.0-0.5	quartz	36
24	0.19	1.6	2.65	0.9-0.5	0.9-0.3	quartz	31
25	0.28	1.7	2.65	0.9-0.4	1.0-0.3	quartz	31
26	0.16	1.9	2.65	0.9-0.5	0.7-0.3	quartz	33
28	0.14	1.8	2.66	0.9-0.3	0.7-0.1	quartz	24

Notes: * values not determined by sieving

Table A.1 Results of classification and direct shear tests

Soil	Spec.vol υ		permeability k ($\times 10^{-3}$ m/s)		dry unit weight (kN/m^3)		bulk unit weight (kN/m^3)	
	L	D	L	D	L	D	L	D
6	1.83	1.63	3.6	1.7	14.2	15.9	18.6	19.7
11	1.82	1.64	3.7	1.9	14.3	15.8	18.7	19.6
21	1.97	1.77	.31	.20	13.2	14.7	18.1	18.9
23	2.02	1.76	.28	.21	12.9	14.7	17.9	19.0
24	1.80	1.61	6.6	3.2	14.4	16.1	18.8	19.8
25	1.78	1.60	7.9	3.9	14.6	16.3	18.9	19.9
26	1.82	1.57	5.1	2.2	14.3	16.5	18.7	20.1
28	1.92	1.70	2.0	1.1	13.8	15.3	18.3	19.3

Notes: L denotes loose samples

D denotes dense samples

Table A.2 Results of permeability and density tests

Test	Nature of test	Specific volume	Dry unit weight (kN/m^3)	Bulk unit weight (kN/m^3)
Maximum density	wet	1.65	15.75	19.61
	dry	1.74		
Minimum density	wet	1.94		
	dry	2.16	12.07	17.29

Table A.3 Results of relative density tests, soil 23

Transducer (serial number)	Transducer range (kPa)	Typical Calibration constant (millivolts/ kPa/volt)	Temperature calibration (equivalent kPa/°C/volt)
2756	35	6.11	0.03
2757	35	5.35	0.04
2930	100	5.32	0.01
2941	100	5.69	0.01
2943	100	5.59	0.01
3201	100	3.65	NOTE1

Notes

1. Temperature sensitivity of transducer 3201 was not determined.

Table C.1 Typical calibration constants and temperature calibration of miniature pore pressure transducers

Transducer/ interface channel (serial number/ channel number)	Resolution error (equivalent kPa)	Noise (equivalent kPa)	Drift (equivalent kPa)	Accuracy (kPa)
2756/3	0.03	0.02	0.06	0.05
2757/4	0.03	0.02	<0.24	0.05
2930/5	0.04	0.02	0.08	0.06
2941/6	0.04	0.02	0.12	0.06
2943/7	0.04	0.02	0.08	0.06
3201/4	0.06	0.03	0.10	0.09

Notes

1. Transducer T2757 appears to have been damaged during the testing programme, exhibiting increasing drift before failing.
2. Characteristics are based upon a supply voltage of five volts.

Table C.2 Characteristics and accuracy of the combined logging system

Soil Layer	Test 139 Depth (m)	Test 139 Specific volume	Test 137 Depth (m)	Test 137 Specific volume	Test 138 Depth (m)	Test 138 Specific volume
1	0-0.086	1.93	0-0.025	1.71	0-0.024	1.72
2	0.086-0.213	1.86	0.025-0.123	1.74	0.024-0.091	1.73
3	0.213-0.333	1.79	0.123-0.218	1.70	0.091-0.187	1.71
4	0.333-0.459	1.75	0.218-0.307	1.67	0.187-0.278	1.68
5	0.459-0.571	1.73	0.307-0.407	1.65	0.278-0.372	1.77
6			0.407-0.487	1.65	0.372-0.474	1.67
7			0.487-0.547	1.65	0.474-0.563	1.66
8			0.547-0.617	1.65	0.563-0.610	1.60

Table D.1 Results of tests to study variations in soil density within test beds

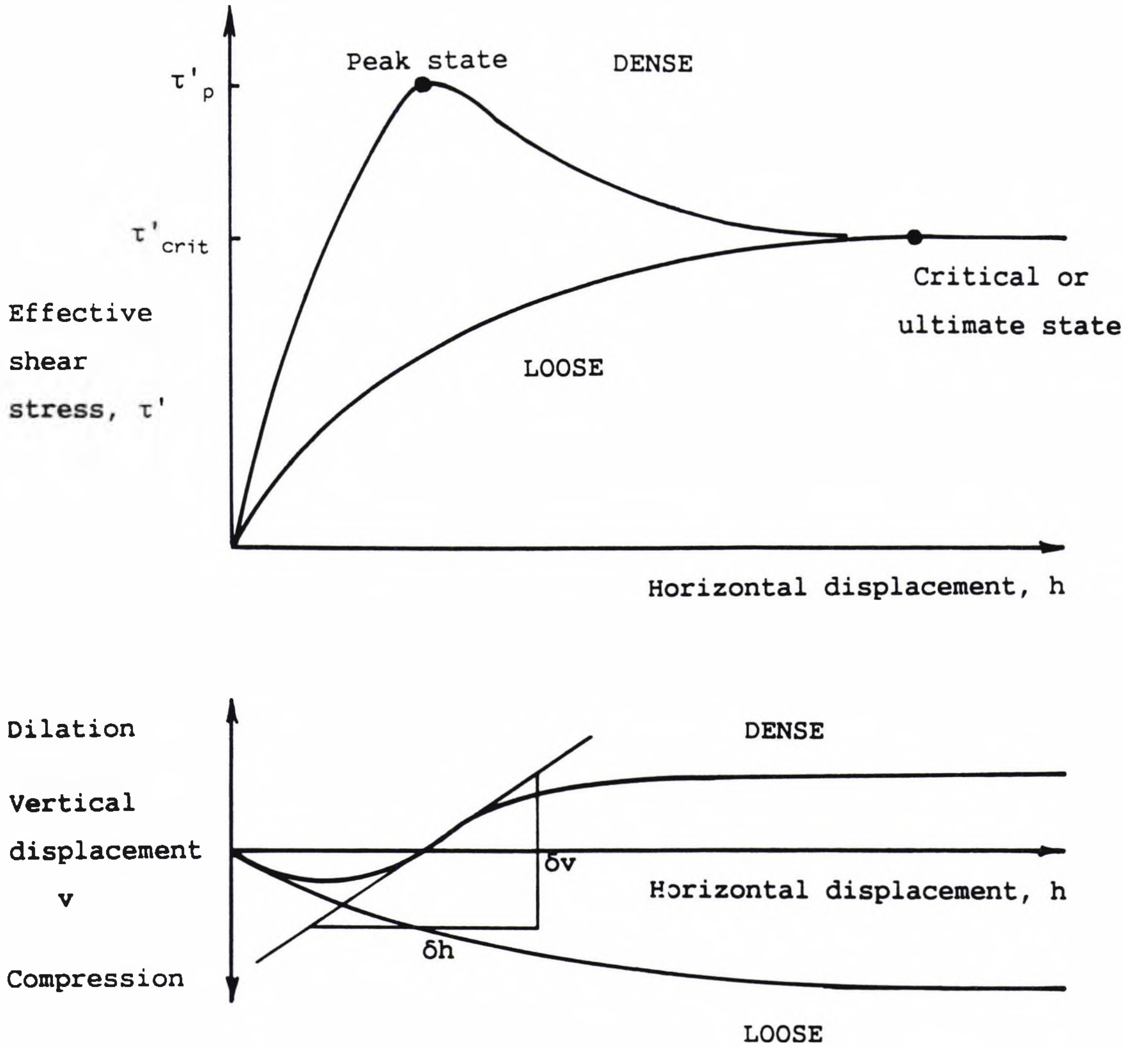

Figure 2.1 Peak and critical states in drained shear tests

Note Taylors Therom predicts that the rate of dilation ($\delta v/\delta h$) is a maximum at the peak state

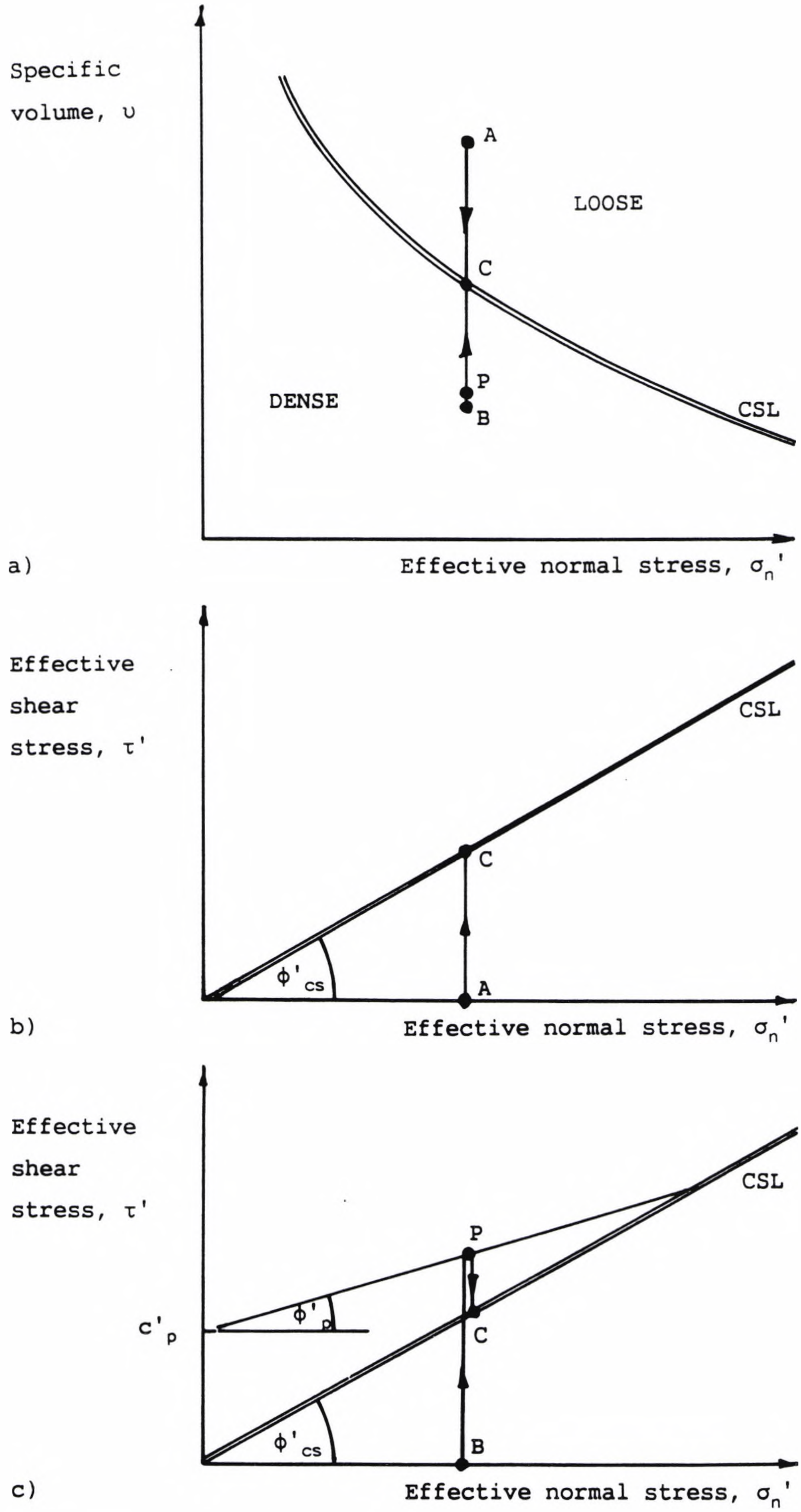

Figure 2.2 State paths for drained shear tests

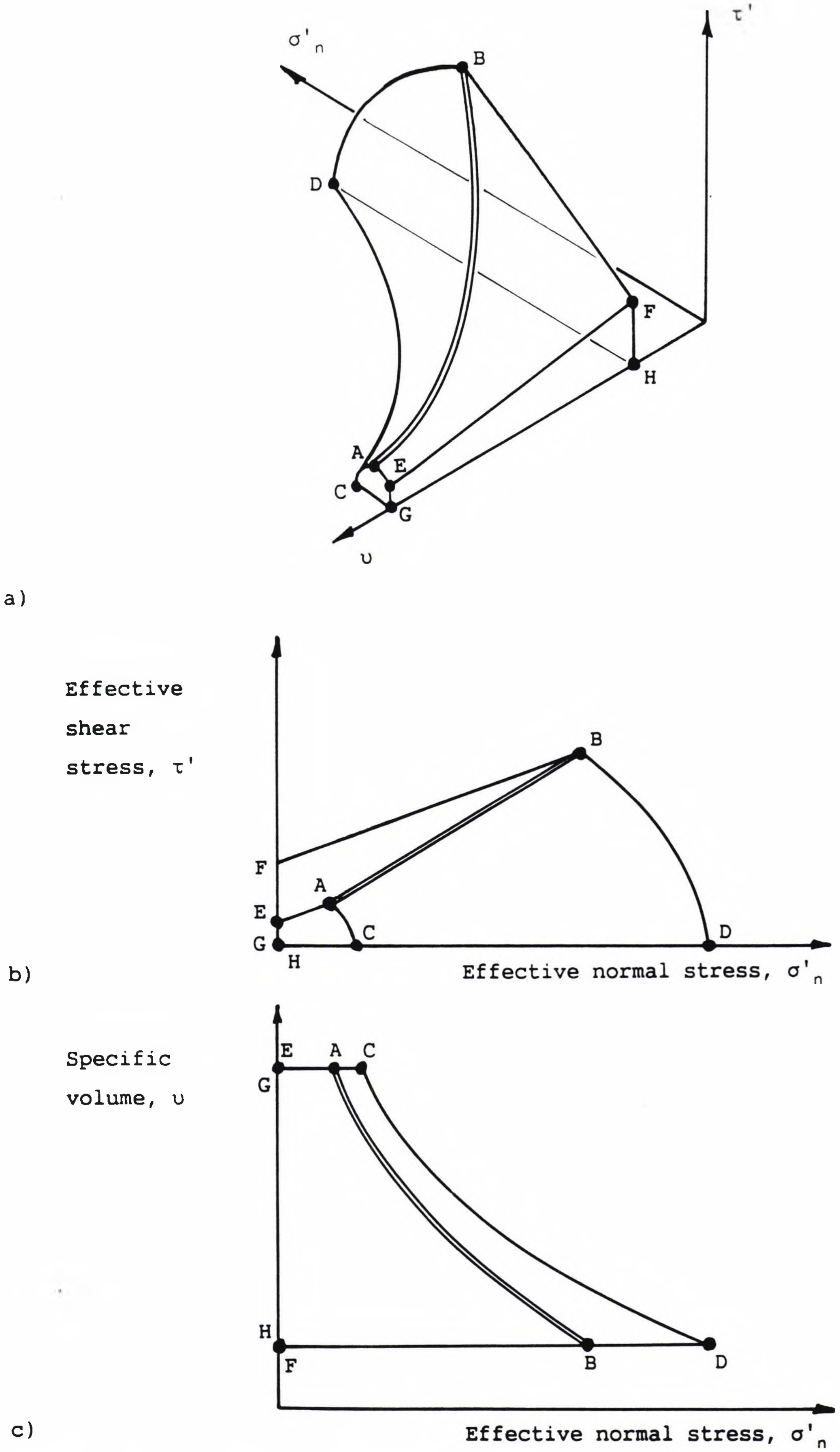

Figure 2.3 The state boundary surface

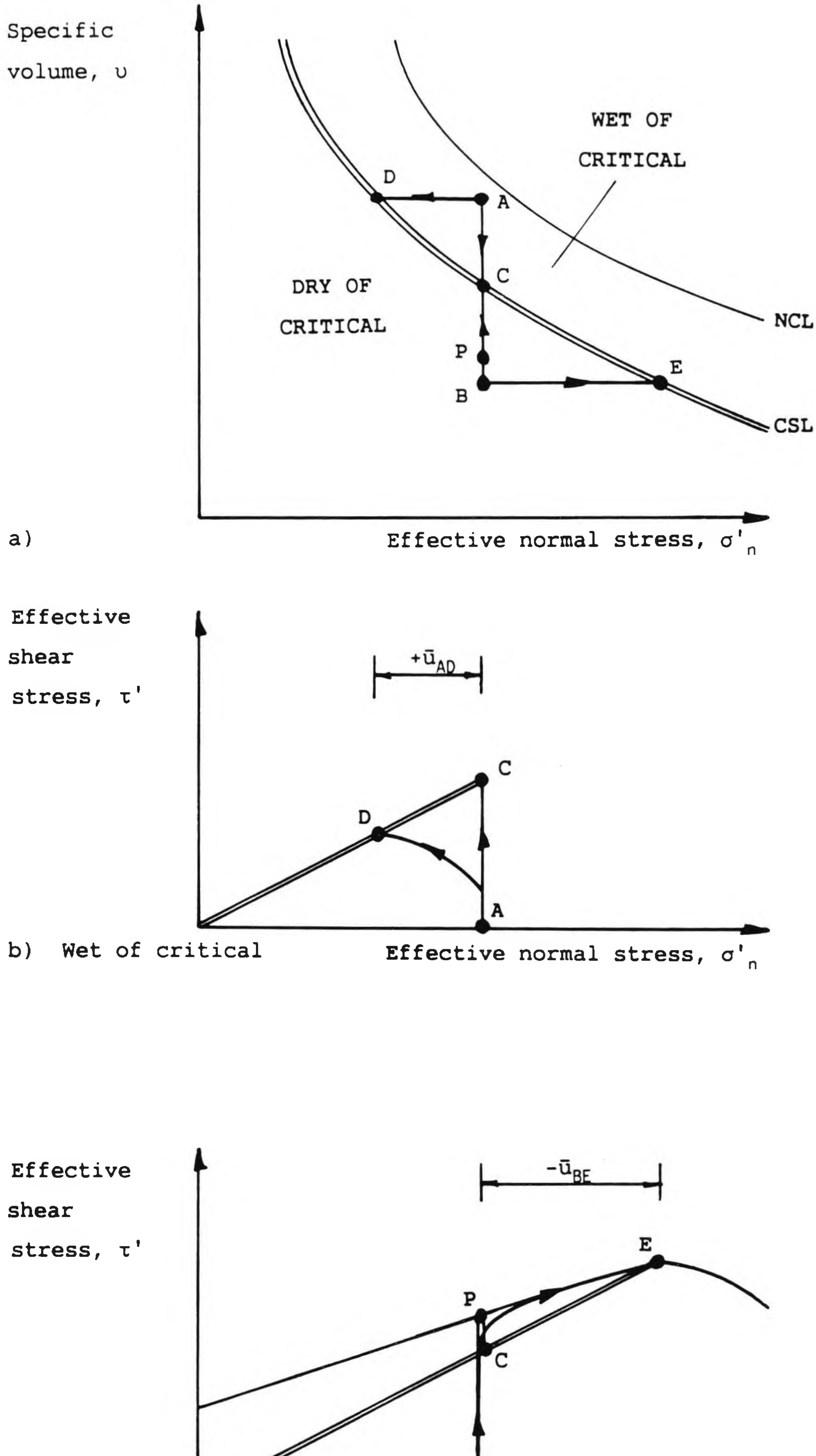

Figure 2.4 Wet and dry of critical soil behaviours

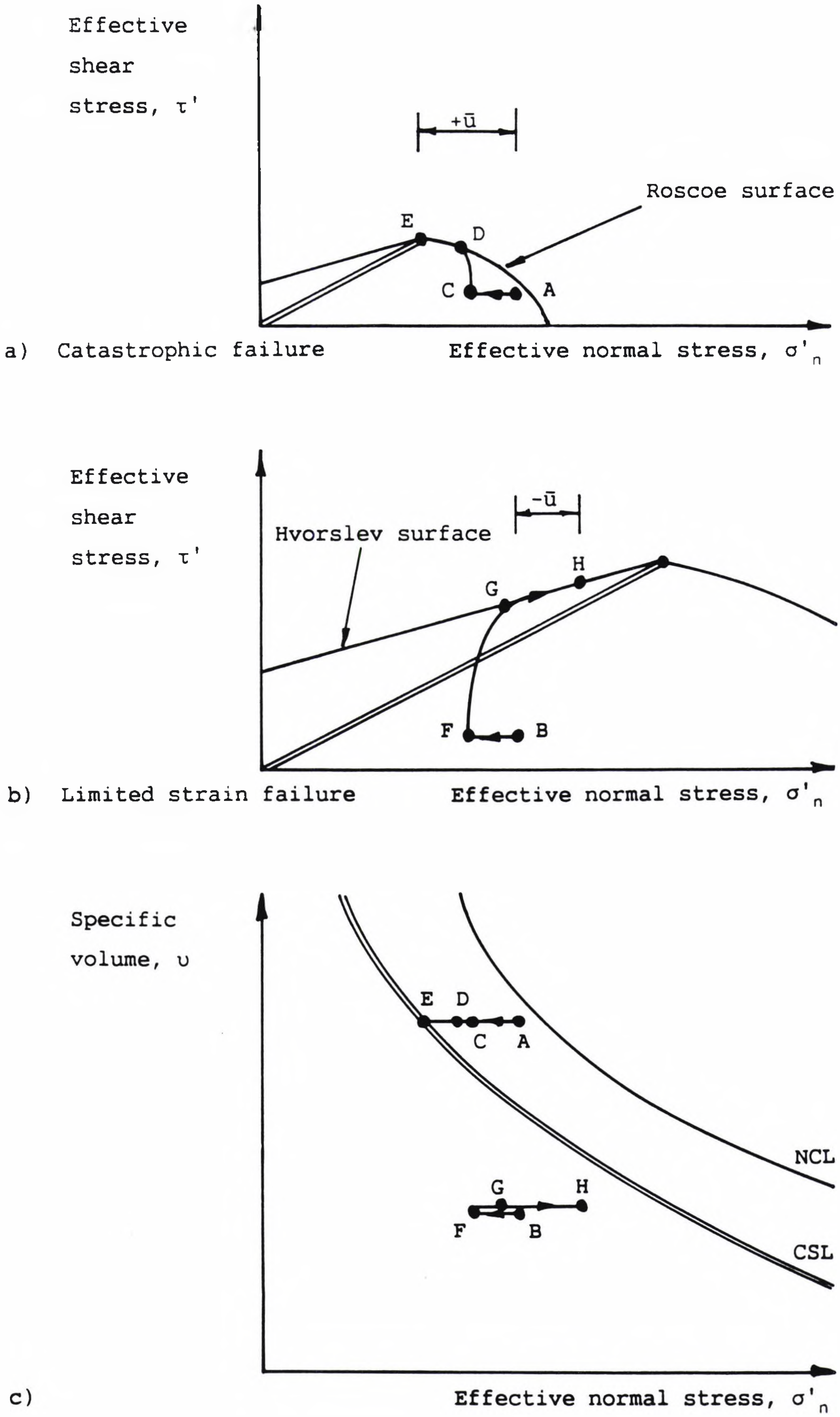

Figure 2.5 Types of soil failure due to increased pore pressures

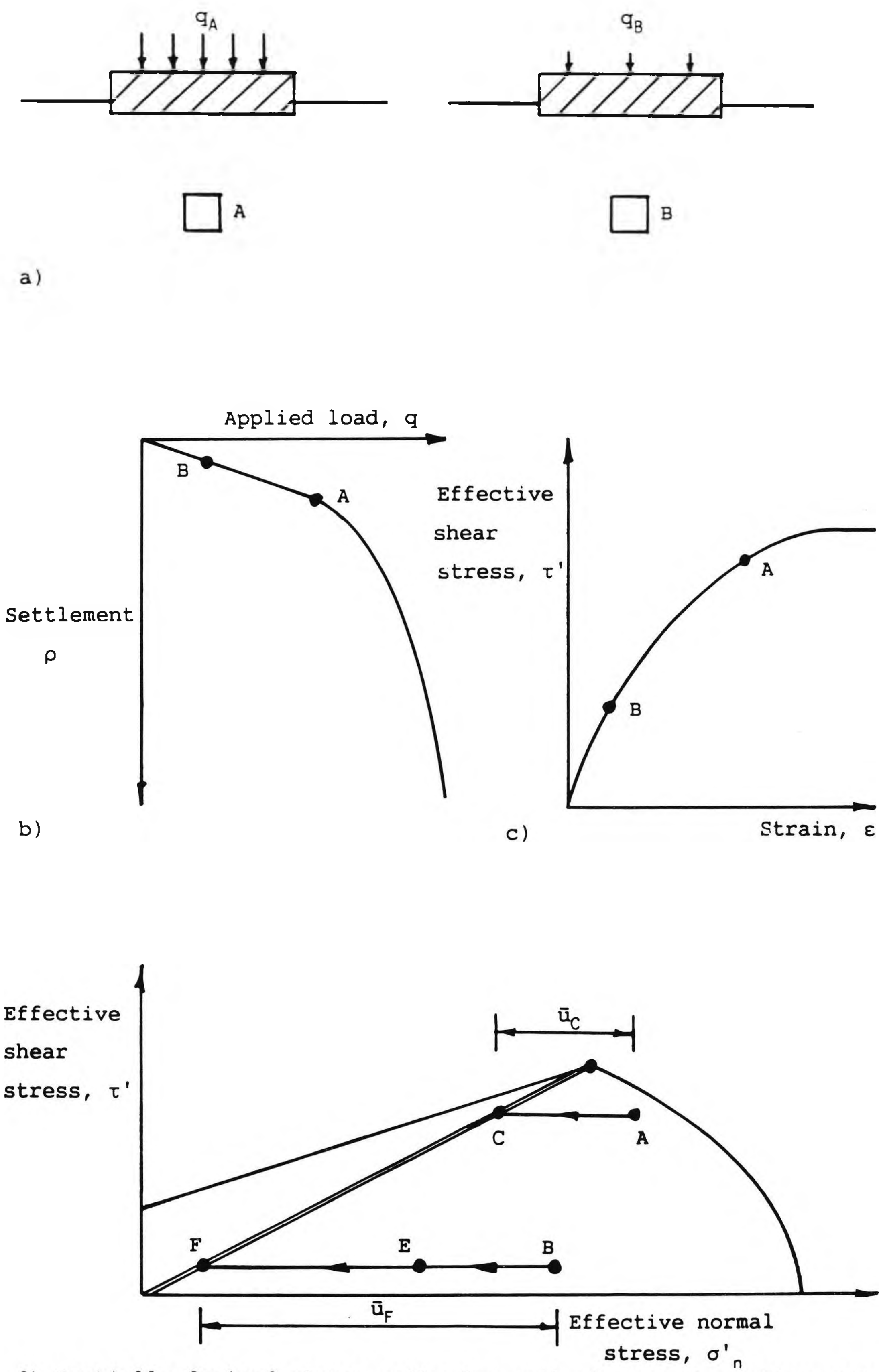

d) Partially drained stress paths for soil elements to achieve CSL

Figure 2.6 Liquefaction at large effective stresses

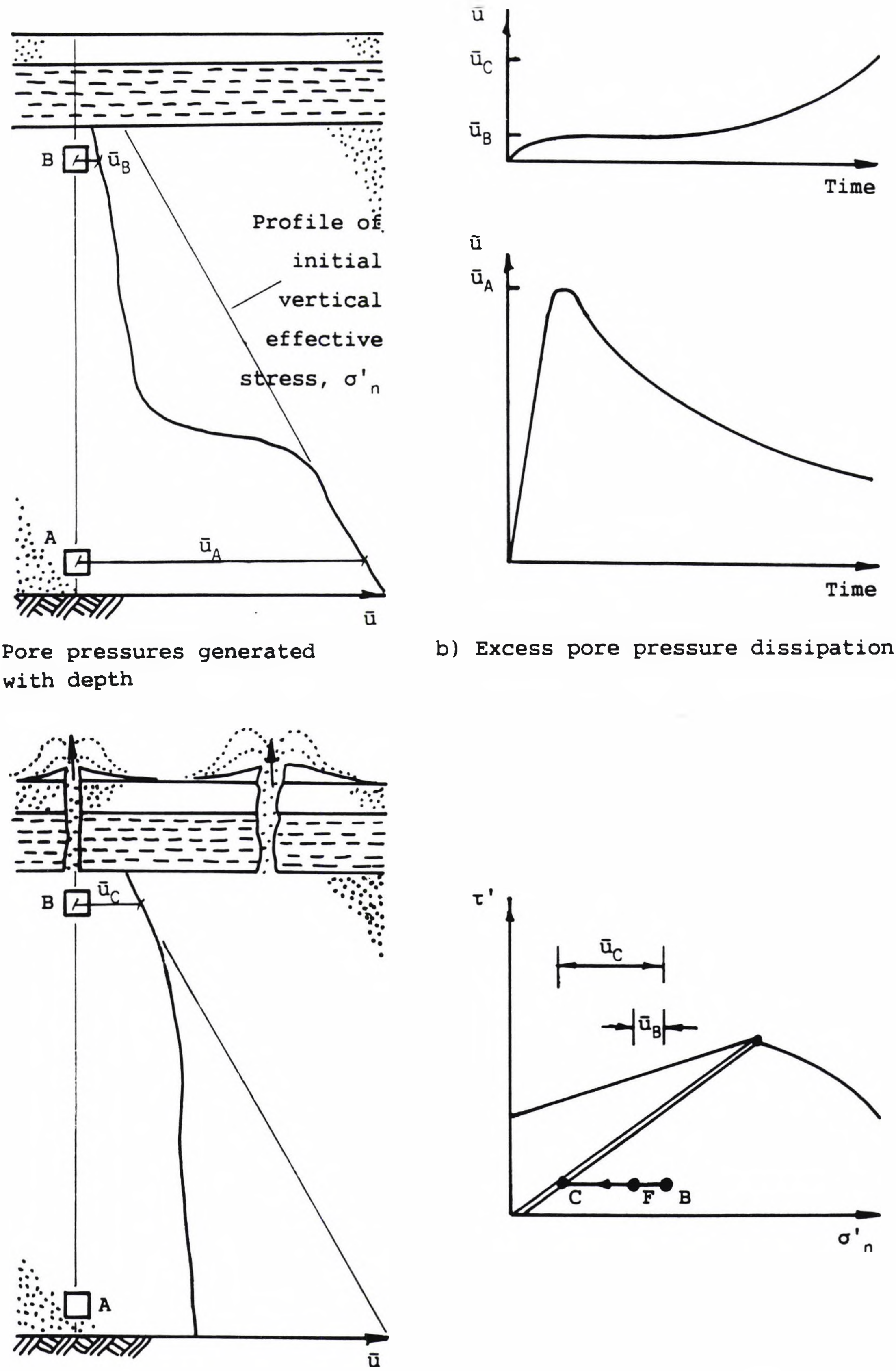

a) Pore pressures generated with depth

b) Excess pore pressure dissipation

c) Delayed near surface liquefaction failure

d) Stress path of element B

Figure 2.7 Non-coincident liquefaction

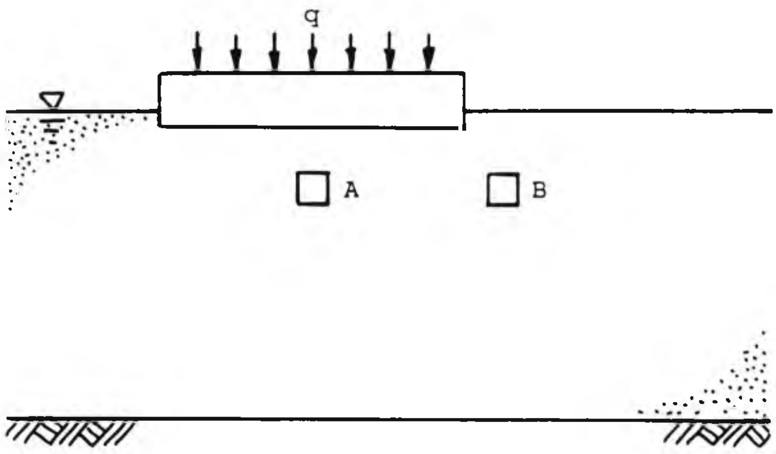

a) Soil profile

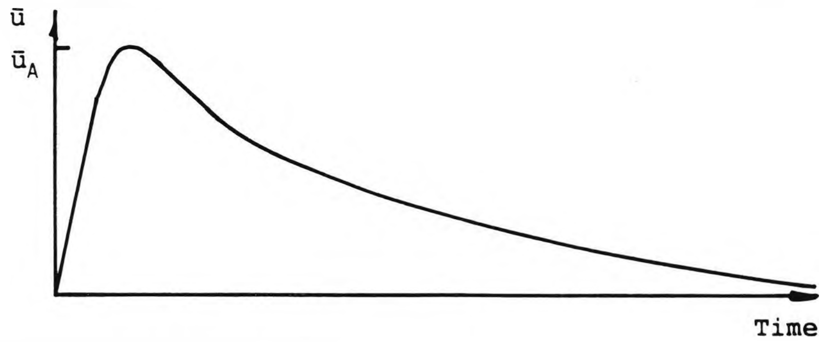

b) Excess pore pressures at A

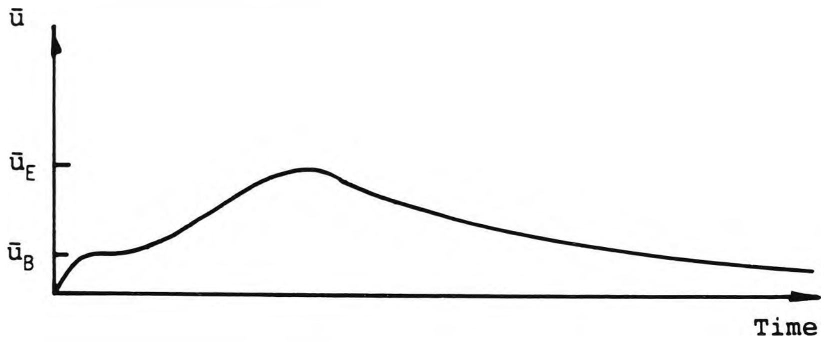

c) Excess pore pressures at B

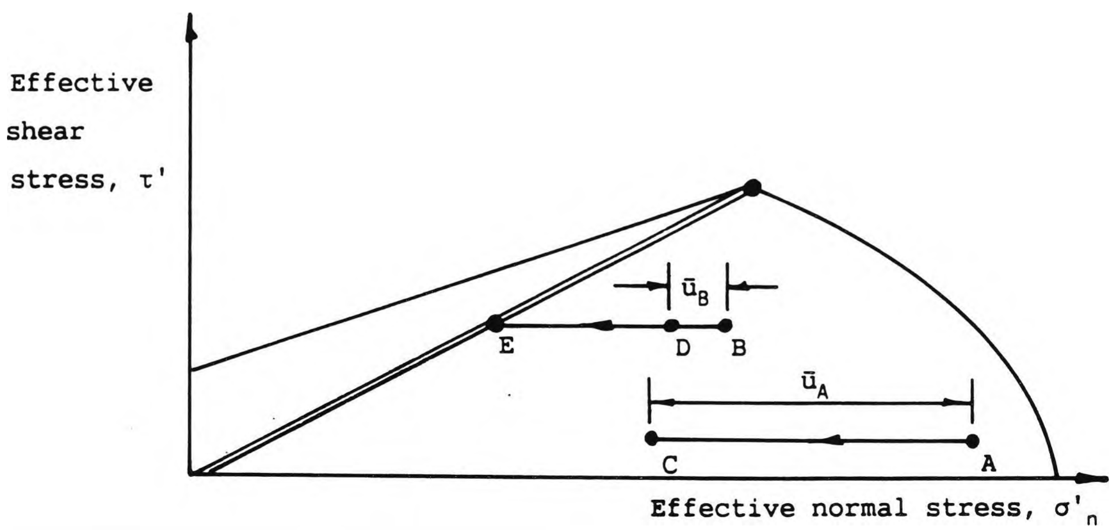

d) Stress paths of soil elements

Figure 2.8 Liquefaction beneath a structure

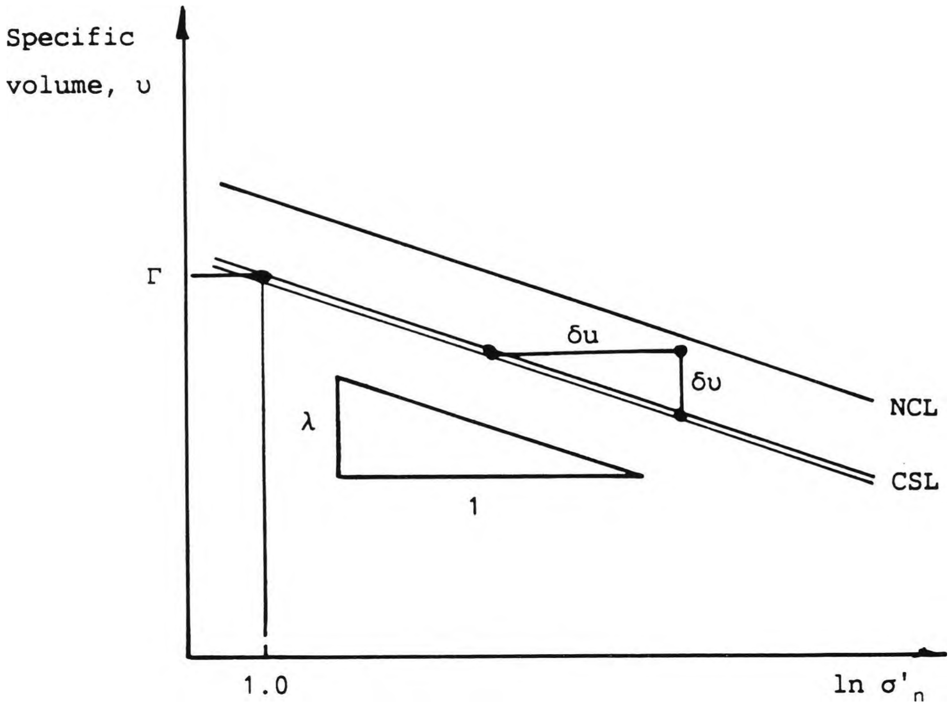

Figure 2.9 Geometry of the critical state line

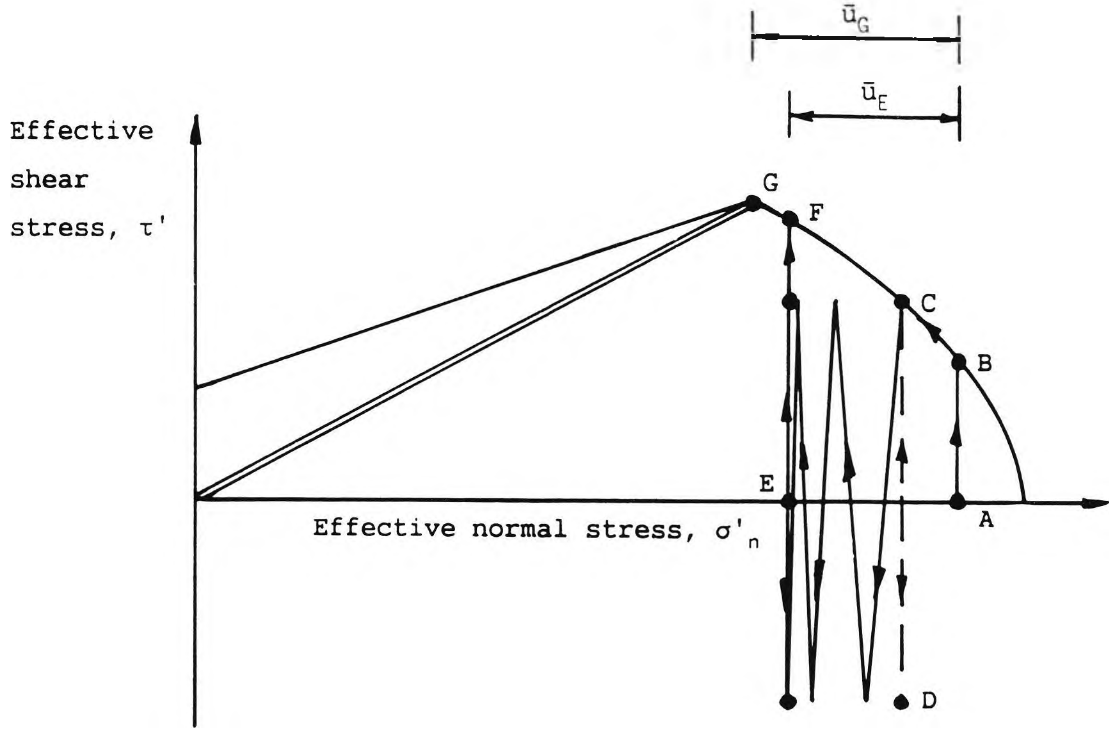

a) Cyclic loading of a wet of critical soil state

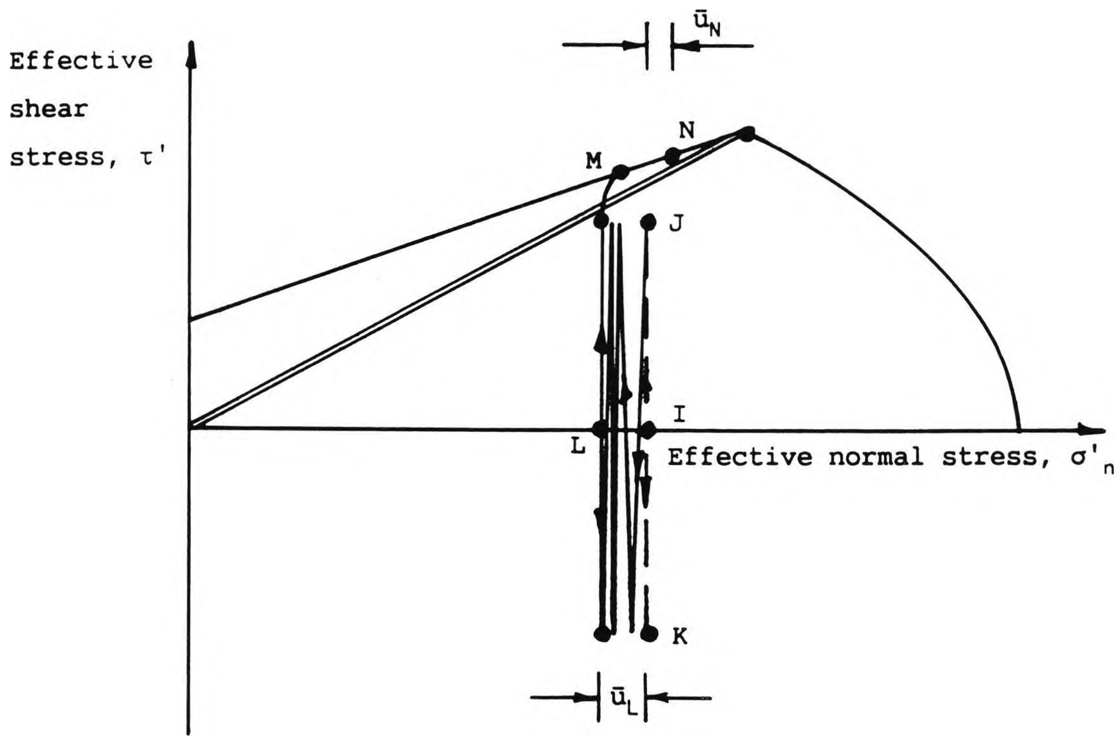

b) Cyclic loading of a dry of critical soil state

Figure 2.10 Stress paths for cyclic loading

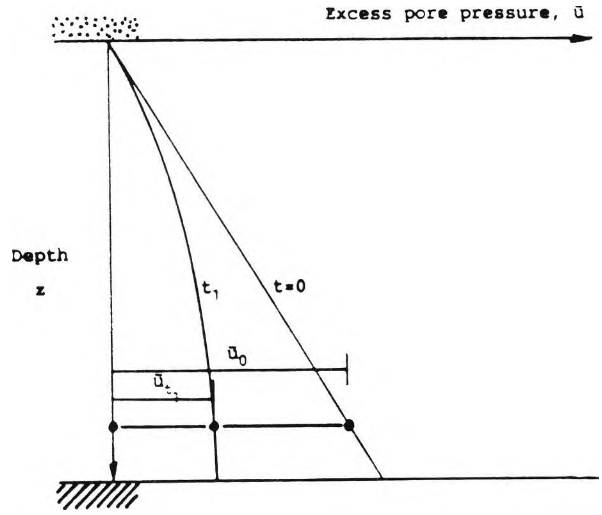

a) Isochrones of excess pore pressure for one-way drainage towards surface (after Dwyer, 1986)

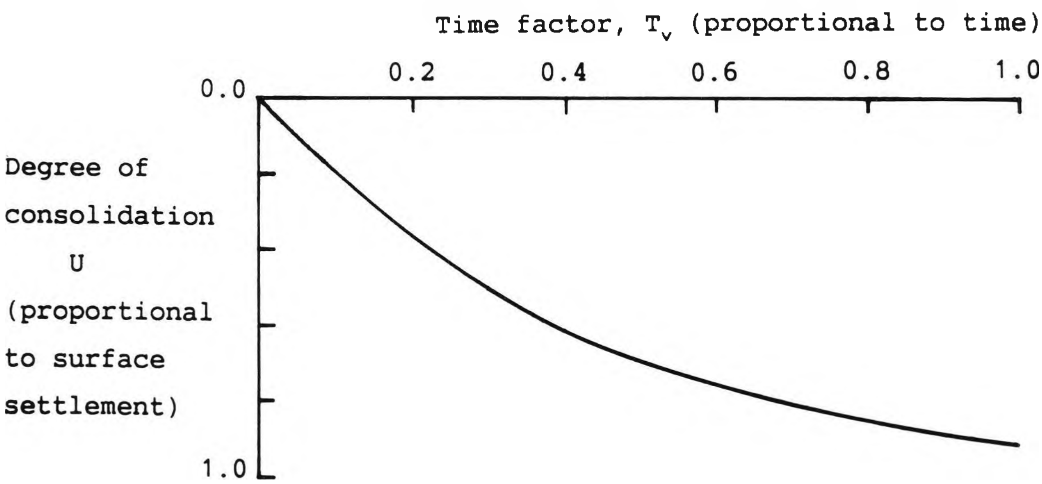

b) Surface settlement with time

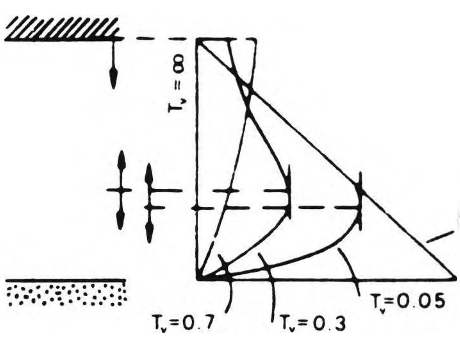

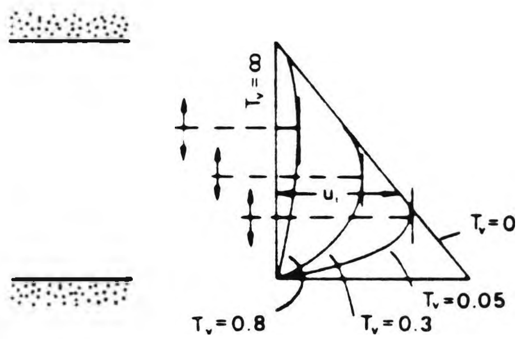

c) Isochrones of excess pore pressure for one-way drainage towards base

d) Isochrones of excess pore pressure for two-way drainage

(after Craig, 1987)

Figure 2.11 Excess pore pressure dissipation and surface settlement by one- dimensional consolidation

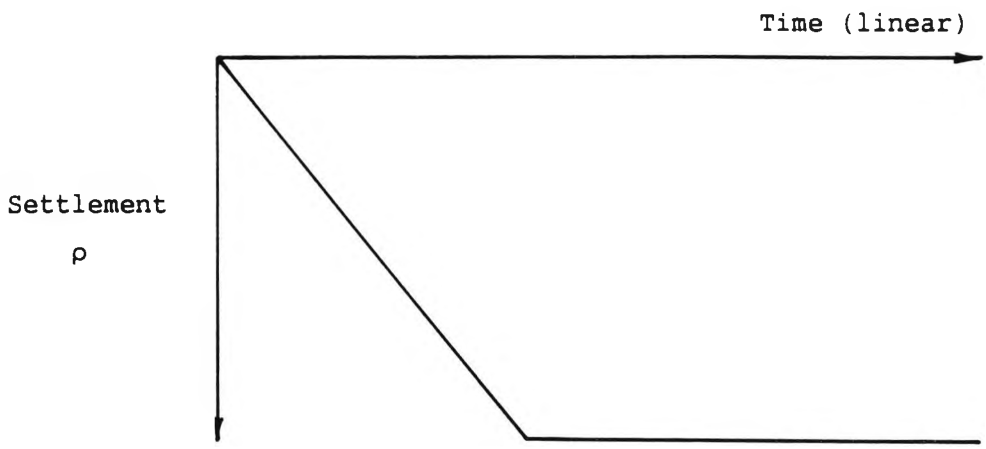

a) Surface settlement

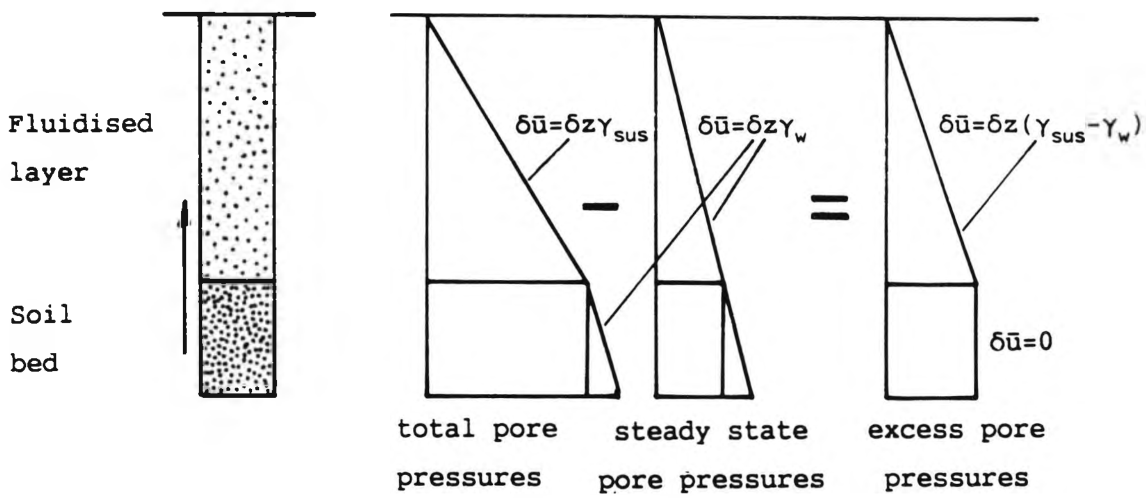

b) Pore pressures in a resedimenting soil bed

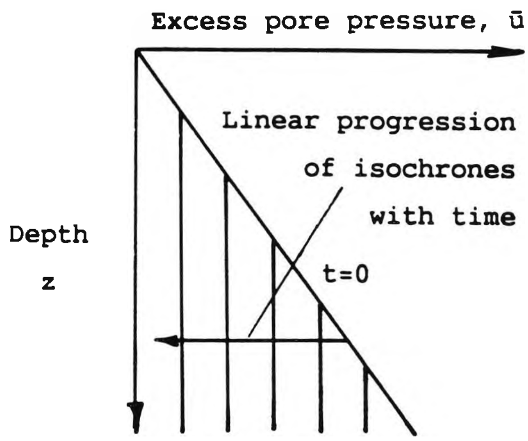

c) Isochrones of excess pore pressure within a resedimenting soil bed

Figure 2.12 Excess pore pressure dissipation and surface settlement by hindered settling

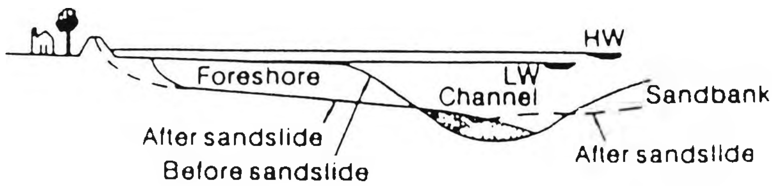

Figure 3.1 Section through Dutch coastal defences, before and after flow slide failure (after Lindenberg and Koning, 1981)

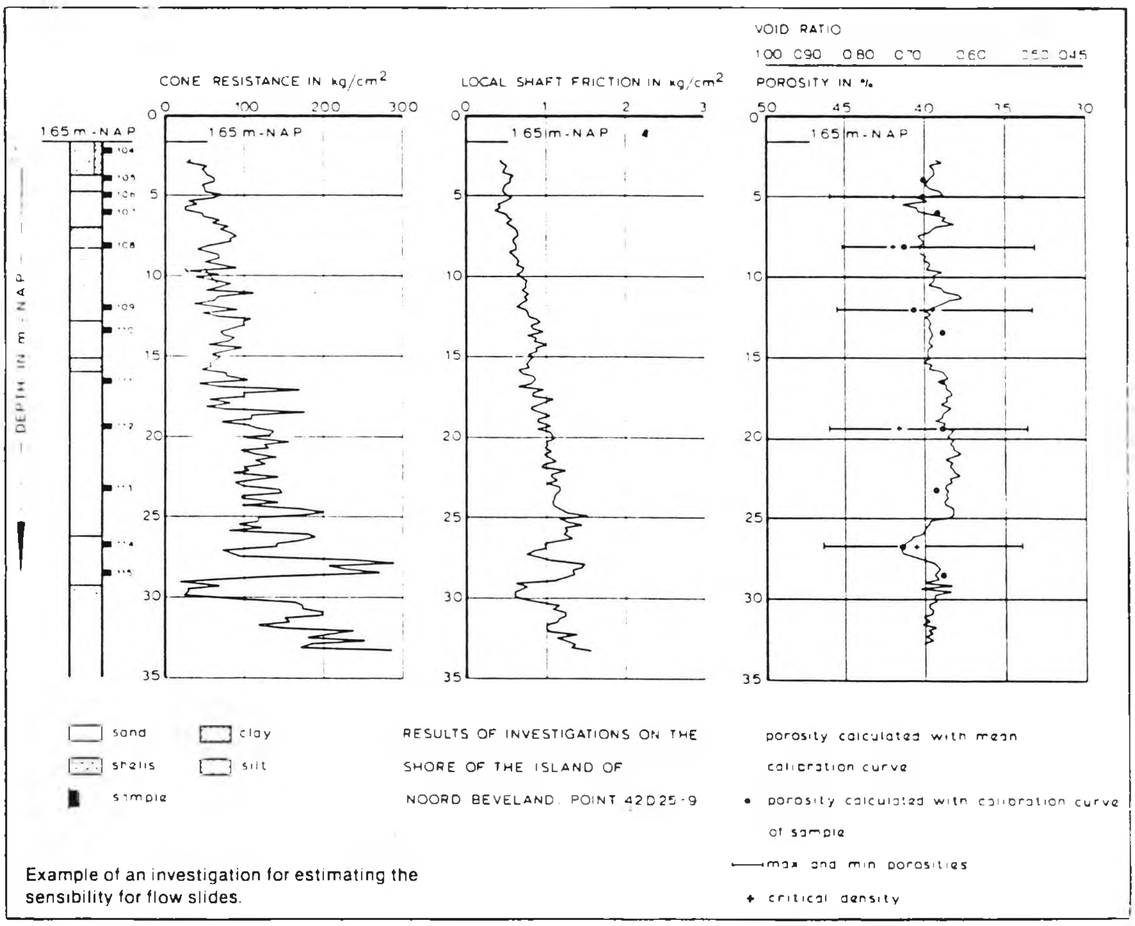

Figure 3.2 Example of results of an investigation to assess the sensitivity of Dutch coastal deposits to flow slide failure (after Delft, 1984)

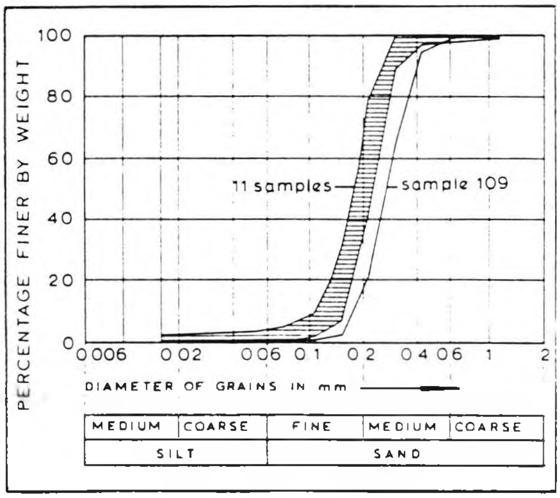

Figure 3.3 Grading envelope of sands from Dutch coastal deposits (after Delft, 1984)

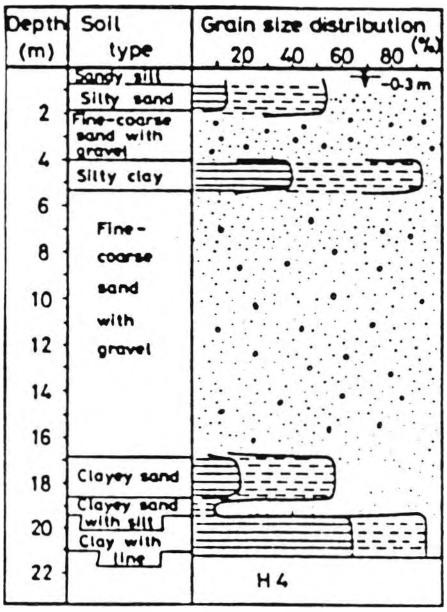

Figure 3.4 Soil profile associated with liquefaction failure induced by the 1977 Vrance earthquake (after Ishihara and Perlea, 1984)

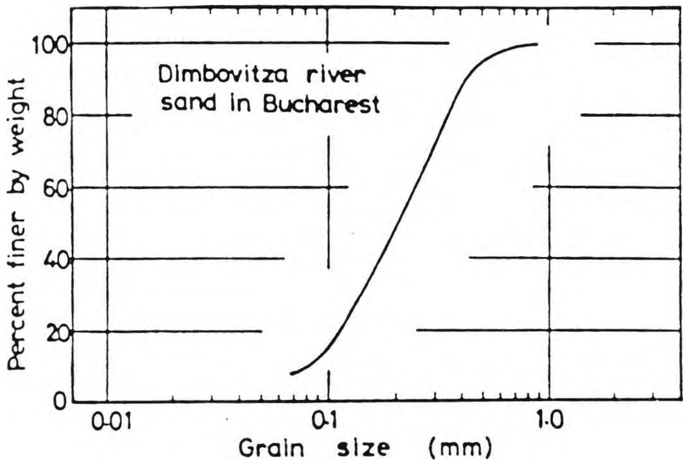

Figure 3.5 Particle size distribution curve of principal sand layer associated with liquefaction failures of 1977 Vrance earthquake (after Ishihara and Perlea, 1984)

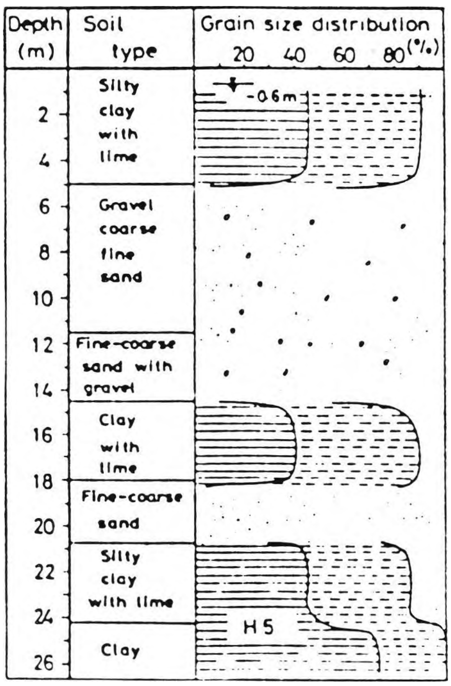

Figure 3.6 Soil profile subjected to 1977 Vrance earthquake which did not show signs of liquefaction failure (after Ishihara and Perlea, 1984)

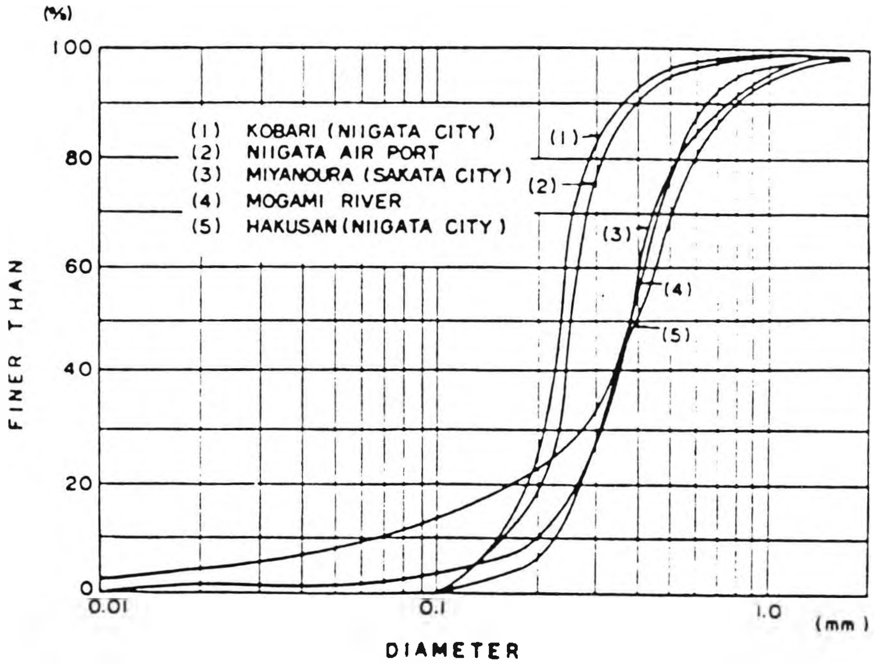

Figure 3.7 Range of particle size distribution curves for soils associated with liquefaction failures at Niigata, 1964 (after the Japanese Society of Soil Mechanics and Foundation Engineering, 1966)

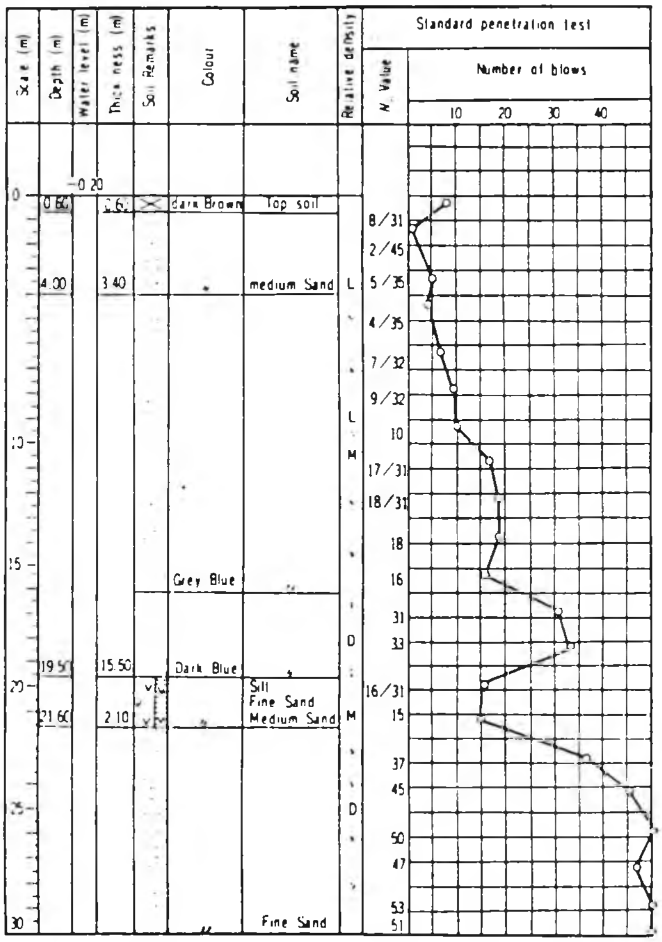

Figure 3.8 Soil profile near pier of Shianogawa Bridge, Niigata (after the Japanese Society of Soil Mechanics and Foundation Engineering, 1966)

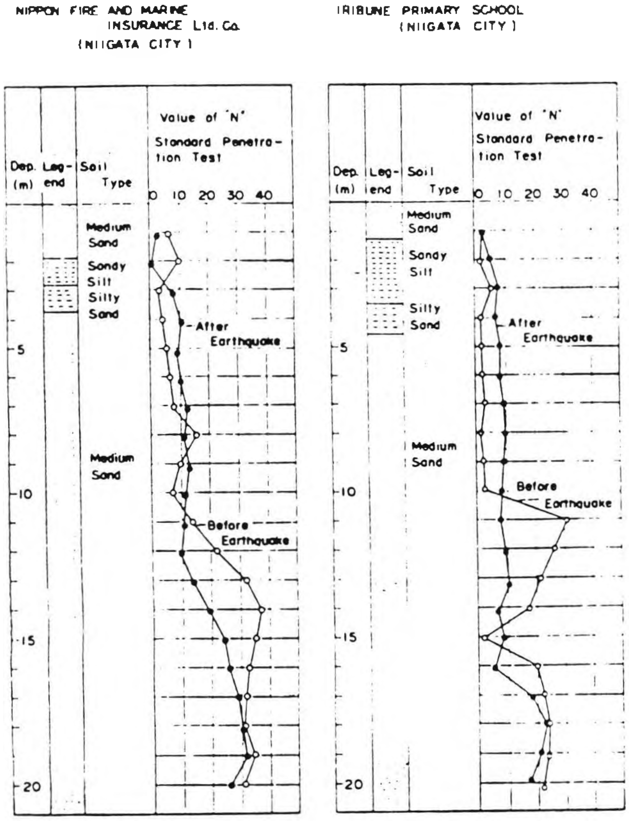

Figure 3.9 Soil profiles and results of standard penetration test performed near structures showing signs of liquefaction failure, Niigata (after the Japanese Society of Soil Mechanics and Foundation Engineering, 1966)

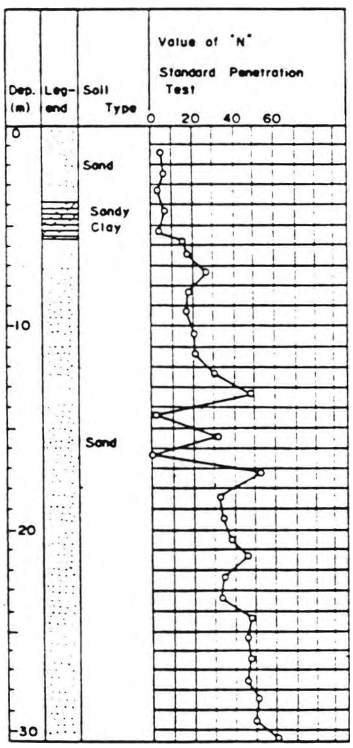

Figure 3.10 Soil profile at Hakusan transformer substation, Niigata (after the Japanese Society of Soil Mechanics and Foundation Engineering, 1966)

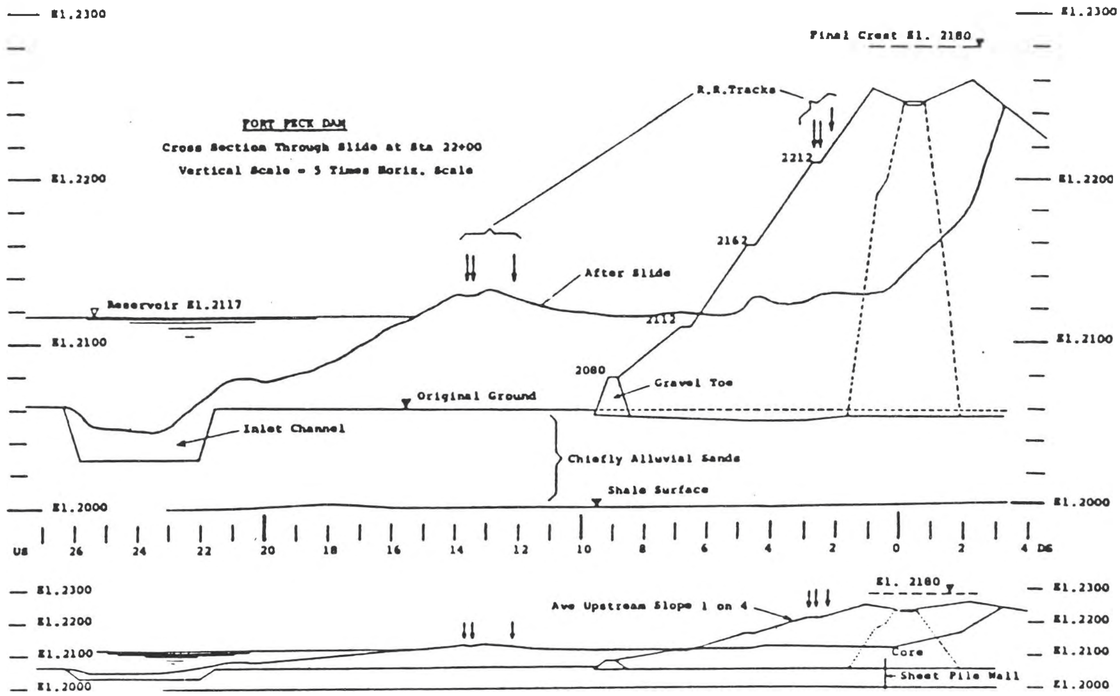

Figure 3.11 Section through Fort Peck Dam before and after partial collapse, 1938 (after Casagrande, 1975)

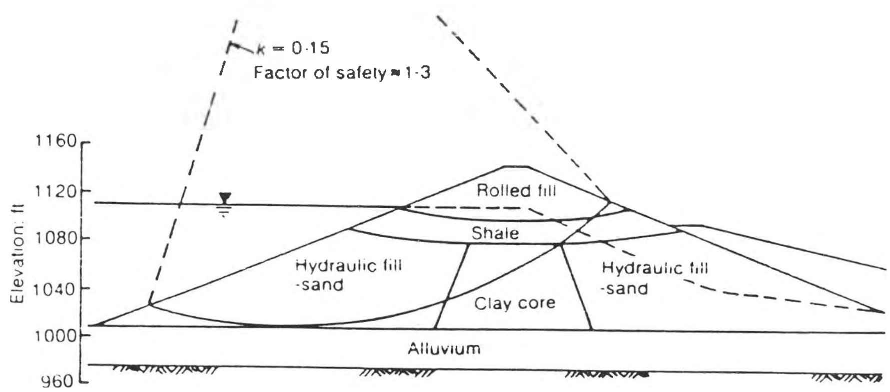

Figure 3.12 Lower San Fernando Dam before collapse (after Seed, 1979b)

Figure 3.13 Ground cracking and initial flow of water at ground level, Niigata 1964 (after Seed, 1970)

Figure 3.14 Sand vents produced by flow of groundwater, Niigata 1964 (after Seed, 1970)

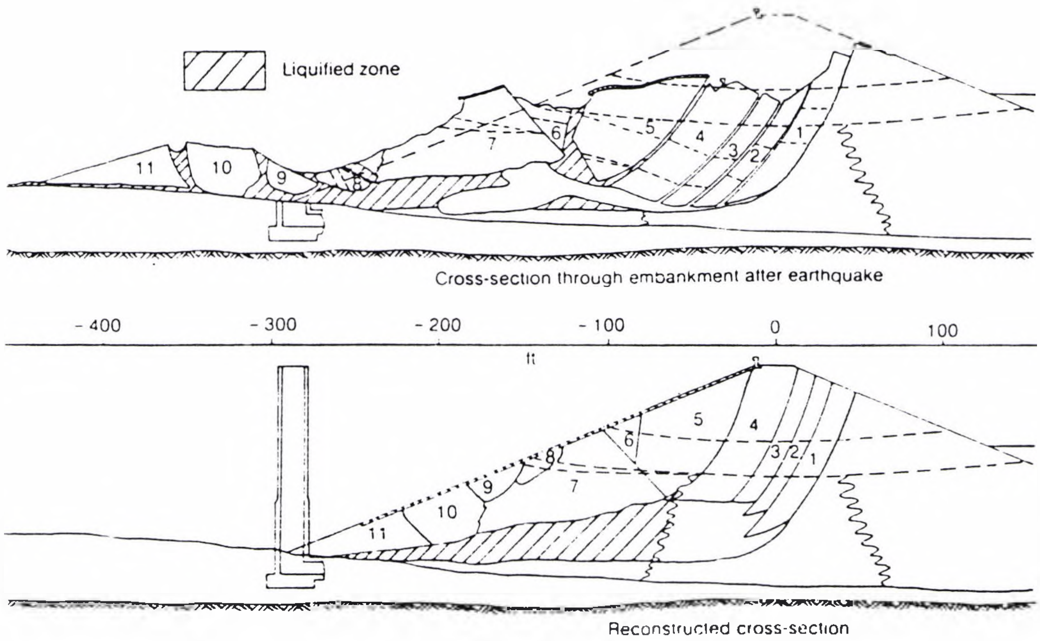

Figure 3.15 **Lower San Fernando Dam after collapse (after Seed, 1979b)**

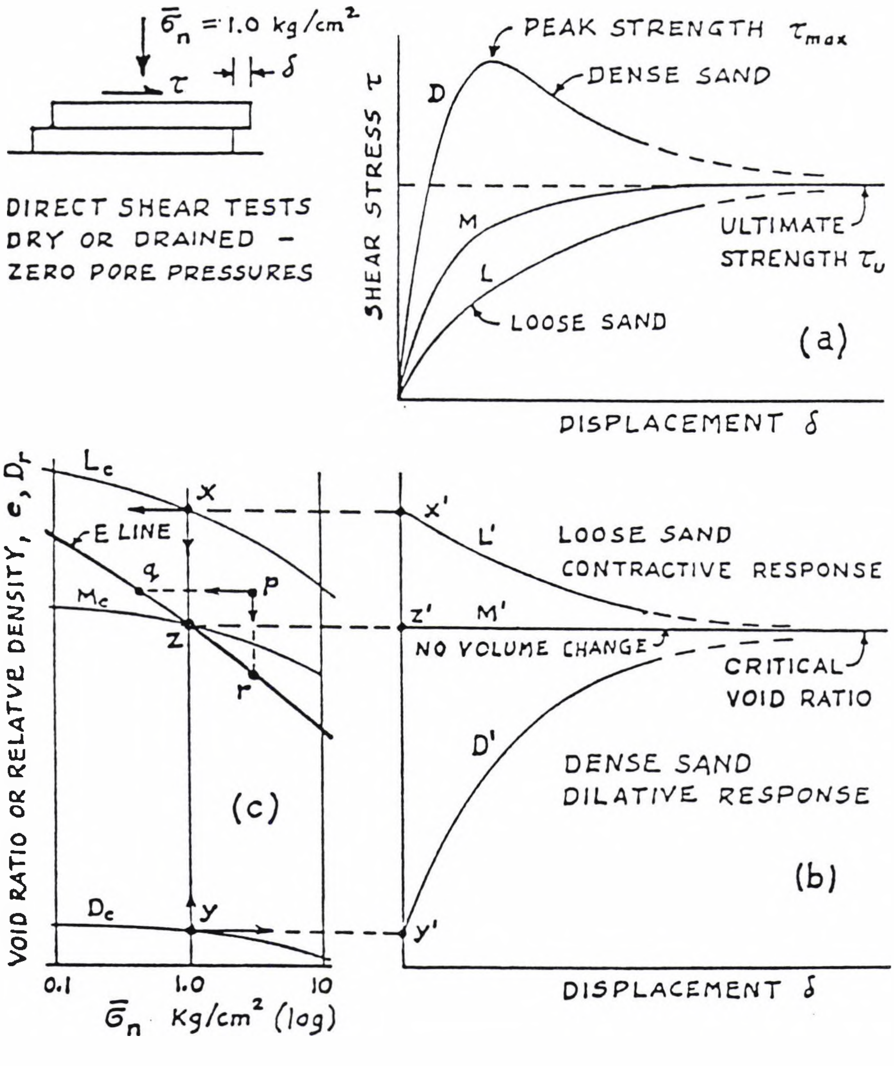

Figure 3.16 Early hypothesis of critical void ratio (after Casagrande, 1975)

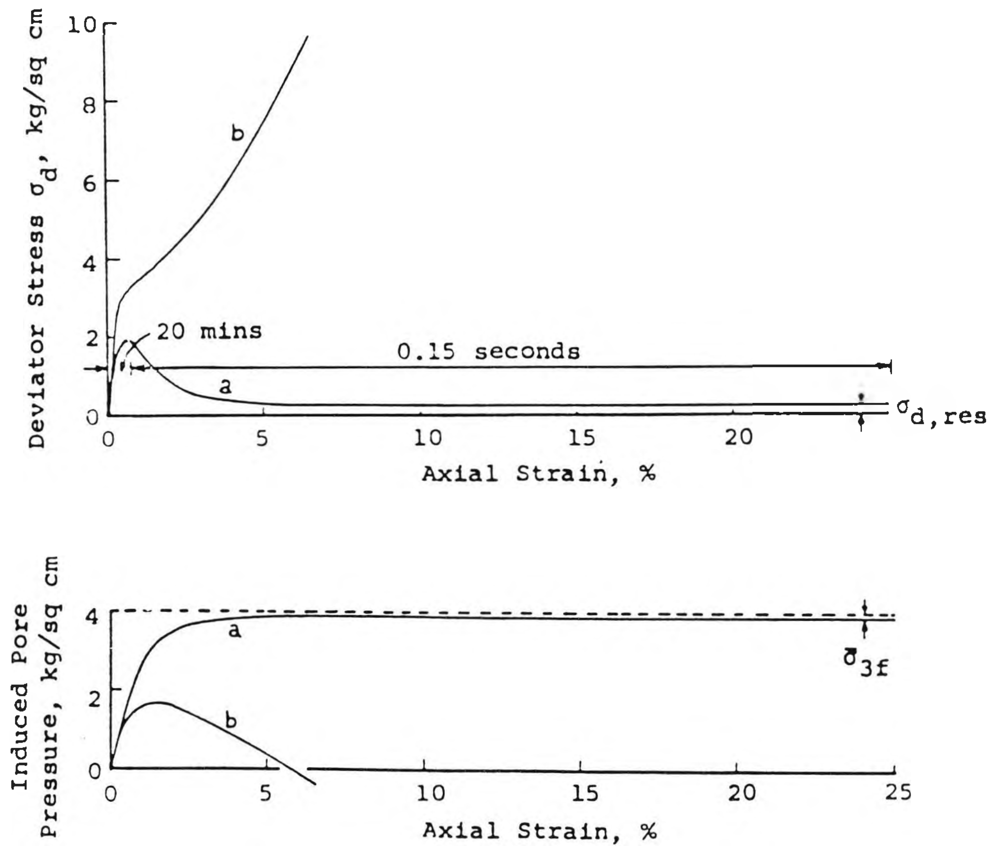

Figure 3.17 Critical void ratio approach, typical test date (after Castro, 1969)

Notes

i) a denotes loose samples

ii) b denotes dense samples

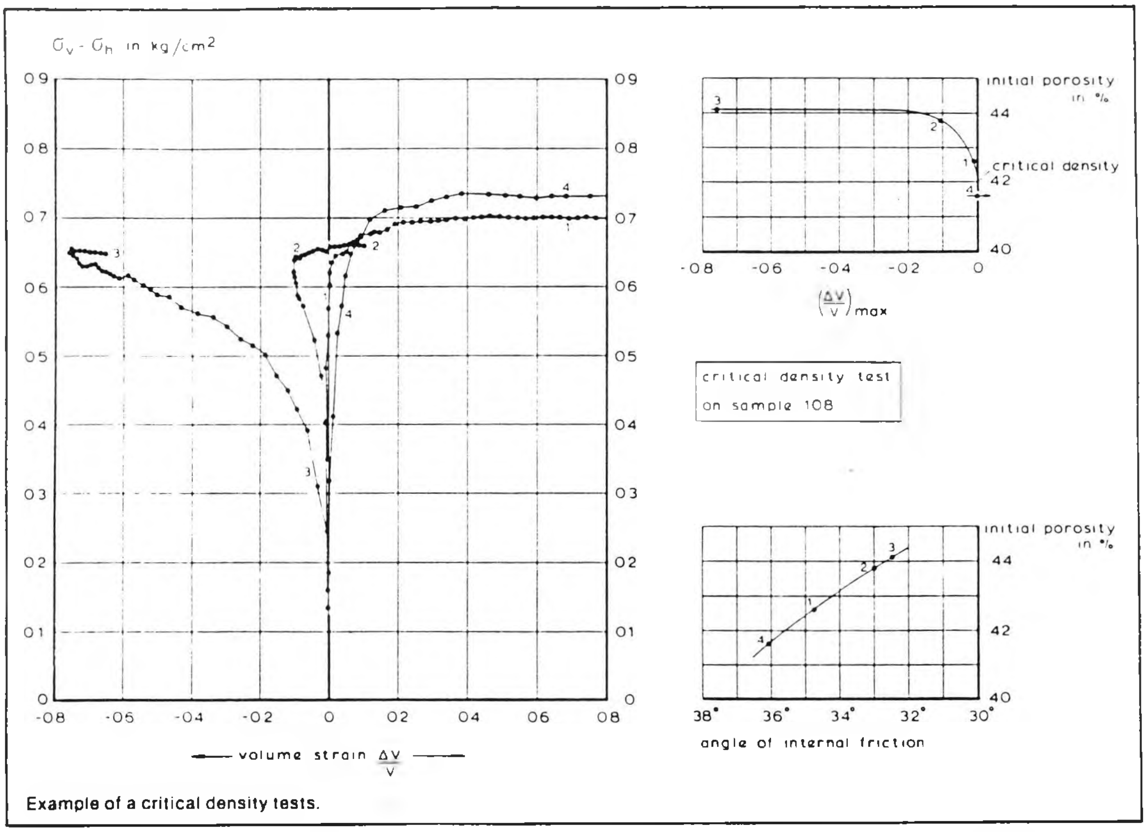

Figure 3.18 An example of test data to define a soils critical density (after Delft, 1984)

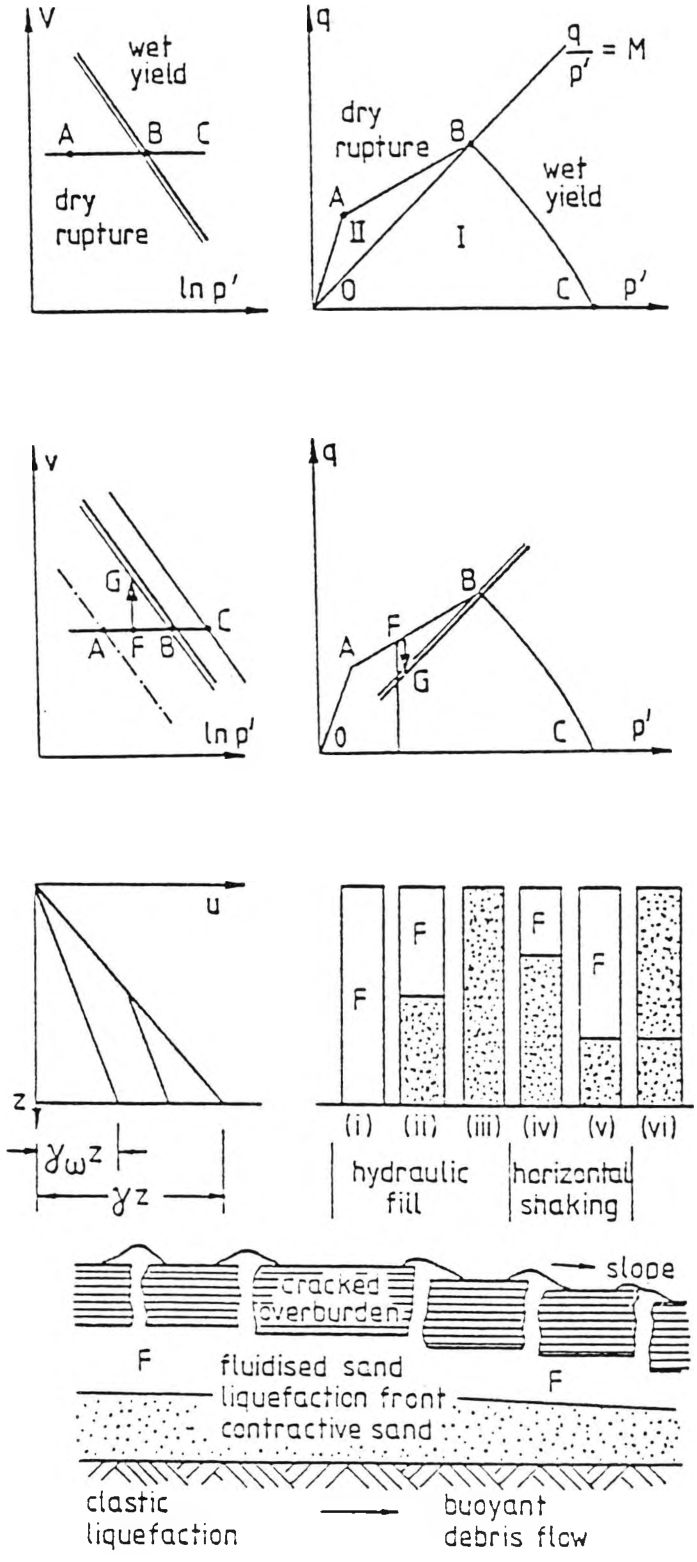

Figure 3.19 **A model of soil profile liquefaction (after Schofield, 1981)**

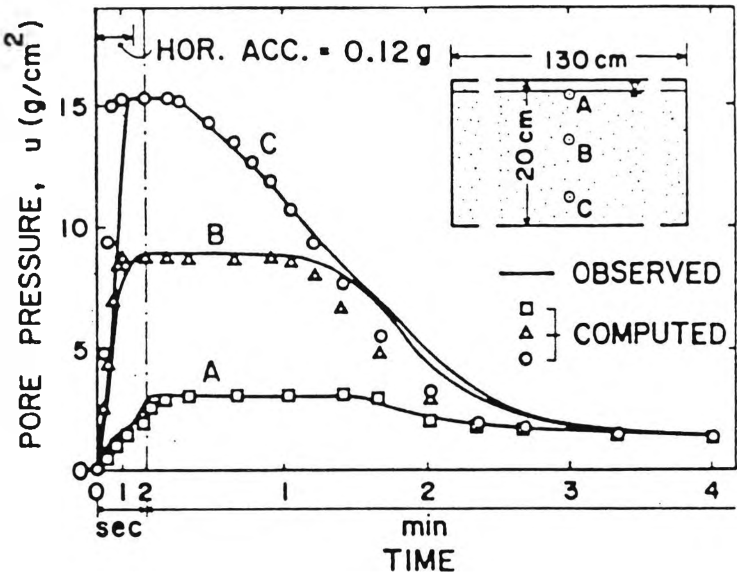

Figure 3.20 Computed and observed excess pore pressure response for a vibrating table test with a bed of loose sand (after Yoshimi, 1977)

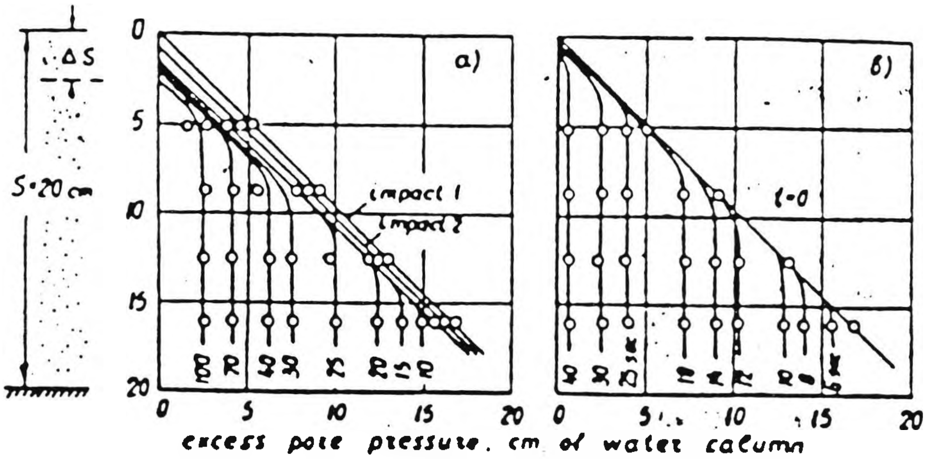

Figure 3.21 Isochrones of excess pore pressure dissipation observed after impact loading of a loose sand bed (after Florin and Ivanov, 1961)

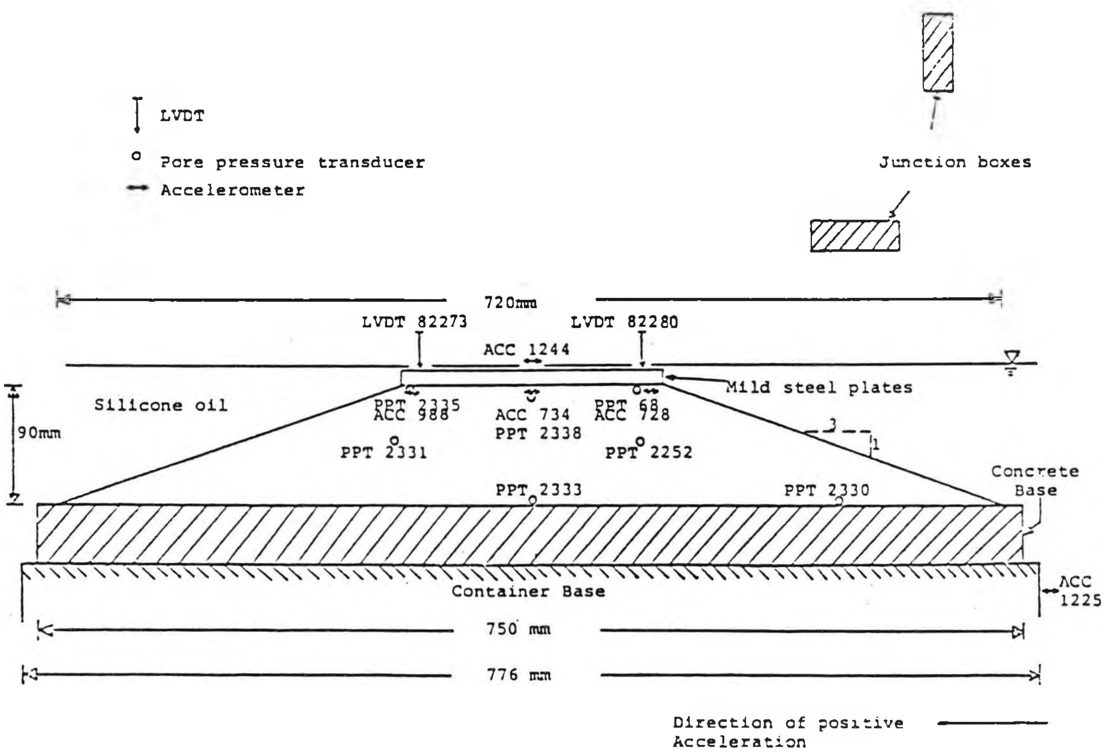

Figure 3.22 Configuration of a centrifuge test on a model island subjected to a simulated earthquake (Test FHL02C) (after Lee and Schofield, 1984)

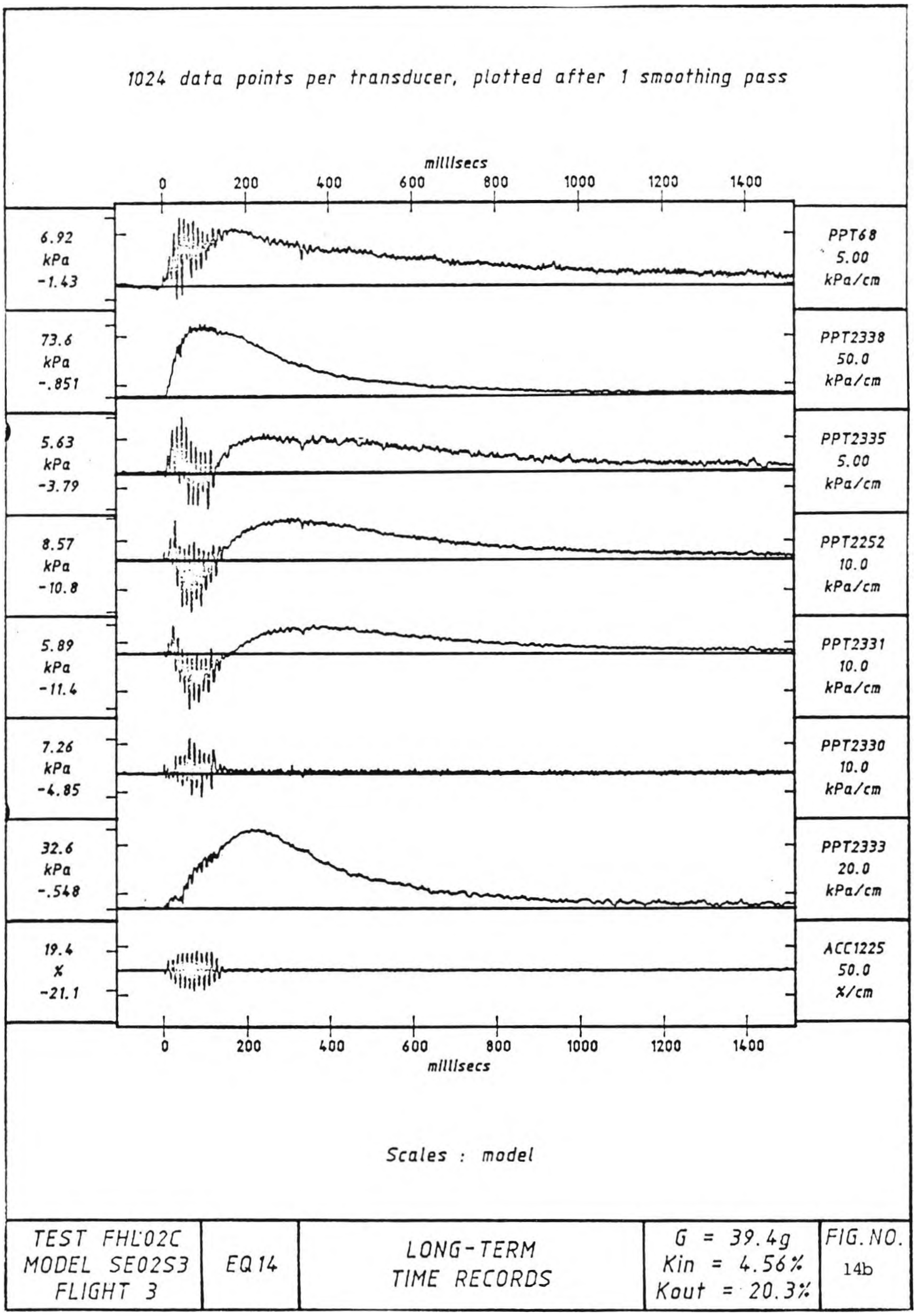

Figure 3.23 Selected results of centrifuge Test FHL02C (after Lee and Schofield, 1984)

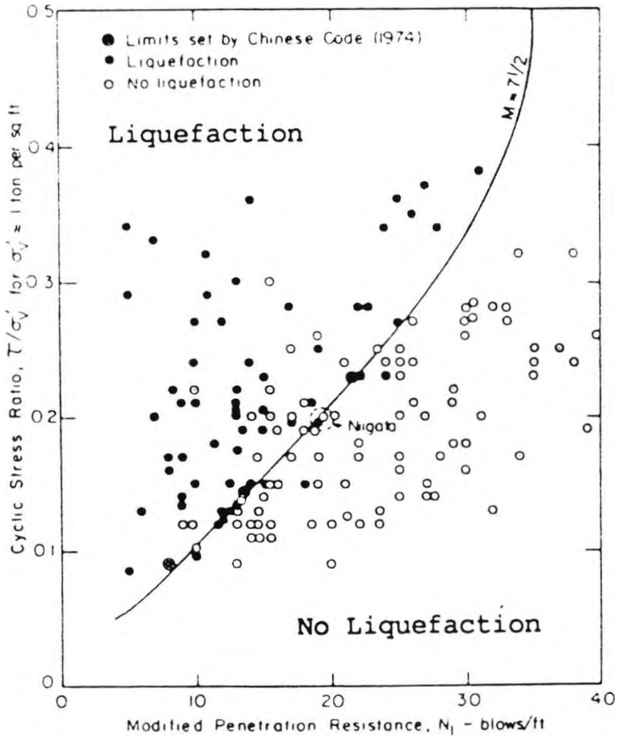

Figure 3.24 Data adopted to define the design curve for sands (D_{50} >0.25mm) subjected to magnitude 7.5 earthquakes, SPT method (after Seed et al, 1983)

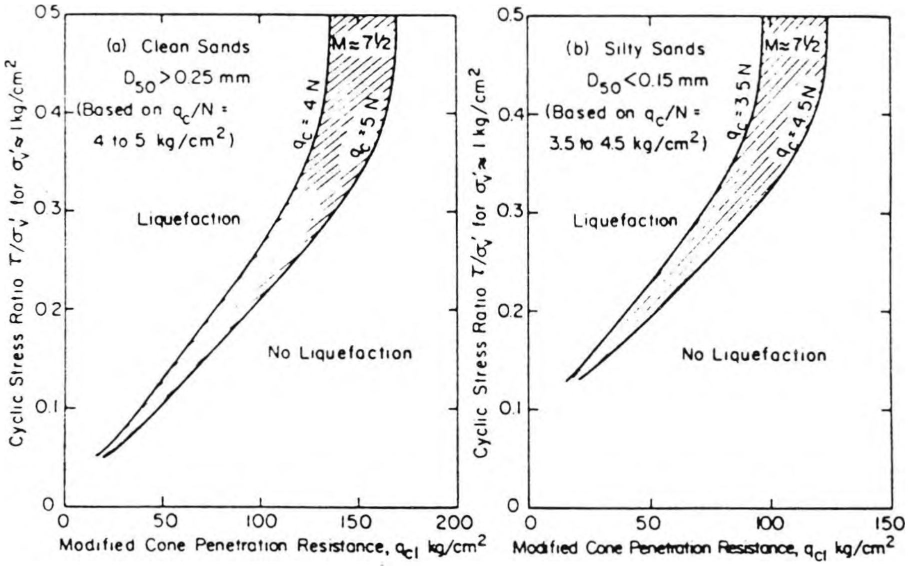

Figure 3.25 Proposed design charts for clean sands and silty sands subjected to magnitude 7.5 earthquakes, CPT method (after Seed et al, 1983)

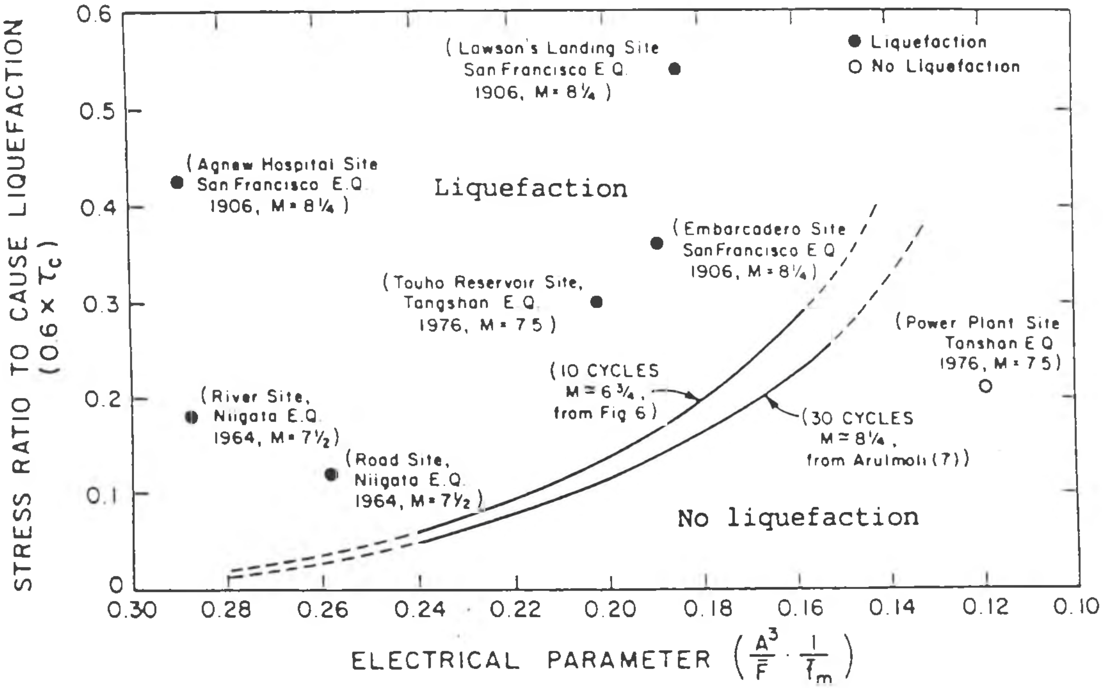

Figure 3.26 Summary of field test results for the electrical resistivity method (after Arulmoli et al, 1981)

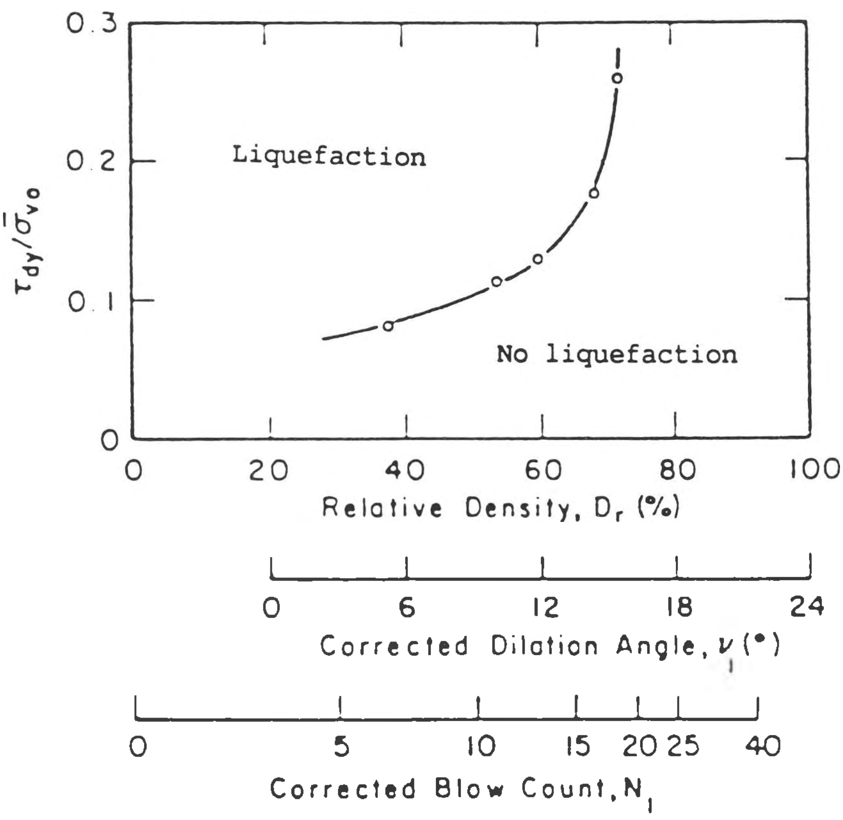

Figure 3.27 Proposed correlation between liquefaction potential and dilation angle (after Vaid et al, 1981)

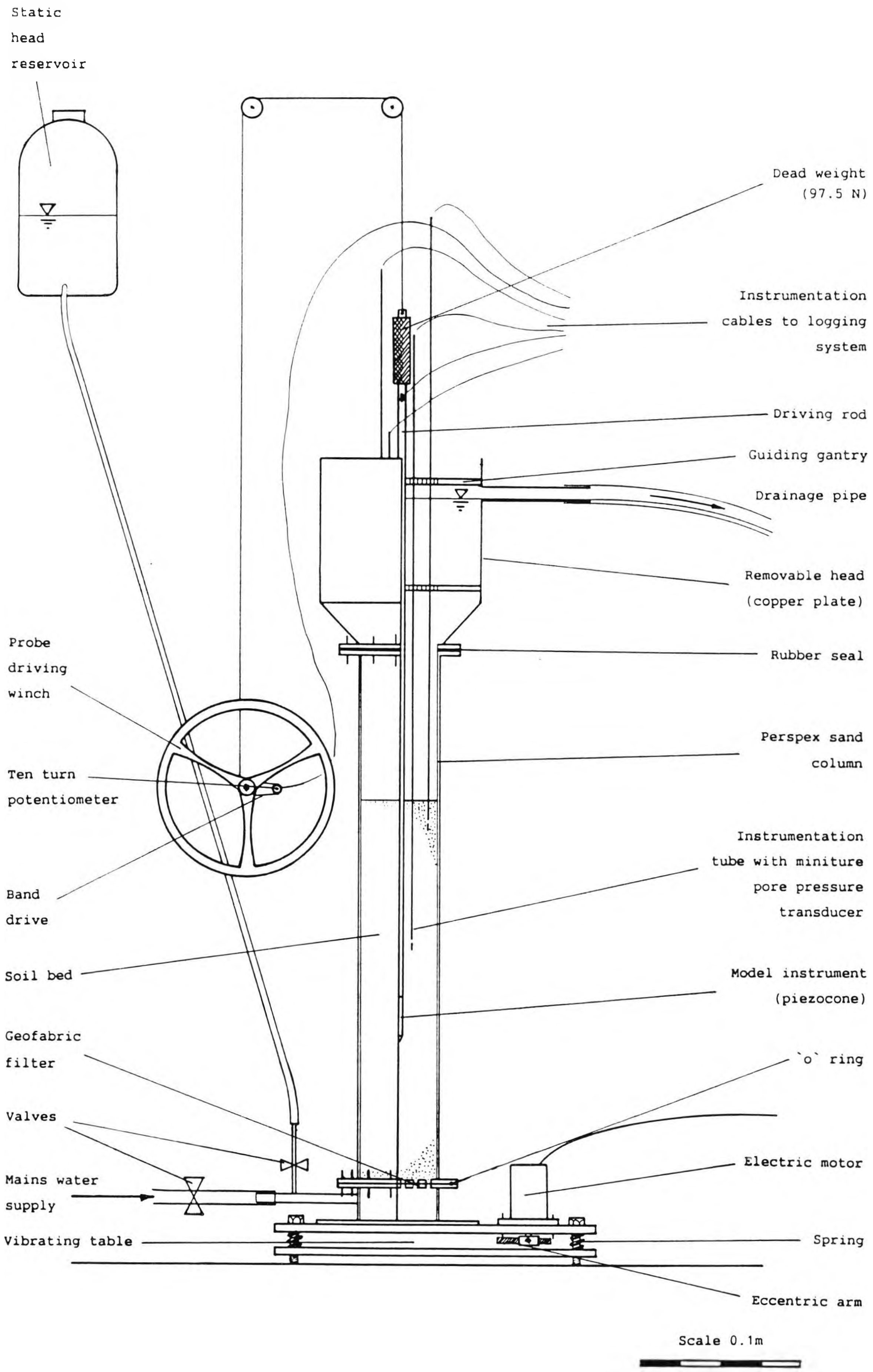

Figure 4.1 Sand column apparatus (half-section)

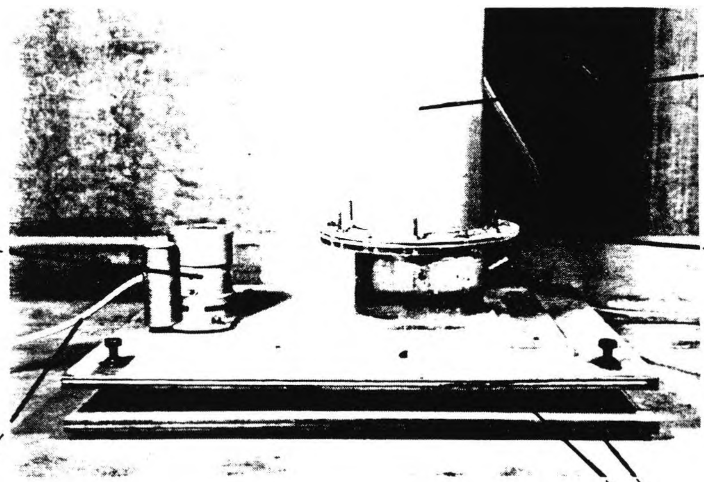

Figure 4.2 Vibrating table

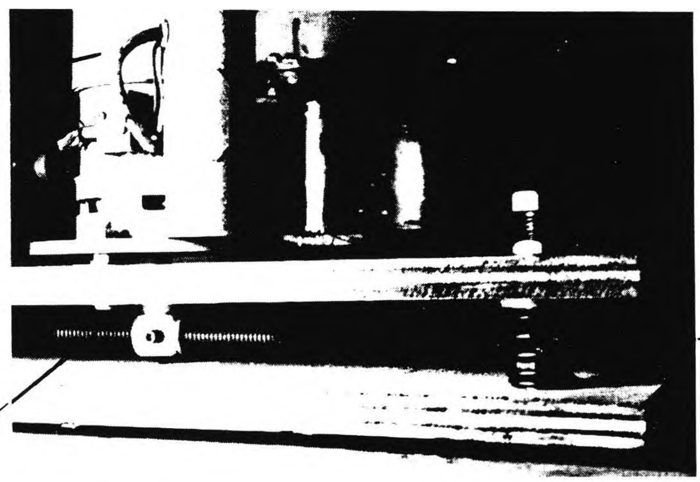

Figure 4.3 Eccentric weight and motor of the vibrating table

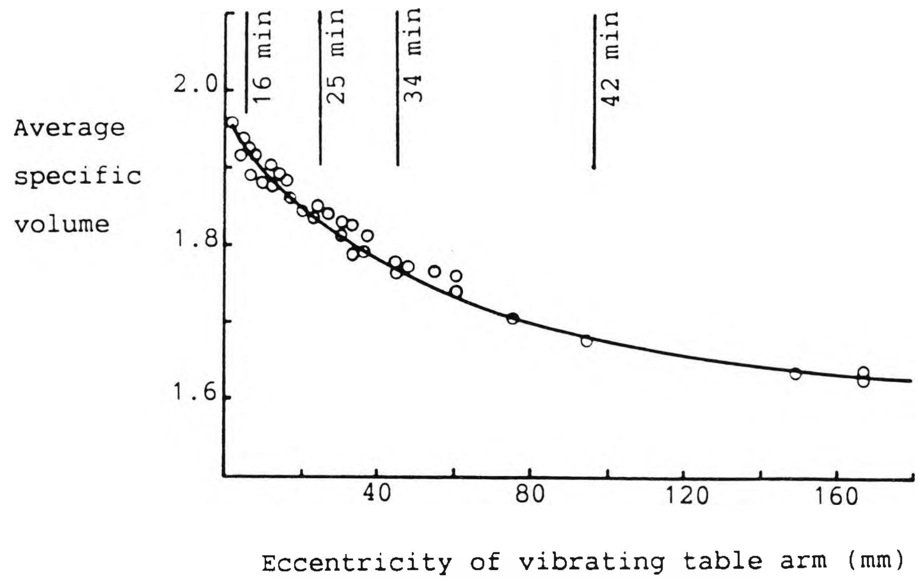

Figure 4.4 Vibrating table calibration curve

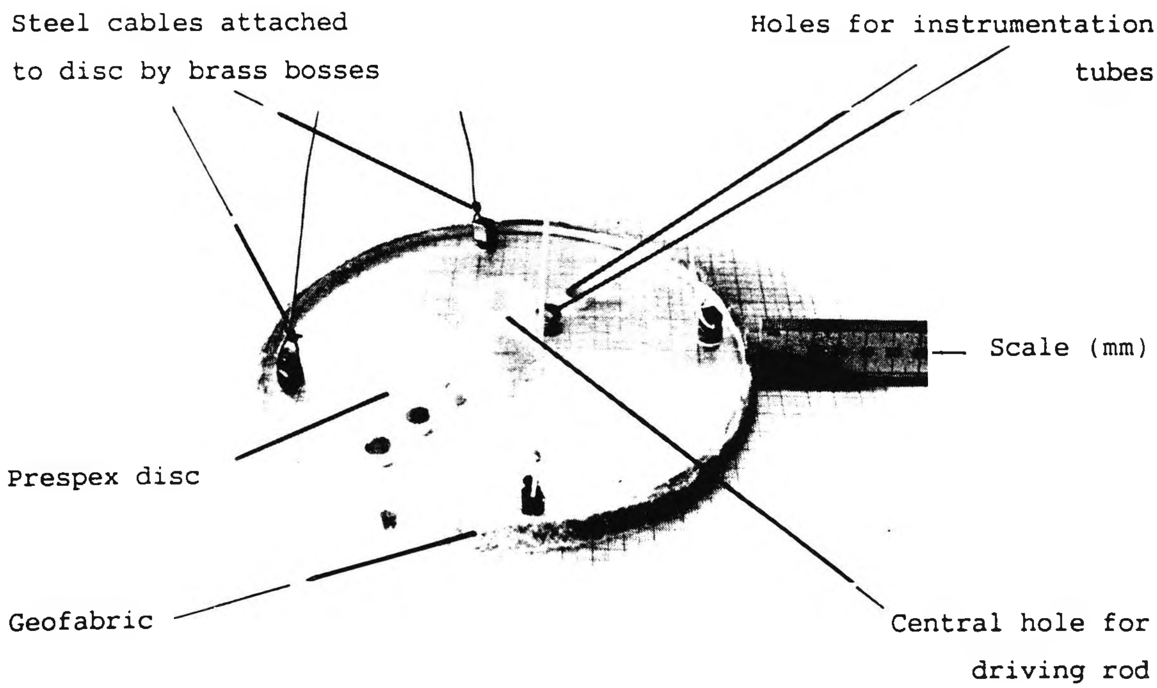

Figure 4.5 Surcharge disc

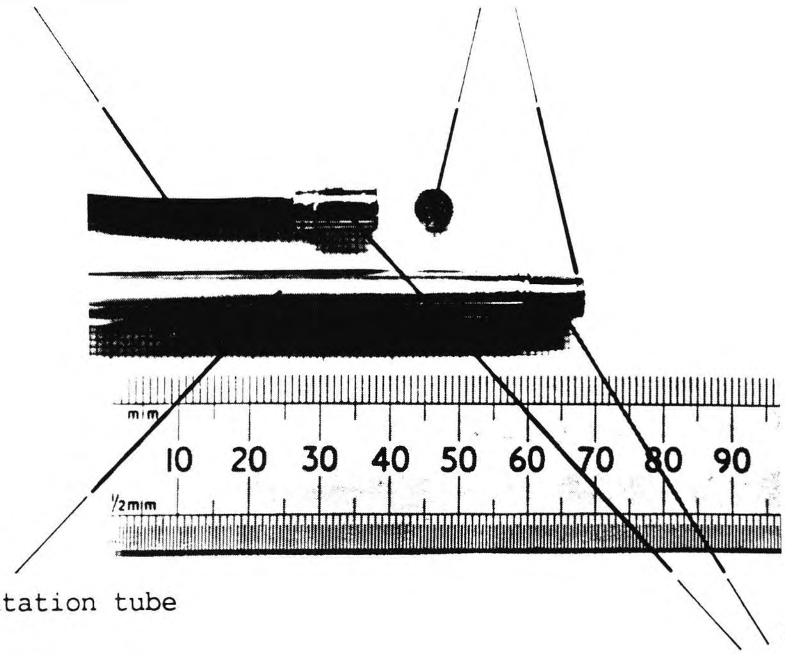

Figure 4.6 Instrumentation tube and miniature pore pressure transducer

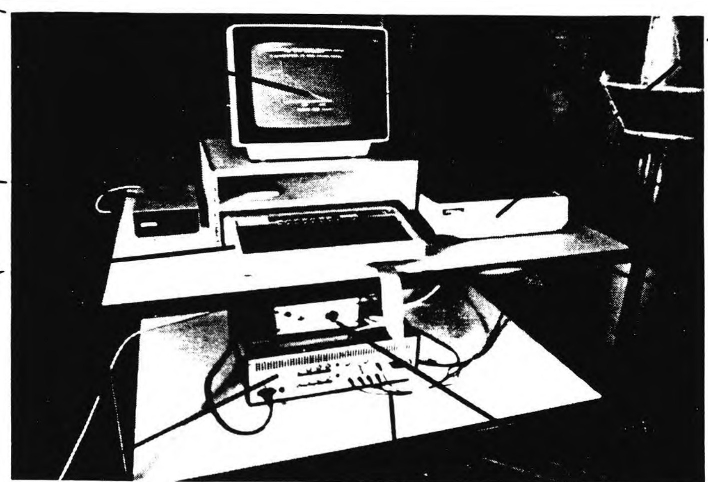

Figure 4.7 Computer controlled data logging system

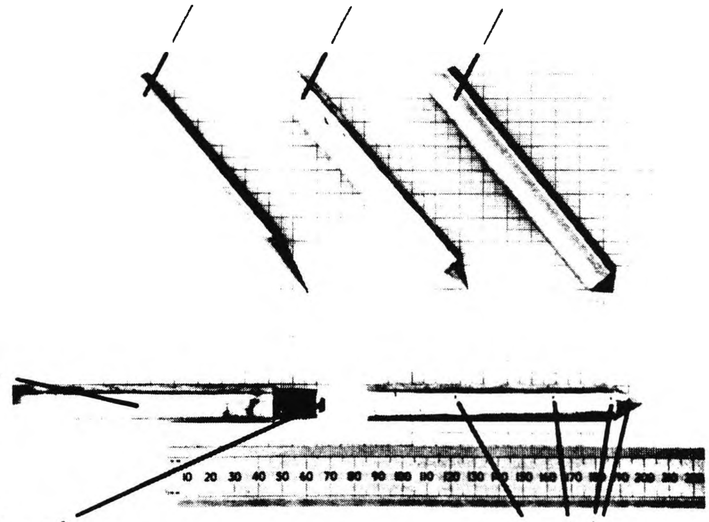

Figure 4.8 Cones and piezocones

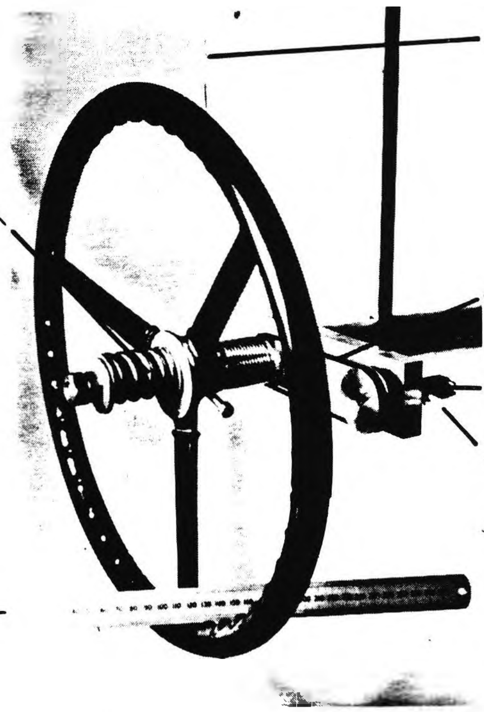

Figure 4.9 Cone driving mechanism

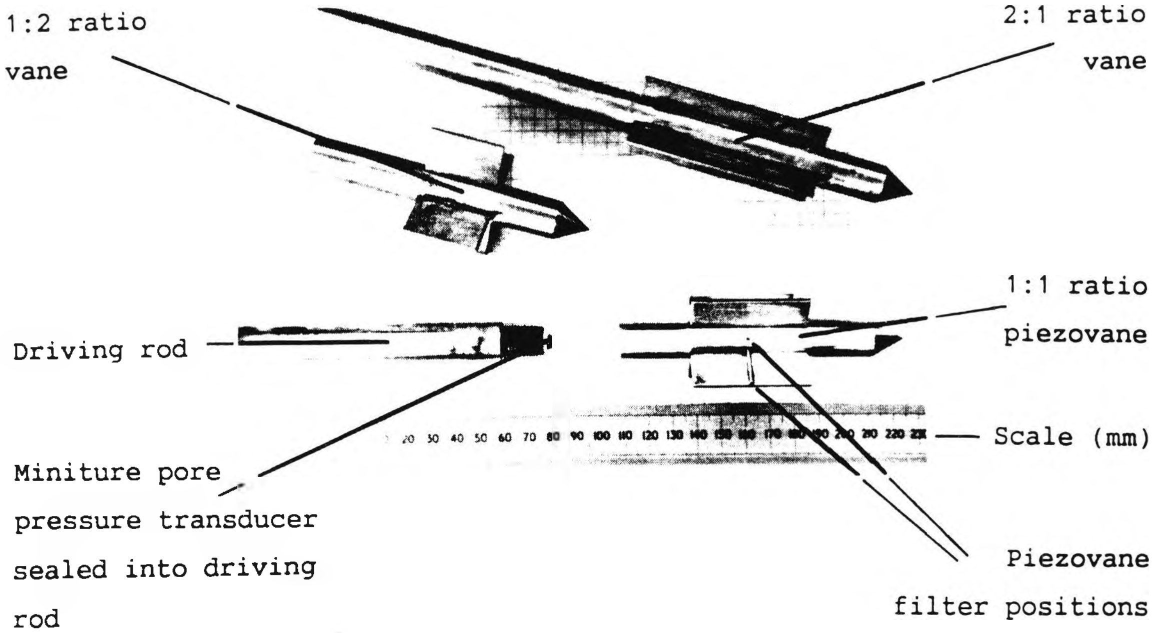

Figure 4.10 Vanes and piezovanes

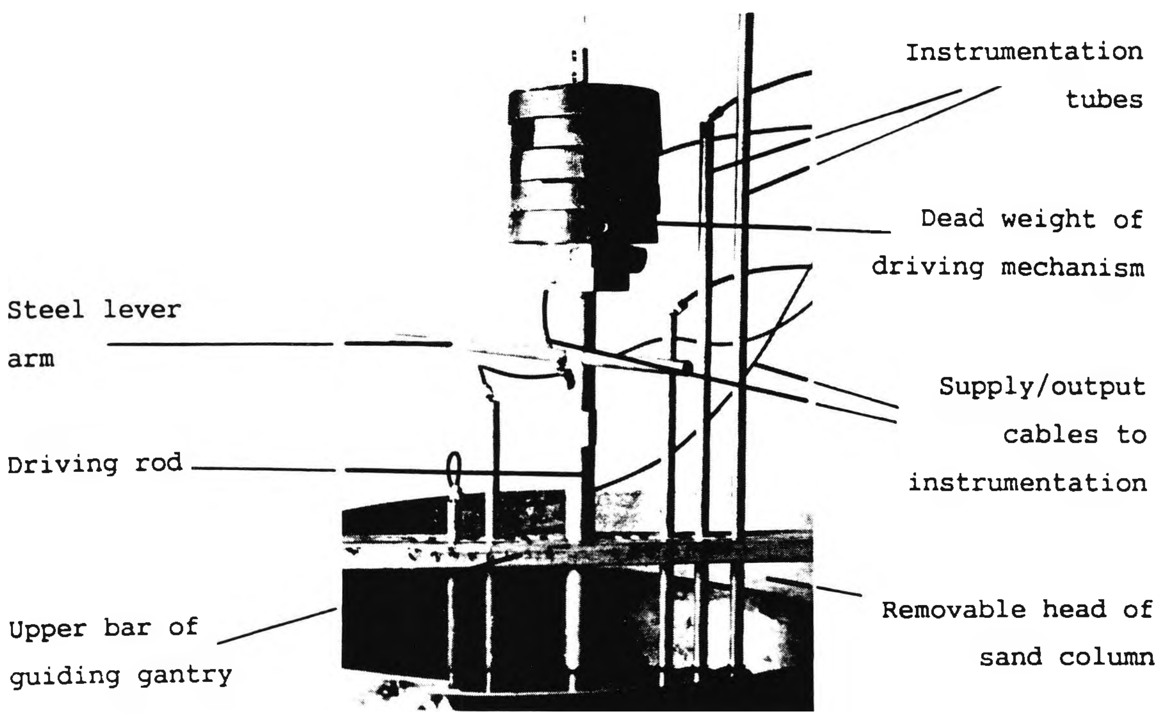

Figure 4.11 Vane rotating mechanism

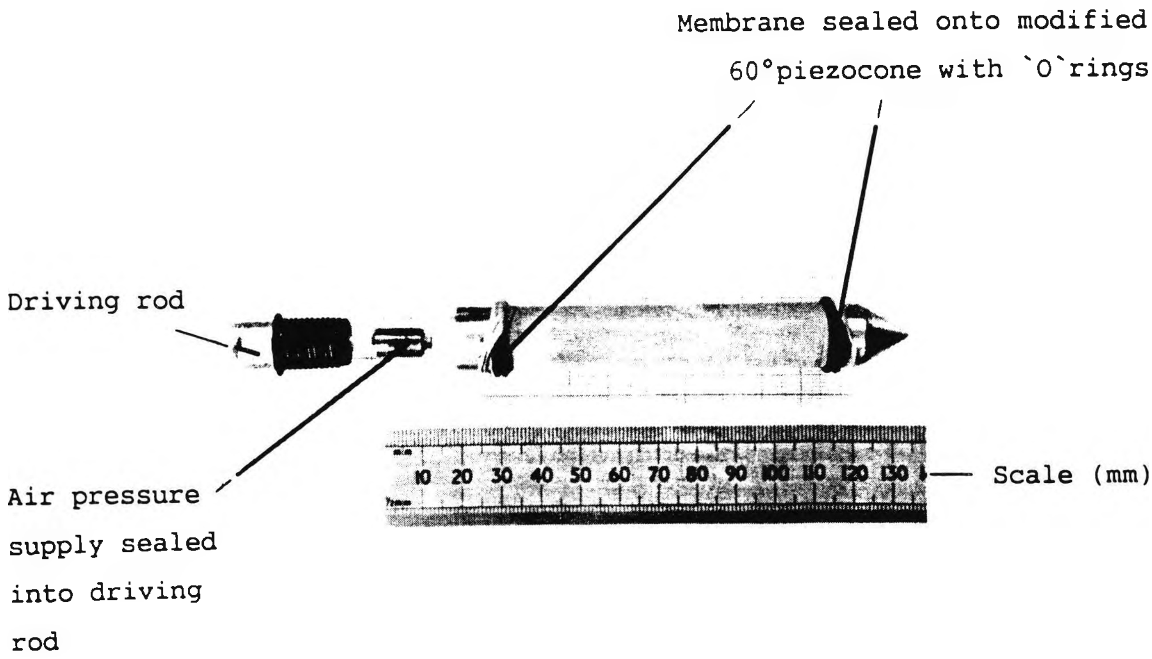

Figure 4.12 Expanding membrane probe

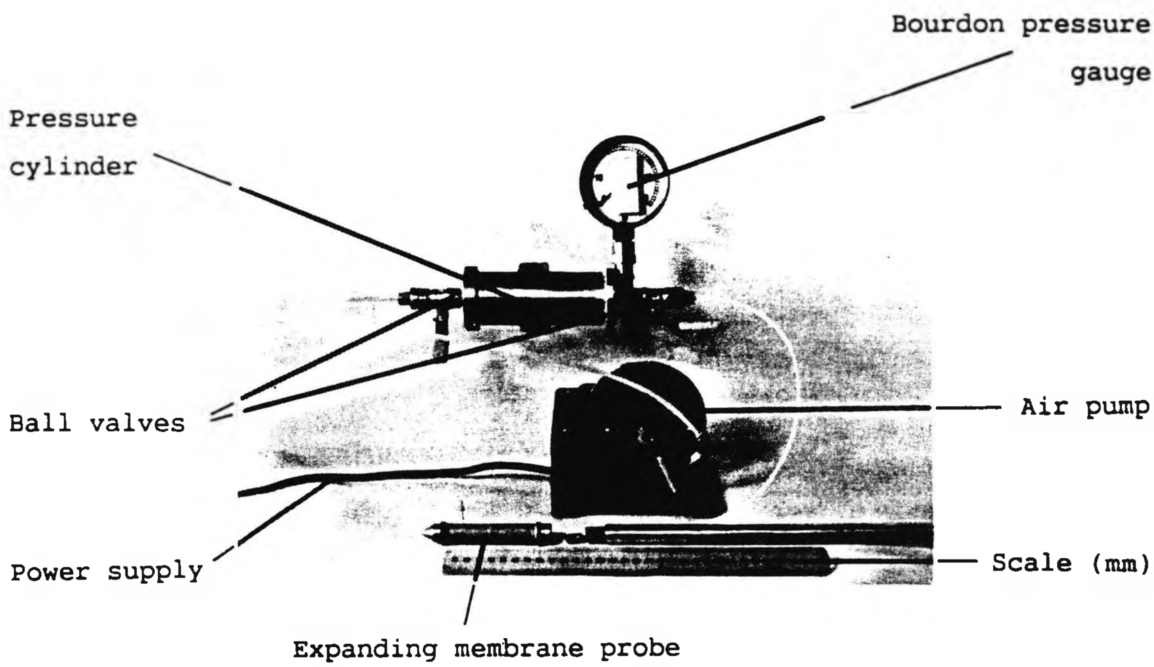

Figure 4.13 Pressure system for expanding membrane probe

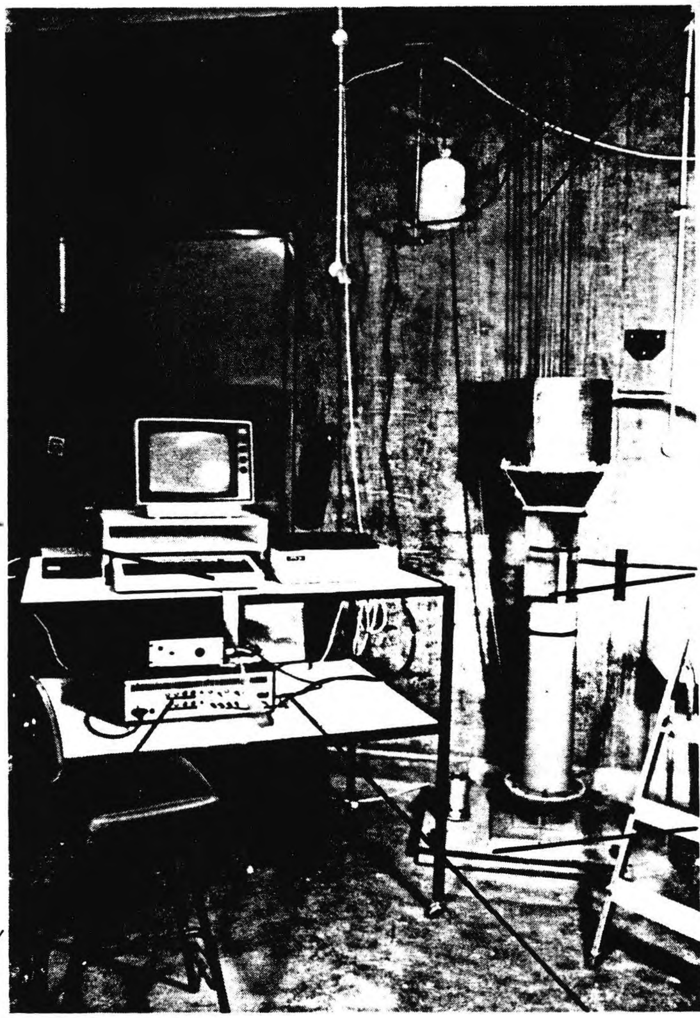

Figure 4.14 Assembled laboratory equipment

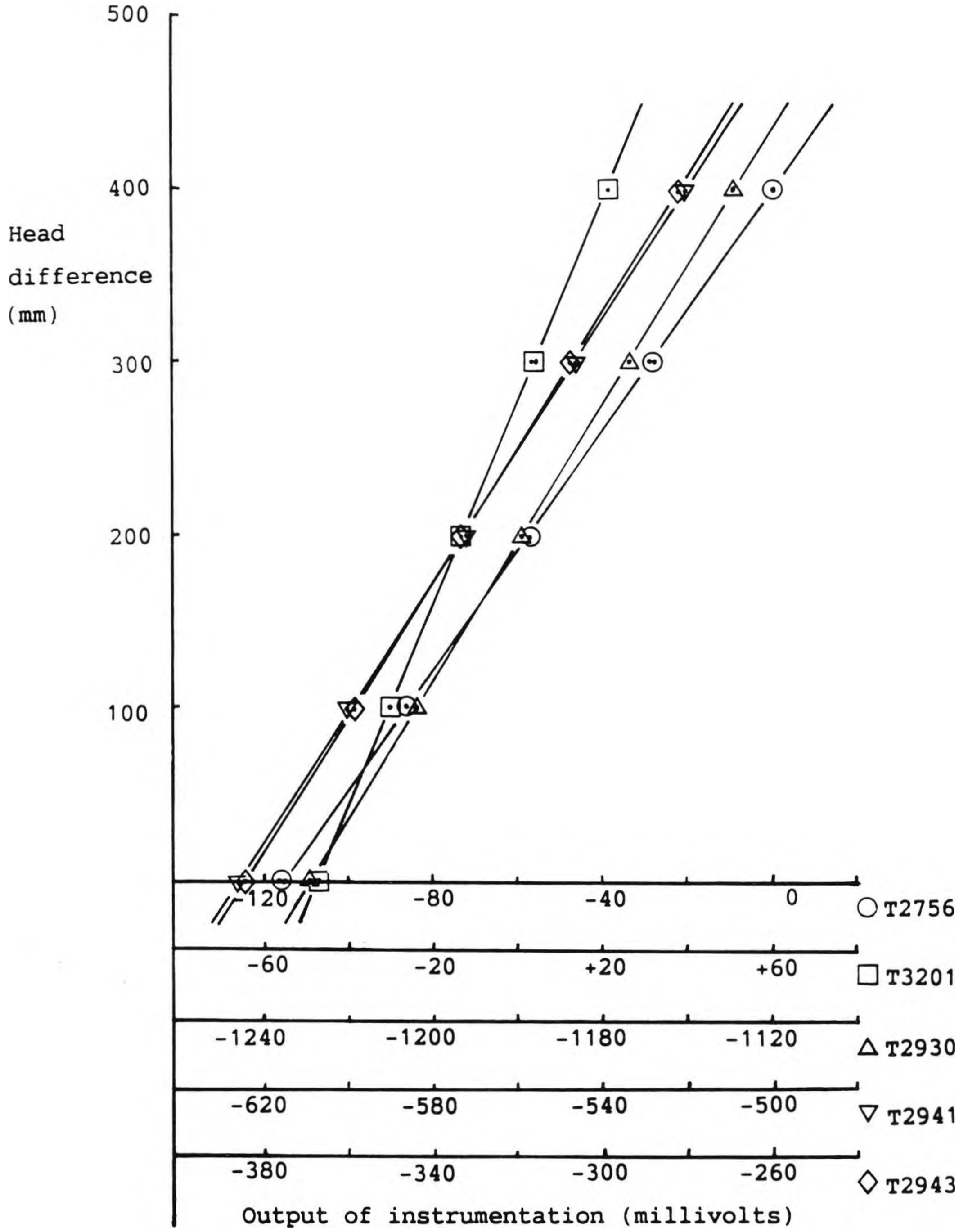

Figure 5.1 Calibration plot for test 182 - 185

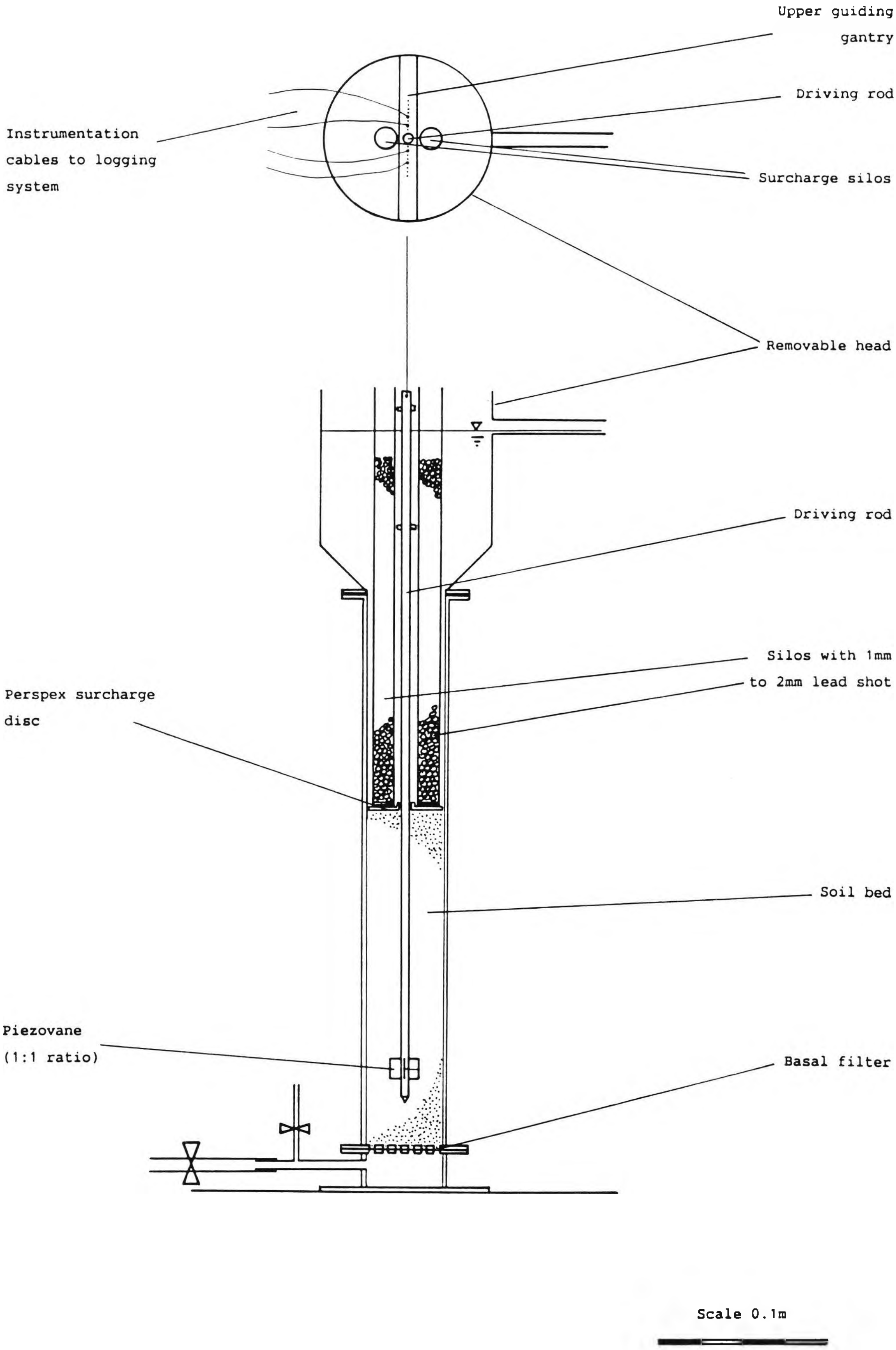

Figure 5.2 Surcharge apparatus assembled inside the sand column (cross- section)

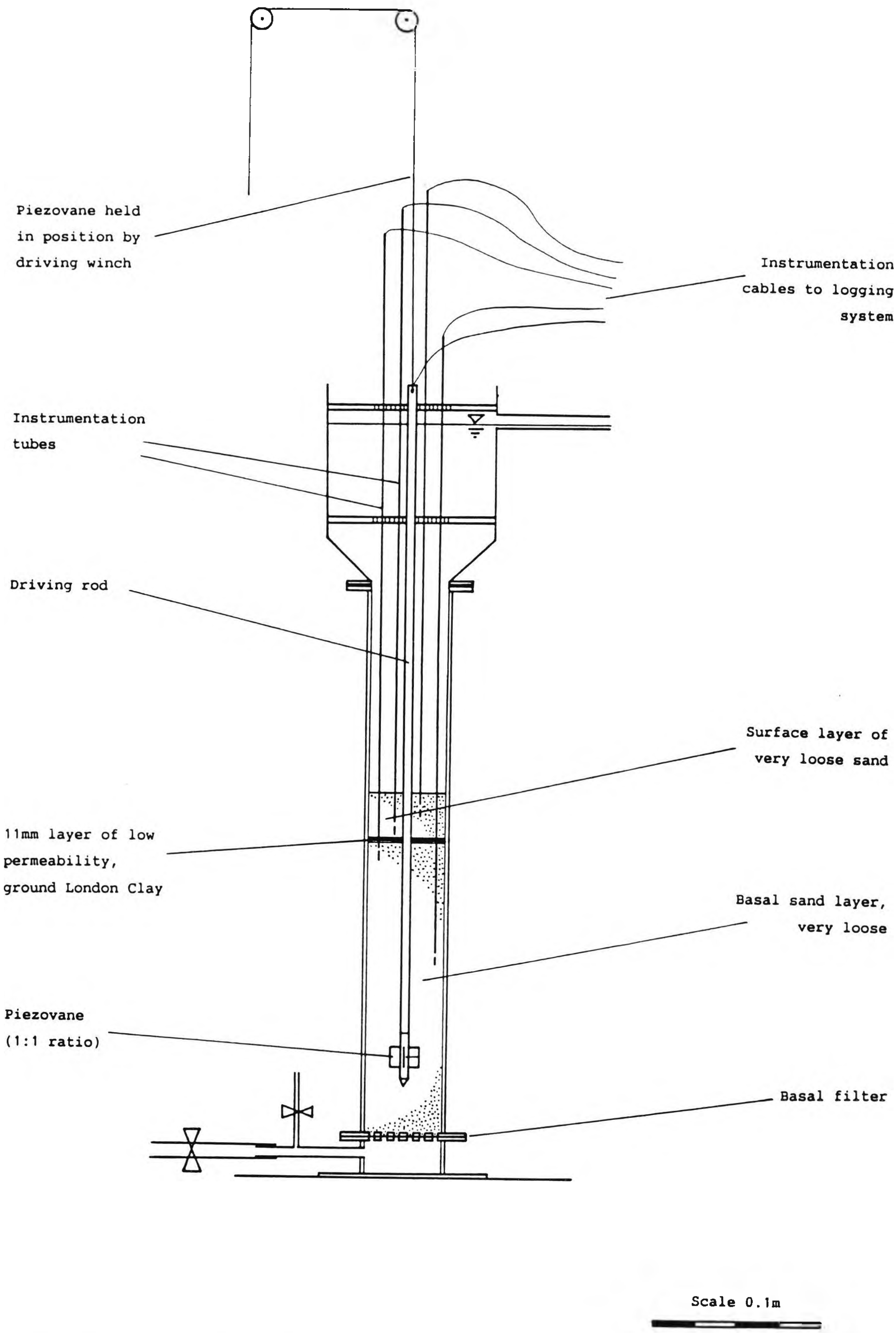

Figure 5.3 Configuration of sand column test 182 - 185 (cross- section)

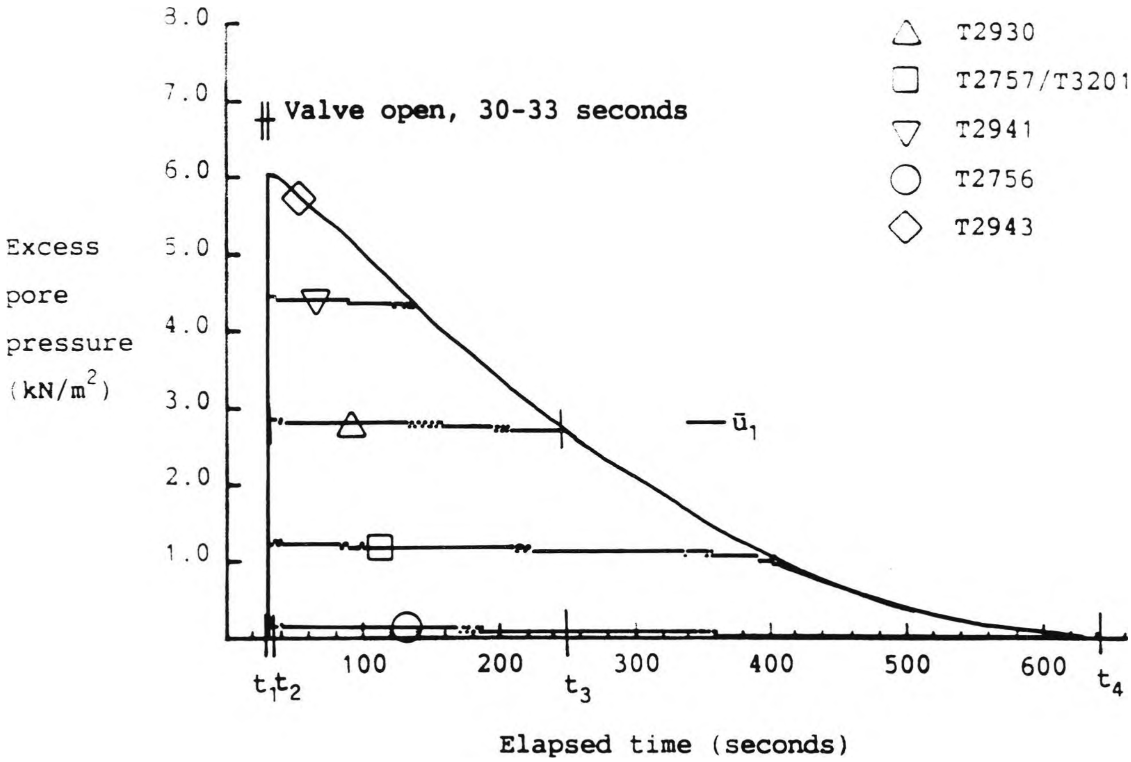

Figure 6.1 An example of a Class I excess pore pressure response, test 42

(The results of this test are summarised in Table 6.3)

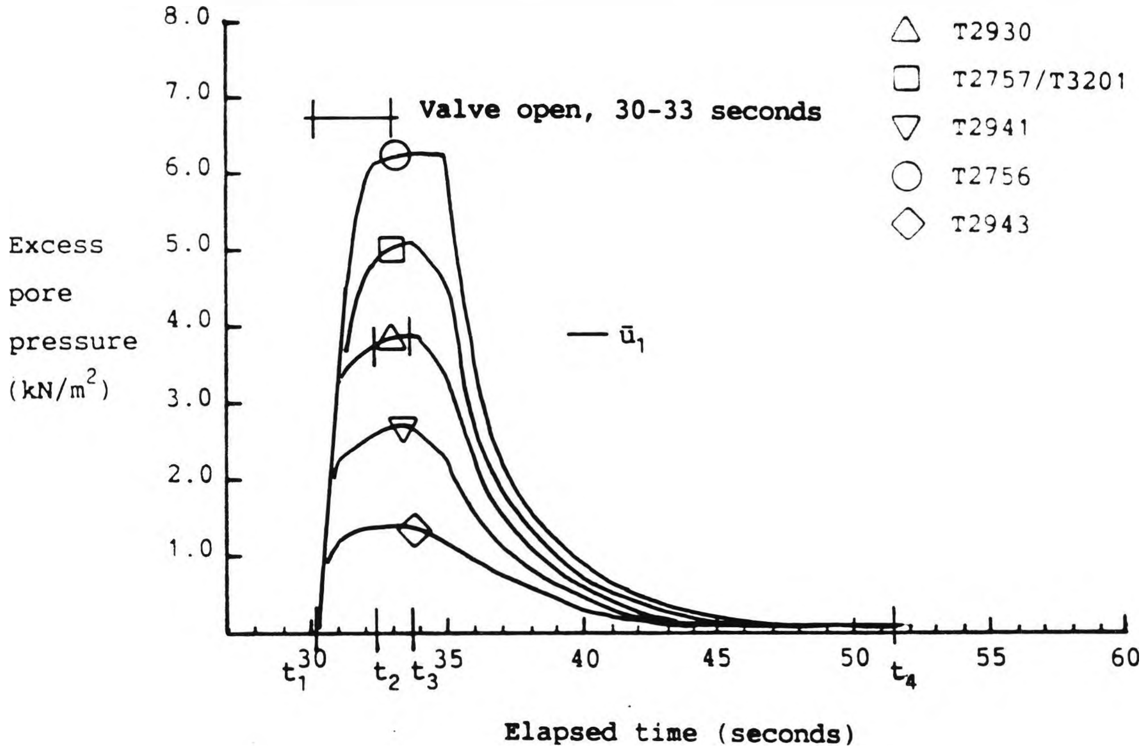

Figure 6.2 An example of a Class II excess pore pressure response, test 0

(The results of this test are summarised in Table 6.3)

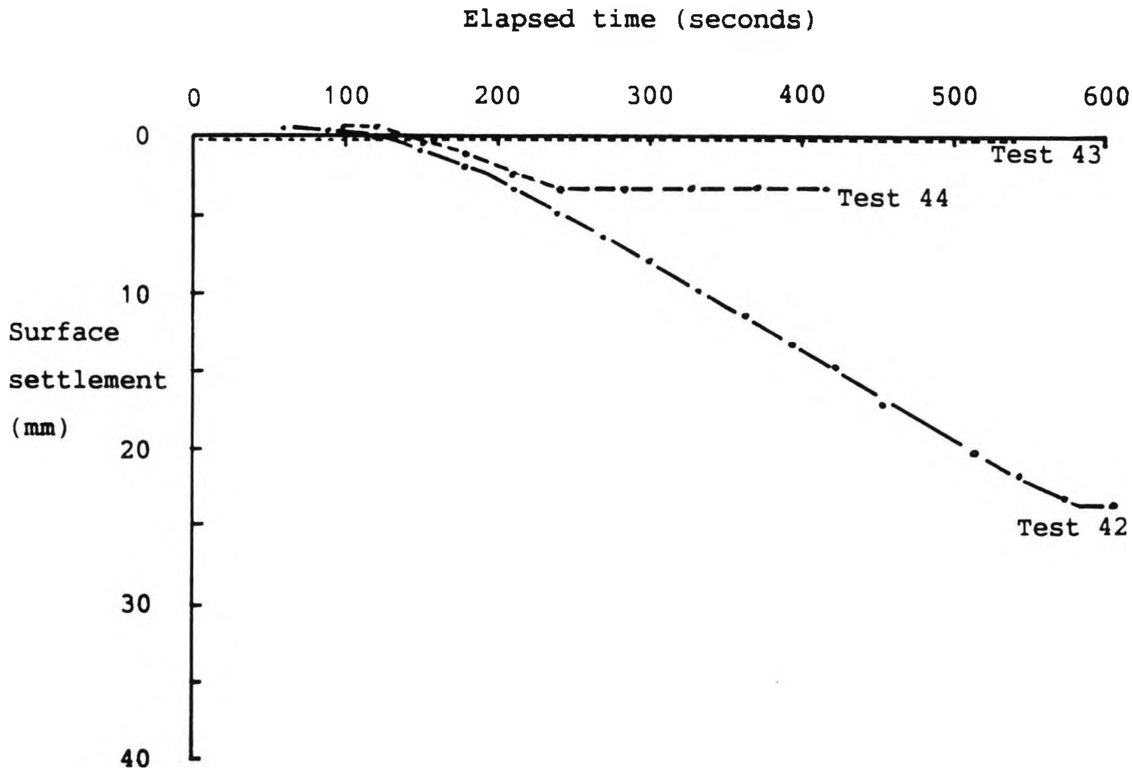

Figure 6.3 Surface settlement recorded in tests 42,43 and 44

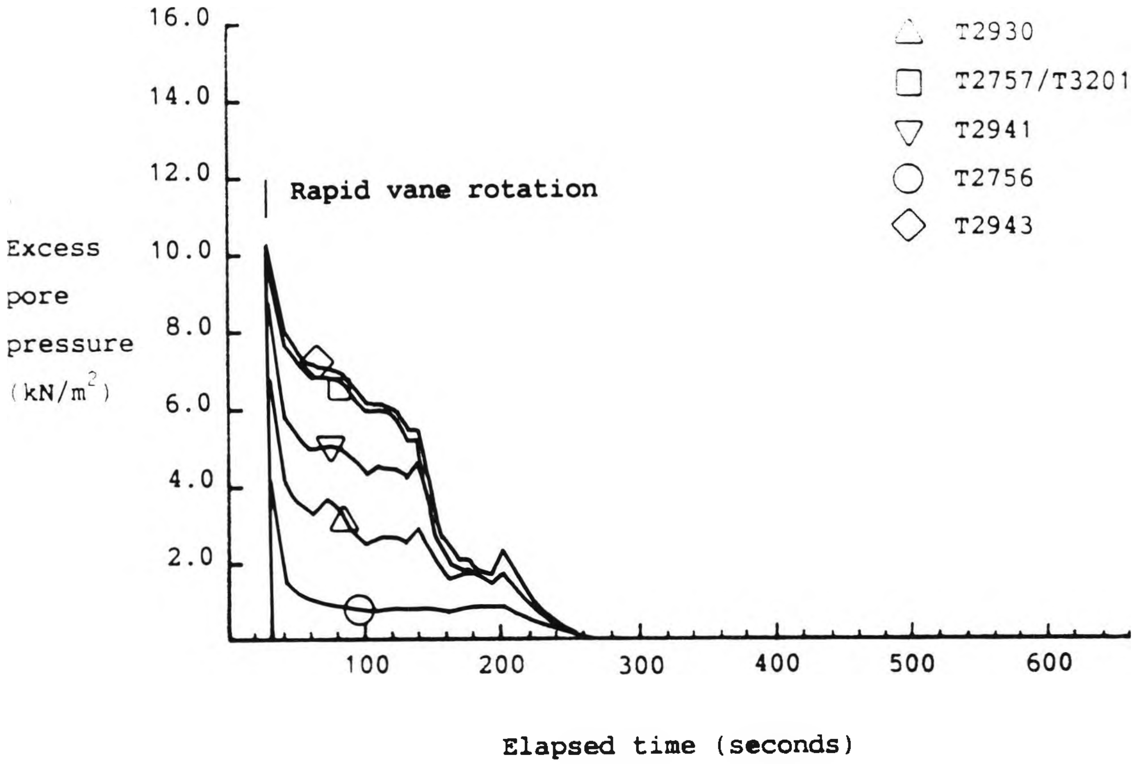

Figure 6.4 **Excess pore pressure response recorded in test 180**

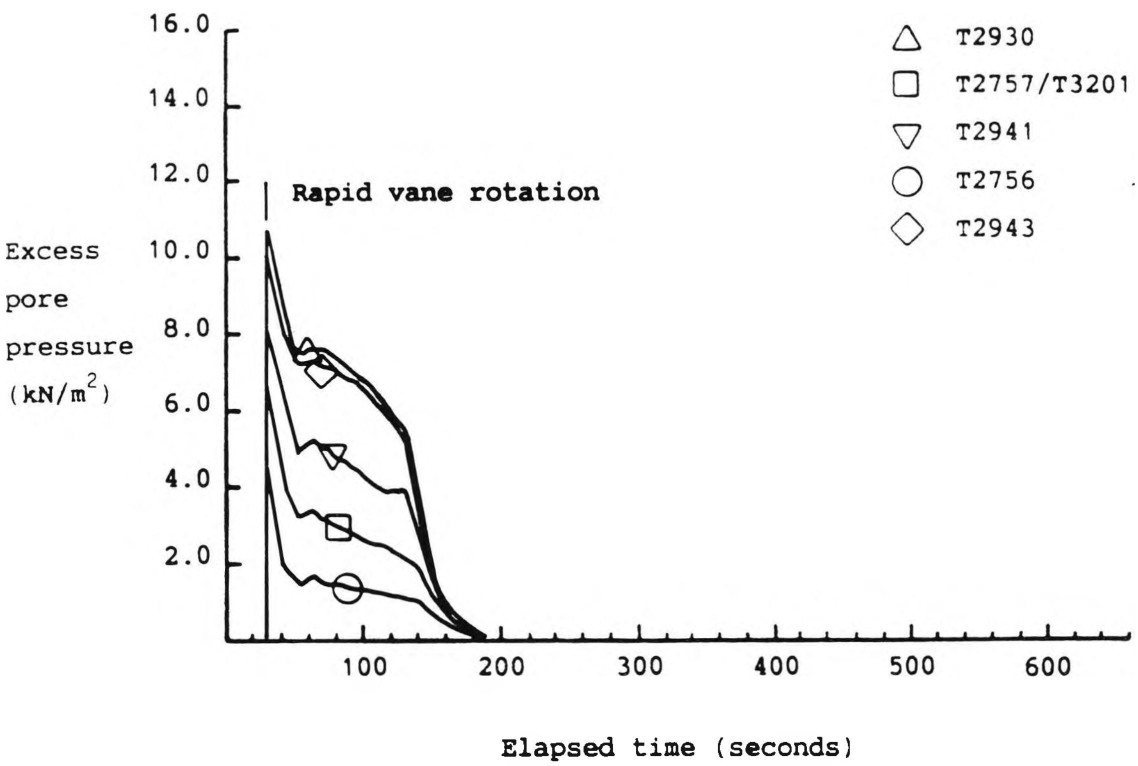

Figure 6.5 **Excess pore pressure response recorded in test 181**

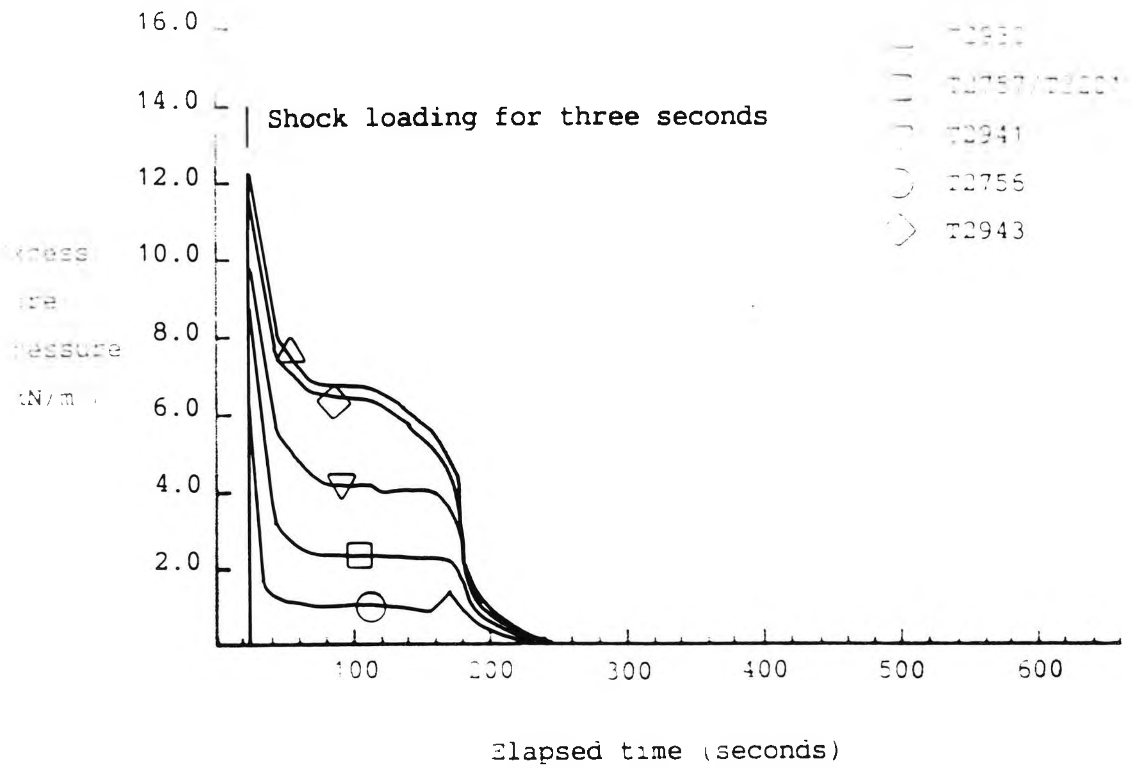

Figure 6.6 Excess pore pressure response recorded in test 186

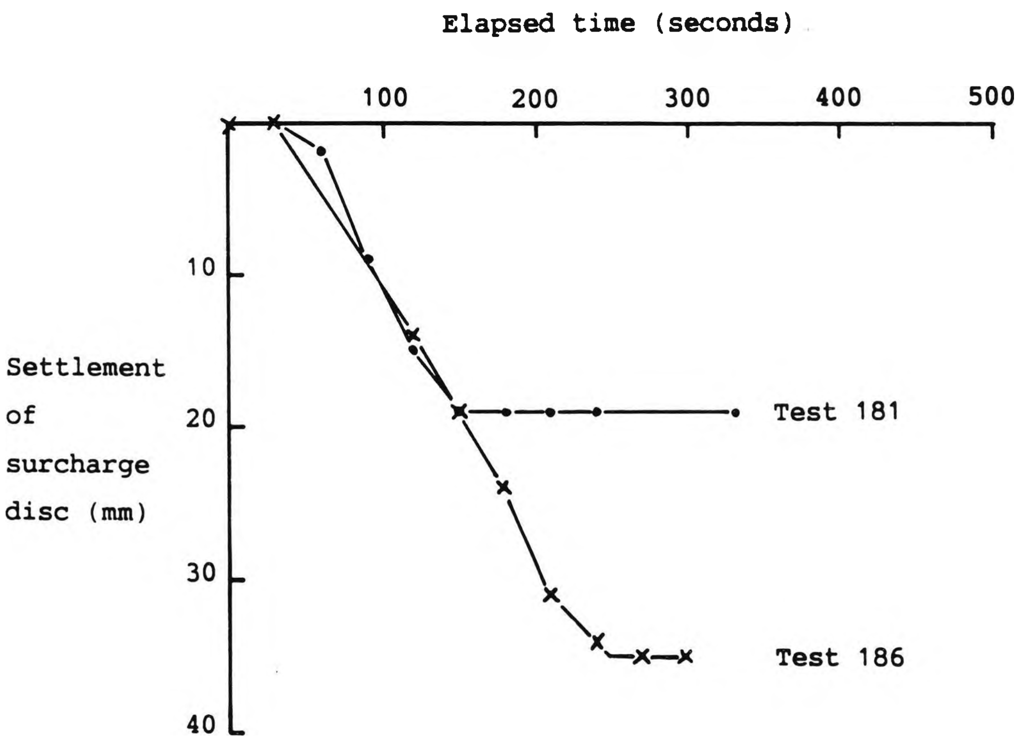

Figure 6.7 Settlement of surcharge disc recorded in tests 181 and 186

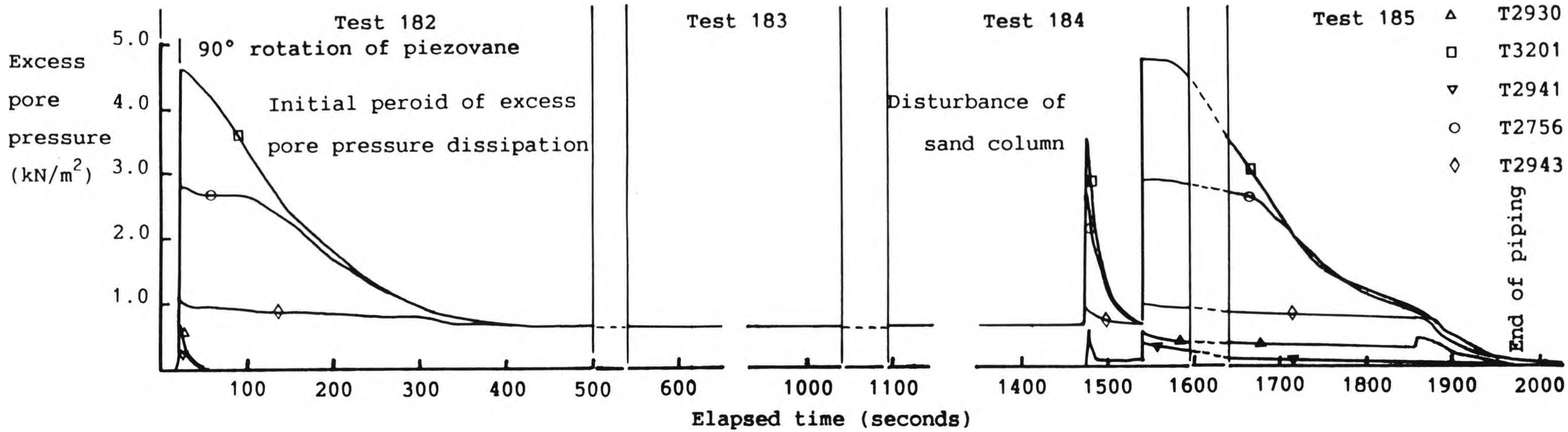

Figure 6.8 Excess pore pressures recorded in test 182 - 185

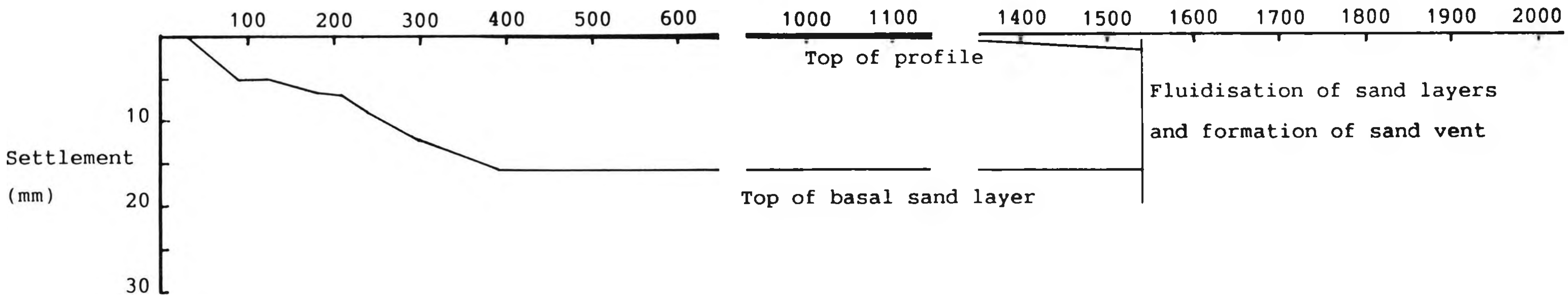

Figure 6.9 Observations of settlement recorded in test 182 - 185

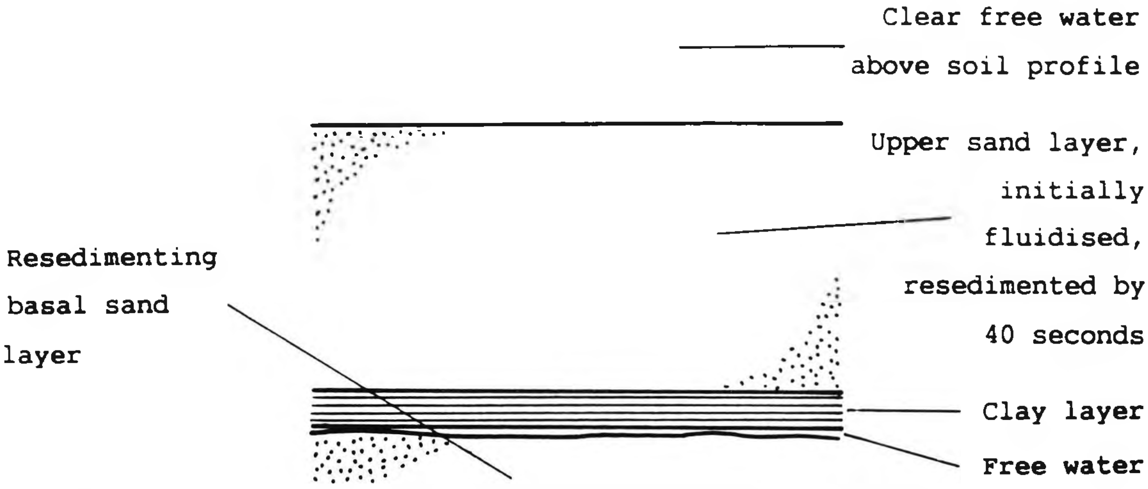

a) layer of free water forming beneath clay layer, from 30 seconds

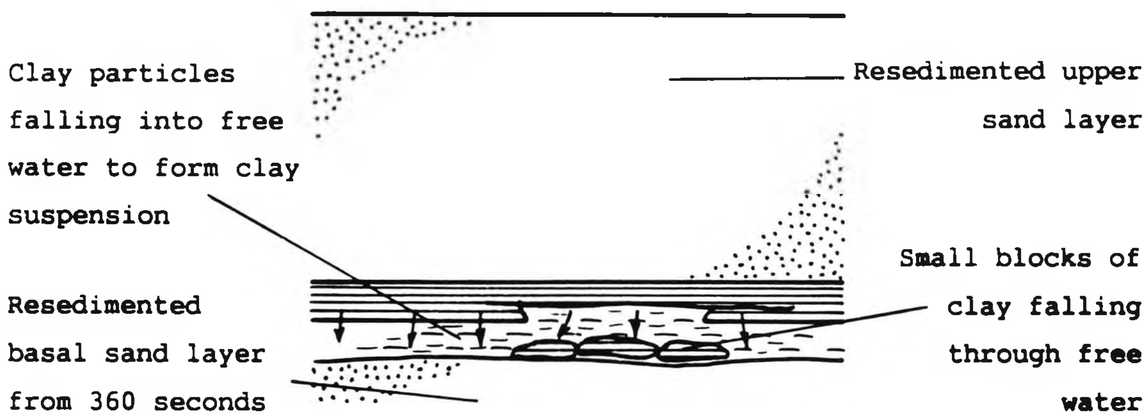

b) progressive collapse of clay layer from base, 30 to 1540 seconds

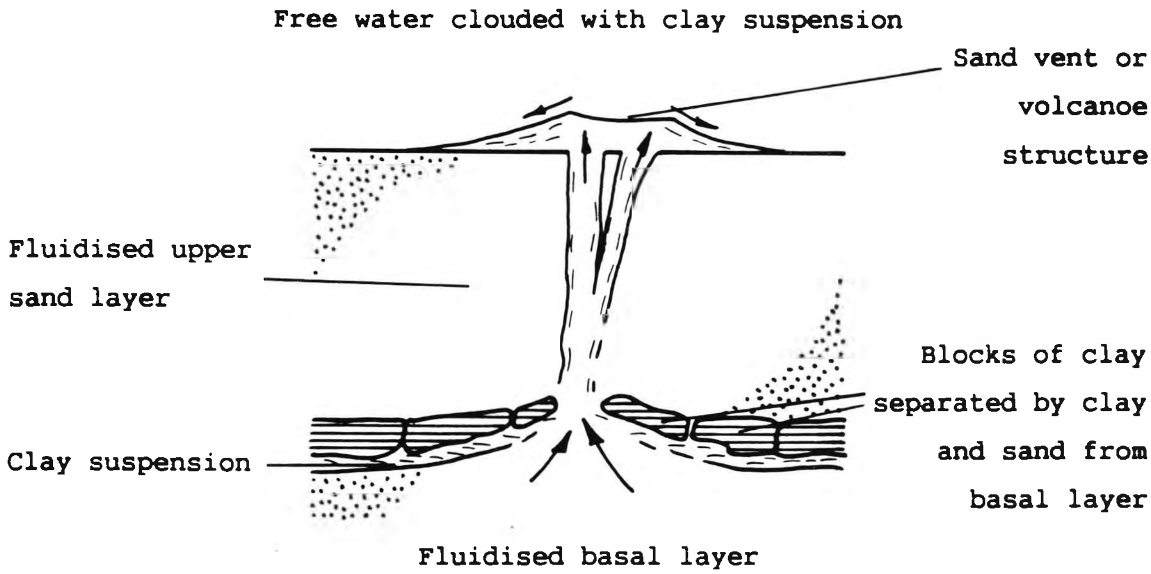

c) rupture of clay layer and formation of sand vent after upward buldging of clay layer at 1540 seconds

Figure 6.10 Soil behaviours observed in test 182 - 185

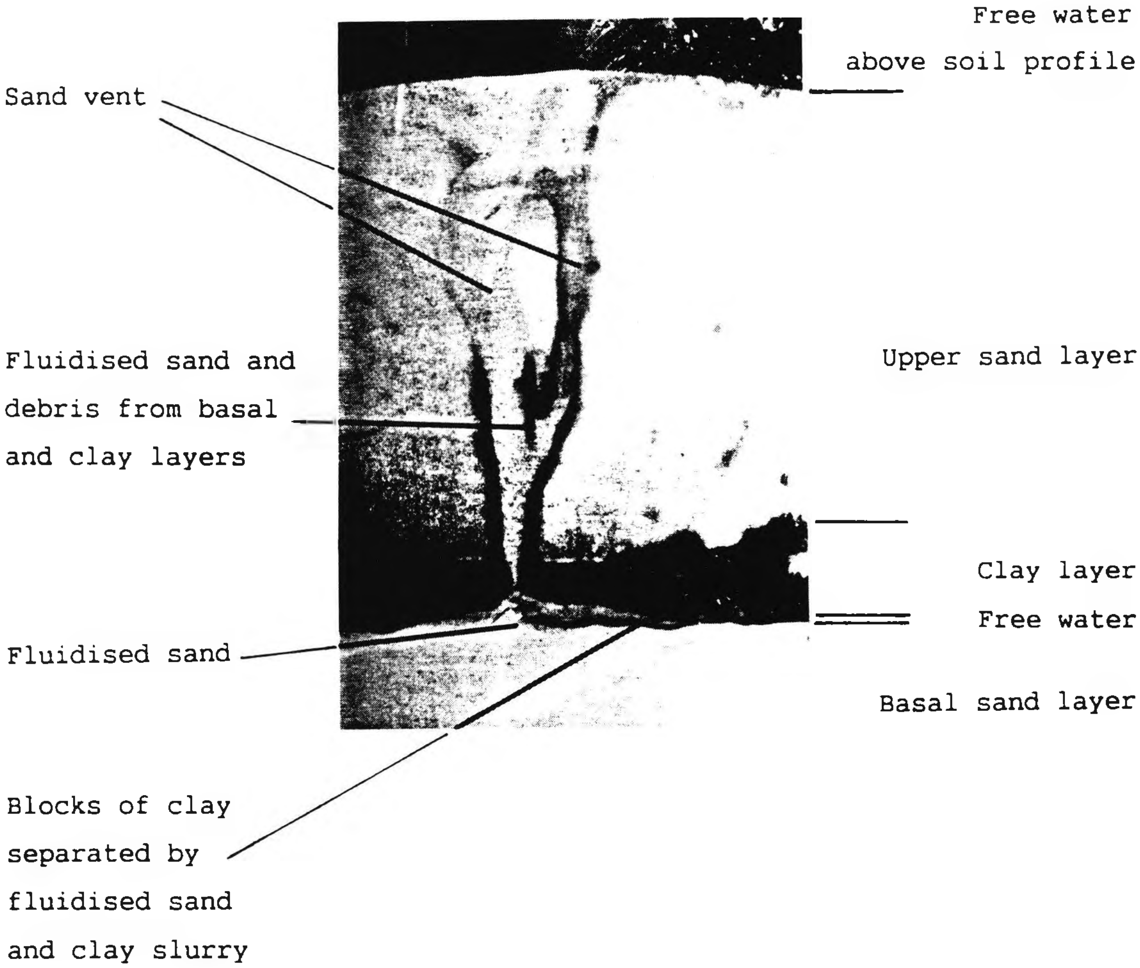

Figure 6.11 Soil profile at the end of test 182 - 185

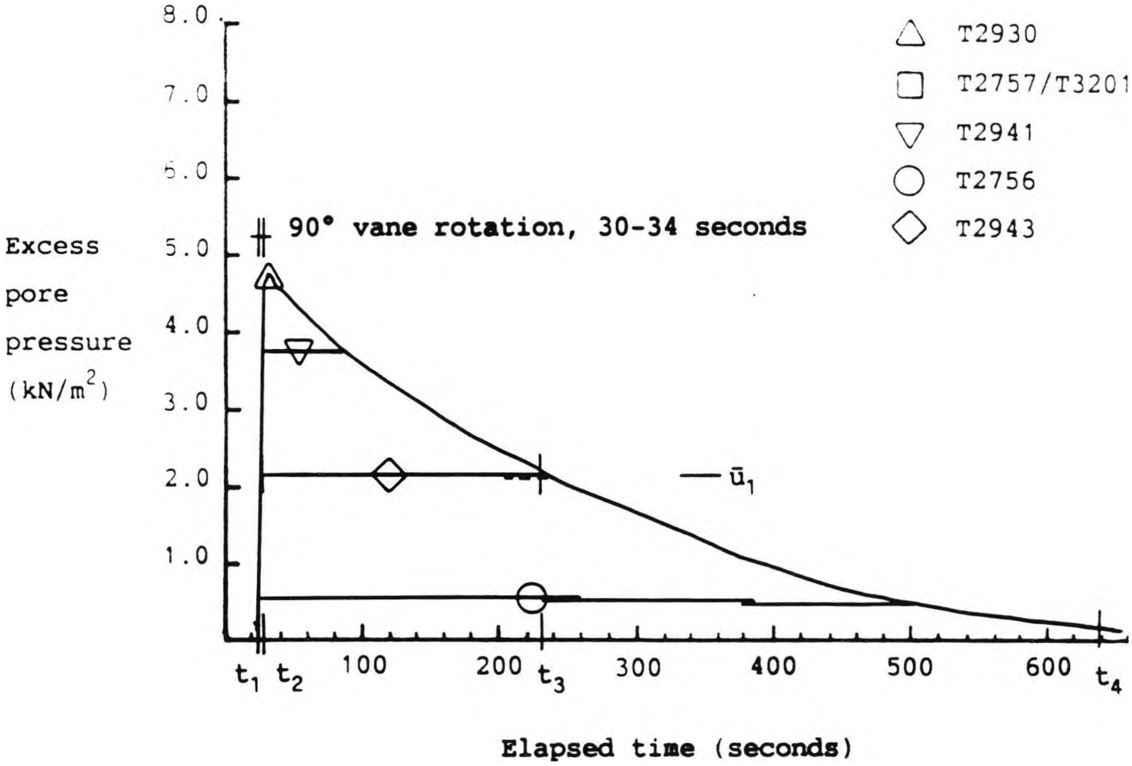

Figure 6.12 An example of a Class I (vane) excess pore pressure response, test 100
(The results of this test are summarised in Table 6.7)

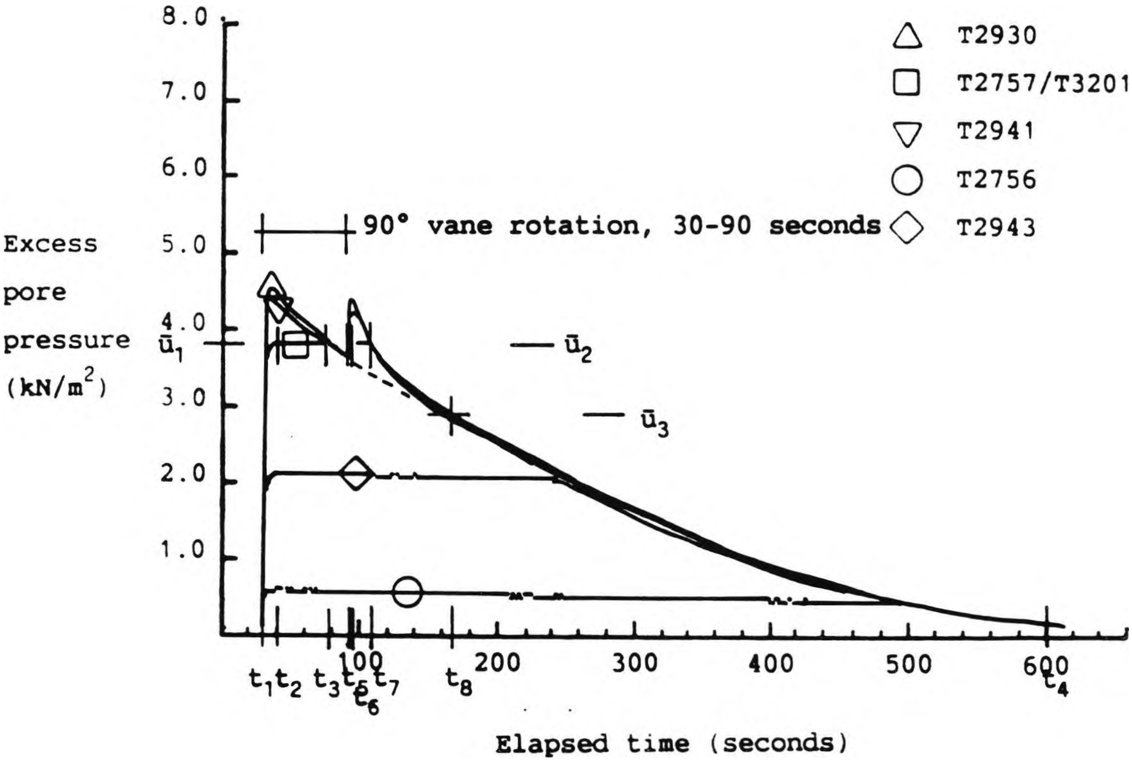

Figure 6.13 An example of a Class Ia (vane) excess pore pressure response, test 93
(The results of this test are summarised in Table 6.4)

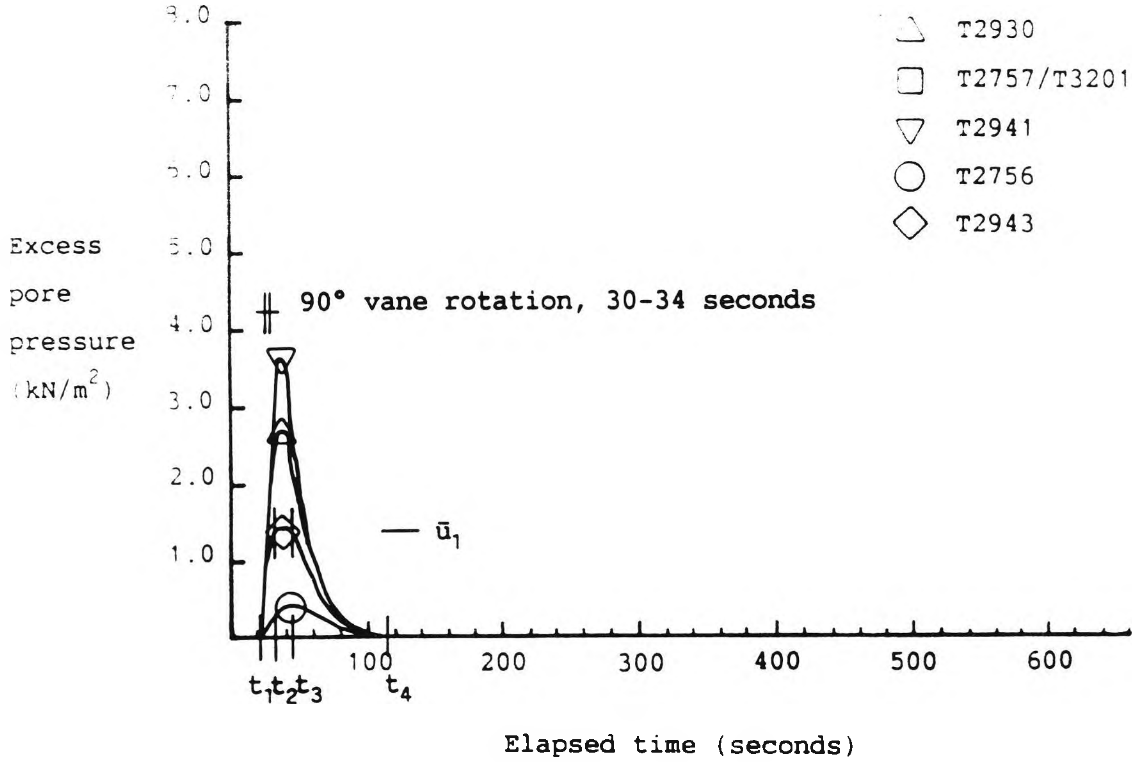

Figure 6.14 **An example of a Class II (vane) excess pore pressure response, test 117**

(The results of this test are summarised in Table 6.10)

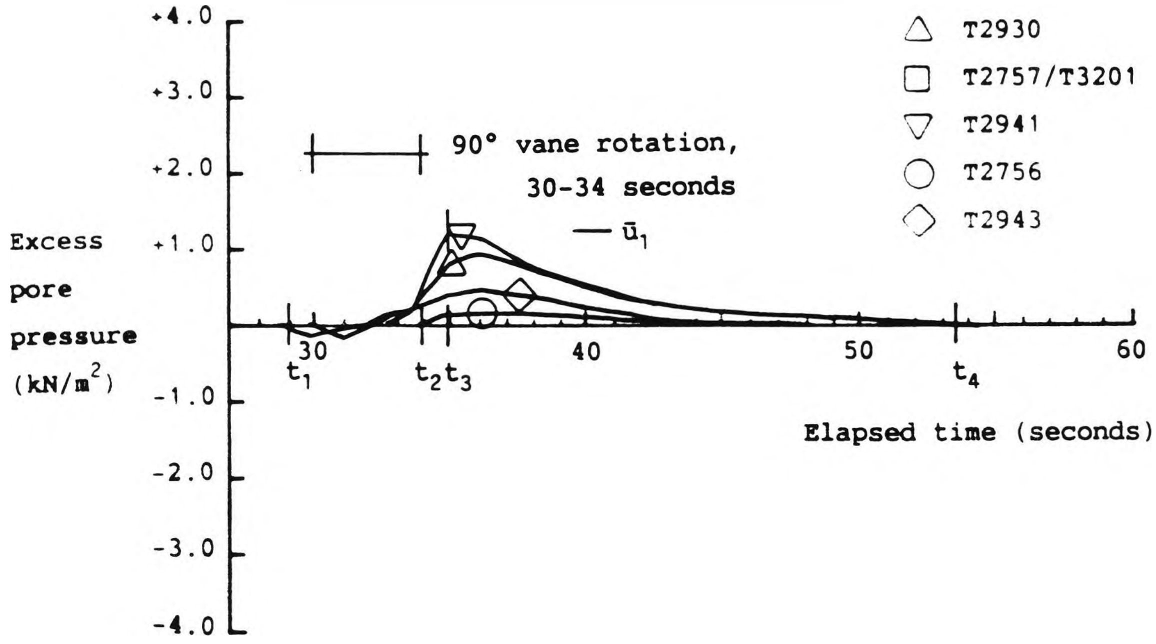

Figure 6.15 **An example of a Class III (vane) excess pore pressure response, test 103**

(The results of this test are summarised in Table 6.7)

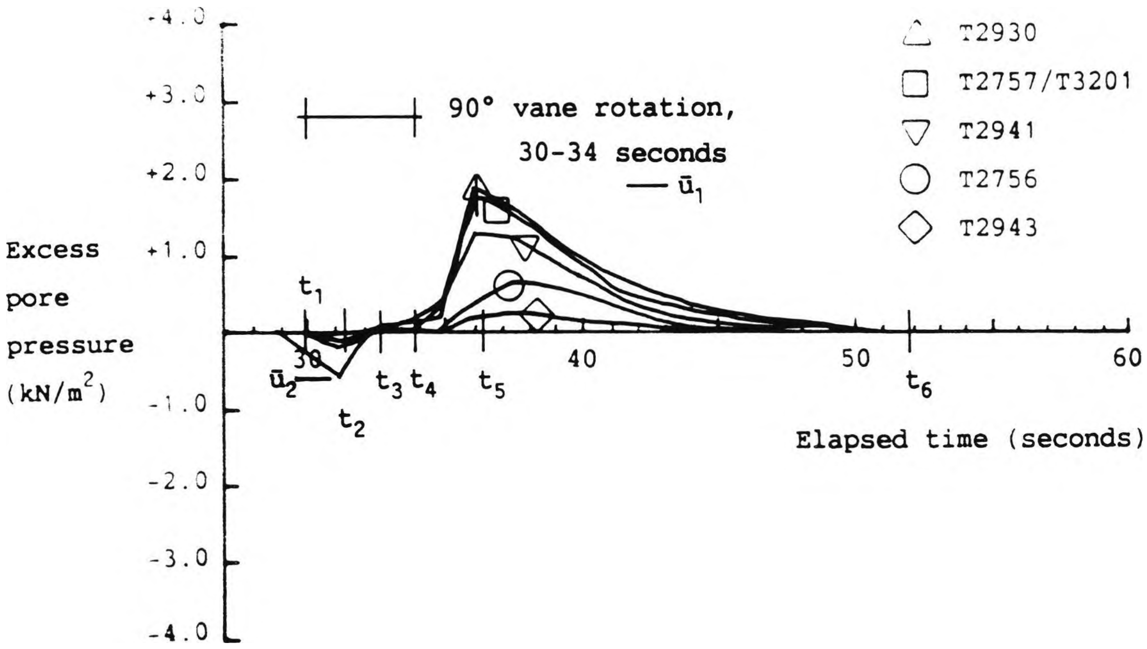

Figure 6.16 An example of a Class IV (vane) excess pore pressure response, test 95

(The results of this test are summarised in Table 6.5)

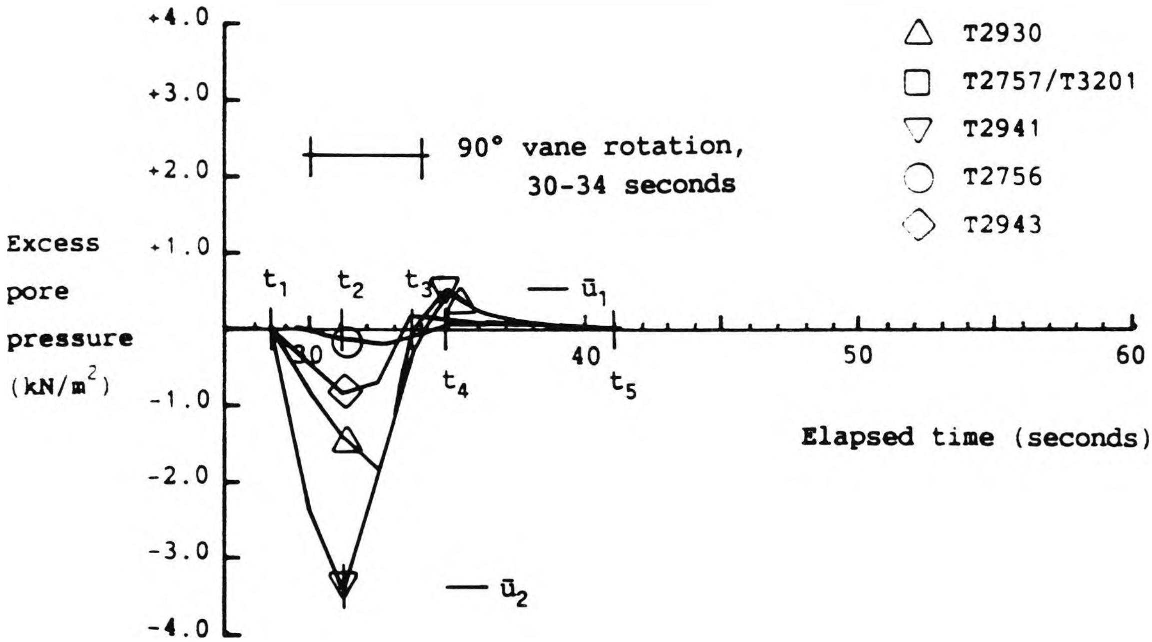

Figure 6.17 An example of a Class V (vane) excess pore pressure response, test 109

(The results of this test are summarised in Table 6.8)

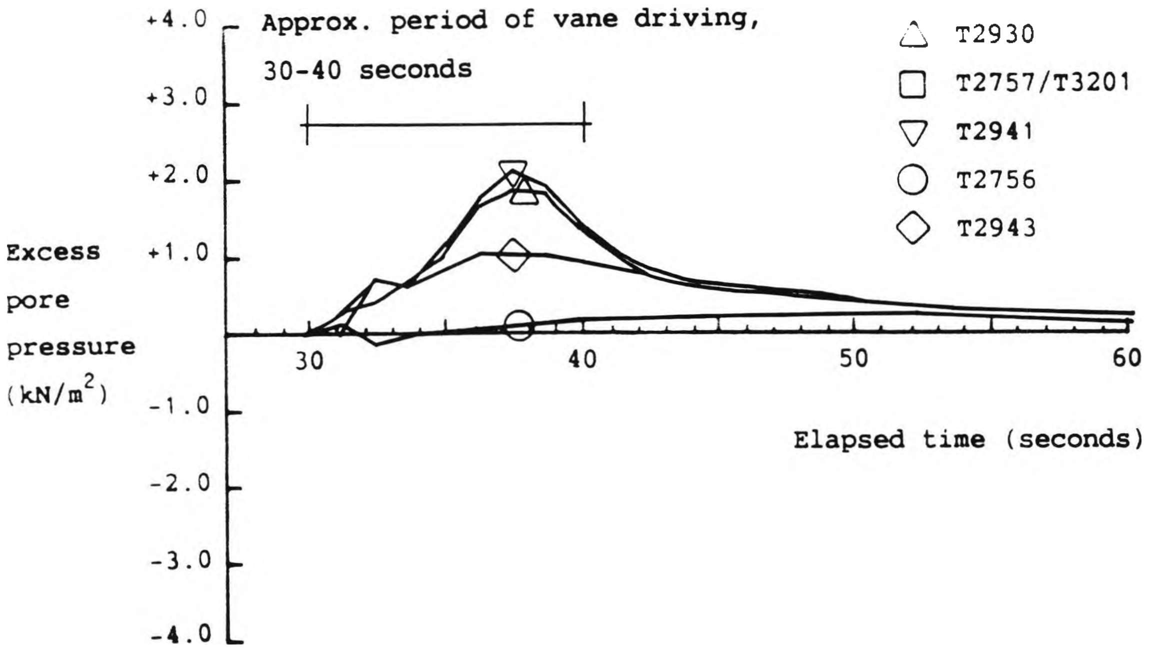

Figure 6.18 A Class III (cone) excess pore pressure response recorded in vane test 114

(The results of this test are summarised in Table 6.9)

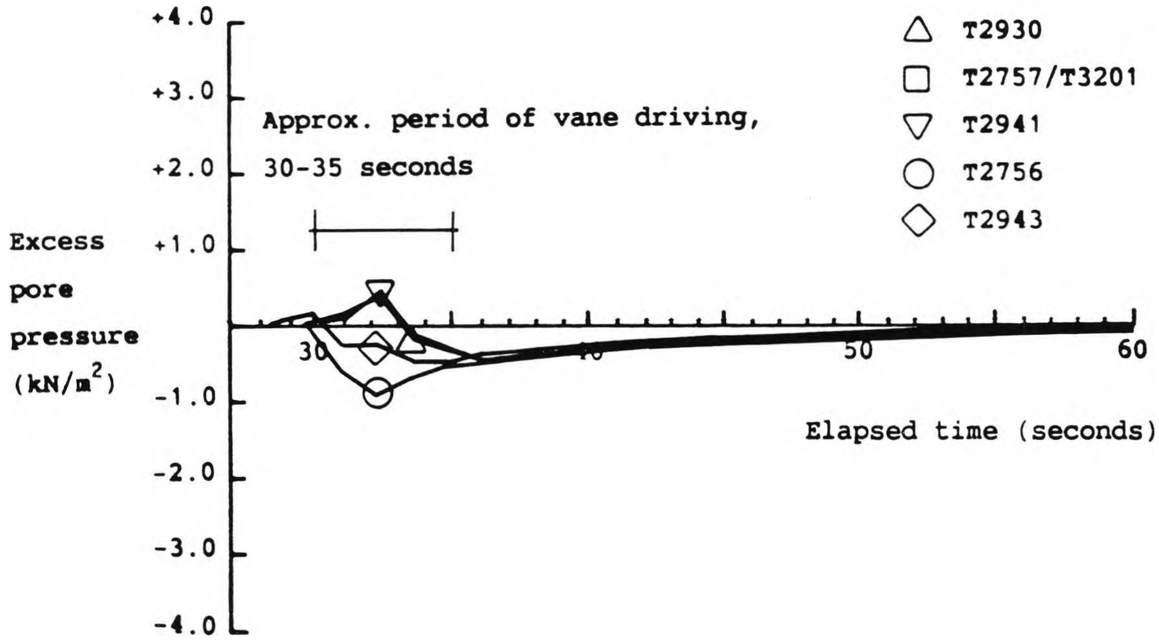

Figure 6.19 A Class IV (cone) excess pore pressure response recorded in vane test 112

(The results of this test are summarised in Table 6.9)

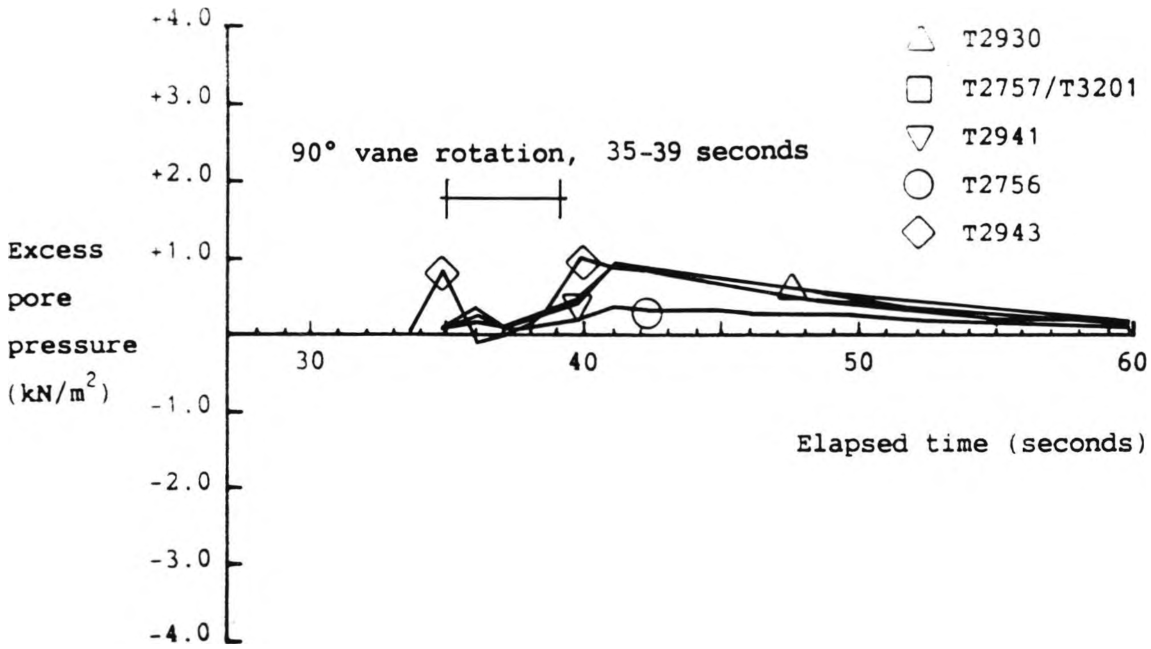

Figure 6.20 A Class III (vane) excess pore pressure response recorded in test 115

(The results of this test are summarised in Table 6.10)

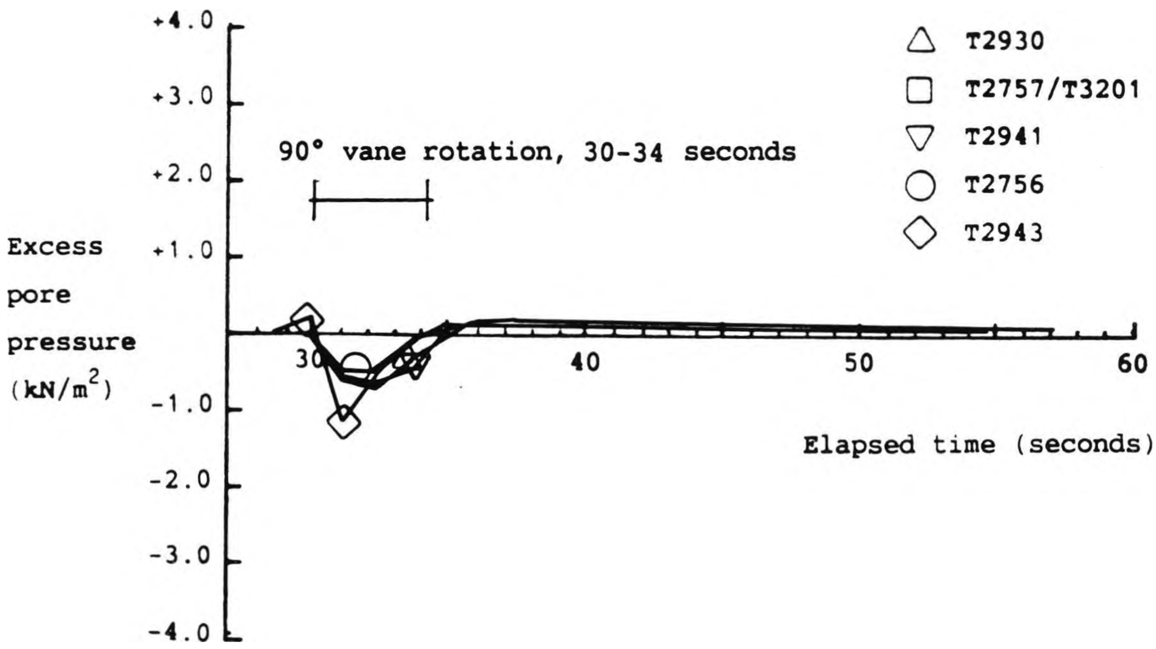

Figure 6.21 A Class V (vane) excess pore pressure response recorded in test 113

(The results of this test are summarised in Table 6.10)

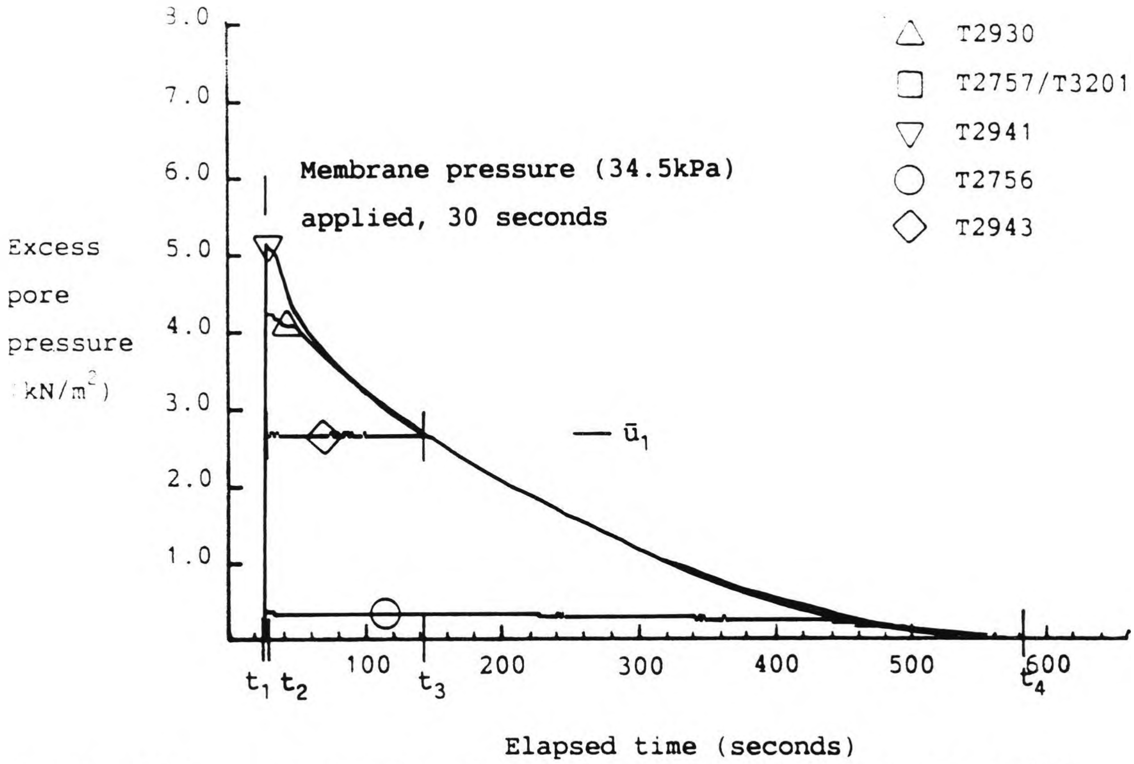

Figure 6.22 An example of a Class I (expanding membrane probe) excess pore pressure response, test 132

(The results of this test are summarised in Table 6.16)

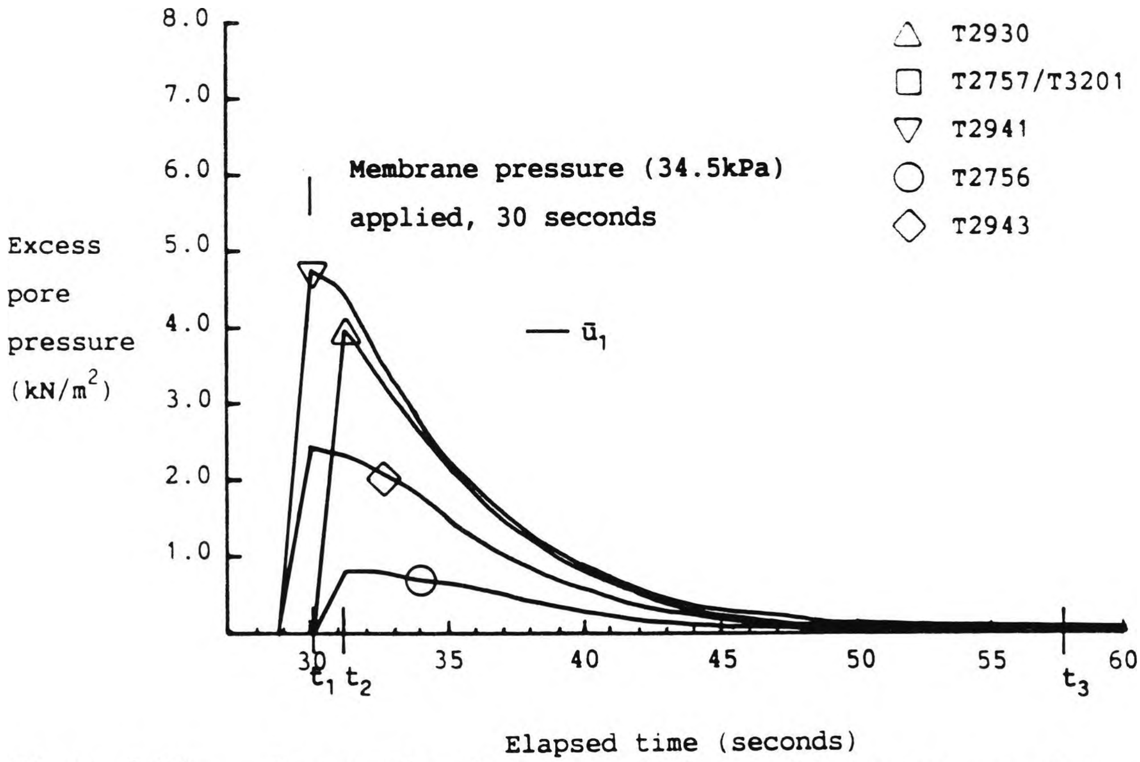

Figure 6.23 An example of a Class II (expanding membrane probe) excess pore pressure response, test 136

(The results of this test are summarised in Table 6.16)

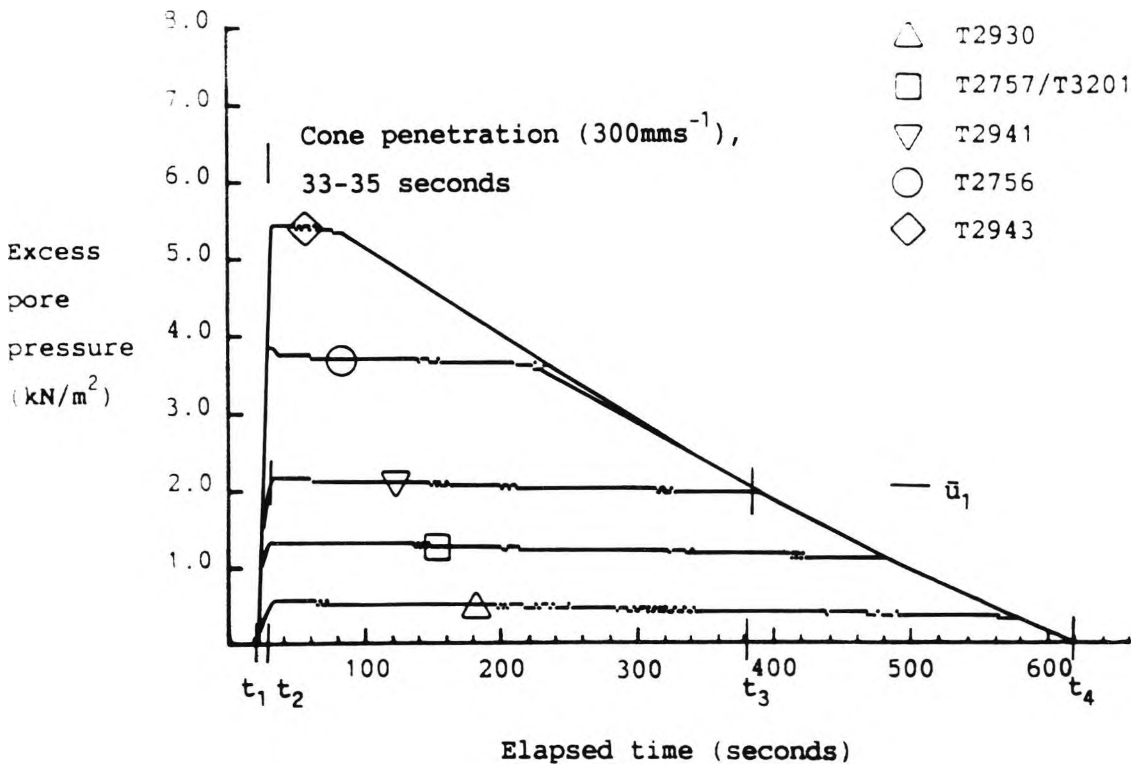

Figure 6.24 An example of a Class I (cone) excess pore pressure response, test 56

(The results of this test are summarised in Table 6.17)

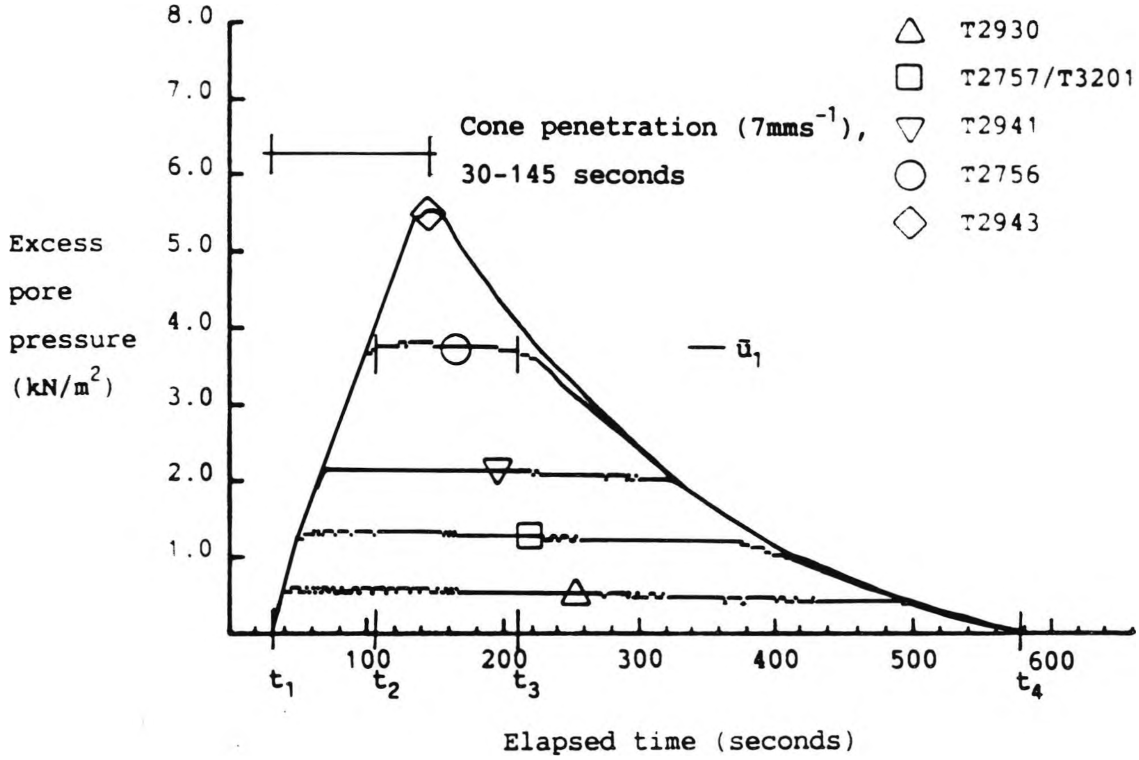

Figure 6.25 An example of a Class I (cone) excess pore pressure response, test 57

(The results of this test are summarised in **Table 6.17**)

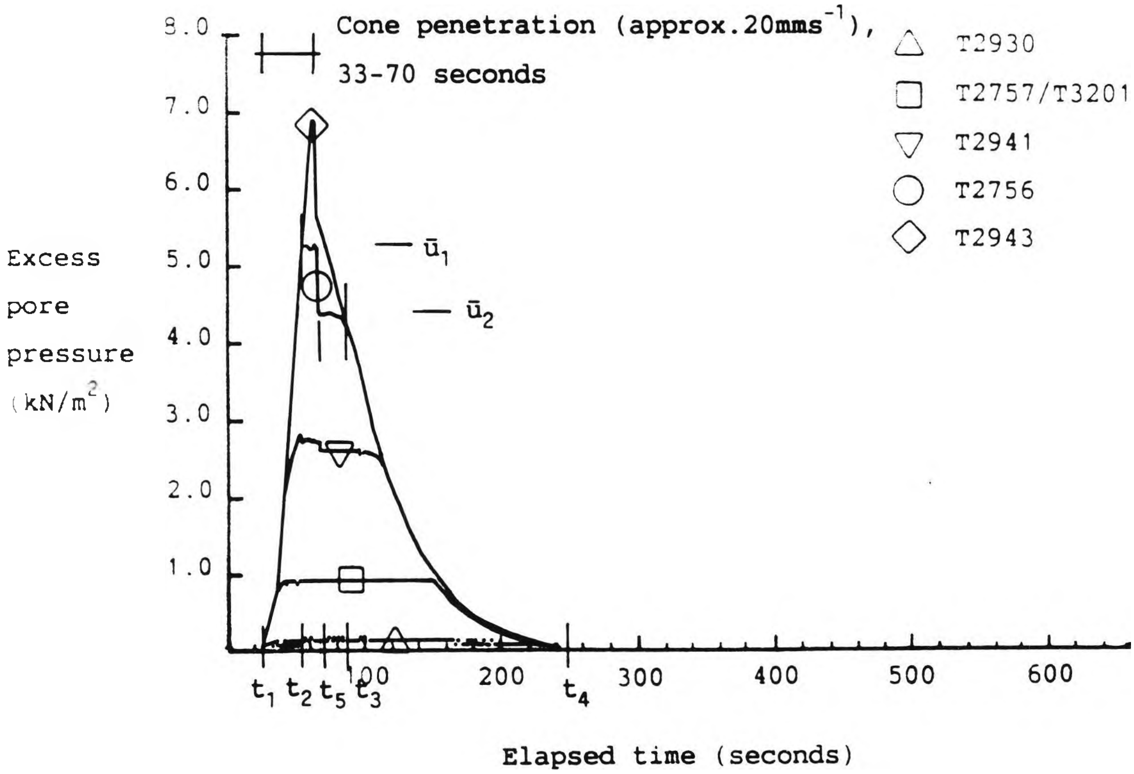

Figure 6.26 **An example of a Class Ia (cone) excess pore pressure response, test 63**

(The results of this test are summarised in Table 6.19)

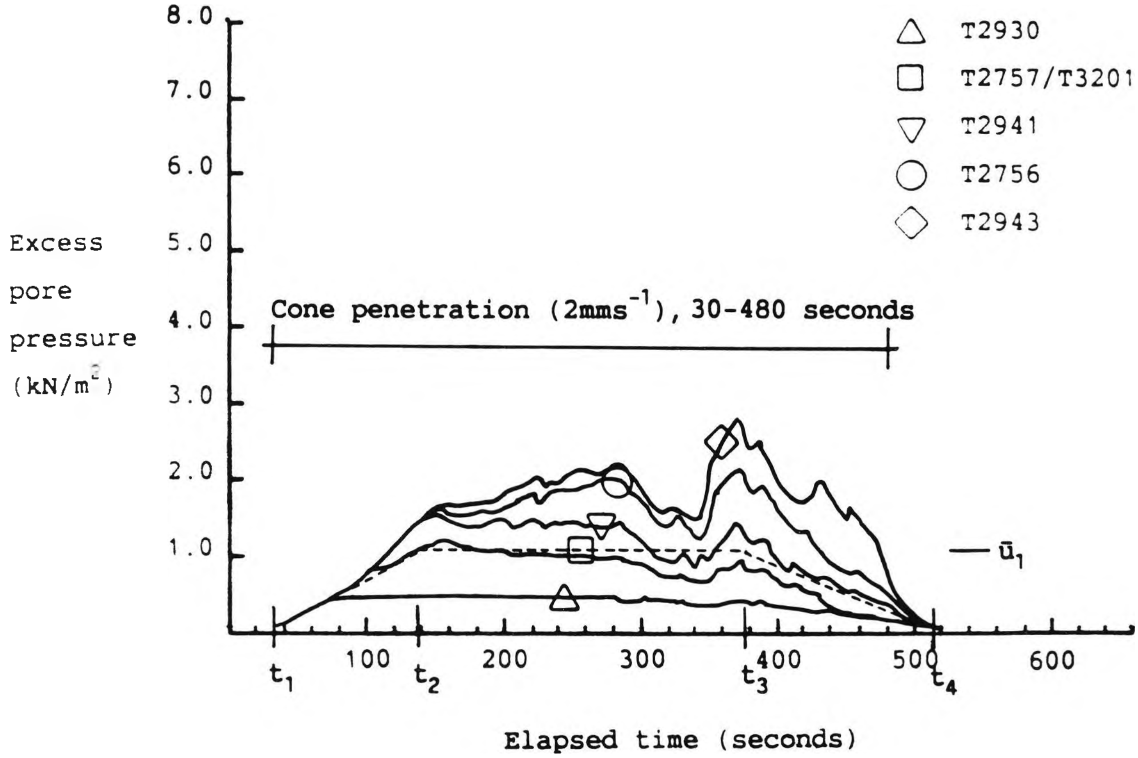

Figure 6.27 **An example of a Class II (cone) excess pore pressure response, test 67**

(The results of this test are summarised in Table 6.18)

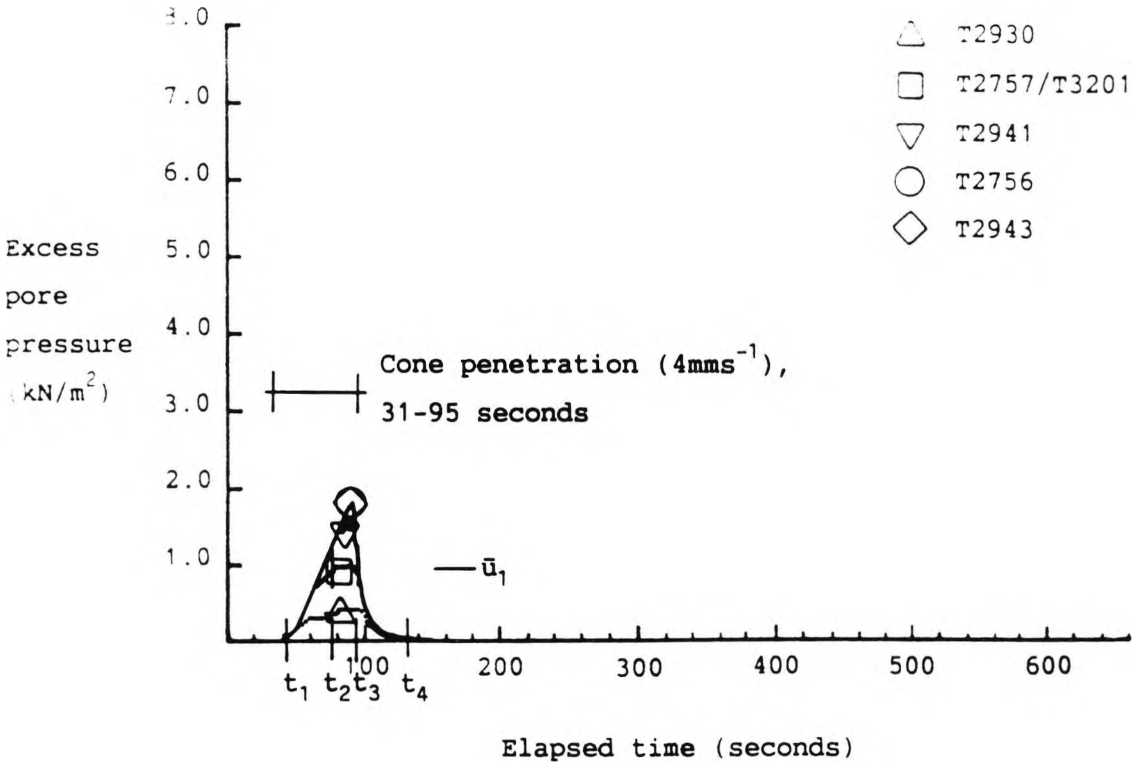

Figure 6.28 An example of a Class II (cone) excess pore pressure response, test 88
(The results of this test are summarised in Table 6.20)

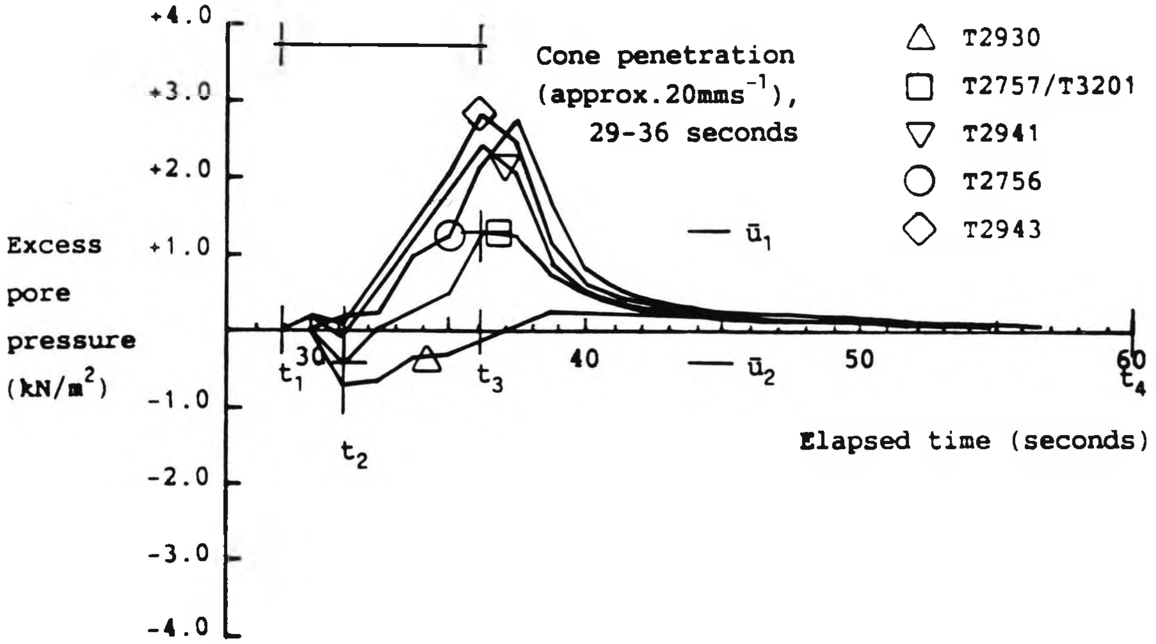

Figure 6.29 An example of a Class III (cone) excess pore pressure response, test 81
(The results of this test are summarised in Table 6.22)

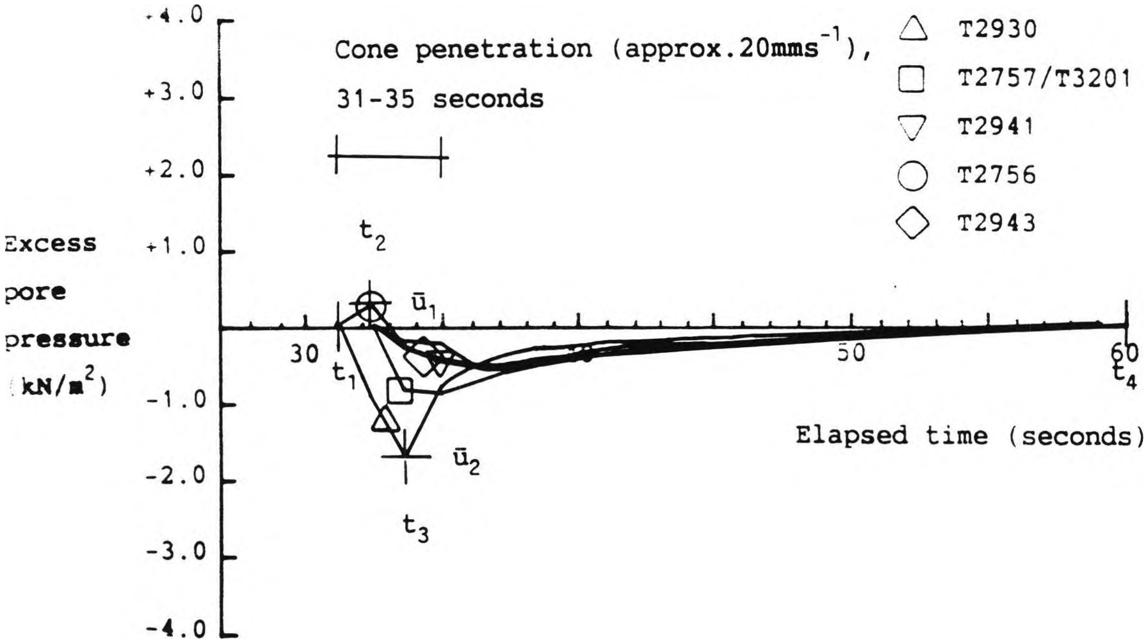

Figure 6.30 An example of a Class IV (cone) excess pore pressure response, test 75

(The results of this test are summarised in Table 6.24)

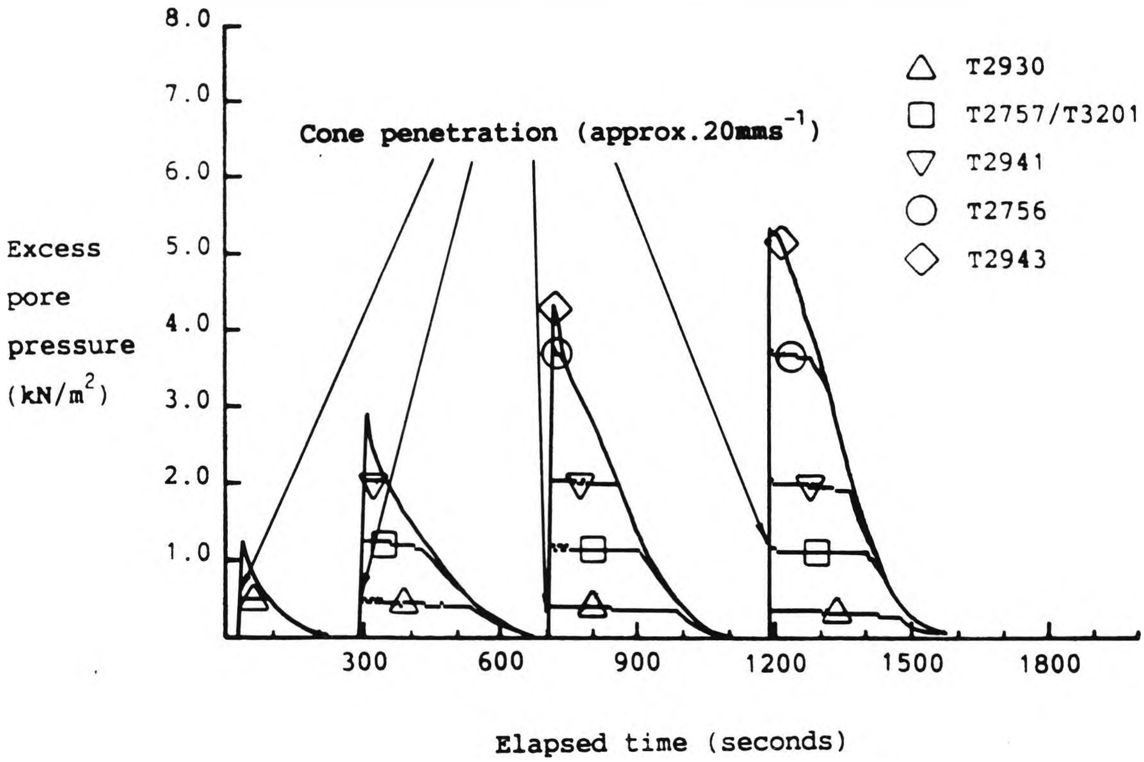

Figure 6.31 Excess pore pressure response recorded in test 69

(The results of this test are summarised in Table 6.18)

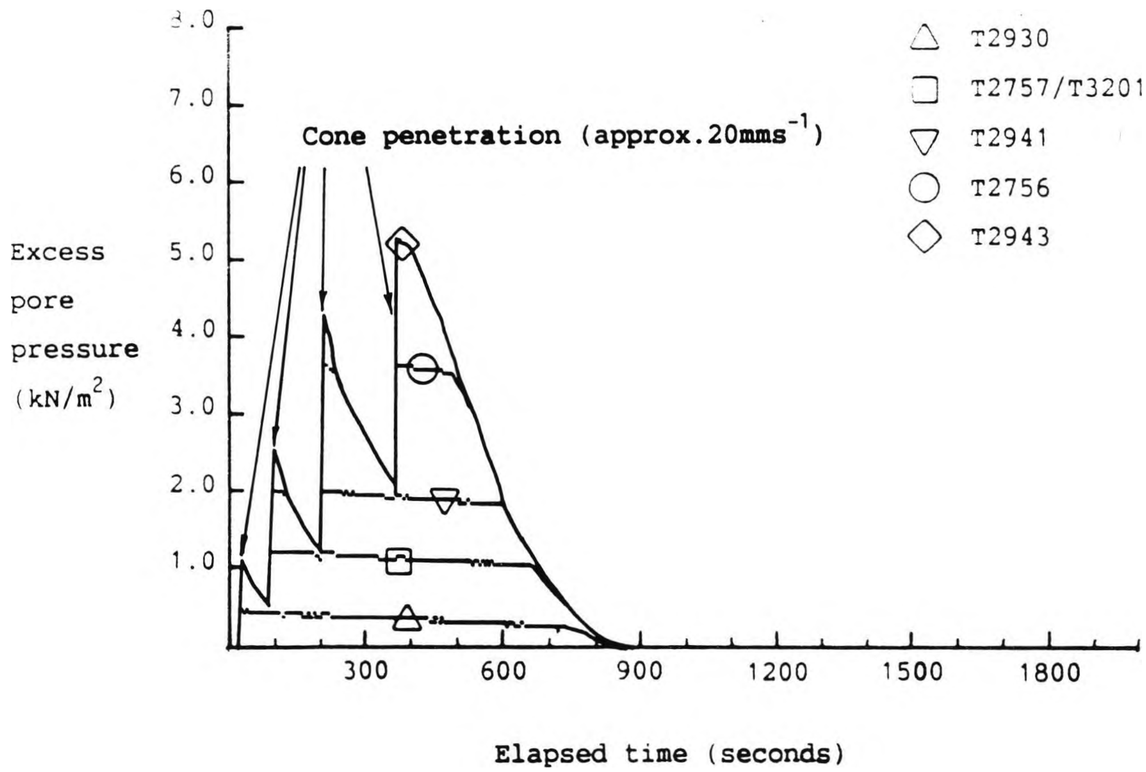

Figure 6.32 Excess pore pressure response recorded in test 70
(The results of this test are summarised in Table 6.18)

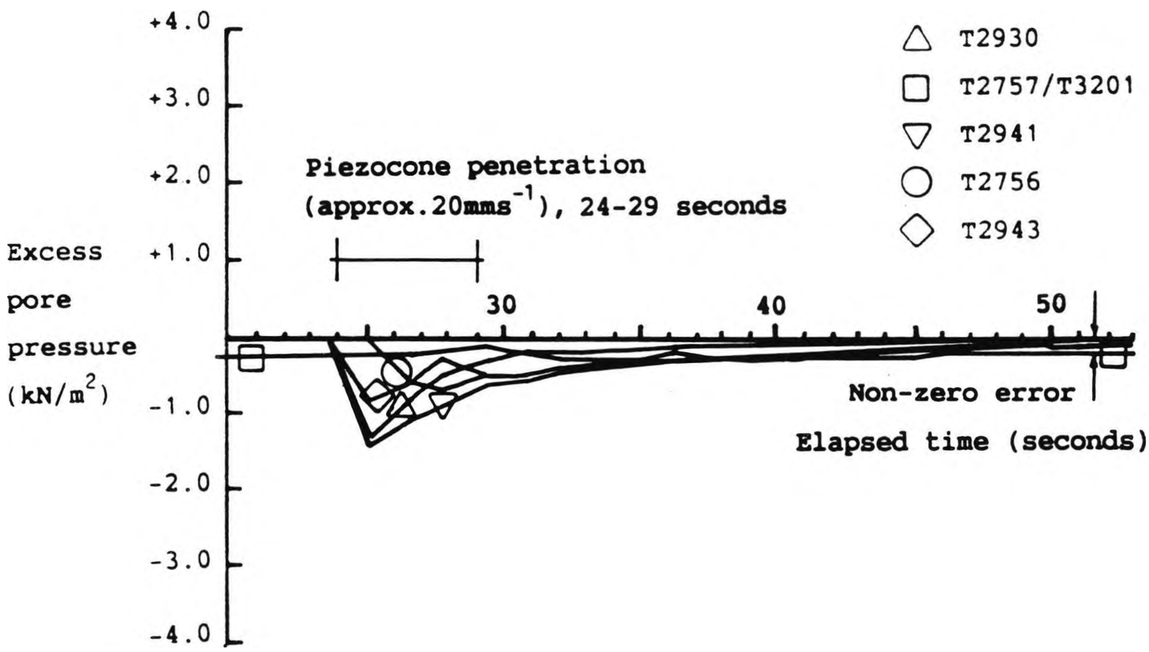

Figure 6.33 Excess pore pressure response recorded in piezocone test 164
(The results of this test are summarised in Table 6.28)

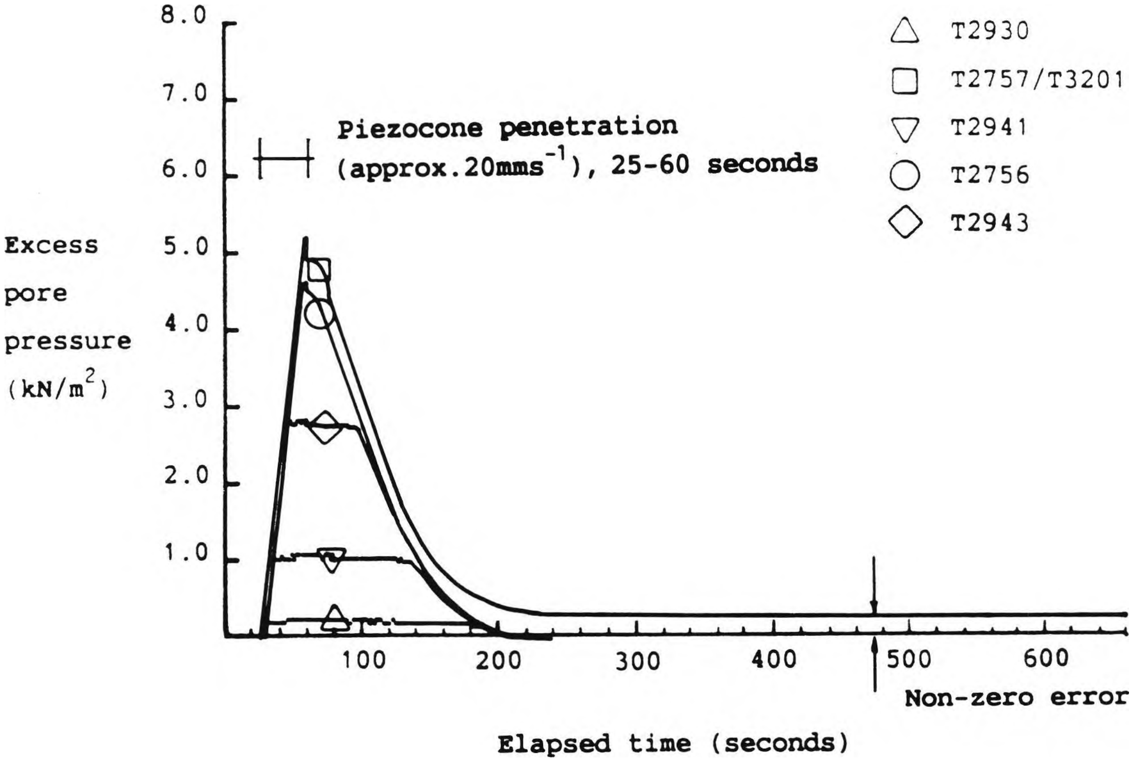

Figure 6.34 Excess pore pressure response recorded in piezocone test 161

(The results of this test are summarised in Table 6.27)

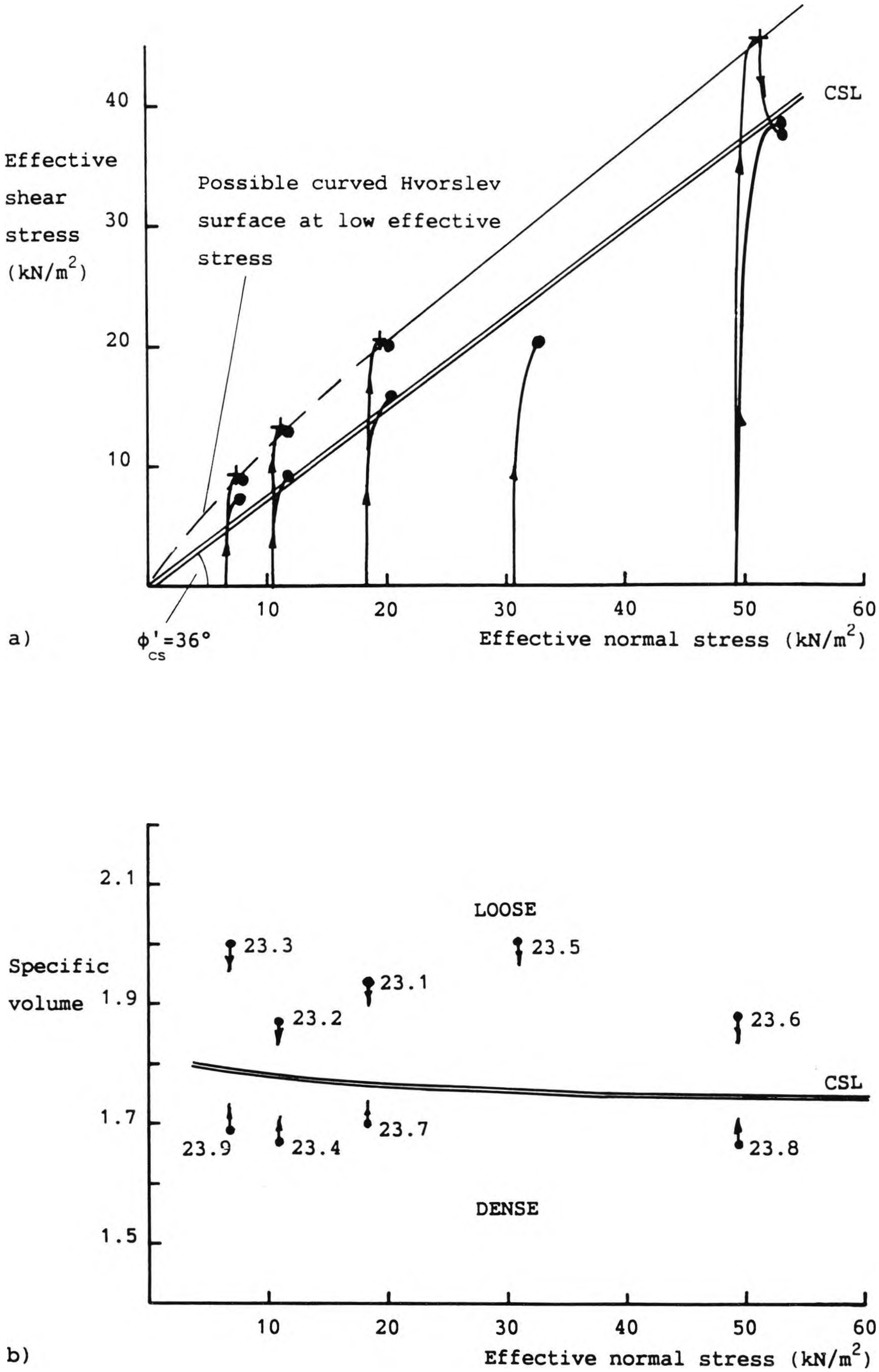

Figure 7.1 Wet and dry soil states, drained behaviour

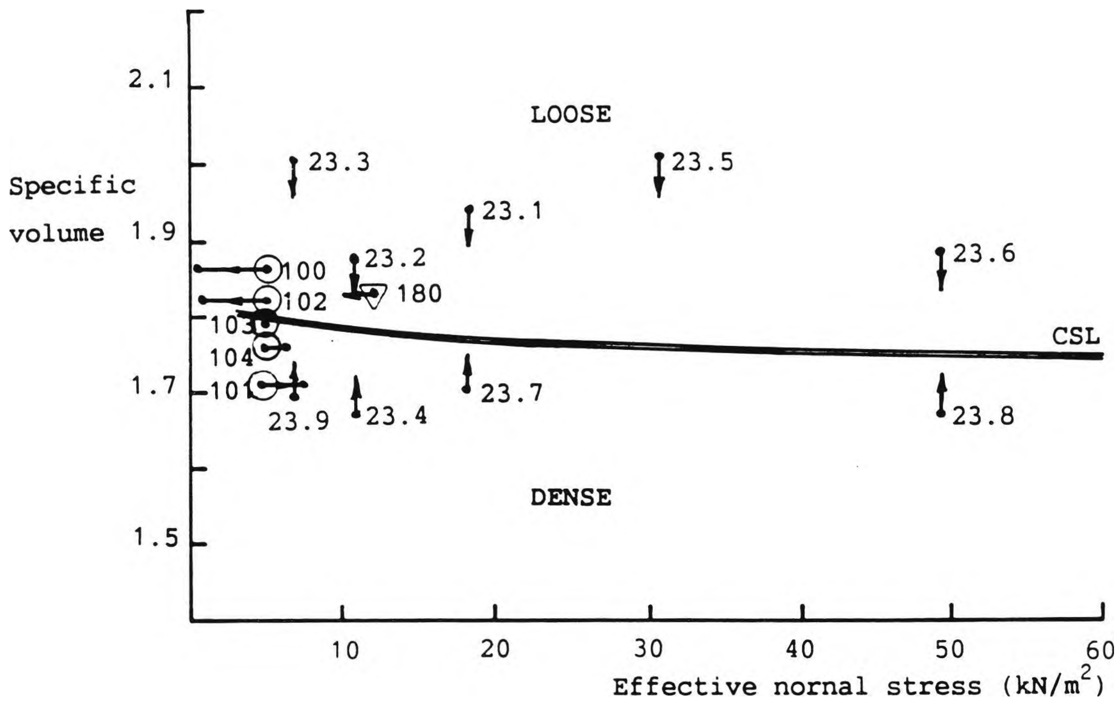

Figure 7.2 Wet and dry soil states, undrained behaviour

Notes

180 Sand column test at increased effective stress level

103 Rapid vane test in sand column

23.1 Drained direct shear test

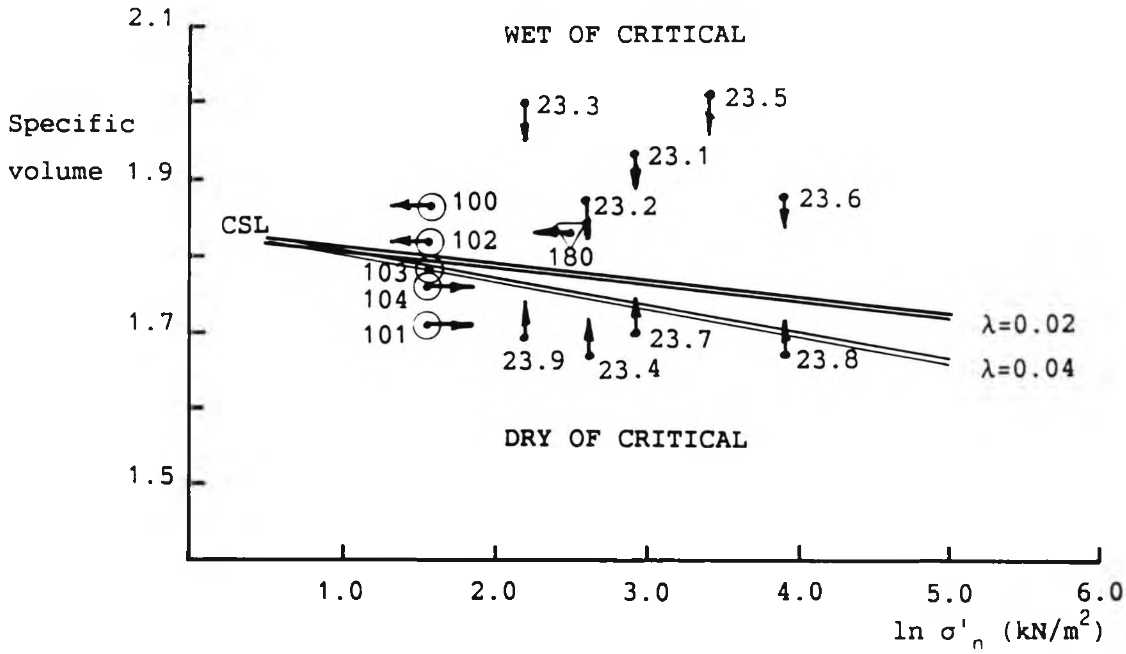

Figure 7.3 Geometry of the critical state line of soil 23

Notes

180 Sand column test at increased effective stress level

103 Rapid vane test in sand column

23.1 Drained direct shear test

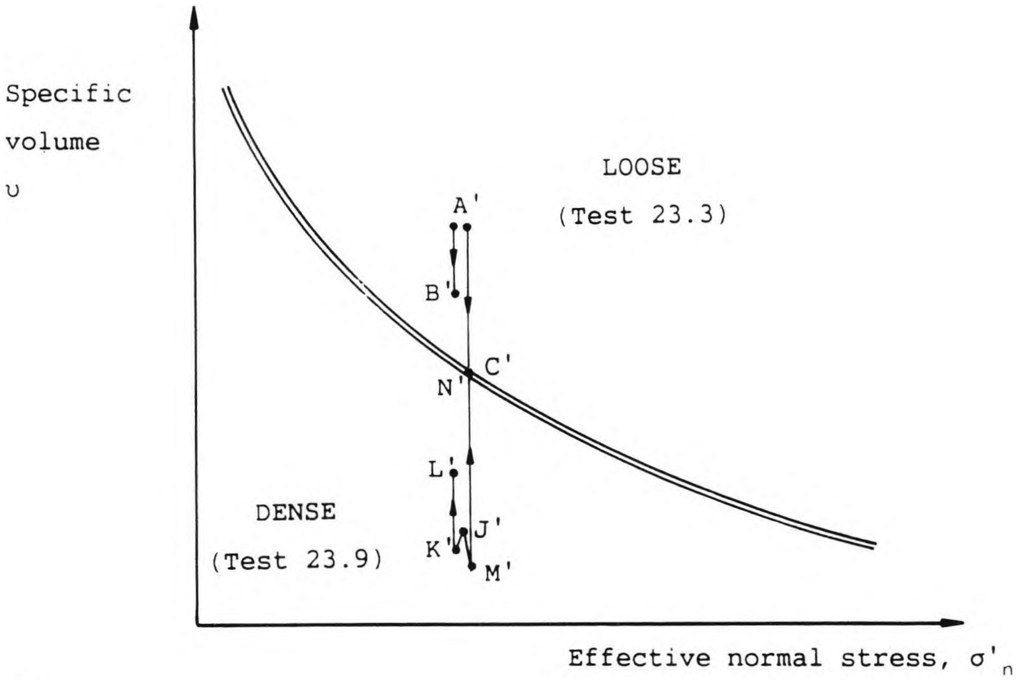

a)

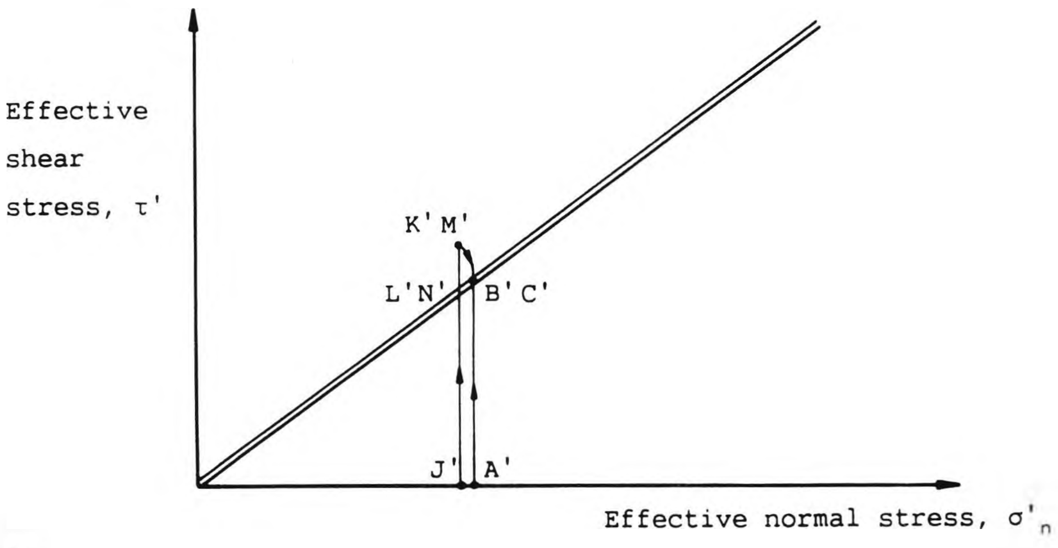

b)

Figure 7.4 Assumed drained stress paths in direct shear tests 23.3 and 23.9

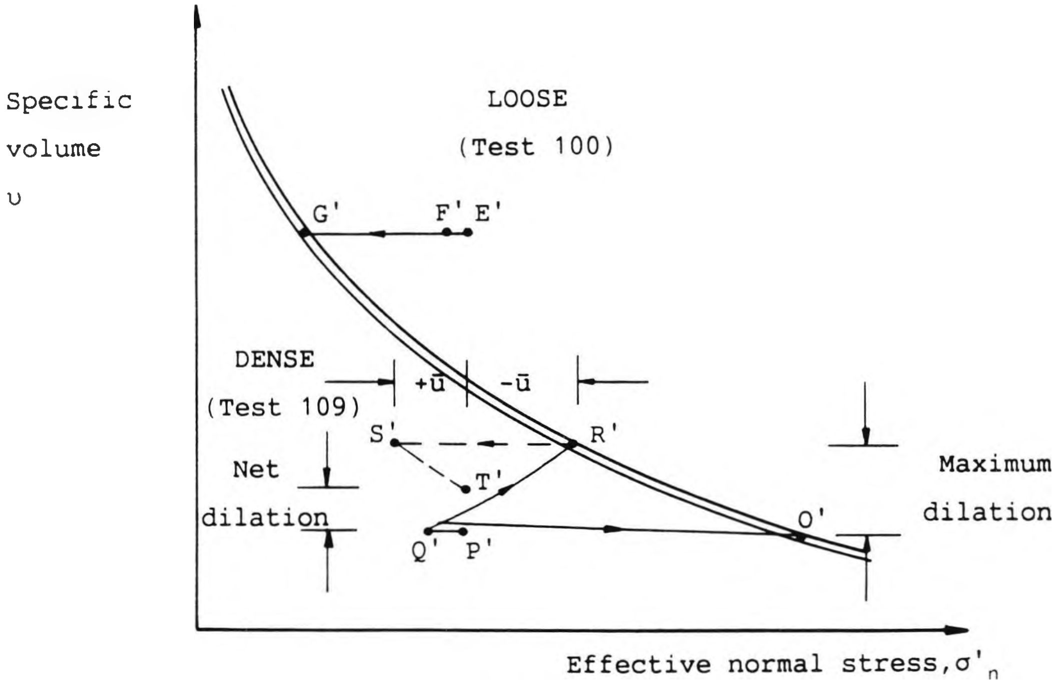

a)

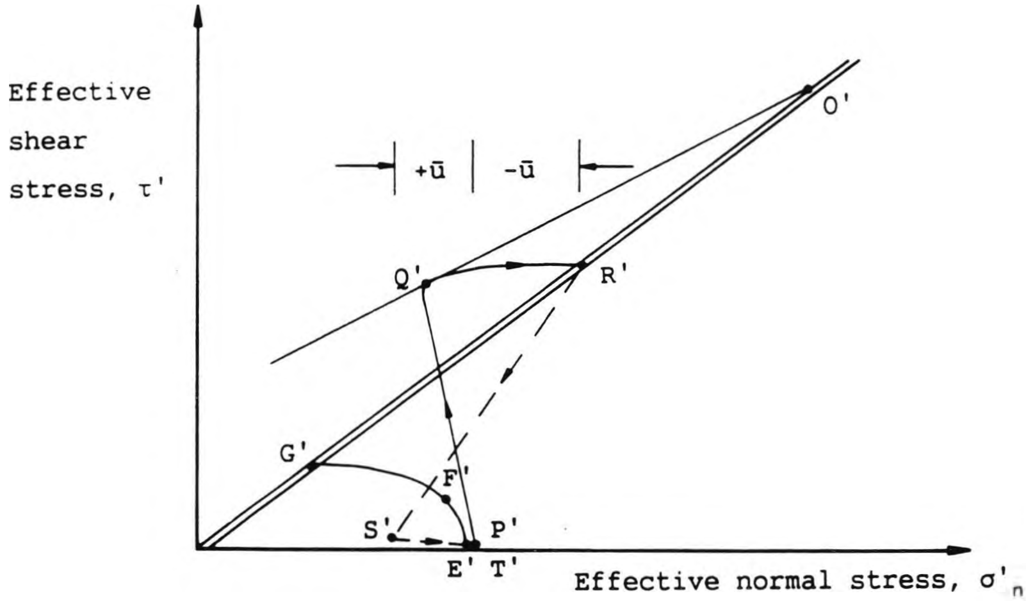

Figure 7.5 Assumed undrained stress paths in sand column tests 100 and 109

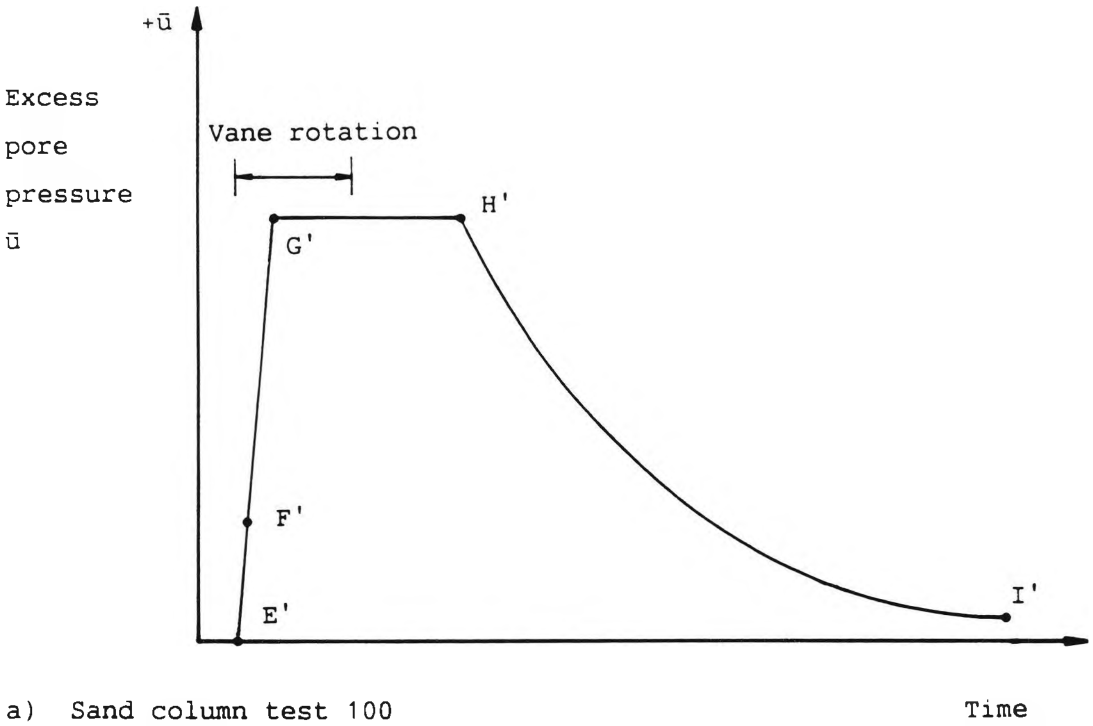

a) Sand column test 100

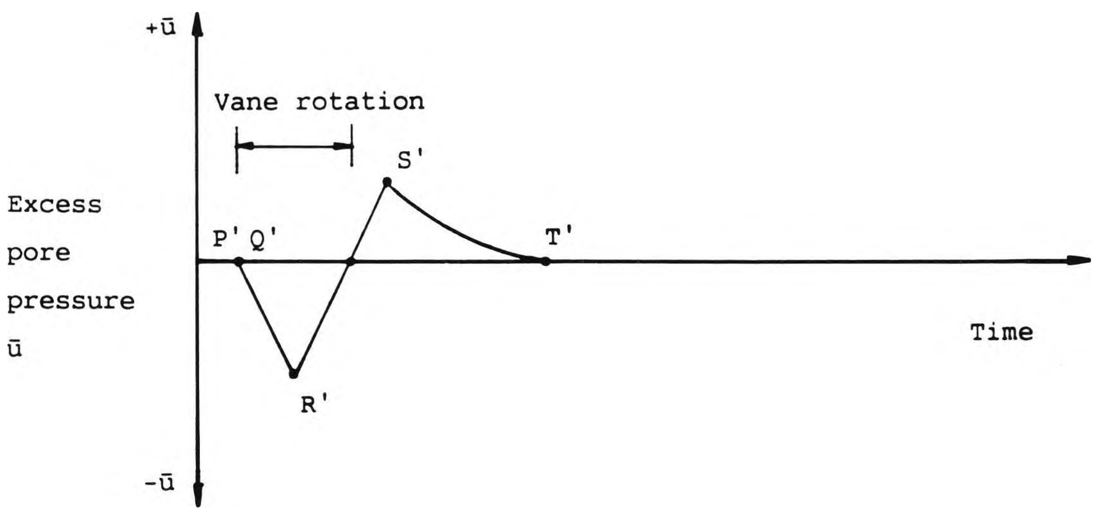

b) Sand column test 109

Figure 7.6 Idealised excess pore pressures recorded in sand column tests 100 and 109

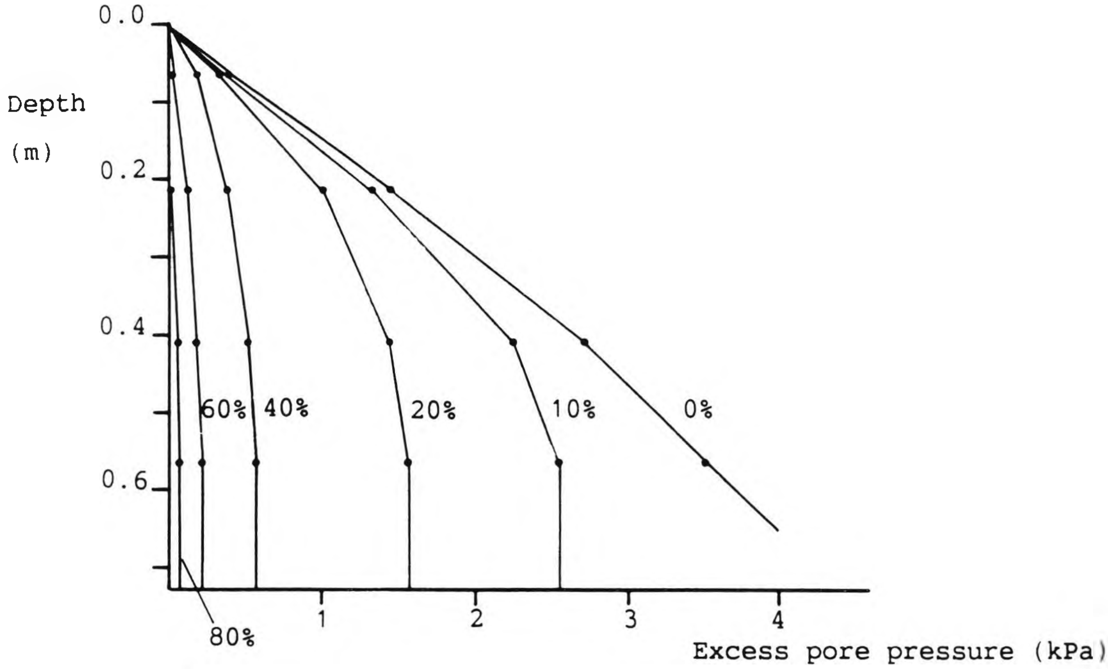

Figure 7.7 Excess pore pressure dissipation recorded in test 117

Note 1 In Figures 7.7 and 7.8 isochrones are for percentage time to full excess pore pressure dissipation, and not average degree of consolidation.

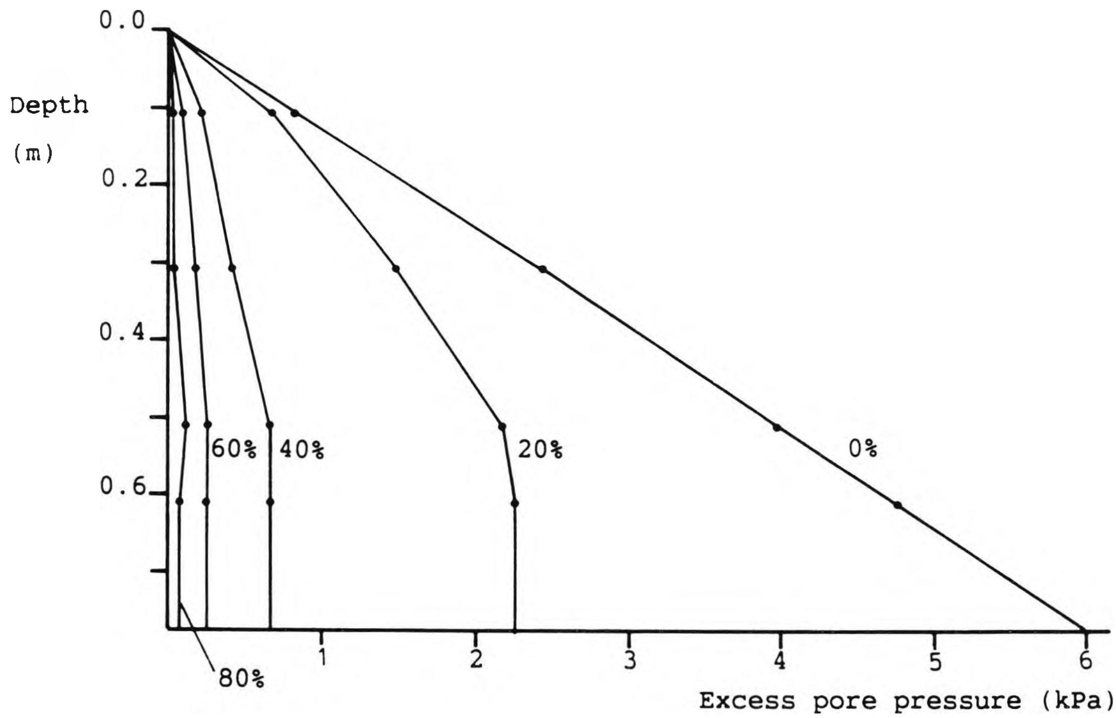

Figure 7.8 Excess pore pressure dissipation recorded in test 136

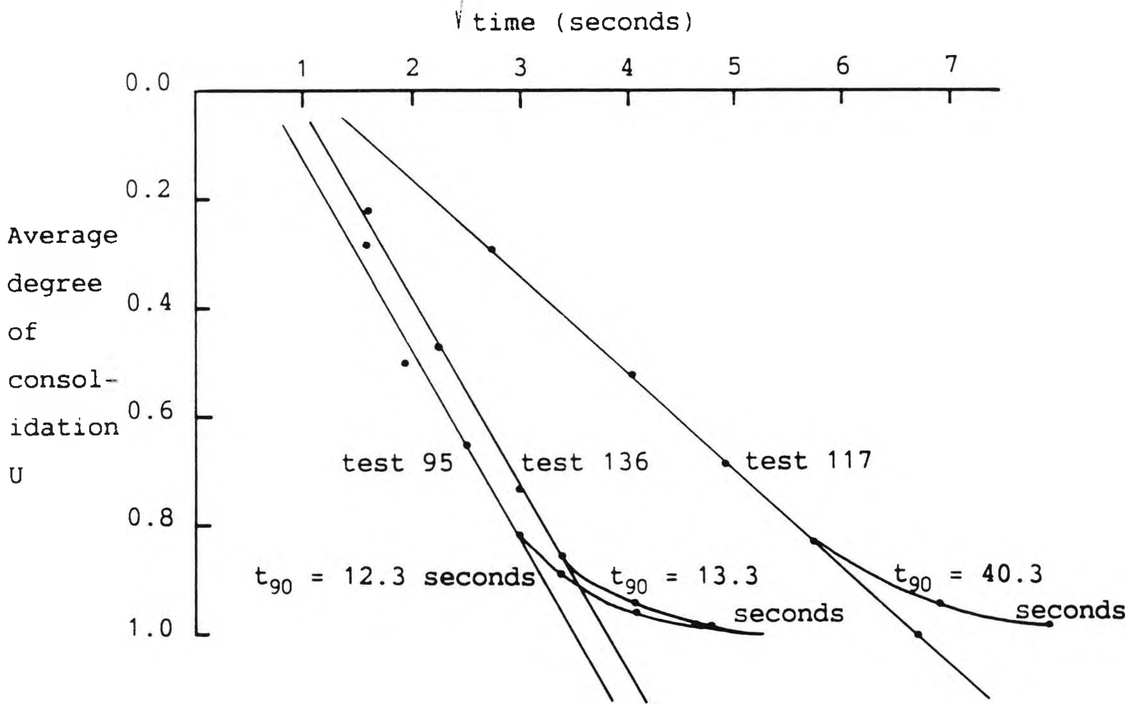

Figure 7.9 Excess pore pressure dissipation by consolidation, average degree of consolidation - square root time

Notes 1 $c_v = \frac{H^2 T_v}{t}$ at t_{90} $T_v = 0.940$

2 Average degree of consolidation values are derived from area beneath initial and subsequent isochrones

3 No zero adjustment made

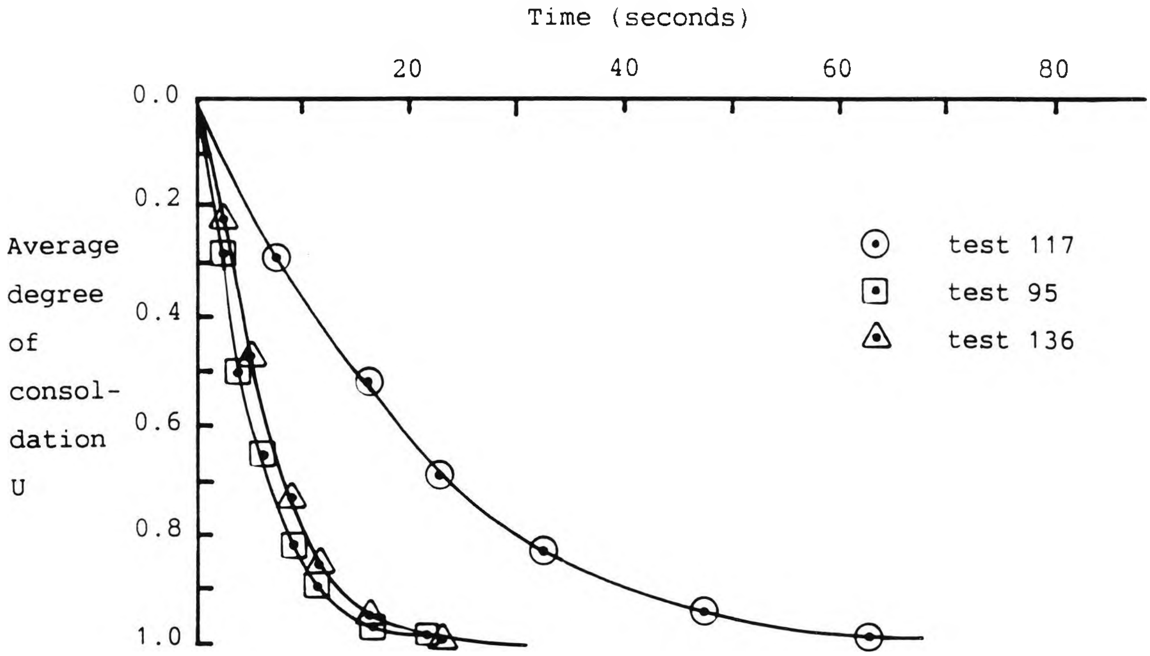

Figure 7.10 Excess pore pressure dissipation by consolidation, average degree of consolidation - linear time

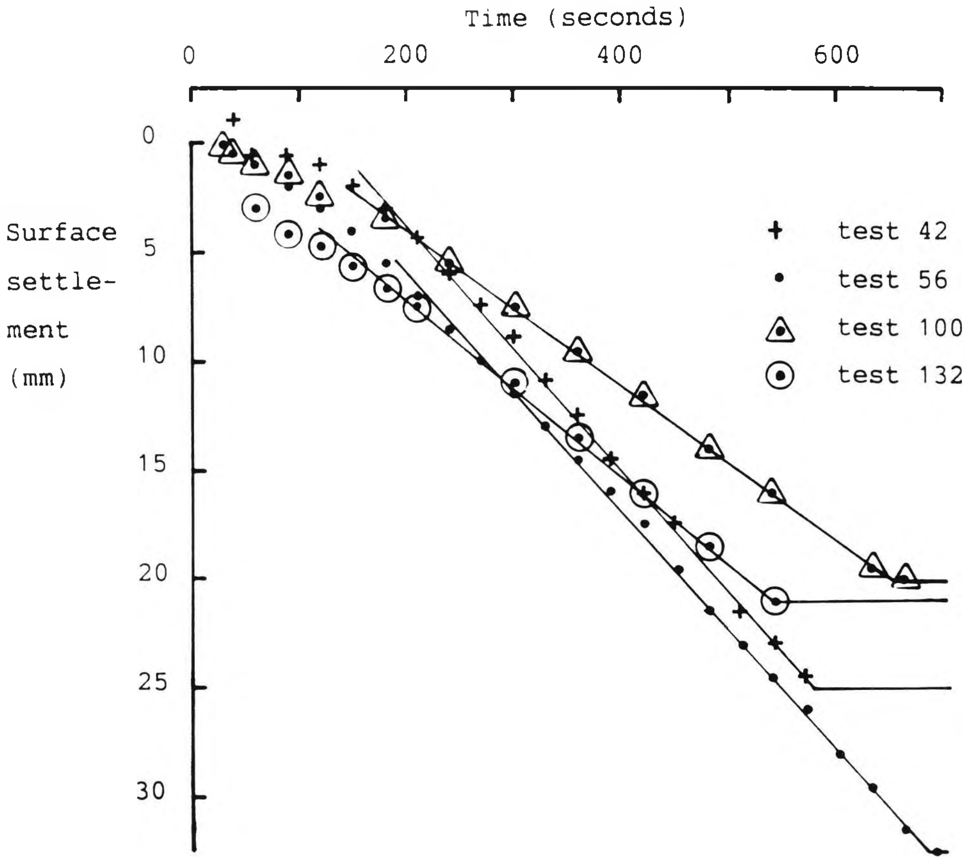

Figure 7.11 Surface settlements observed in sand column tests 42, 56, 100 and 132

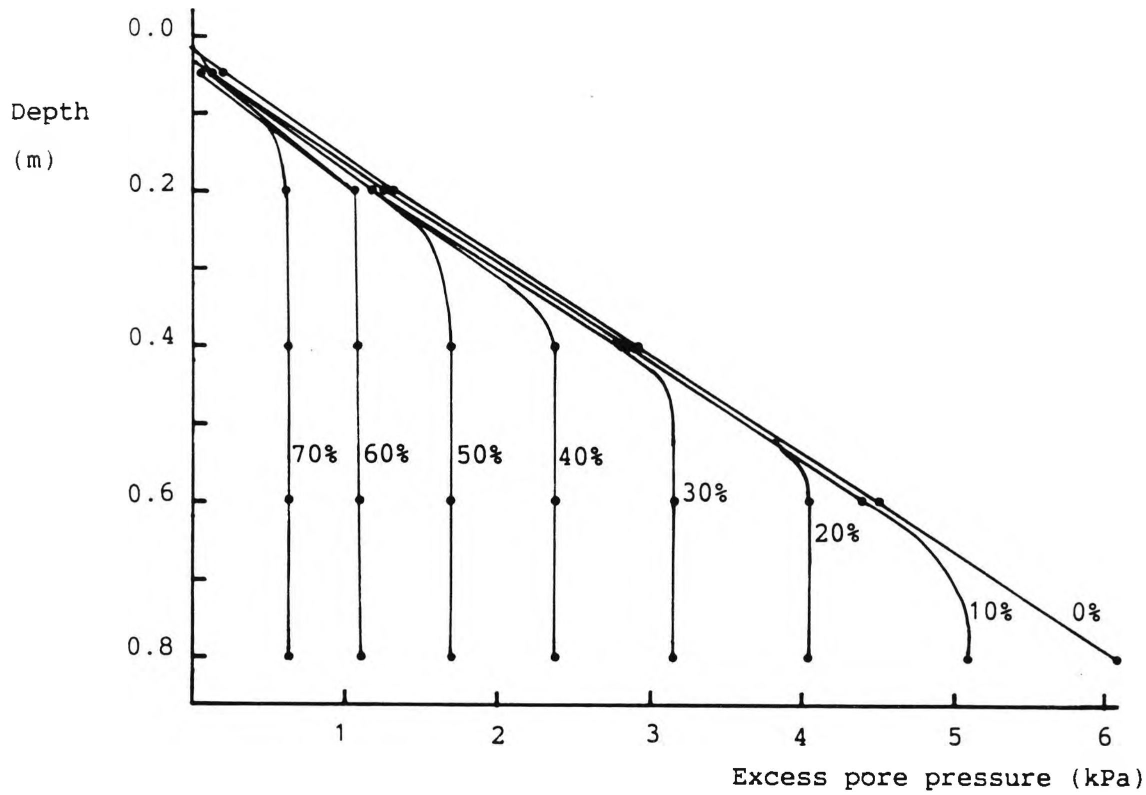

Figure 7.12 Excess pore pressure dissipation recorded in test 42

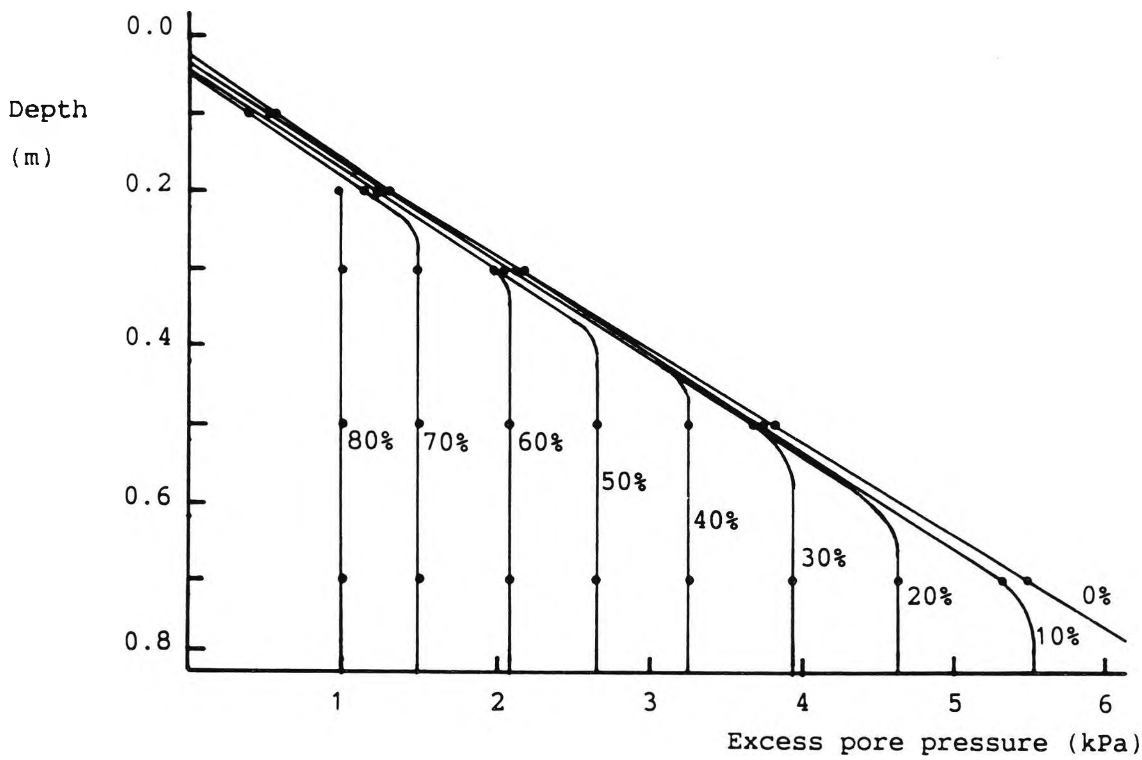

Figure 7.13 Excess pore pressure dissipation recorded in test 56

<u>Note 1</u> In Figures 7.12 and 7.13 isochrones are for percentage time to full excess pore pressure dissipation, and not average degree of consolidation.

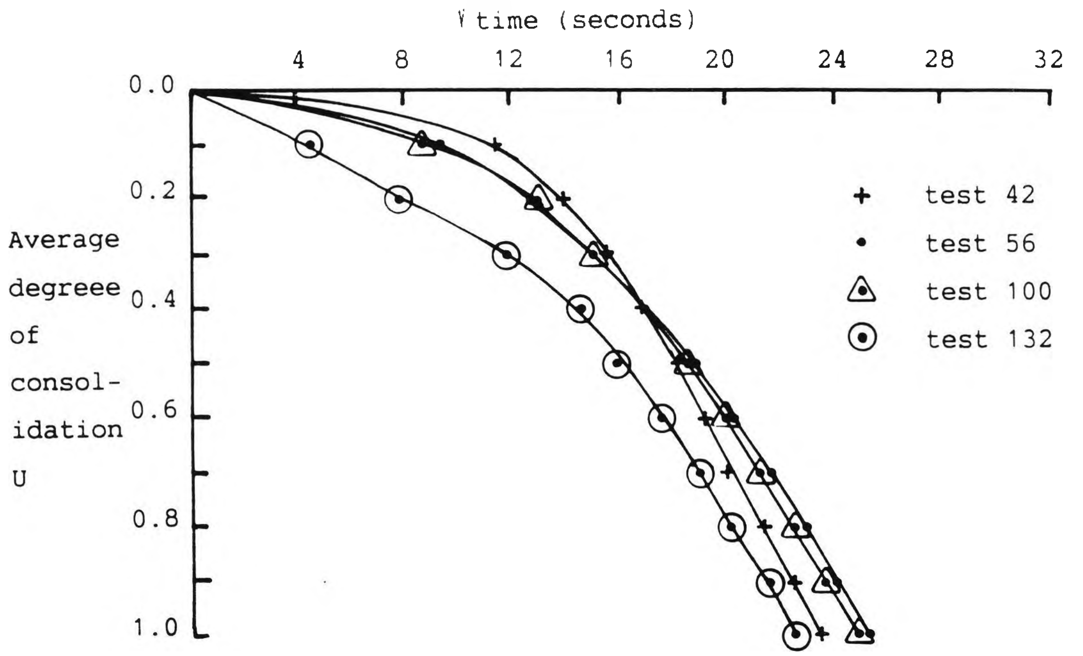

Figure 7.14 Excess pore pressure dissipation by hindered settling, average degree of consolidation - square root time

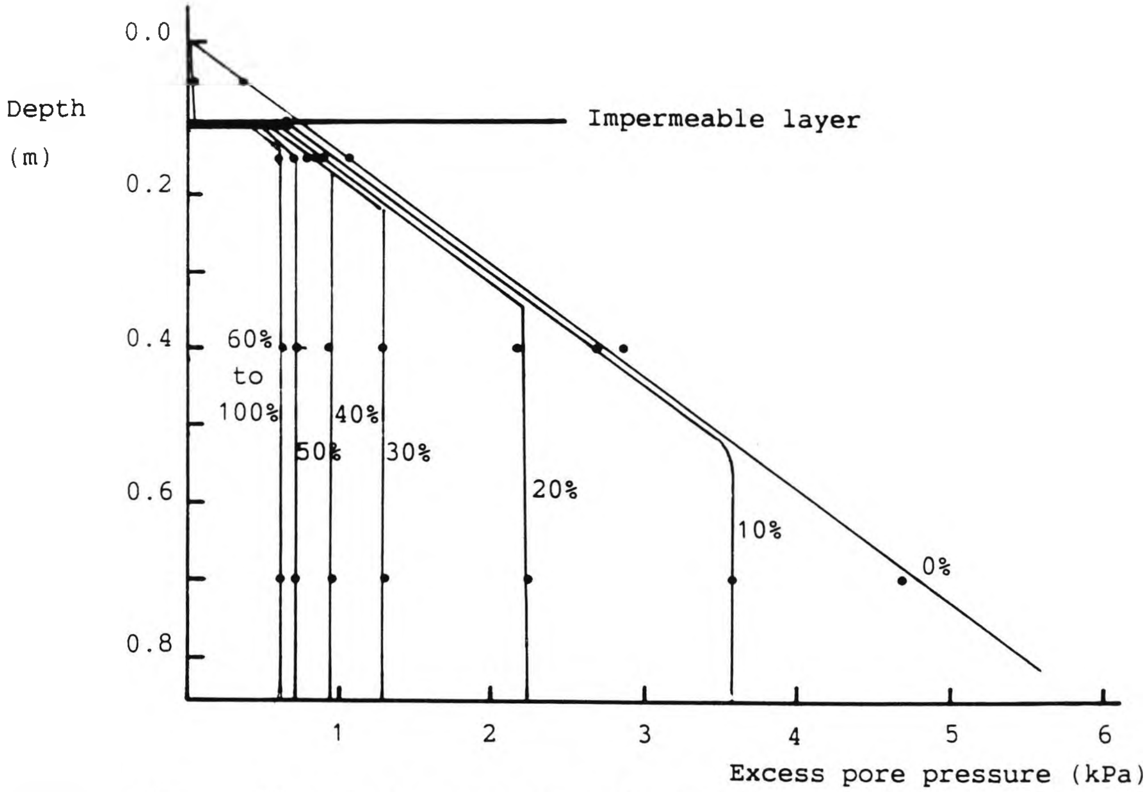

Figure 7.15 Excess pore pressure dissipation recorded in test 182-185, 20 sec to 400 sec

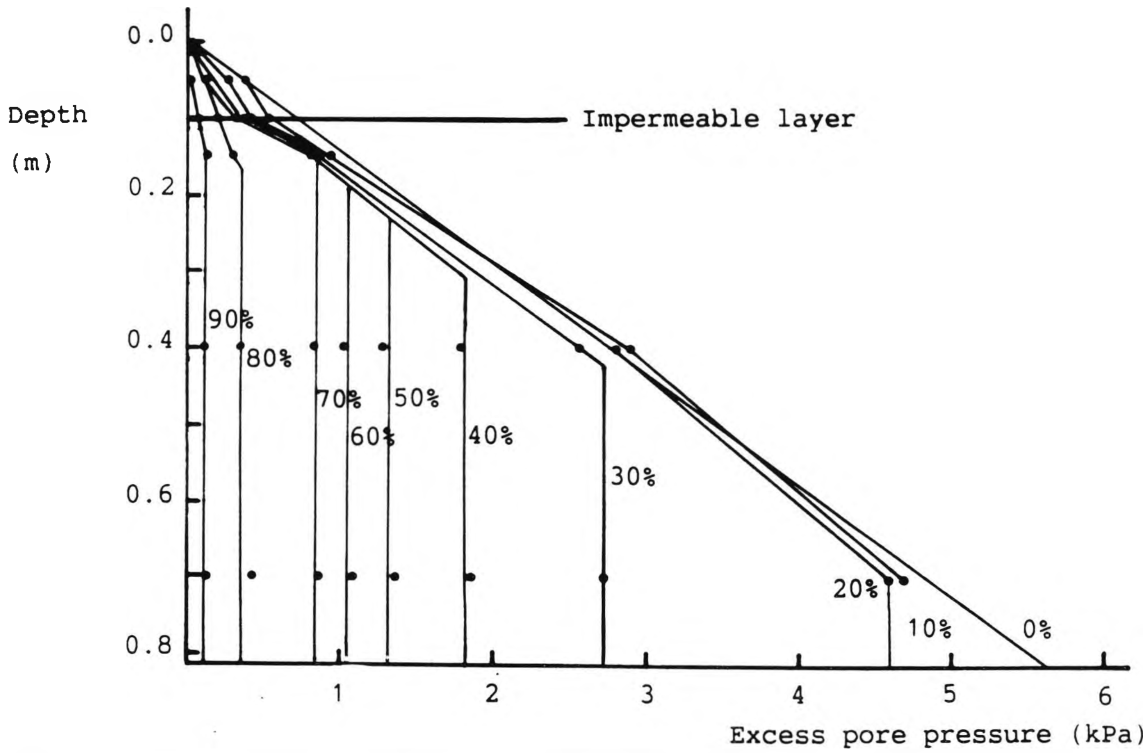

Figure 7.16 Excess pore pressure dissipation recorded in test 182-185, 1540 sec to 2000 sec

Note 1 In Figures 7.15 and 7.16 isochrones are for percentage time to full excess pore pressure dissipation, and not average degree of consolidation.

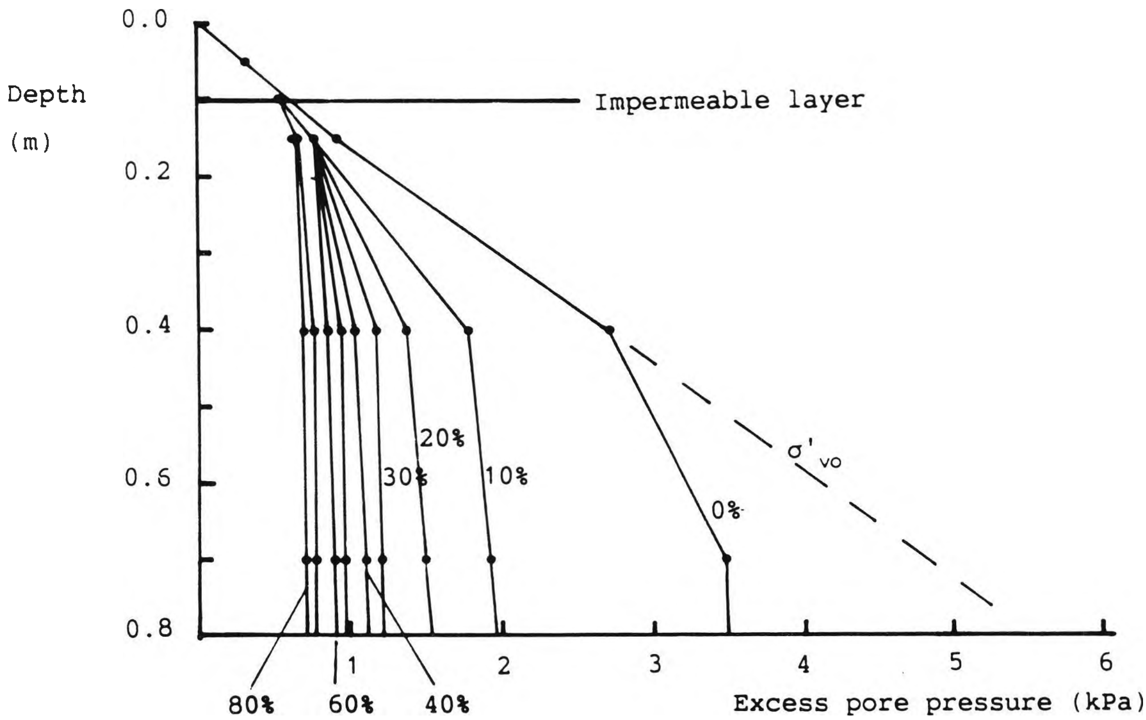

Figure 7.17 Excess pore pressure dissipation recorded in test 182-185, 1480 sec to 1530 sec

Note 1 In Figure 7.17 isochrones are for percentage time to full excess pore pressure dissipation, and not average degree of consolidation.

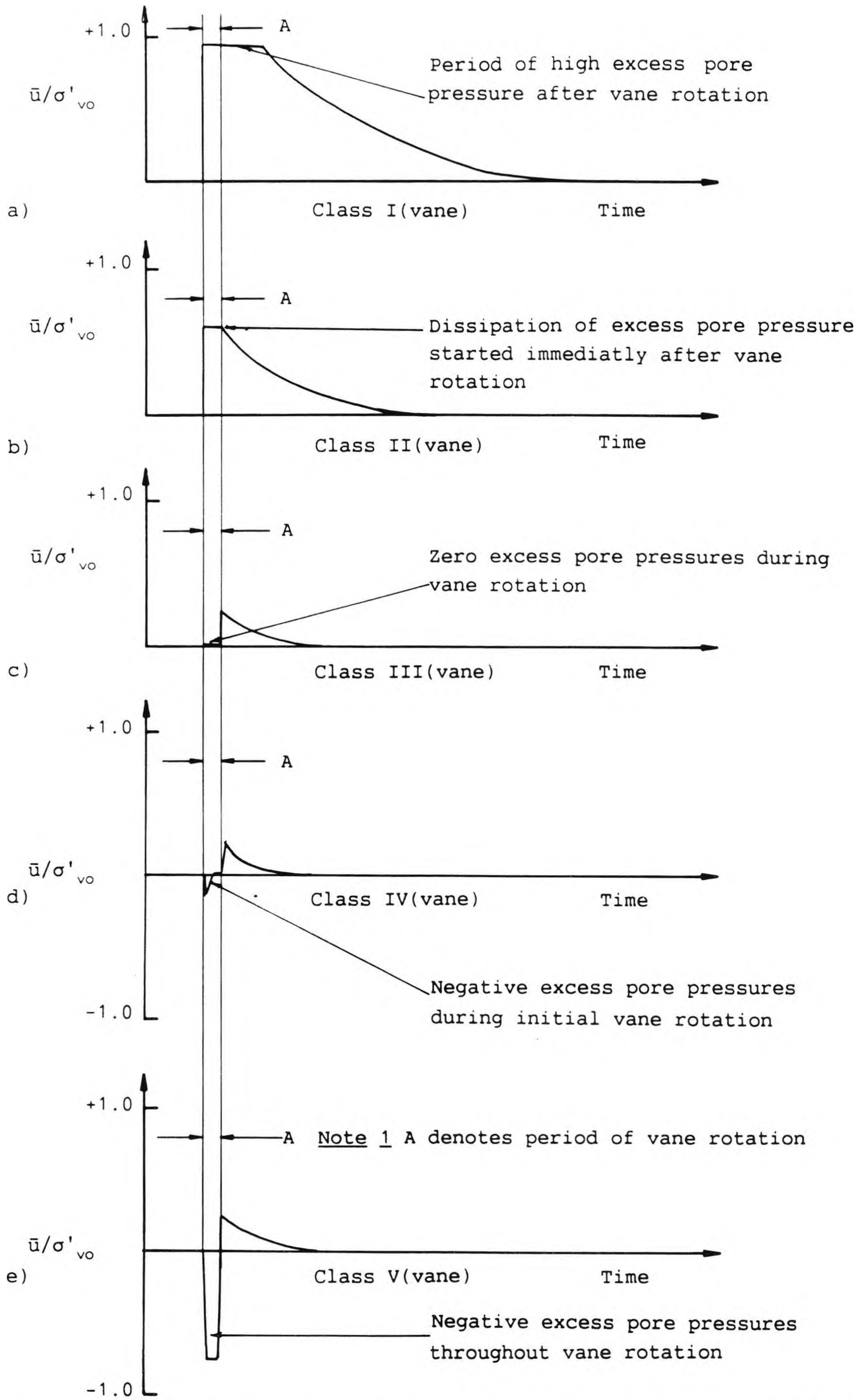

Figure 7.18 Schematic sketches of excess pore pressures recorded during vane tests

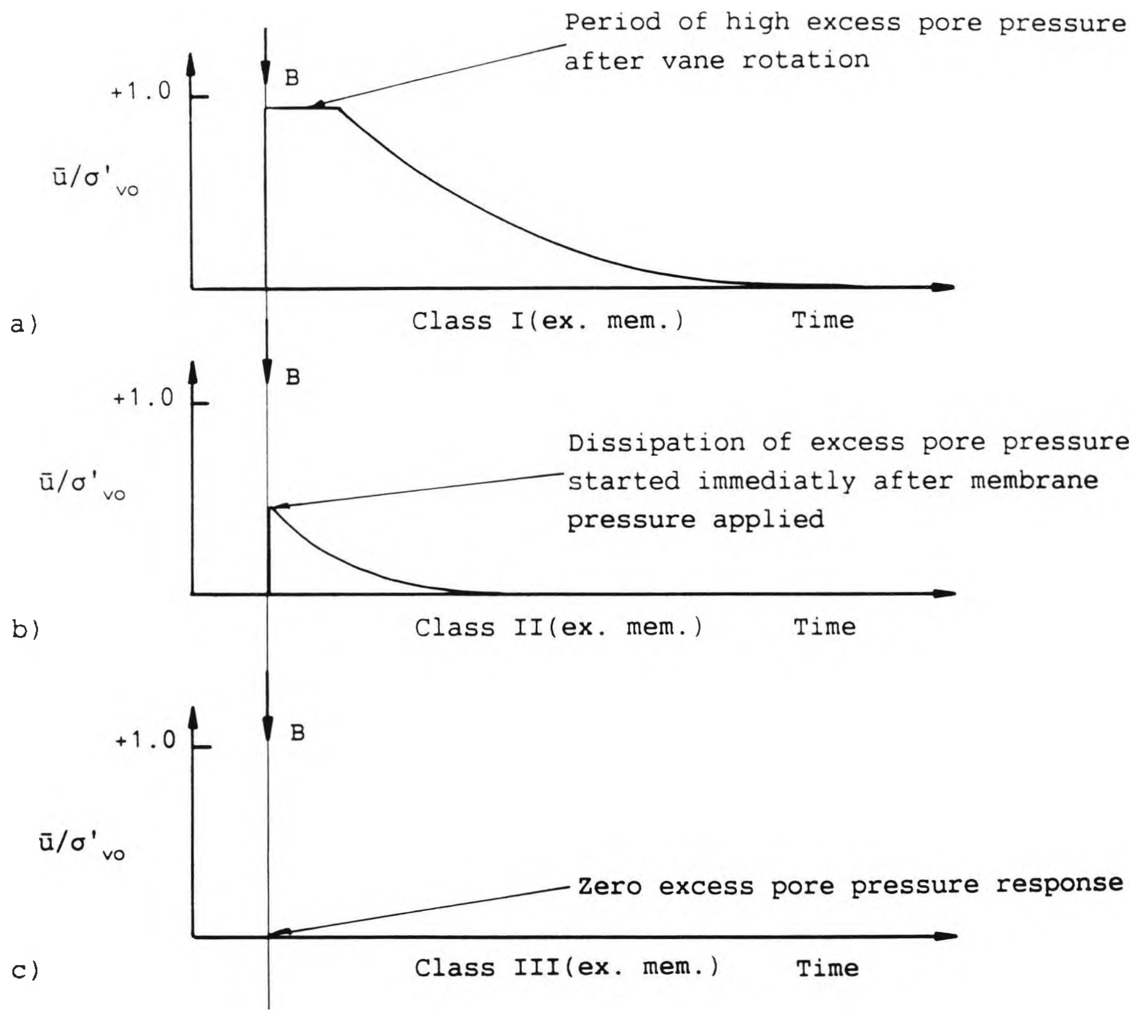

Figure 7.19 Schematic sketches of excess pore pressures recorded during expanding membrane probe tests

Note 1 B denotes time at which pressure applied to expanding membrane

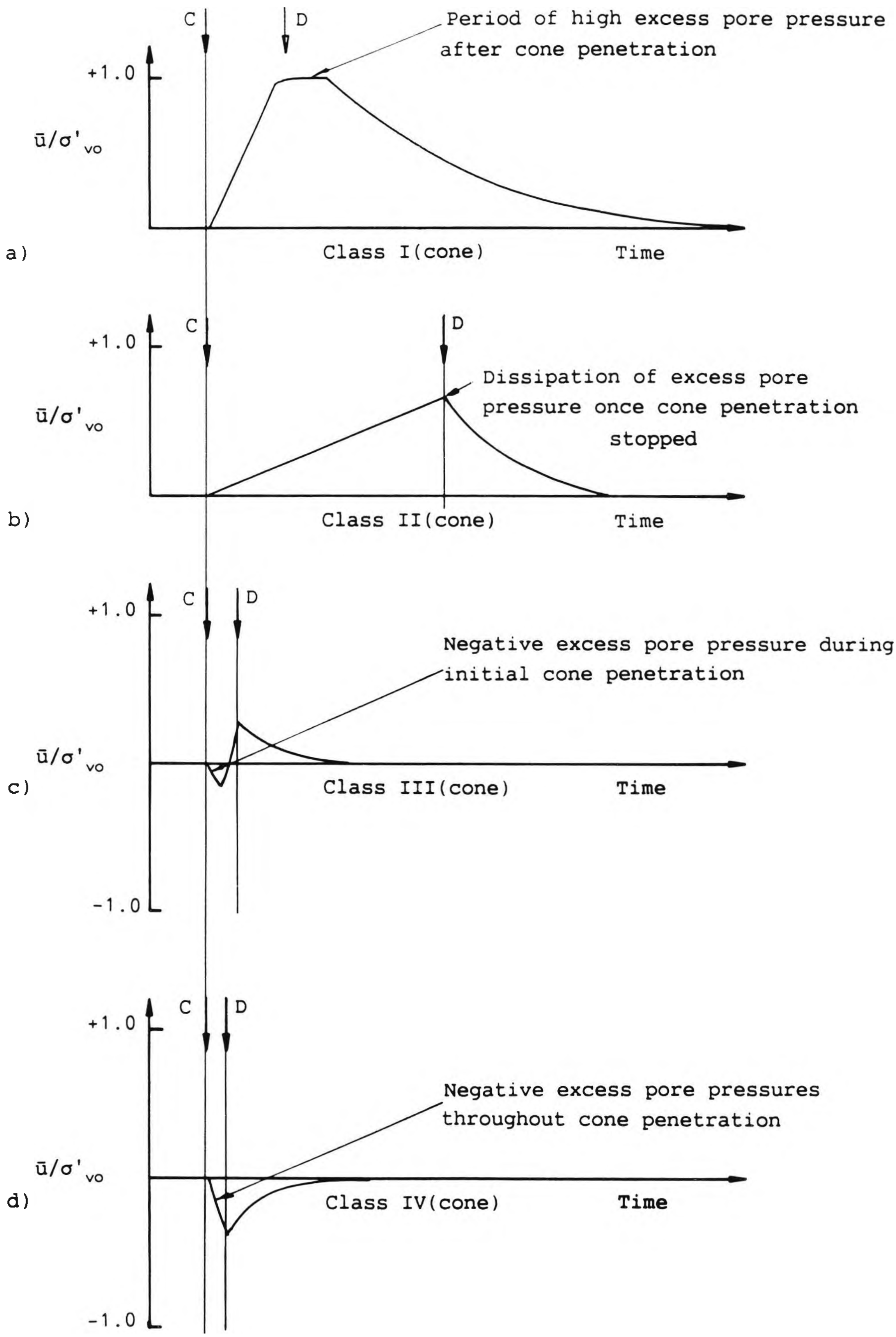

Figure 7.20 Schematic sketches of excess pore pressures recorded during cone tests

<u>Note</u> <u>1</u> C denotes time at which cone entered soil bed

<u>2</u> D denotes end of cone penetration

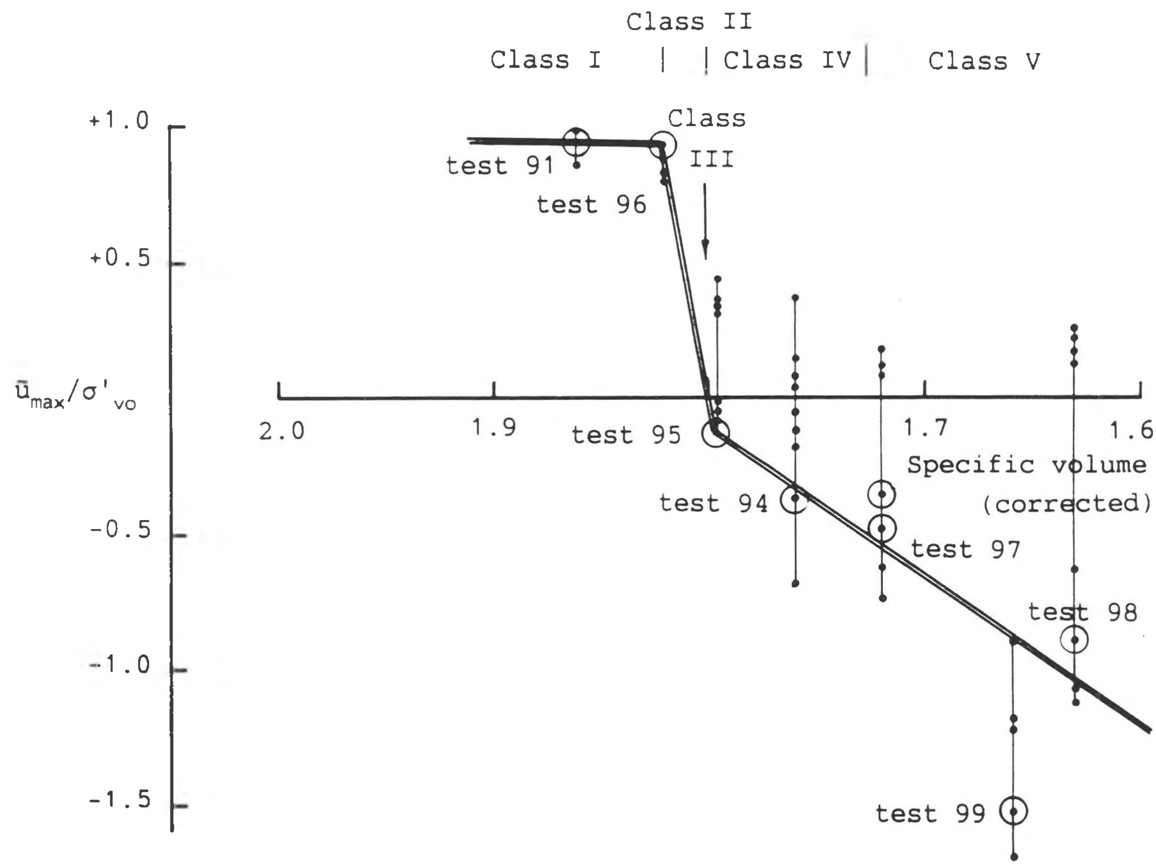

Figure 7.21 Excess pore pressure - specific volume for 1:1 ratio vane

<u>Note 1</u> ⊙ denotes transducer closest to instrument

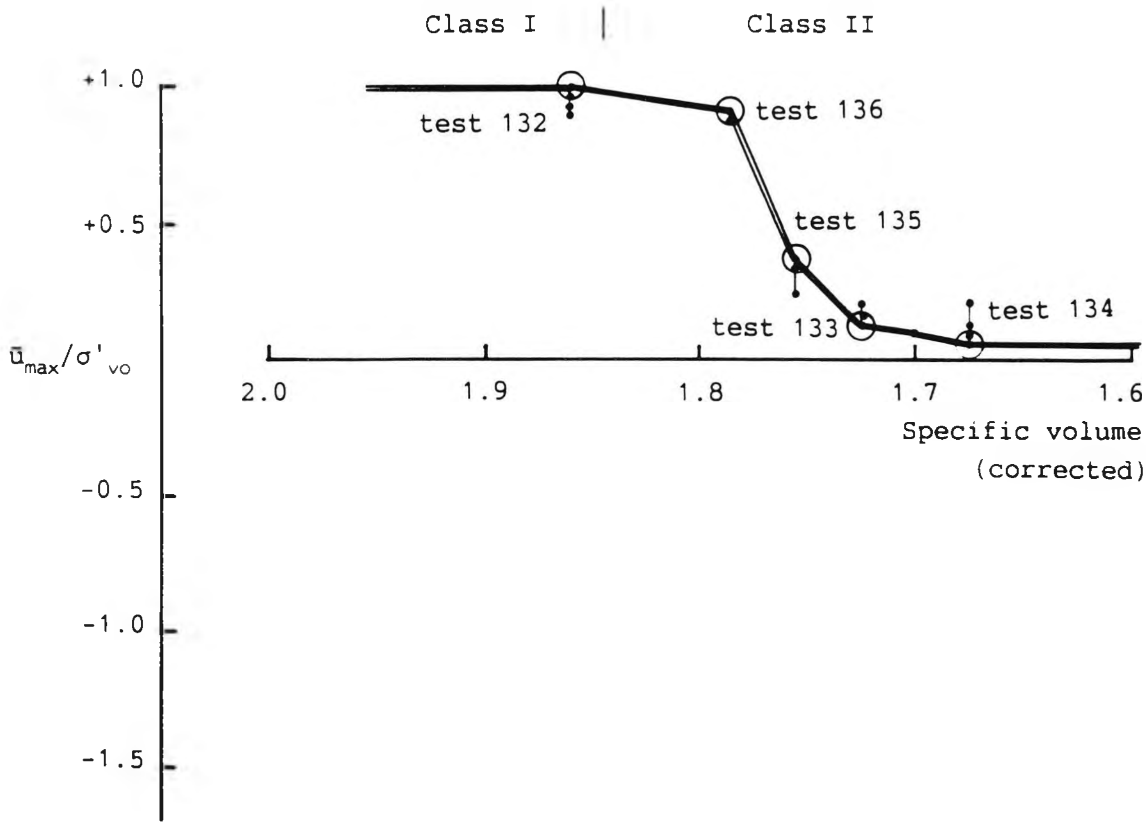

Figure 7.22 Excess pore pressure - specific volume for expanding membrane probe

<u>Note 1</u> ⊙ denotes transducer closest to instrument

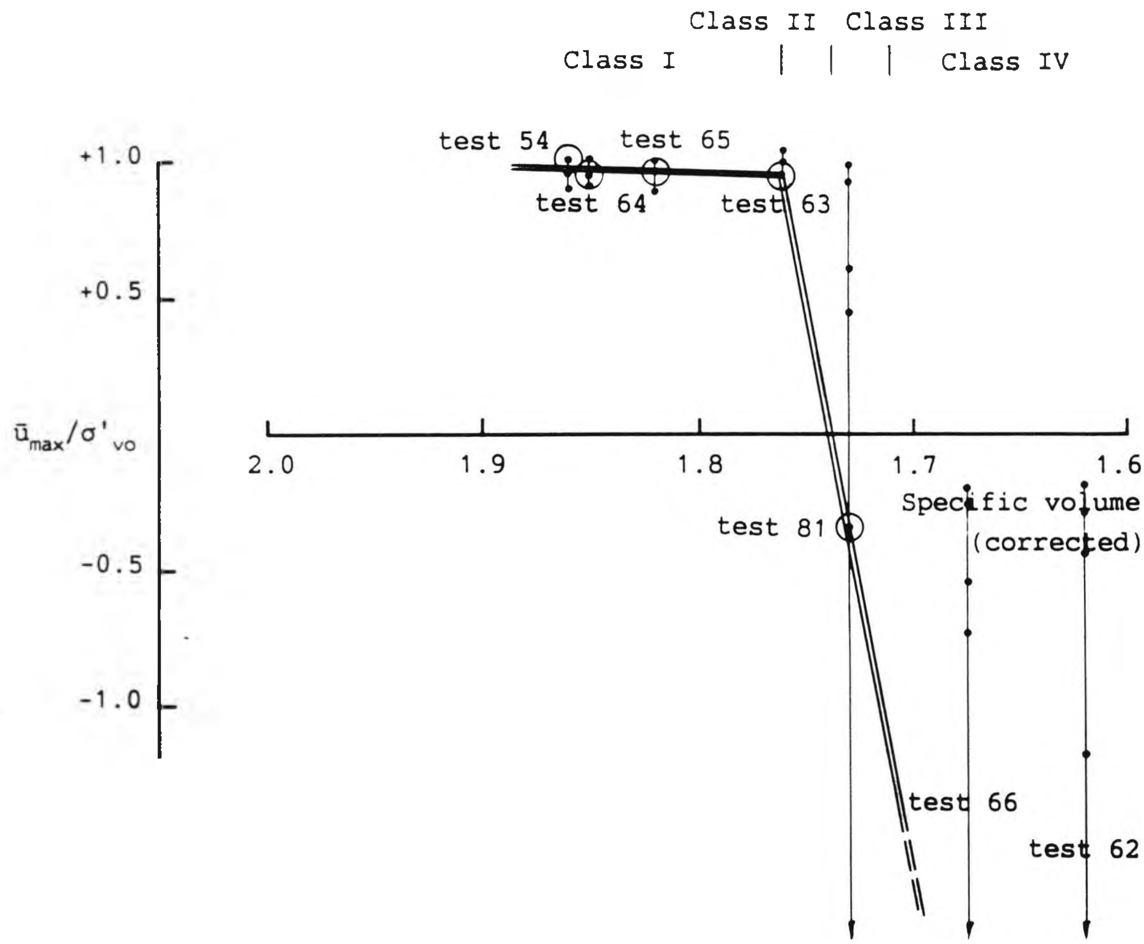

Figure 7.23 Excess pore pressure - specific volume for 60° cone

Note 1 ⊙ denotes transducer closest to instrument

2 Specific volume values have been corrected to give values at the base of the soil bed, including tests where only partial cone penetration was achieved

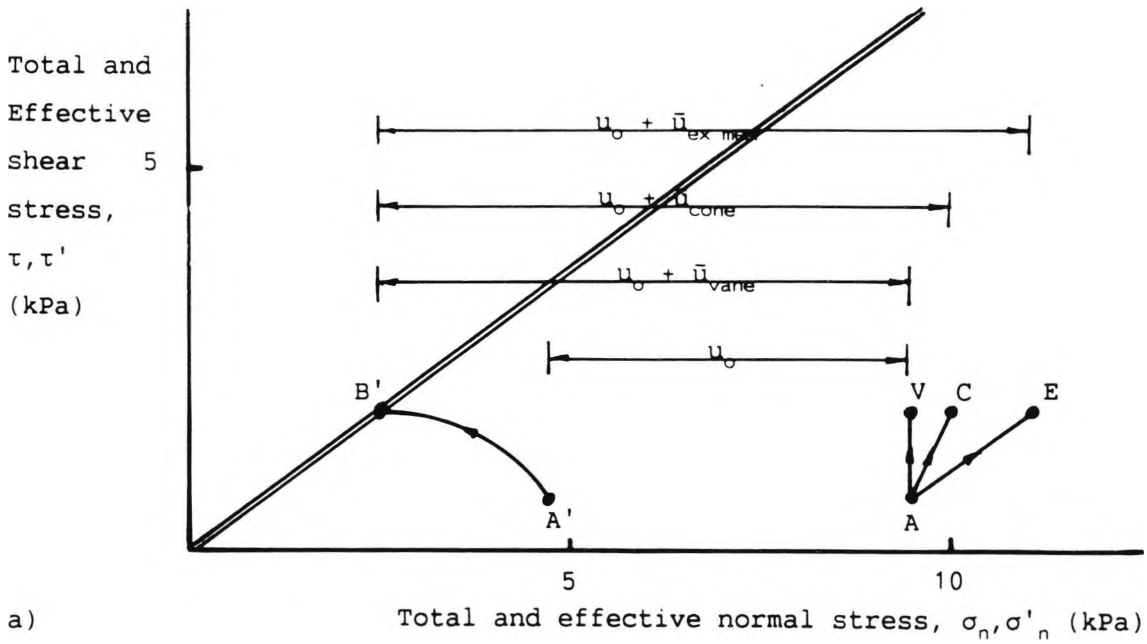

a)

A'B' denotes effective stress path

AV denotes total stress path for vane

AC denotes total stress path for cone

AE denotes total stress path for expanding membrane probe

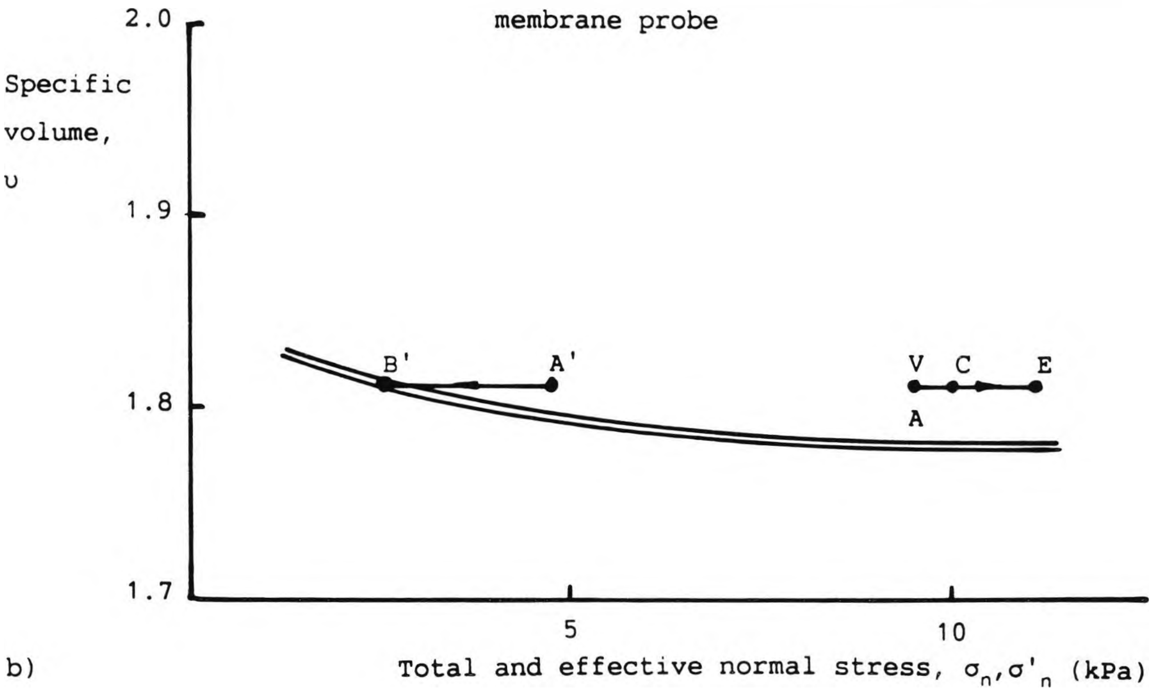

b)

Figure 7.24 Assumed undrained stress paths for model instruments loading soil initially wet of critical

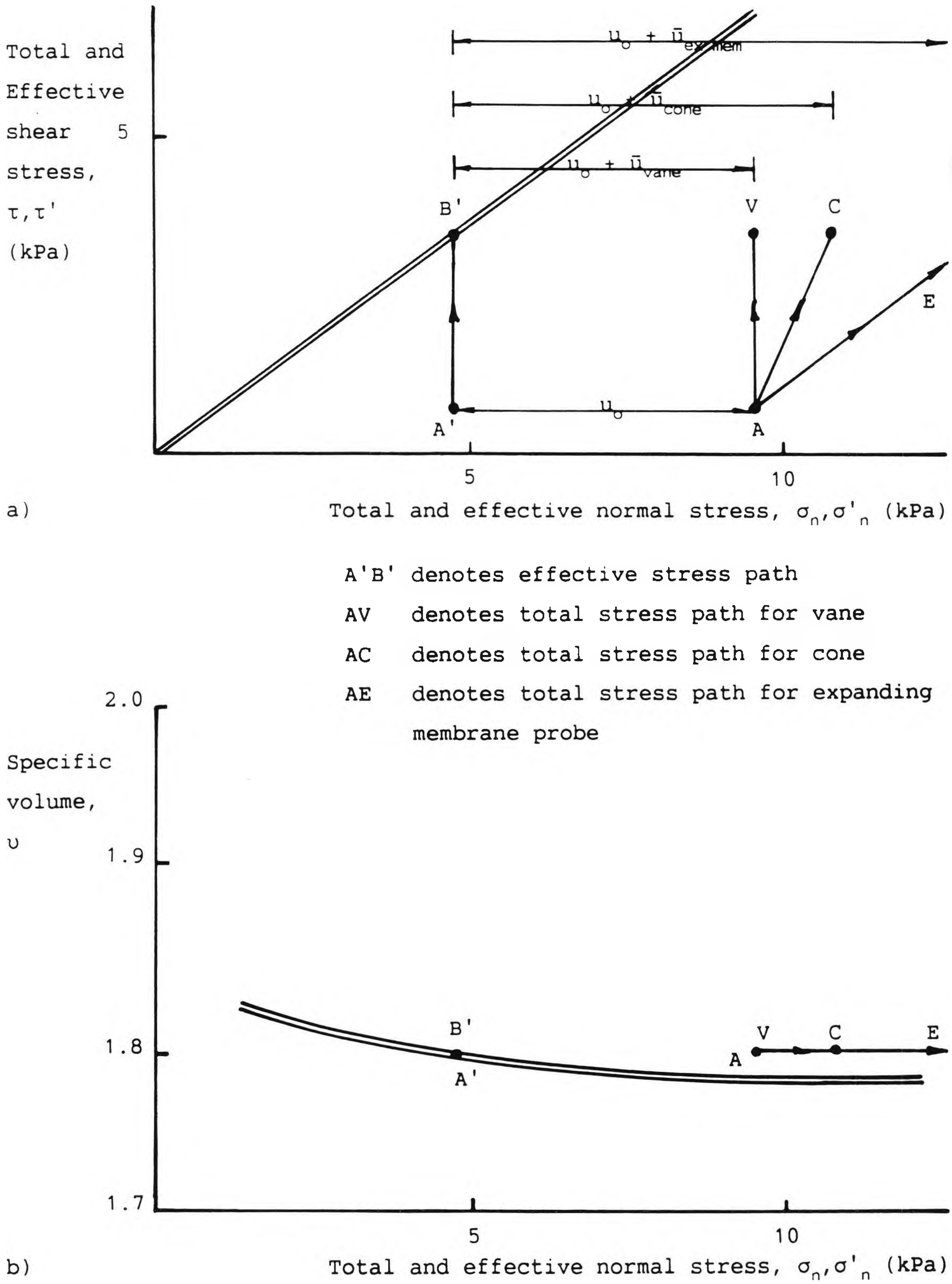

Figure 7.25 Assumed undrained stress paths for model instruments loading soil initially beneath the critical state line

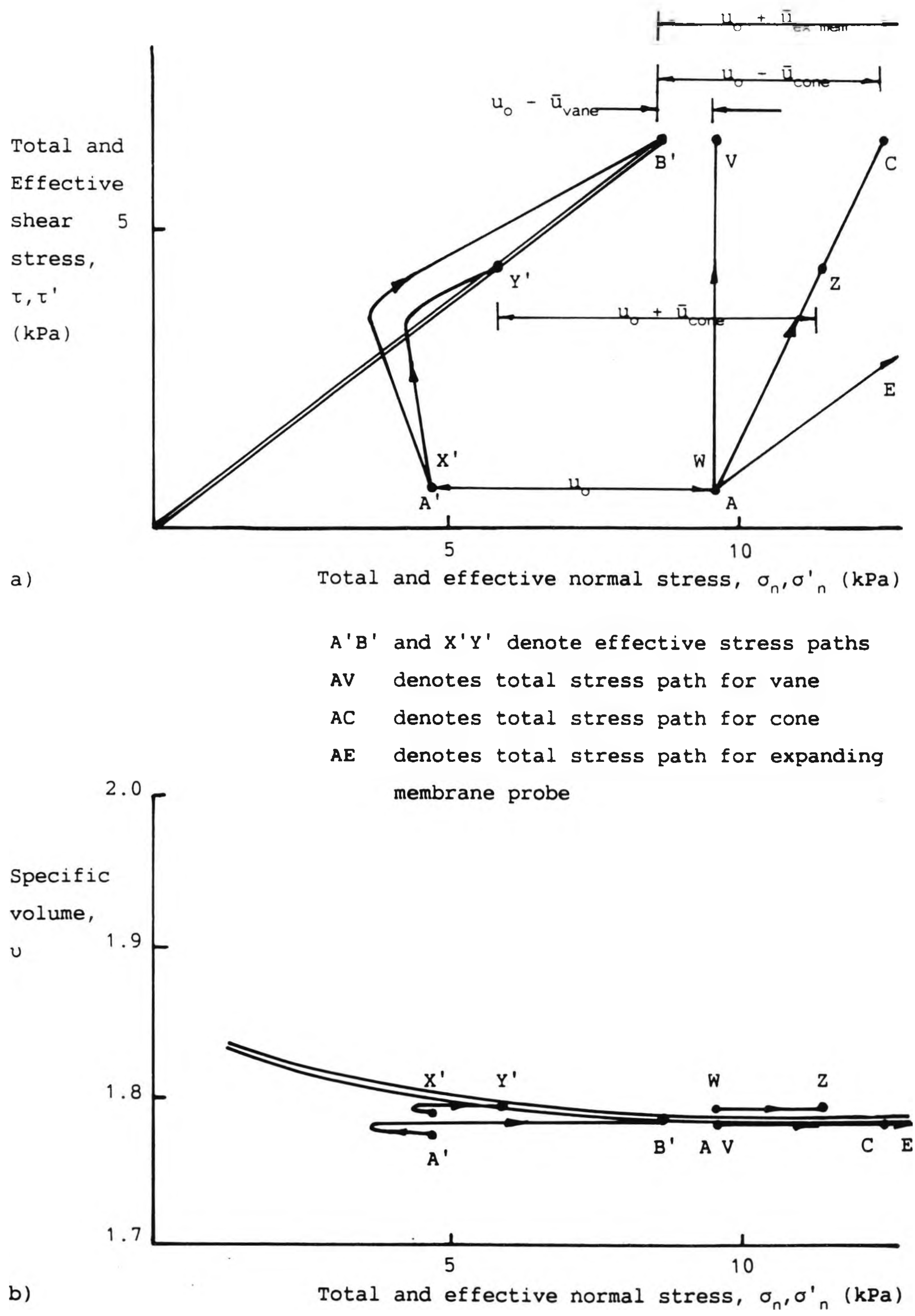

Figure 7.26 Assumed undrained stress paths for model instruments loading soil initially dry of critical

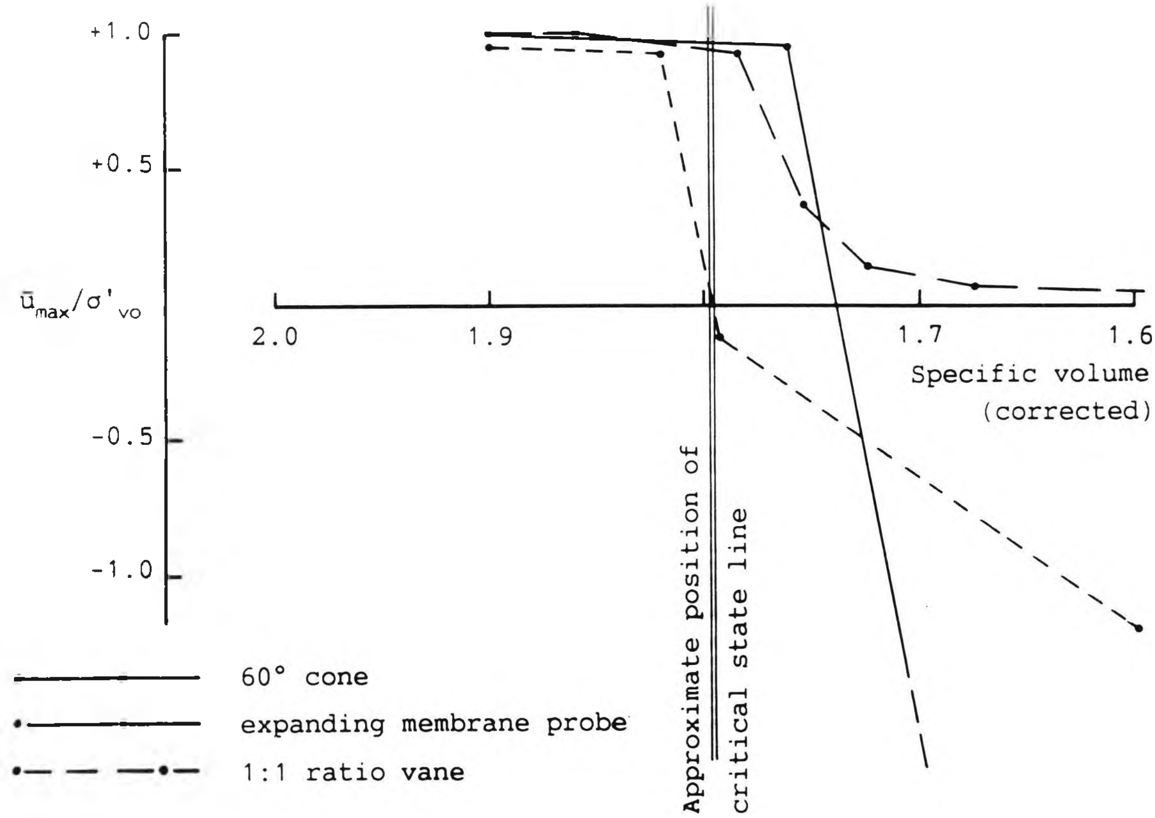

Figure 7.27 Summary plot of excess pore pressure - specific volume for various types of model in situ instruments

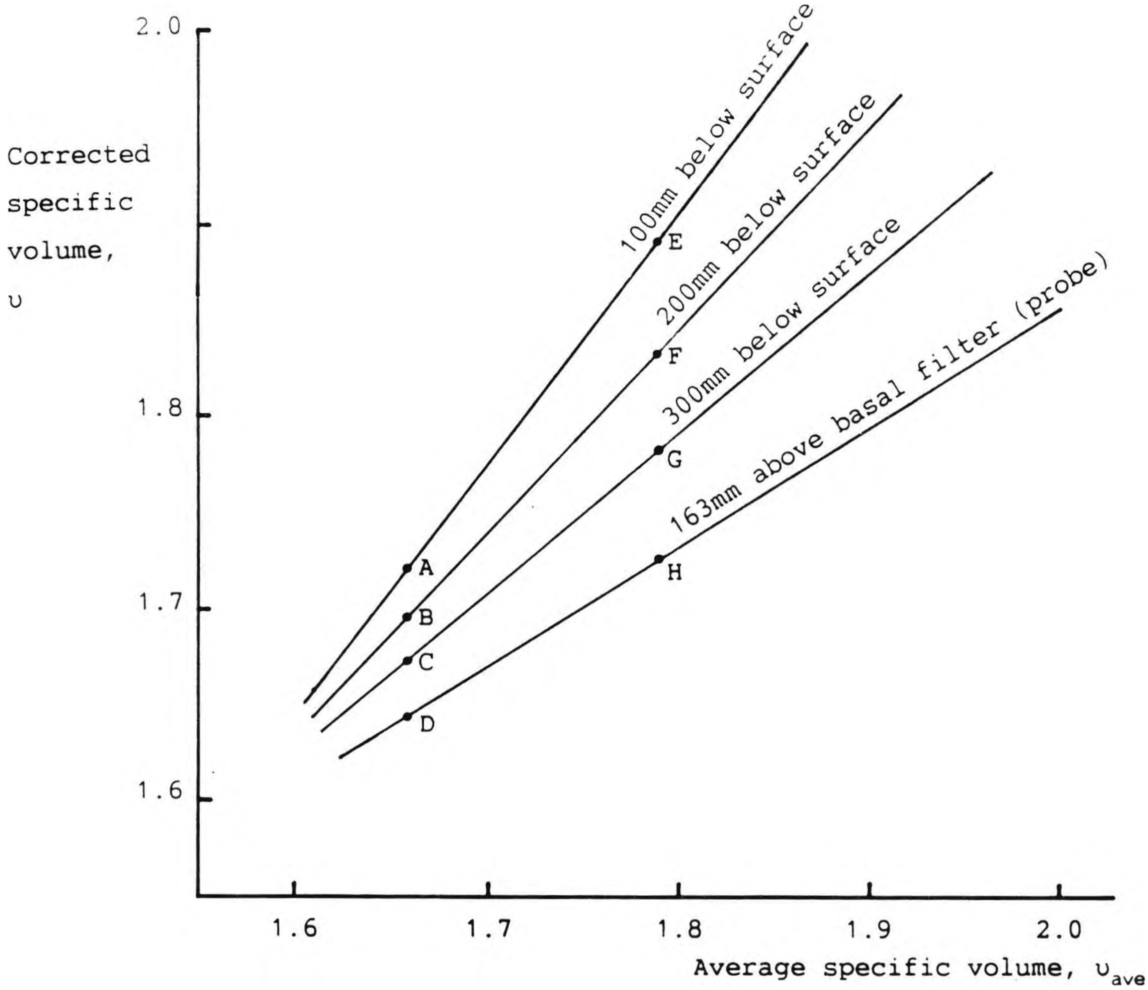

Figure 7.28 Correction for specific volume at the base of soil beds

<u>Note</u> The approximate method of correction shown above was derived from the testing to establish variations in soil density within soil beds prepared in the sand column, refer Appendix D. Figure 7.28 was constructed as follows;

<u>1</u> A to H were derived from the difference between assumed average, and measured specific volume values shown in Figure D.2.

<u>2</u> A simple linear correction was assumed by interpolation between associated values ie. AE, BF, CG and DH.

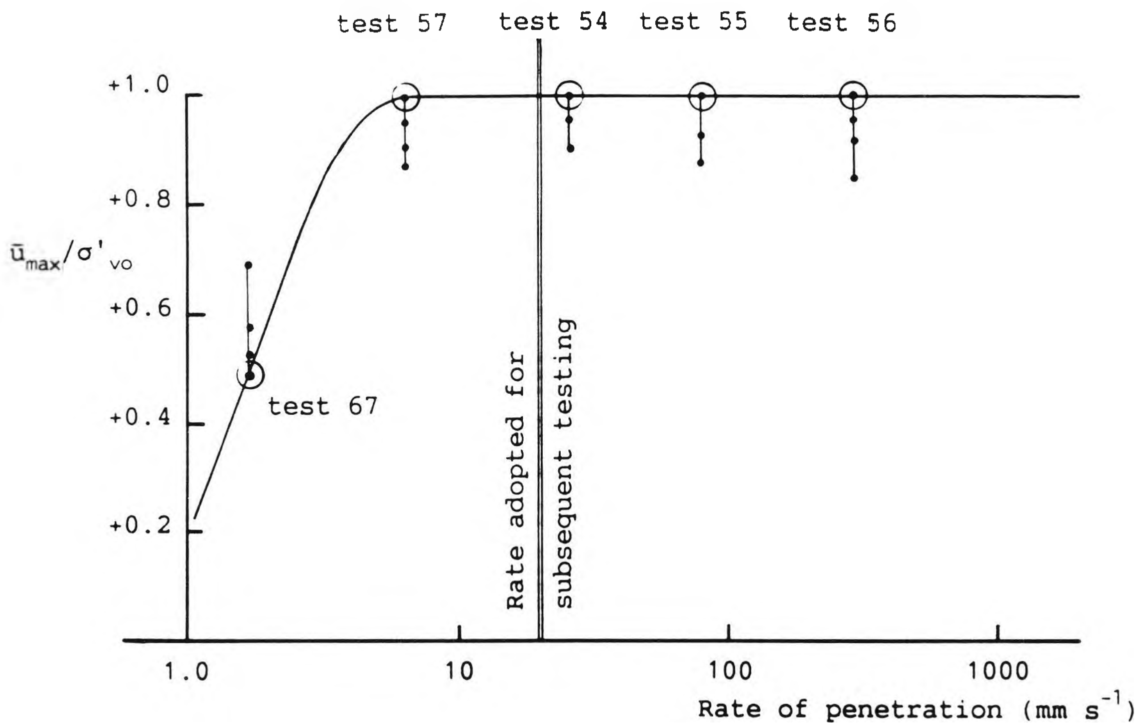

Figure 7.29 Excess pore pressure - rate of penetration for 60° cone driven into very loose soil beds

Note 1 ⊙ denotes transducer closest to instrument

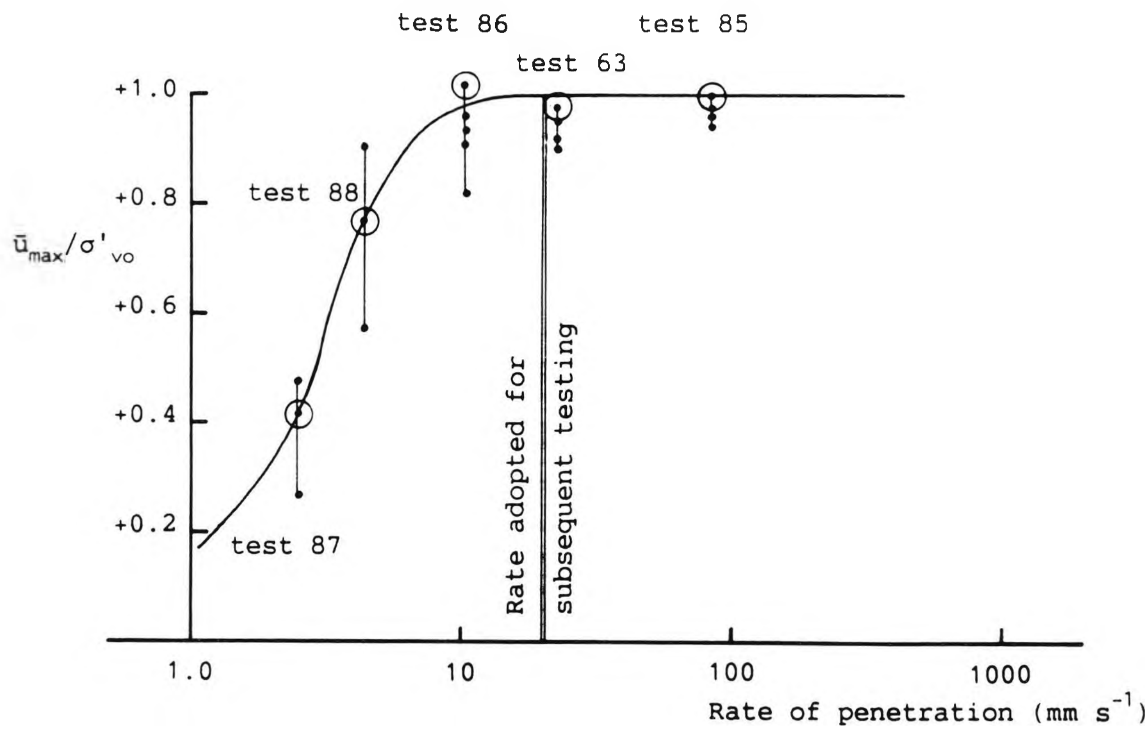

Figure 7.30 Excess pore pressure - rate of penetration for 60° cone driven into medium dense soil beds

Note 1 ⊙ denotes transducer closest to instrument

2 Partial cone penetration achieved in tests 87 and 88

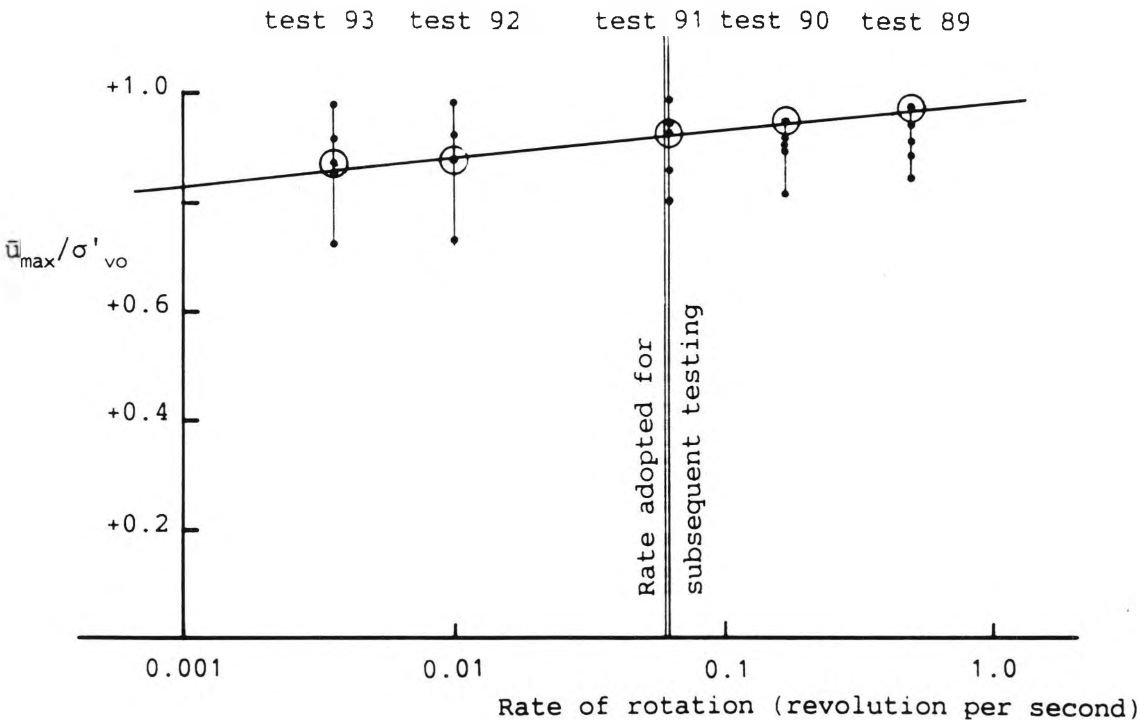

Figure 7.31 Excess pore pressure - rate of rotation for 1:1 ratio vane in very loose soil beds

Note 1 ⊙ denotes transducer closest to instrument

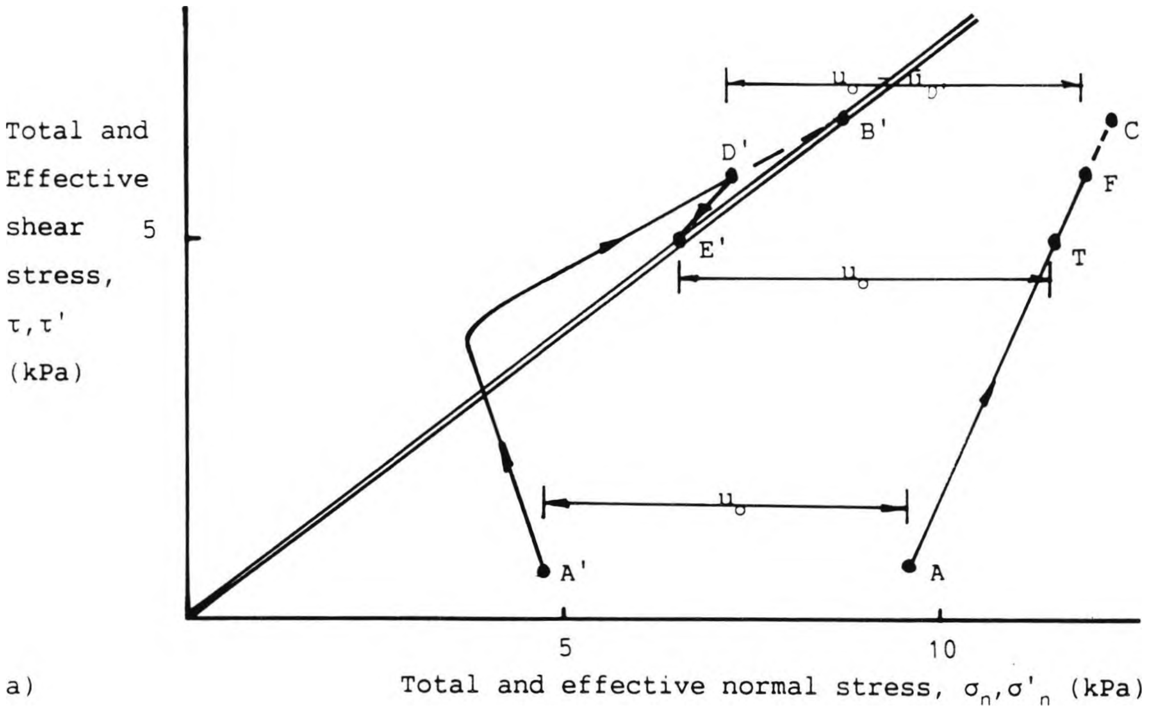

a)

A'D'E' denotes partially drained effective stress path

A'D'B' denotes undrained effective stress path

AFC denotes undrained total stress path

AFT denotes partially drained total stress path

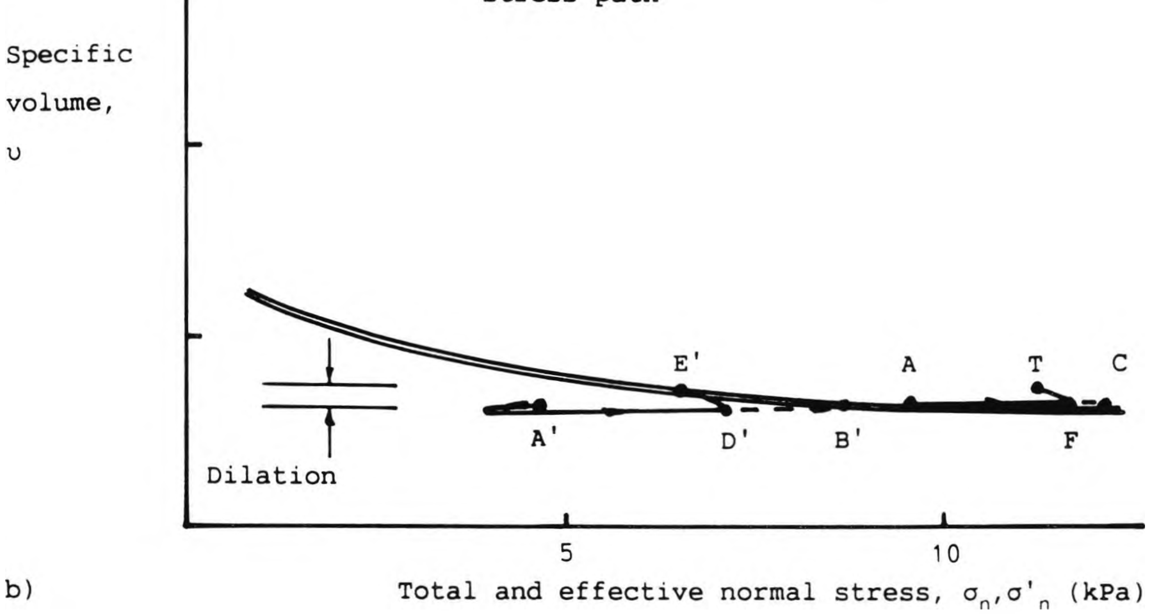

b)

Figure 7.32 Assumed locally drained stress paths for a cone loading soil initially dry of critical

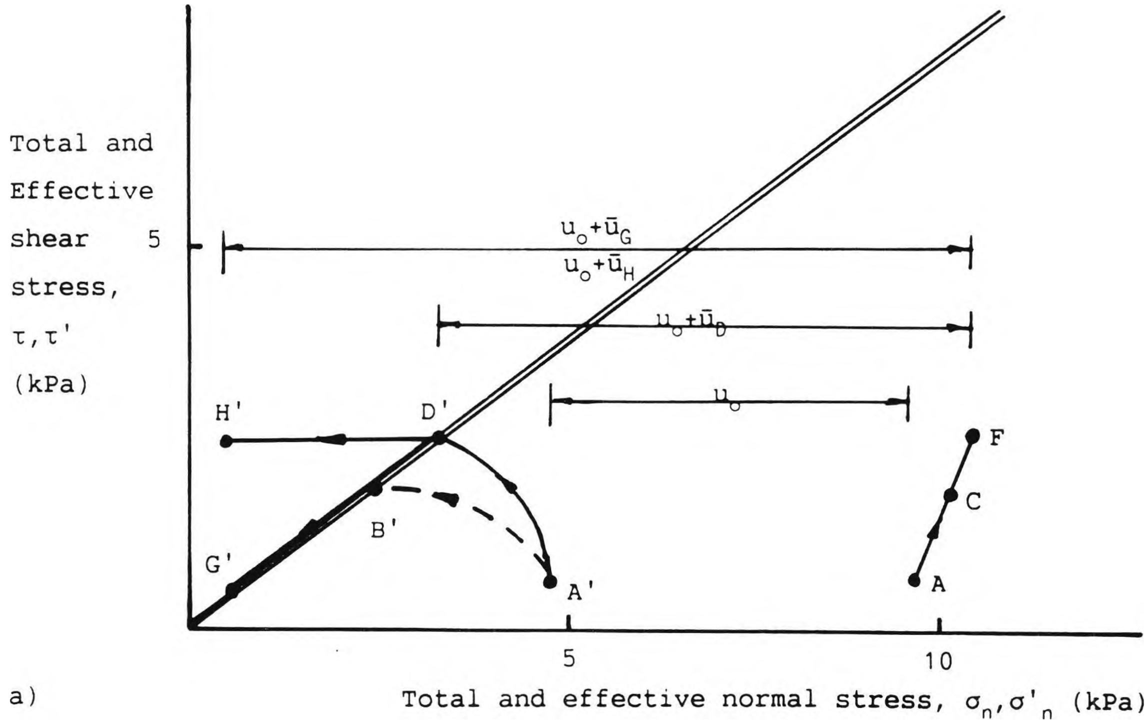

a) Total and effective normal stress, σ_n, σ'_n (kPa)

A'D'G' and A'D'H' denote partially drained effective stress paths

A'B' denotes undrained effective stress path

AF denotes partially drained total stress path

AC denotes undrained total stress path

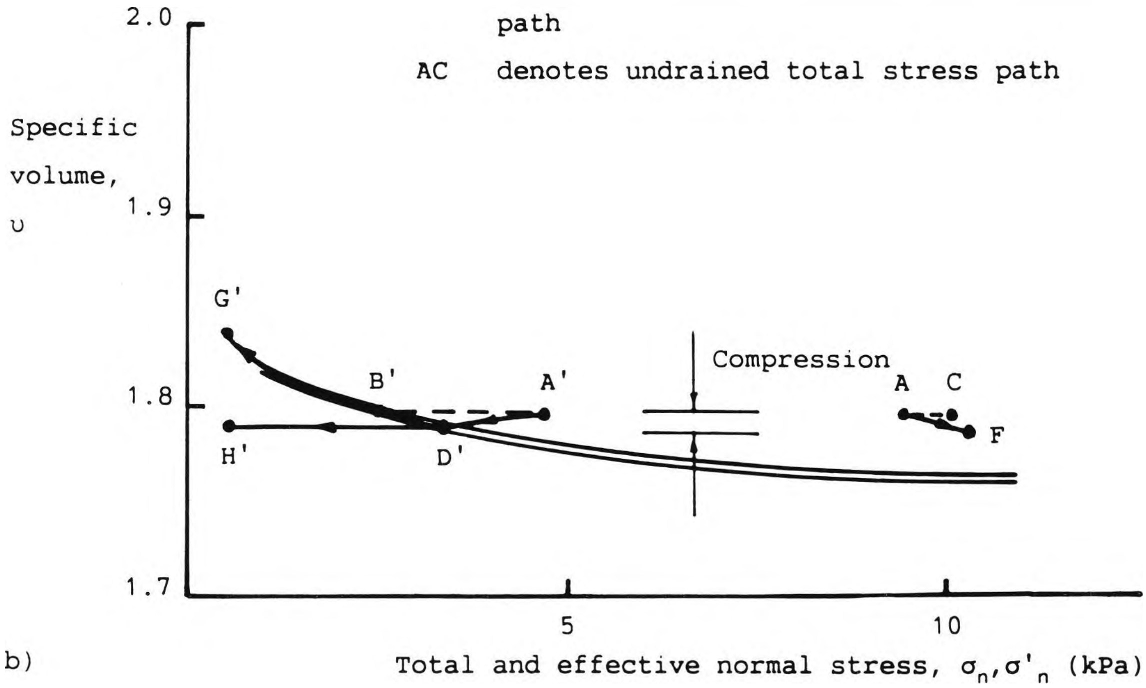

b) Total and effective normal stress, σ_n, σ'_n (kPa)

Figure 7.33 Assumed locally drained stress paths for a cone loading soil initially wet of critical

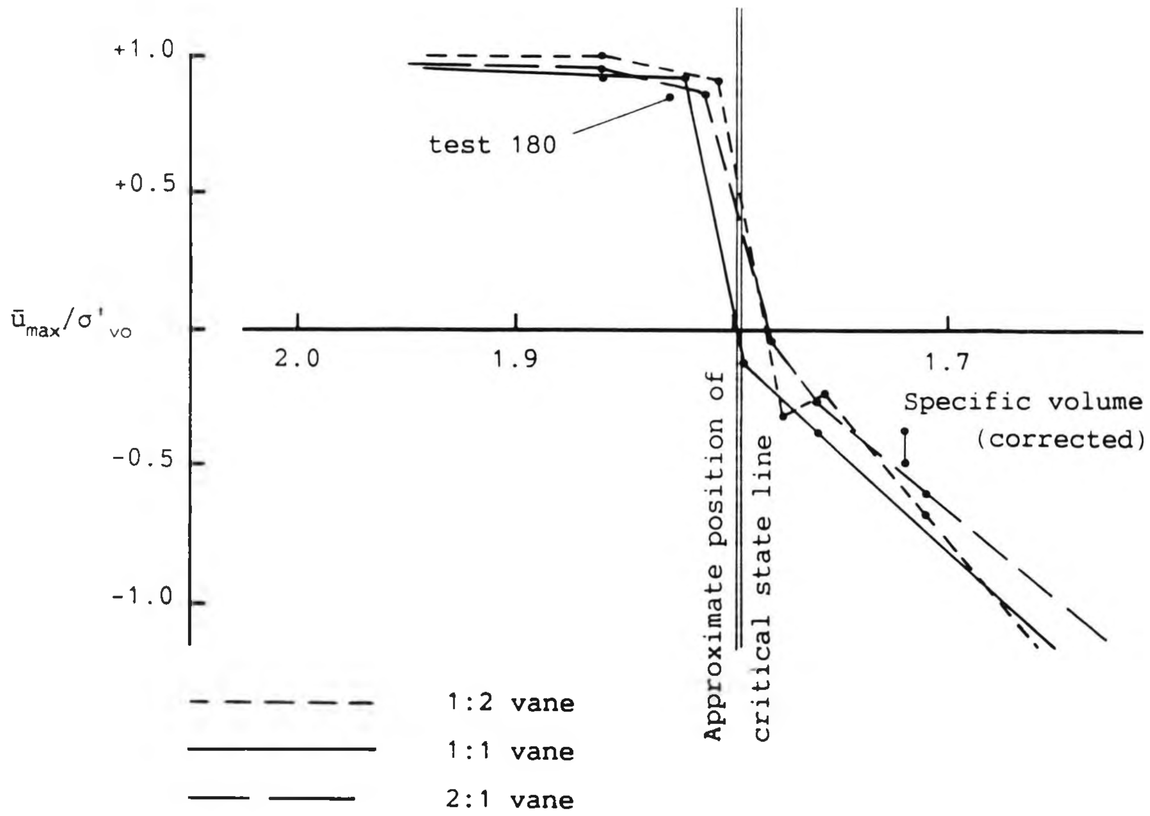

Figure 7.34 Excess pore pressure - specific volume for various vane geometries

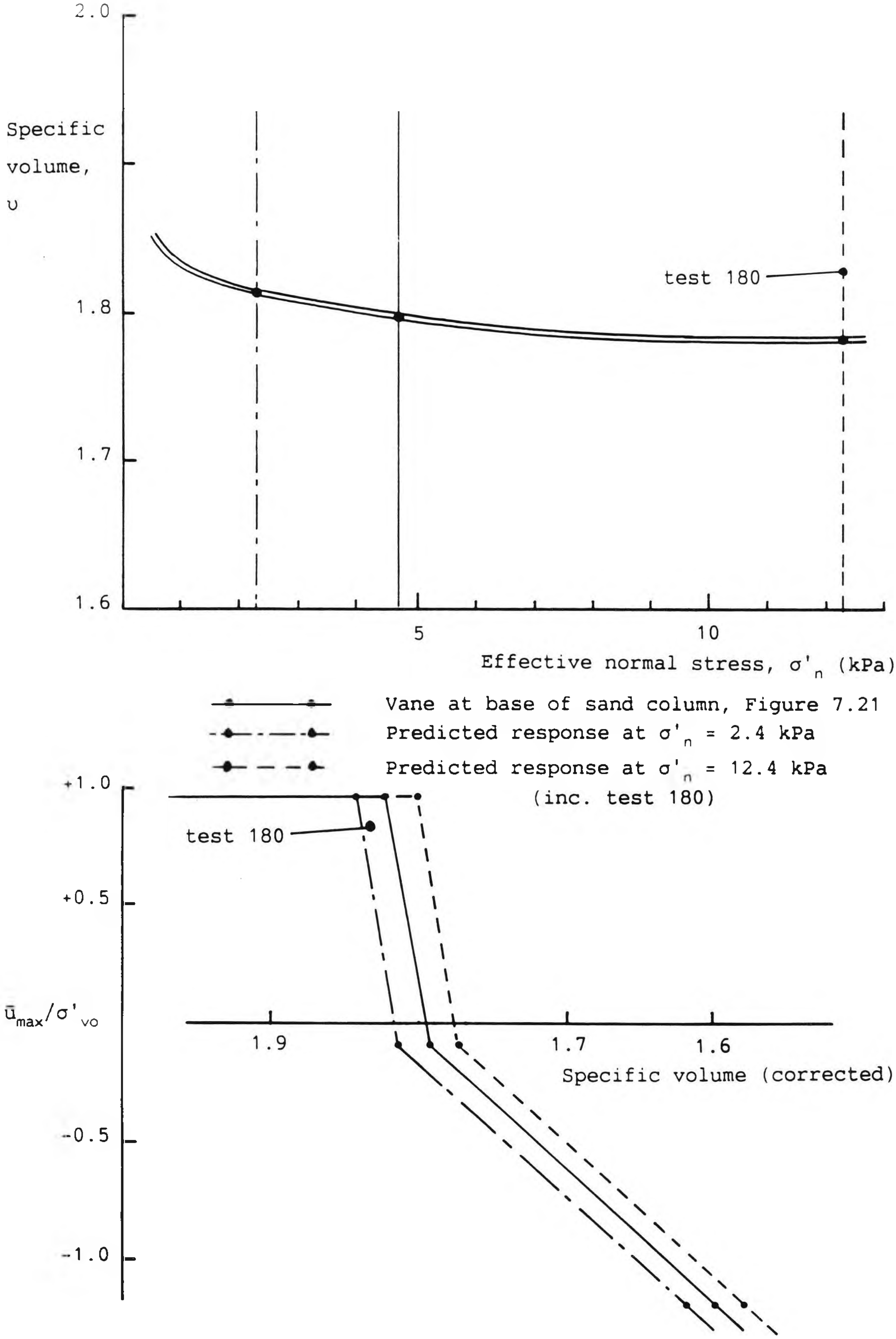

Figure 7.35 Predicted effect of stress level upon excess pore pressures recorded in vane tests

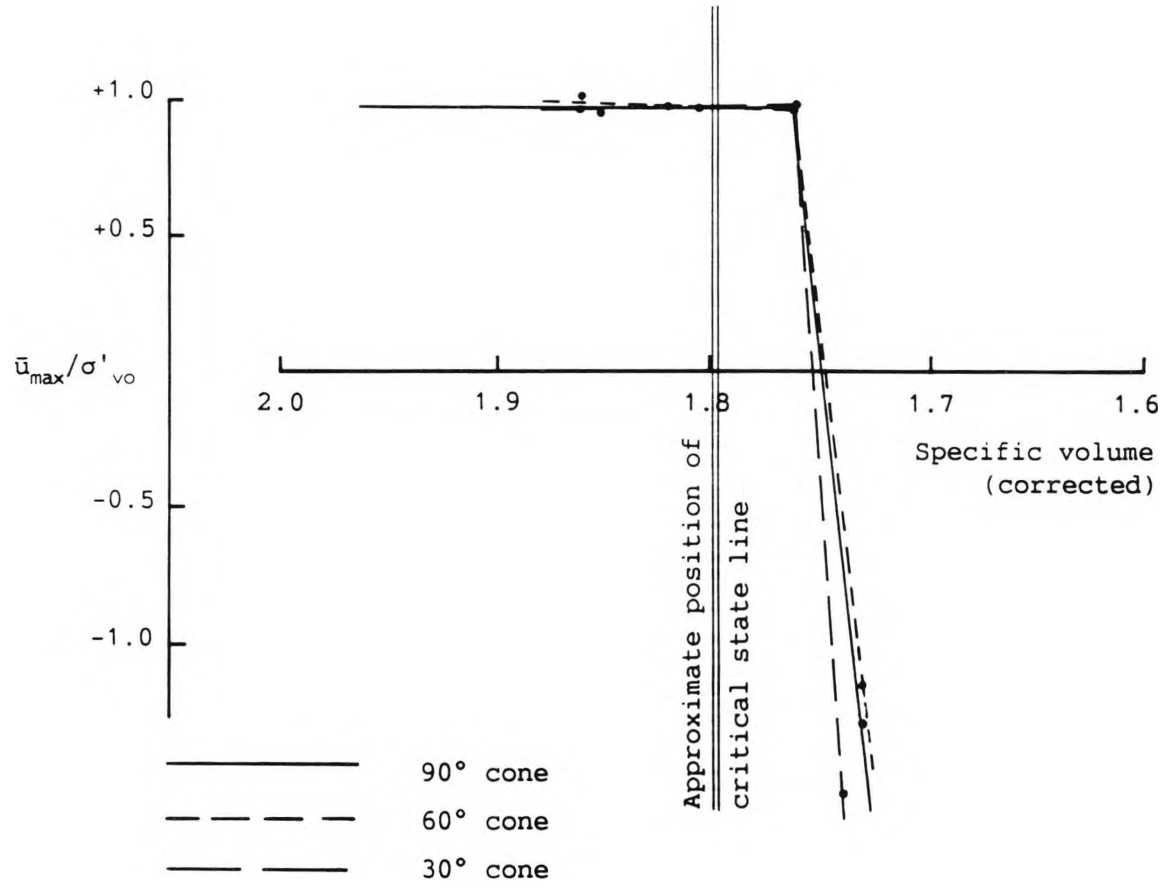

Figure 7.36 Excess pore pressure - specific volume for various cone geometries

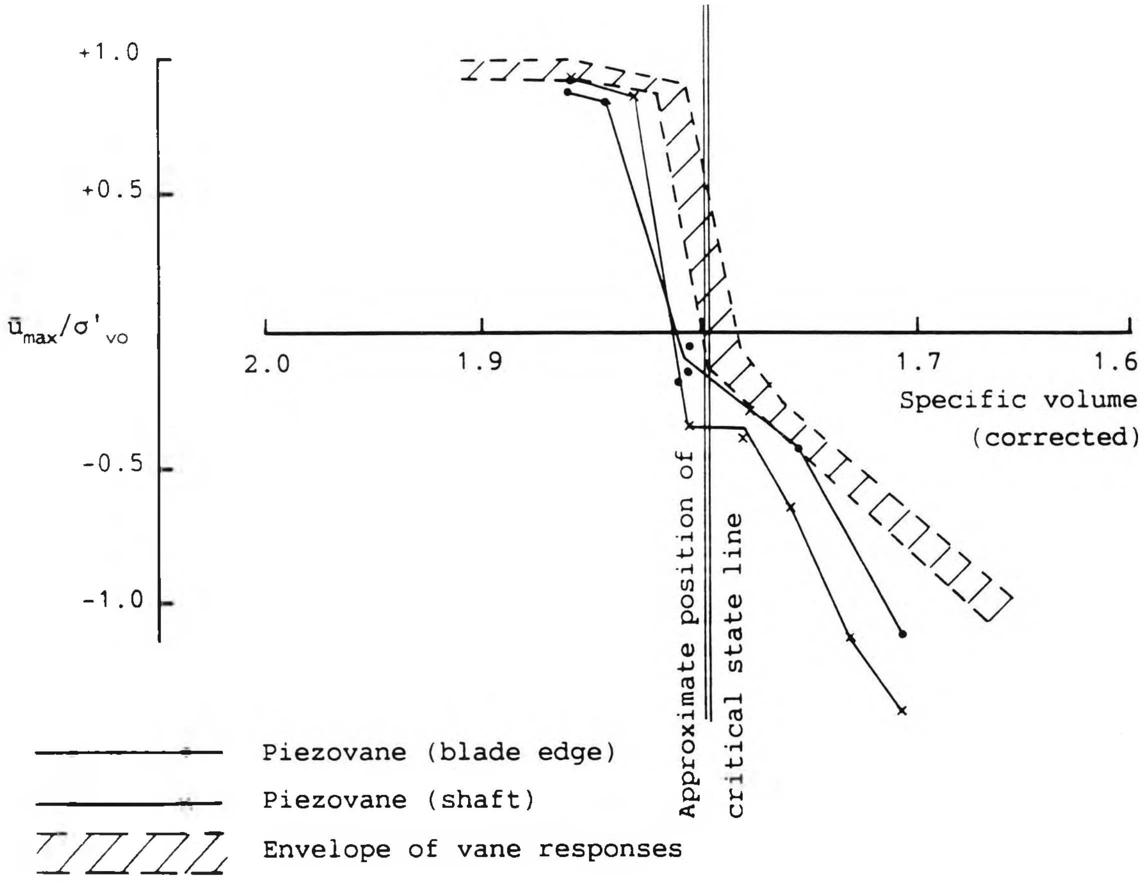

Figure 7.37 Excess pore pressure - specific volume for 1:1 ratio piezovane

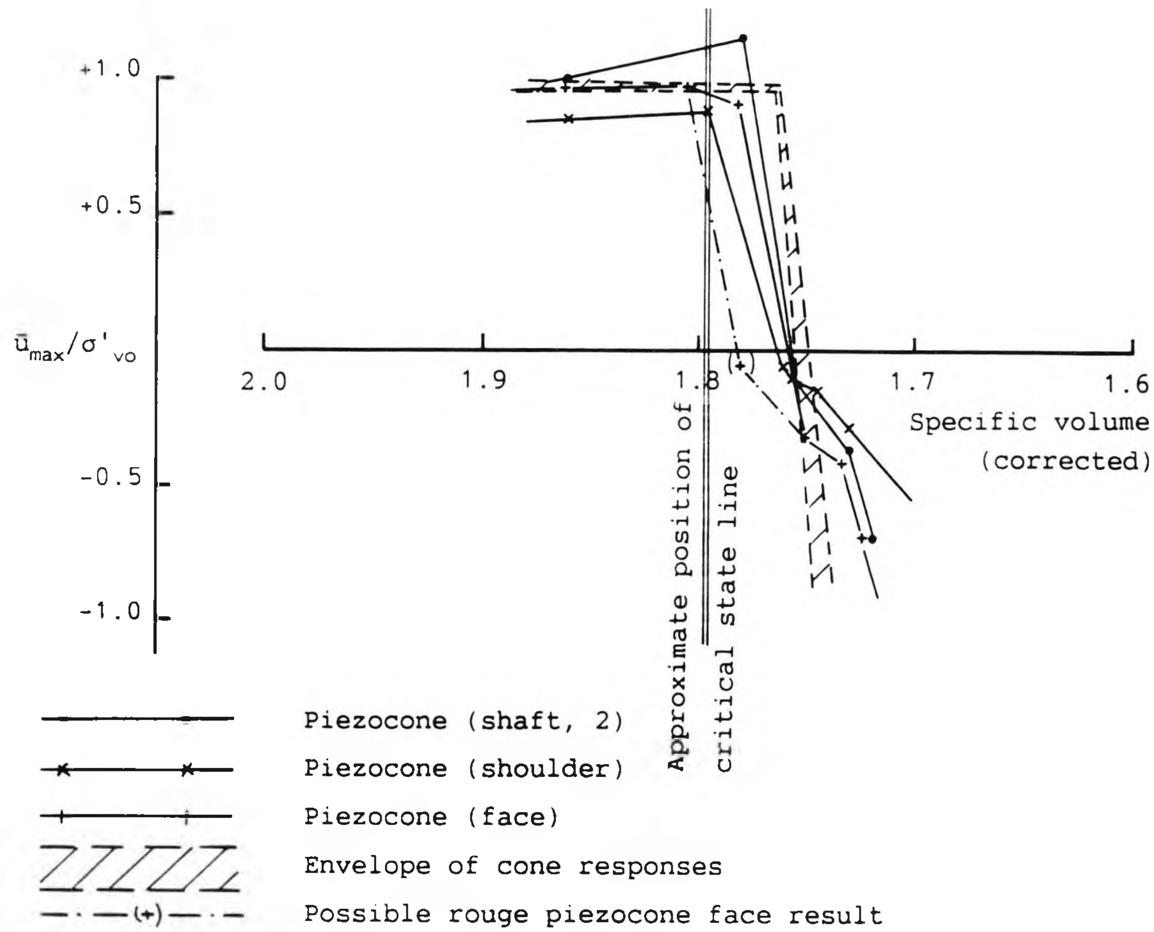

Figure 7.38 Excess pore pressure - specific volume for 60° piezocone

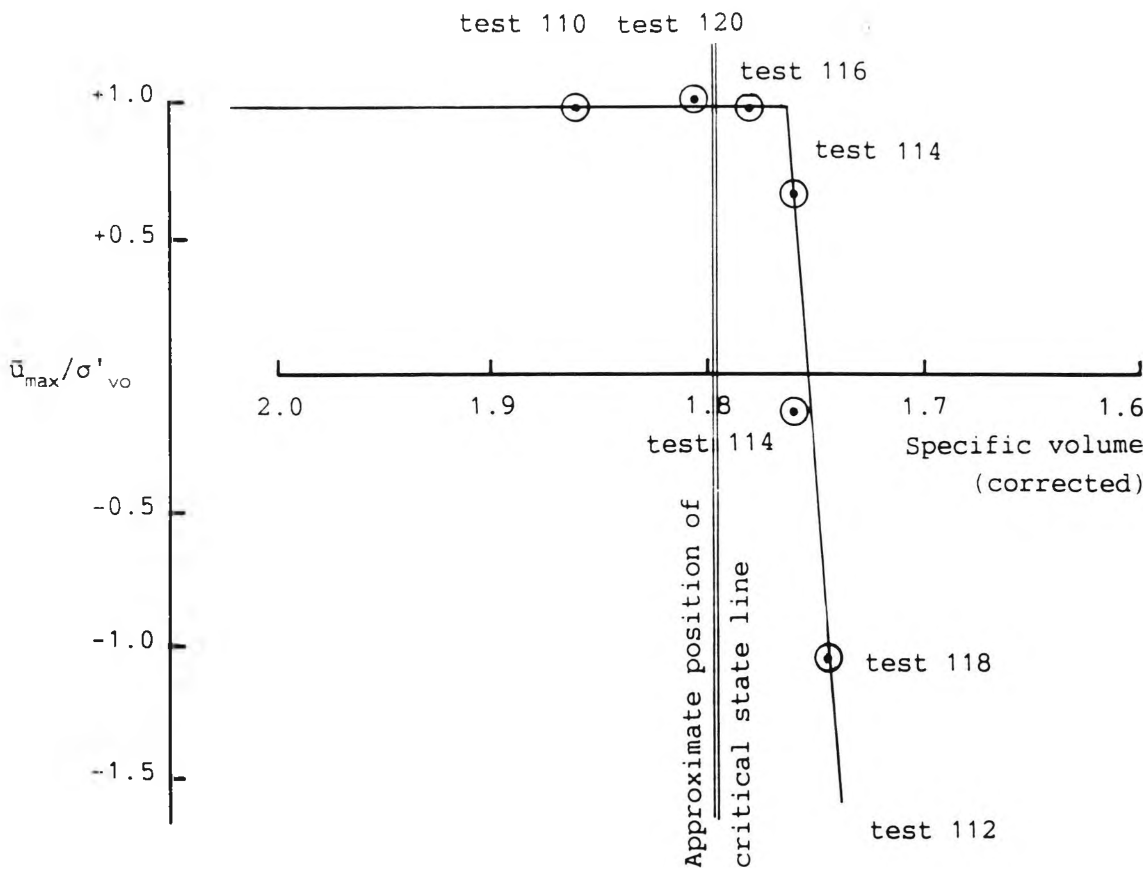

Figure 7.39 Excess pore pressure - specific volume for 1:1 ratio vane driven into soil beds at approximately 20mm s^{-1}

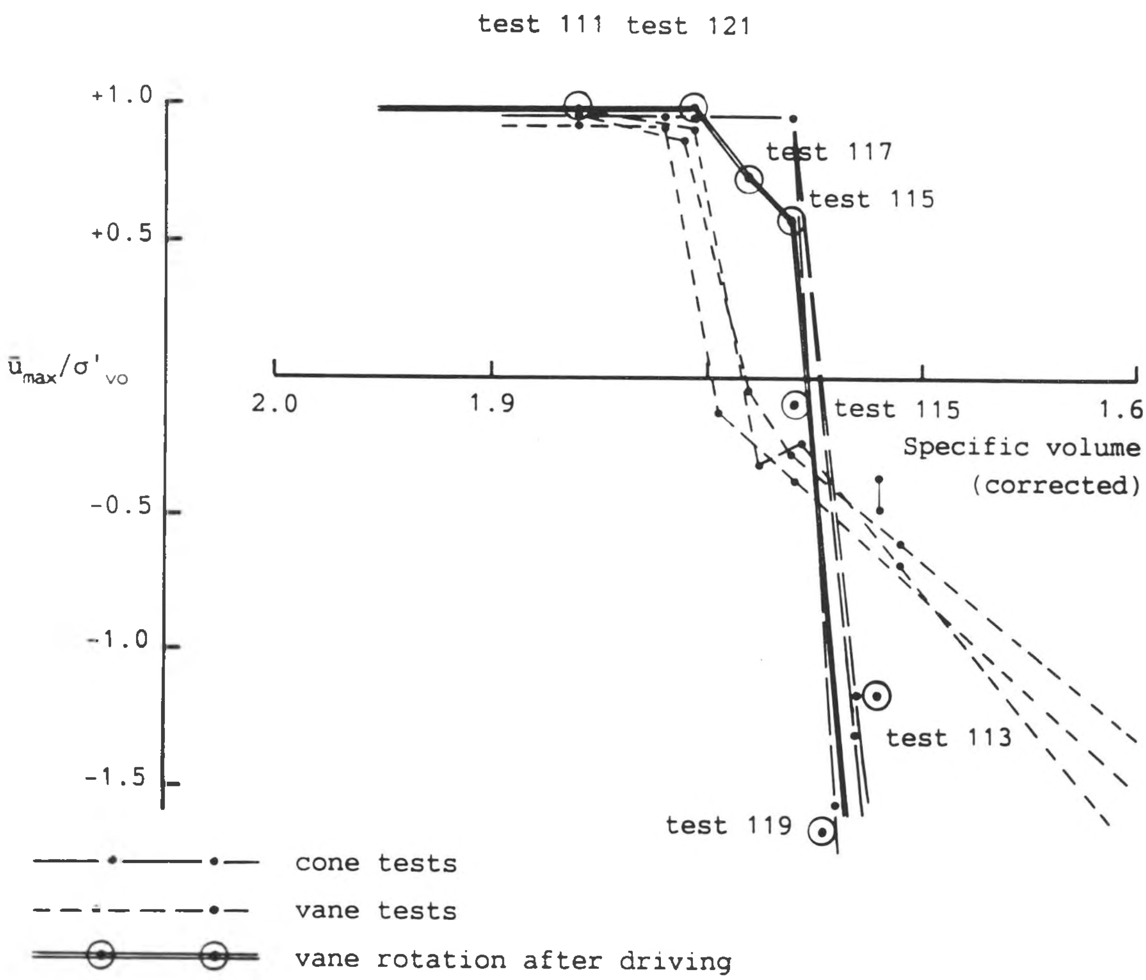

Figure 7.40 Excess pore pressure - specific volume for 1:1 ratio vane rotated in a soil bed after installation by driving

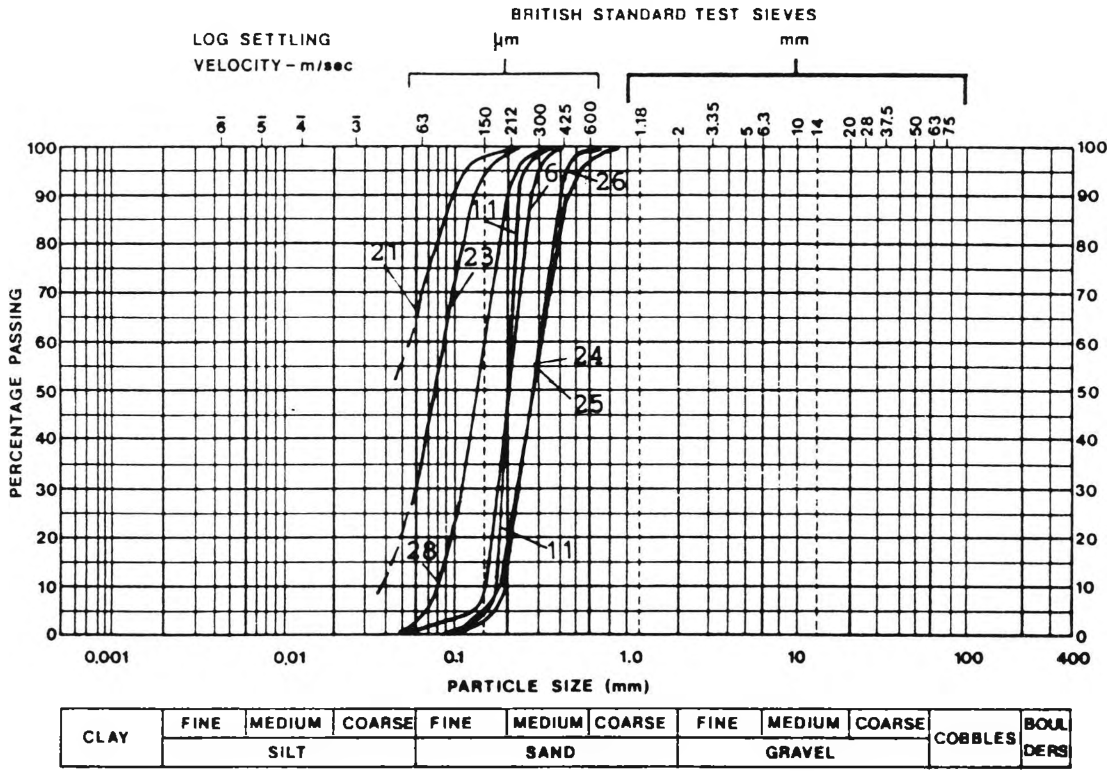

Soil 6	Folkestone harbour sand
Soil 11	Camber Sands windblown sand
Soil 21	Pegwell Bay sandy silt
Soil 23	British Industrial Sand, grade HH
Soil 24	British Industrial Sand, grade T
Soil 25	British Industrial Sand, grade 50
Soil 26	British Industrial Sand, grade 65
Soil 28	British Industrial Sand, grade 110(H)

Figure A.1 Particle size distribution plots of soils tested in the direct shear apparatus

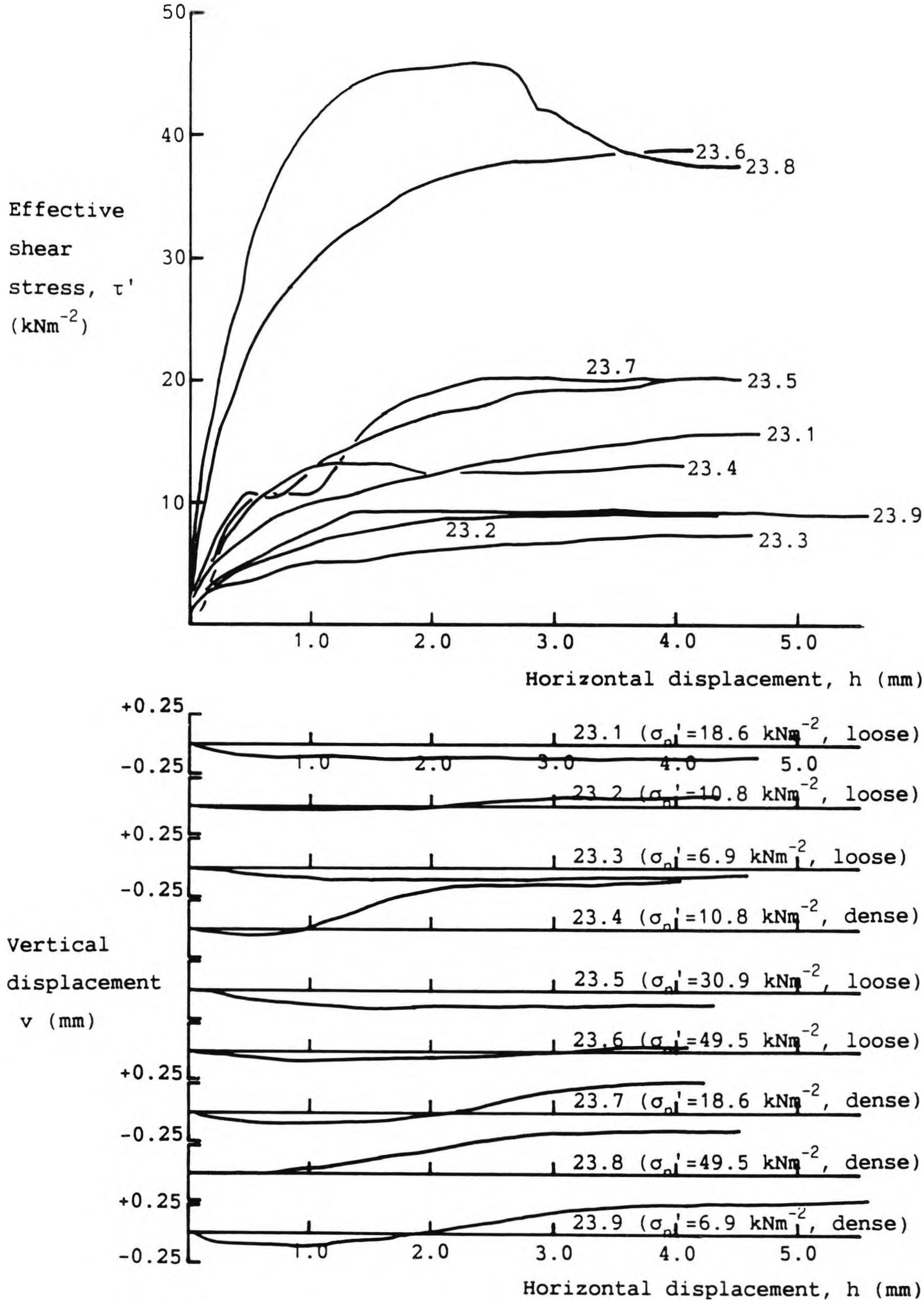

Figure A.2 Direct shear tests with soil 23

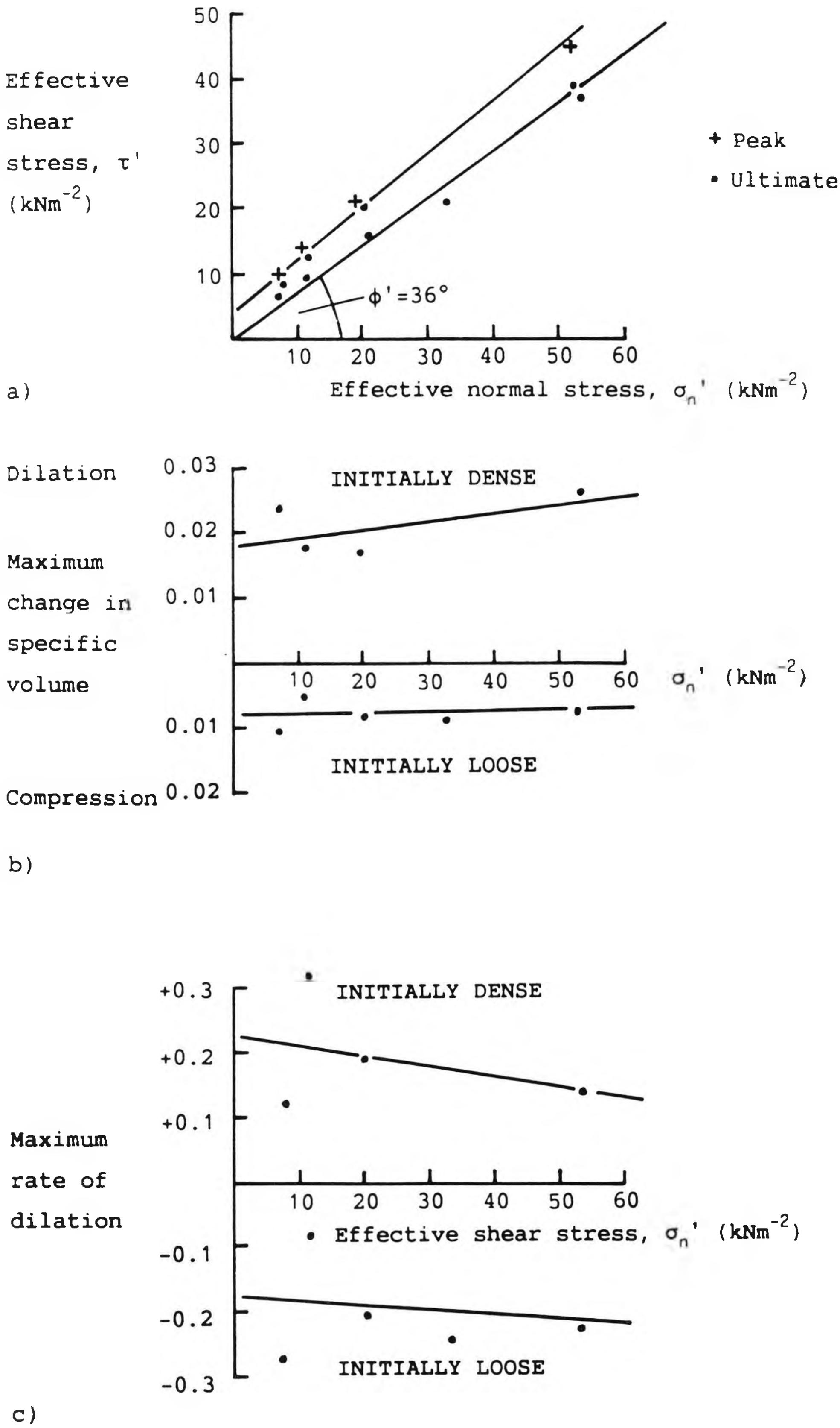

Figure A.3 Summary of direct shear test data, soil 23

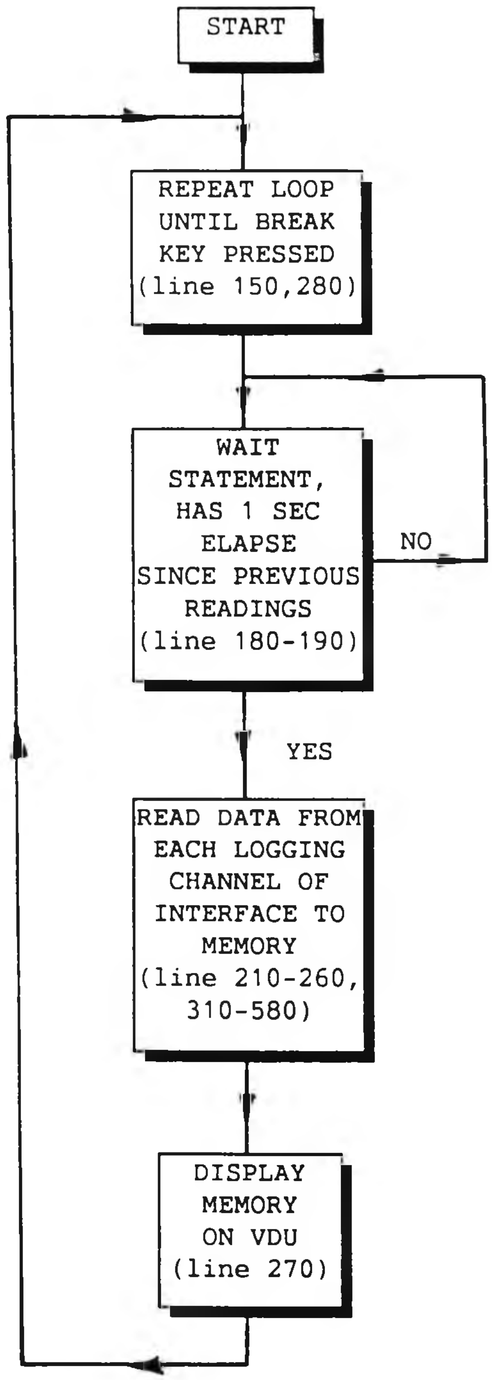

Figure B.1 Flow chart of continuous logging programs CONLOG and PEN1

```
 10 REM*******************************
 20 REM*                             *
 30 REM* CONLOG : CONtinues LOGging  *
 40 REM*           program           *
 50 REM*                             *
 60 REM* Commissioned : 15.7.85      *
 70 REM*      By : C.A.Jessett       *
 80 REM*                             *
 90 REM*******************************
100 PROCinit
110 @%=&20006
120 DIM U(1,5)
130 ET=-1
140 REM**********CONTINUES*LOOP******
150 REPEAT
160 REM**********TIME*INTERVAL*******
170 TO=TIME
180 IF (TIME-TO)/100>(ET+1) GOTO 210
190 GOTO 180
200 REM**********READING*SEQUENCE****
210 U(1,0)=FNread_trans(1)
220 U(1,1)=FNread_trans(3)
230 U(1,2)=FNread_trans(4)
240 U(1,3)=FNread_trans(5)
250 U(1,4)=FNread_trans(6)
260 U(1,5)=FNread_trans(7)
270 PRINT U(1,0),U(1,1),U(1,2),U(1,3),U(1,4),U(1,5)
280 UNTIL FALSE
290 END
300 REM****DEFINE*READING*PROCEDURE**
310 DEFFNread_trans(channel%)
320 LOCALdelay%
330 *FX15,0
340 ?PB=(MUX+channel%+8)
350 ?PC=1:PC=3:?PC=1
360 ?PB=ADI
370 ?PC=1:?PC=3:?PC=1
380 ?PB=(ADI+1)
390 ?PC=1:?PC=3:?PC=1
400 FORdelay%=1 TO 700 : NEXT
410 ?PB=(ADI+2)
420 ?PC=1:?PC=3:?PC=1
430 LSB=?PA
440 ?PB=(ADI+4)
450 ?PC=1:?PC=3:?PC=1
460 MSB=?PA
470 RES=LSB+(MSB AND 15)*256
480 IF(MSB AND 32)=32 THEN RES=RES*-1
490 =RES
500 DEFPROCinit
510 PA=&FC00
520 PB=PA+1
530 PC=PB+1
540 CR=PC+1
550 ?CR=144
560 ADI=112
570 MUX=160
580 ENDPROC
```

Figure B.2 Program listing of CONLOG

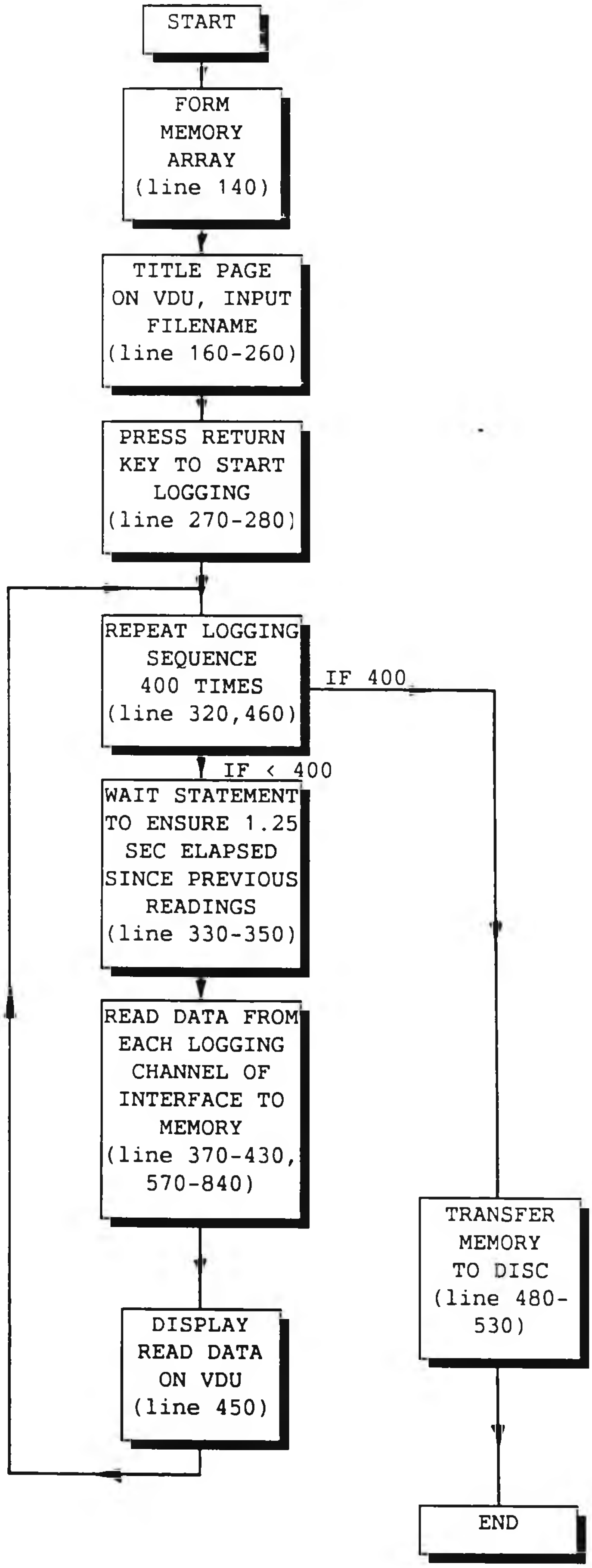

Figure B.3 Flow chart of test logging programs UDISL05 and PEN2

```
10 REM********************************
20 REM* UDISLO5 : excess pore        *
30 REM*           pressure (U)       *
40 REM*           DISsipation        *
50 REM*           LOgging program    *
60 REM*           5 channels         *
70 REM*                              *
80 REM* Commissioned : 1.7.85        *
90 REM*       By : C.A.Jessett       *
100 REM*                             *
110 REM*******************************
120 PROCinit
130 @%=&20006
140 DIM U(401,6)
150 REM*********TITLE*PAGE***********
160 CLS:PRINT:PRINT
170 PRINT"                WELCOME TO"
180 PRINT:PRINT
190 PRINT CHR$(141);CHR$(136);"                UDISLO5"
200 PRINT CHR$(141);CHR$(136);"                UDISLO5"
210 PRINT:PRINT:PRINT
220 PRINT"      The excess pore pressure (U)
                DISsipation LOgging program"
230 PRINT:PRINT:PRINT:PRINT
240 INPUT"   Please supply name of data file for
            logging and press RETURN key
                                        "F$
250 PRINT:PRINT"                         THANK YOU"
260 X = OPENOUT(F$)
270 PRINT:INPUT"Press RETURN key to commence logging"
                START
280 CLS
290 REM**********LOGGING*LOOP********
300 REM**********TIME*INTERVAL*******
310 T0=TIME
320 FOR I=1 TO 401
330 ET=(TIME-T0)/100
340 IF ET>(I-1.008)*1.25 THEN 370
350 GOTO 330
360 REM*********LOGGING*SEQUENCE******
370 U(I,0)=ET              :REM ELAPSE TIME
380 U(I,1)=FNread_trans(1):REM Ch1/SUPPLY VOLTAGE
390 U(I,2)=FNread_trans(3):REM Ch3/T2756
400 U(I,3)=FNread_trans(4):REM Ch4/T2757
410 U(I,4)=FNread_trans(5):REM Ch5/T2930
420 U(I,5)=FNread_trans(6):REM Ch6/T2941
430 U(I,6)=FNread_trans(7):REM Ch7/T2943
440 REM***DISPLAY*DATA*ON*SCREEN*****
450 PRINT U(I,0);" "U(I,1);" "U(I,2);" "U(I,3);" "
          U(I,4);" "U(I,5);" "U(I,6)
460 NEXT I
470 REM*********SAVE*DATA*ON*DISC*****
480 FOR I=1 TO 401
490 FOR J=0 TO 6
500 PRINT£X,U(I,J)
510 NEXT J
520 NEXT I
530 CLOSE£0
540 CLS
550 END
560 REM****DEFINE*READING*PROCEDURE**
570 DEFFNread_trans(channel%)
580 LOCALdelay%
590 *FX15,0
600 ?PB=(MUX+channel%+8)
610 ?PC=1:?PC=3:?PC=1
620 ?PB=ADI
630 ?PC=1:?PC=3:?PC=1
640 ?PB=(ADI+1)
650 ?PC=1:?PC=3:?PC=1
660 FORdelay%=1 TO 700 : NEXT
670 ?PB=(ADI+2)
680 ?PC=1:?PC=3:?PC=1
690 LSB=?PA
700 ?PB=(ADI+4)
710 ?PC=1:?PC=3:?PC=1
720 MSB=?PA
730 RES=LSB+(MSB AND 15)*256
740 IF(MSB AND 32)=32 THEN RES=RES*-1
750 =RES
760 DEFPROCinit
770 PA=&FC00
780 PB=PA+1
790 PC=PB+1
800 CR=PC+1
810 ?CR=144
820 ADI=112
830 MUX=160
840 ENDPROC
```

Figure B.4 Program listing of UDISLO5

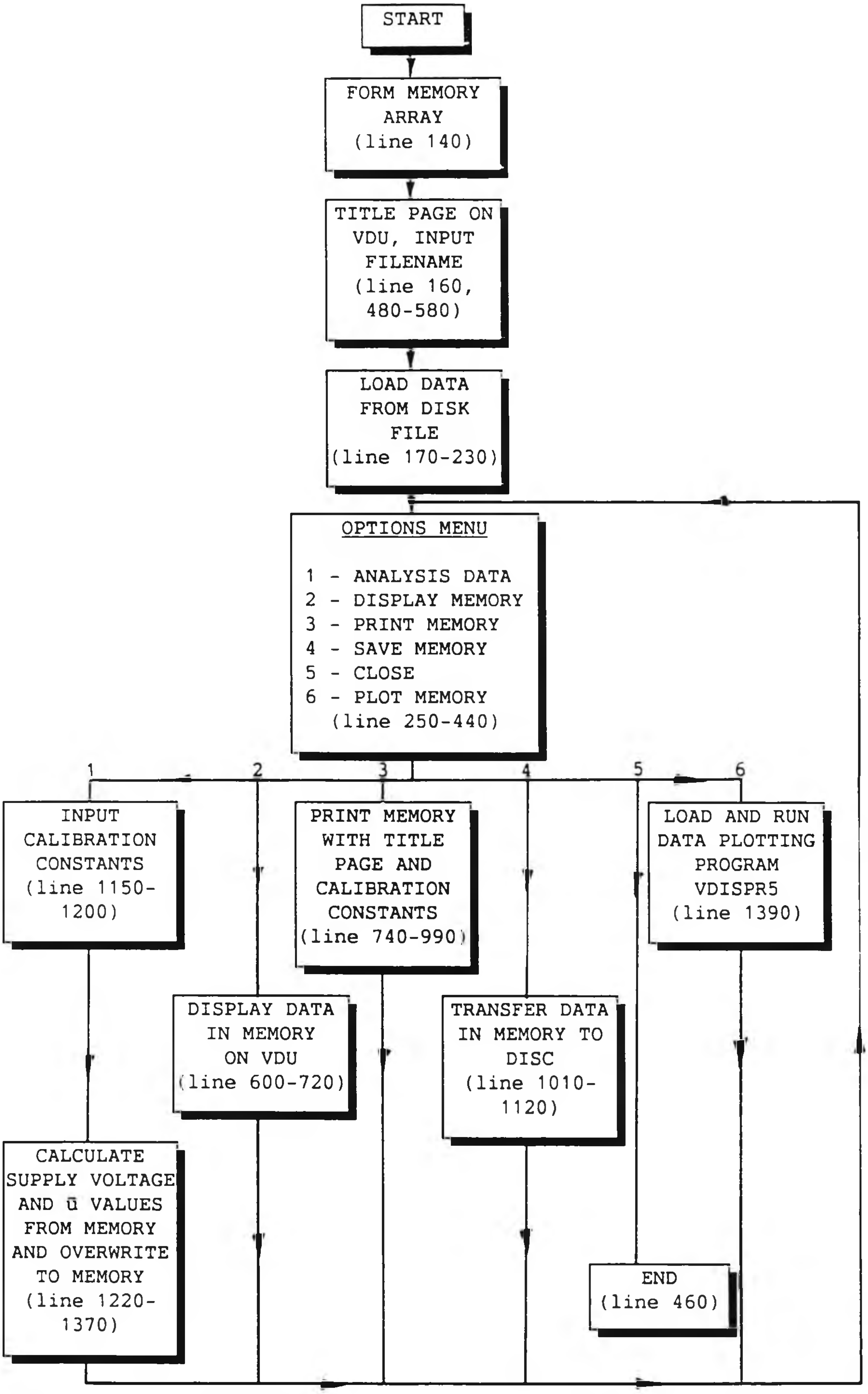

Figure B.5 Flow chart of test data analysis programs PEN3.1 and UDISAN5

```
 10 REM********************************
 20 REM*                              *
 30 REM* UDISAN5 : excess pore        *
 40 REM*           pressure (U)       *
 50 REM*           DISsipation        *
 60 REM*           ANalysis prog.     *
 70 REM*           5 channels         *
 80 REM*                              *
 90 REM* Commissioned : 15.7.85       *
100 REM*       By : C.A.Jessett       *
110 REM*                              *
120 REM********************************
130 CLS
140 DIM U(401,6)
150 REM*****LOAD*DATA*FILE***********
160 GOSUB 470
170 X=OPENIN F$
180 FOR I=1 TO 401
190 FOR J=0 TO 6
200 INPUT£X,U(I,J)
210 NEXT J
220 NEXT I
230 CLOSE£0
240 REM**********OPTIONS*MENU*********
250 CLS
260 PRINT"                OPTIONS"
270 PRINT
280 PRINT
290 PRINT"      Analyse test data      ...(1)"
300 PRINT"      Display data on screen...(2)"
310 PRINT"      Print data             ...(3)"
320 PRINT"      Save data on disc      ...(4)"
330 PRINT"      Close program          ...(5)"
340 PRINT"      Plot data              ...(6)"
350 PRINT"         (final option)          "
360 PRINT
370 INPUT"Select option and press RETURN key       "OP
380 IF OP=1 THEN GOSUB 1130
390 IF OP=2 THEN GOSUB 590
400 IF OP=3 THEN GOSUB 730
410 IF OP=4 THEN GOSUB 1000
420 IF OP=5 THEN GOTO 450
430 IF OP=6 THEN GOSUB 1380
440 GOTO 240
450 CLS
460 END
```

```
470 REM**********TITLE*PAGE***********
480 PRINT:PRINT:PRINT
490 PRINT"              WELCOME TO"
500 PRINT:PRINT
510 PRINT CHR$(141);CHR$(136);"              UDISAN5"
520 PRINT CHR$(141);CHR$(136);"              UDISAN5"
530 PRINT:PRINT:PRINT
540 PRINT"      The excess pore pressure (U)
            DISsipation ANalysis program"
550 PRINT:PRINT:PRINT:PRINT
560 INPUT"   Please supply name of data file for
          analysis and press RETURN key
                                   "F$
570 PRINT:PRINT"                          THANK YOU"
580 RETURN
590 REM*****DISPLAY*DATA*ON*SCREEN***
600 CLS
610 @X=&20105
620 FOR L=1 TO 401 STEP 18
630 PRINT" TIME  S.V  T56  T57  T30  T41  T43"
640 PRINT"  sec volts KPa  KPa  KPa  KPa  KPa":PRINT:PRINT
650 FOR I=L TO L+17
660 IF I=401 GOTO 690
670 PRINT U(I,0),U(I,1),U(I,2),U(I,3),U(I,4),U(I,5),U(I,6)
680 NEXT I
690 PRINT
700 INPUT"Press RETURN to continue data presentation"C$
710 CLS : NEXT L
720 RETURN
```

Figure B.6 Program listing of UDISAN5, line 10 to 720

```
730 REM********PRINT*DATA************
740 CLS
750 @%=&2030A
760 VDU2
770 PRINT"GEOTECHNICAL ENGINEERING RESEARCH CENTRE":PRINT
780 PRINT"           THE CITY UNIVERSITY":PRINT
790 PRINT"  _"
800 PRINT"  U DISSIPATION IN SAND COLUMN,"F$:PRINT:PRINT:PRINT
810 PRINT"  CALIBRATION CONSTANTS USED"
820 PRINT
830 PRINT"           Supply voltage       "SV
840 PRINT"           Transducer 2756      "T56
850 PRINT"           Transducer 2757      "T57
860 PRINT"           Transducer 2930      "T30
870 PRINT"           Transducer 2941      "T41
880 PRINT"           Transducer 2943      "T43
890 PRINT
900 PRINT"  ELAPSE  SUPPLY   T2756   T2757   T2930   T2941   T2943"
910 PRINT"   TIME   VOLTAGE "
920 PRINT"  (sec)   (volts)  (KPa)   (KPa)   (KPa)   (KPa)   (KPa)"
930 PRINT
940 PRINT
950 FOR I=1 TO 401
960 PRINT U(I,0),U(I,1),U(I,2),U(I,3),U(I,4),U(I,5),U(I,6)
970 NEXT I
980 VDU3
990 RETURN
```

```
1000 REM*****SAVE*DATA*ON*DISC********
1010 CLS
1020 PRINT"    TRANSFERING DATA TO DISC"
1030 PRINT
1040 INPUT"Please supply file name    "A$
1050 X=OPENOUT(A$)
1060 FOR I=1 TO 401
1070 FOR J=0 TO 6
1080 PRINT£X,U(I,J)
1090 NEXT J
1100 NEXT I
1110 CLOSE£0
1120 RETURN
1130 REM CALCULATION OF SUPPLY VOLTAGE AND EXCESS PORE PRESSURES
1140 REM   INPUT CALIBRATION CONSTANTS
1150 INPUT"Input: supply voltage calibration (units/volt)        "SV
1160 INPUT"       calibration constant for transducer 2756      "T56
1170 INPUT"       calibration constant for transducer 2757      "T57
1180 INPUT"       calibration constant for transducer 2930      "T30
1190 INPUT"       calibration constant for transducer 2941      "T41
1200 INPUT"       calibration constant for transducer 2943      "T43
1210 REM RETAIN INITIAL TRANS READINGS
1220 IT56=U(1,2)
1230 IT57=U(1,3)
1240 IT30=U(1,4)
1250 IT41=U(1,5)
1260 IT43=U(1,6)
1270 FOR I=1 TO 401
1280 REM*******SUPPLY*VOLTAGE*********
1290 U(I,1)=(U(I,1)/SV)
1300 REM******EXCESS*PORE*PRESSURES***
1310 U(I,2)=(U(I,2)-IT56)/(U(I,1)*T56)
1320 U(I,3)=(U(I,3)-IT57)/(U(I,1)*T57)
1330 U(I,4)=(U(I,4)-IT30)/(U(I,1)*T30)
1340 U(I,5)=(U(I,5)-IT41)/(U(I,1)*T41)
1350 U(I,6)=(U(I,6)-IT43)/(U(I,1)*T43)
1360 NEXT I
1370 RETURN
1380 REM*********GRAPHIC*PLOTTING******
1390 CHAIN"UDISPL5"
```

Figure B.7 Program listing of UDISAN5, line 730 to 1390

GEOTECHNICAL ENGINEERING RESEARCH CENTRE

THE CITY UNIVERSITY

U DISSIPATION IN SAND COLUMN.TEST173

CALIBRATION CONSTANTS USED

Supply voltage	416.000
Transducer 2756	6.136
Transducer	3.655
Transducer 2930	5.327
Transducer 2941	5.640
Transducer 2943	5.536
Potentiometer	1619.000
Initial tip position	0.850

ELAPSE TIME (sec)	TIP POSITION (metres)	SUPPLY VOLTAGE (volts)	T2756 (KPa)	(KPa)	T2930 (KPa)	T2941 (KPa)	T2943 (KPa)
0.010	0.850	4.882	0.000	0.000	0.000	0.000	0.000
1.420	0.850	4.880	0.000	0.000	0.000	0.000	0.000
2.810	0.850	4.880	0.000	0.000	0.000	0.000	0.000
4.210	0.850	4.882	0.000	0.000	0.000	-0.036	0.000
5.600	0.850	4.882	0.000	0.000	0.000	0.000	0.000
7.000	0.850	4.882	0.000	0.000	0.000	0.000	0.000
8.390	0.850	4.880	0.000	0.000	0.000	-0.036	0.000
9.790	0.850	4.880	0.000	0.000	0.000	0.000	0.000
11.[illegible]30	0.850	4.880	0.000	0.000	0.000	0.000	0.000
12.580	0.850	4.882	0.000	0.000	0.000	0.000	0.000
13.970	0.850	4.880	0.000	0.000	0.000	0.000	0.000
15.370	0.850	4.880	0.000	0.000	0.000	0.000	0.000
16.770	0.850	4.880	0.000	0.000	0.000	0.000	0.000
18.160	0.850	4.880	0.000	0.000	0.000	0.000	0.000
19.560	0.850	4.880	0.000	0.000	0.000	0.000	0.000
20.960	0.850	4.882	0.000	0.000	0.000	0.000	0.000
22.360	0.850	4.880	0.000	0.000	0.000	0.000	0.000
23.750	0.850	4.880	0.000	0.000	0.000	0.000	0.000
25.150	0.850	4.880	0.000	0.000	0.000	0.000	0.000
26.550	0.835	4.882	0.200	0.056	0.038	0.036	0.074
27.950	0.812	4.880	0.067	0.280	0.038	0.000	0.000
29.350	0.777	4.880	0.033	0.561	0.077	0.073	0.074
30.740	0.752	4.880	0.134	0.953	0.192	0.218	0.185
32.140	0.720	4.880	0.301	1.233	0.269	0.400	0.407
33.540	0.686	4.880	0.534	1.682	0.308	0.690	0.666
34.930	0.655	4.880	0.735	2.187	0.269	0.945	0.888
36.330	0.633	4.880	1.002	2.691	0.269	1.090	1.036
37.730	0.611	4.880	1.102	3.028	0.308	1.344	1.259
39.120	0.593	4.880	1.336	3.476	0.269	1.344	1.370
40.520	0.574	4.882	1.435	3.811	0.269	1.416	1.480

Figure B.8 Example of the output from PEN3.1.

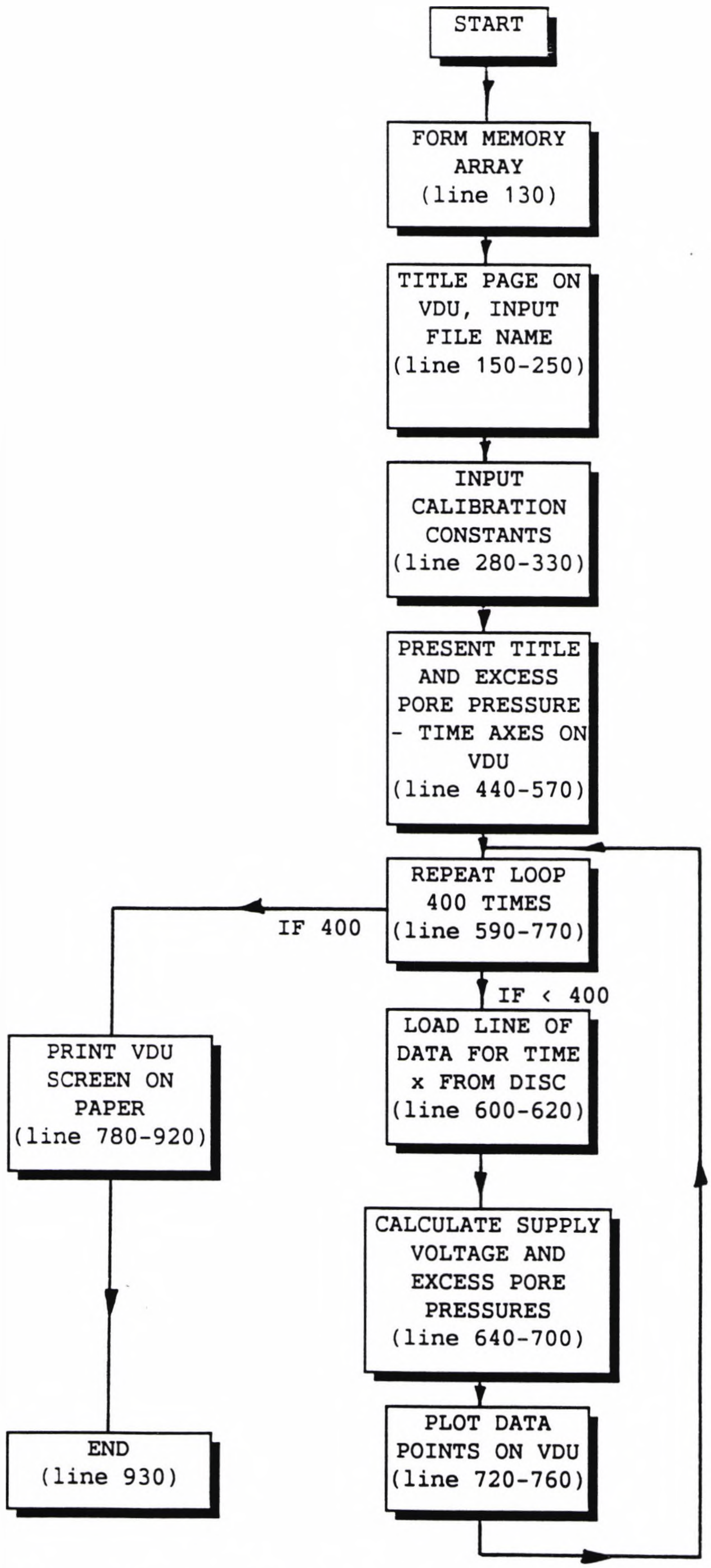

Figure B.9 Flow chart of preliminary data plotting program UDISPR5

```
 10 REM******************************
 20 REM*                            *
 30 REM* UDISPR5 : excess pore      *
 40 REM*           pressure (U)     *
 50 REM*           plotting and     *
 60 REM*           printing prog.   *
 70 REM*                            *
 80 REM* Commissioned : 8.1.86      *
 90 REM*       By : C.A.Jessett     *
100 REM*                            *
110 REM******************************
120 CLS
130 DIM U(6)
140 REM********TITLE*PAGE***********
150 PRINT:PRINT:PRINT
160 PRINT"                 WELCOME TO"
170 PRINT:PRINT
180 PRINT CHR$(141);CHR$(136);"                 UDISPR5"
190 PRINT CHR$(141);CHR$(136);"                 UDISPR5"
200 PRINT:PRINT:PRINT
210 PRINT"       The excess pore pressure (U)
               DISsipation PLotting program"
220 PRINT:PRINT:PRINT:PRINT
230 INPUT"   Please supply name of data file for
             analysis and press RETURN key
                                "F$
240 PRINT:PRINT"                                THANK YOU"
250 S=OPENIN F$
260 REM  CALCULATION OF SUPPLY VOLTAGE AND EXCESS PORE PRESSURES
270 CLS:REM INPUT CALIBRATION CONSTANTS
280 INPUT"Input: supply voltage calibration (units/volt)        "SV
290 INPUT"       calibration constant for transducer 2756       "T56
300 INPUT"       calibration constant for transducer 2757       "T57
310 INPUT"       calibration constant for transducer 2930       "T30
320 INPUT"       calibration constant for transducer 2941       "T41
330 INPUT"       calibration constant for transducer 2943       "T43
340 REM INPUT &SAVE INITIAL READINGS
350 FOR J=0 TO 6
360 INPUT£S,U(J)
370 NEXT
380 IT56=U(2)
390 IT57=U(3)
400 IT30=U(4)
410 IT41=U(5)
420 IT43=U(6)
430 REM*******GRAPHIC*PLOTTING*******
440 MODE 4
450 PLOT 4,250,850:PLOT 5,250,250:PLOT 5,1000,250
460 PLOT 69,400,245:PLOT 69,550,245: PLOT 69,700,245:PLOT 69,850,245
470 PLOT 69,245,325:PLOT 69,245,400:PLOT 69,245,475:PLOT 69,245,540:
    PLOT 69,245,615:PLOT 69,245,690:PLOT 69,245,765
480 PRINT"GEOTECHNICAL ENGINEERING RESEARCH CENTRE"
490 PRINT TAB(10,1);"THE CITY UNIVERSITY"
500 PRINTTAB(3,2);"-"
510 PRINTTAB(3,3);"U DISSIPATION IN SAND COLUMN,"F$
520 PRINTTAB(2,13);"-"
530 PRINTTAB(2,14);"U"
540 PRINTTAB(0,15);"(KPa)"
550 PRINTTAB(4,19);"2.0":PRINTTAB(4,10);"6.0"
560 PRINTTAB(16,25);"200       400"
570 PRINTTAB(14,27);"ELAPSE TIME (sec)"
580 REM*****INPUT DATA FOR PLOTTING**
590 FOR I=2 TO 401
600 FOR J=0 TO 6
610 INPUT£S,U(J)
620 NEXT J
630 REM CALCULATE CO-ORDINATES OF PLOTTING POINTS
640 VOLT=U(1)/SV
650 X=(U(0)*1.5)+250
660 Y56=(((U(2)-IT56)/(VOLT*T56))*75)+250
670 Y57=(((U(3)-IT57)/(VOLT*T57))*75)+250
680 Y30=(((U(4)-IT30)/(VOLT*T30))*75)+250
690 Y41=(((U(5)-IT41)/(VOLT*T41))*75)+250
700 Y43=(((U(6)-IT43)/(VOLT*T43))*75)+250
710 REM********PLOTTING POINTS*******
720 PLOT 69,X,Y56
730 PLOT 69,X,Y57
740 PLOT 69,X,Y30
750 PLOT 69,X,Y41
760 PLOT 69,X,Y43
770 NEXT I
780 REM******LINE PRINT SCREN********
790 VDU2
800 VDU1,27,1,65,1,8
810 FORI=0TO&13FSTEP8
820 VDU1,27,1,75,1,0,1,1
830 FORJ=&7EC7TO&5807STEP-&140
840 FORK=0TO7
850 VDU1,(?(J+I-K))
860 NEXT
870 NEXT
880 VDU1,27,1,13
890 NEXT
900 VDU3
910 INPUT P$
920 MODE 7
930 END
```

Figure B.10   Program listing of UDISPR5

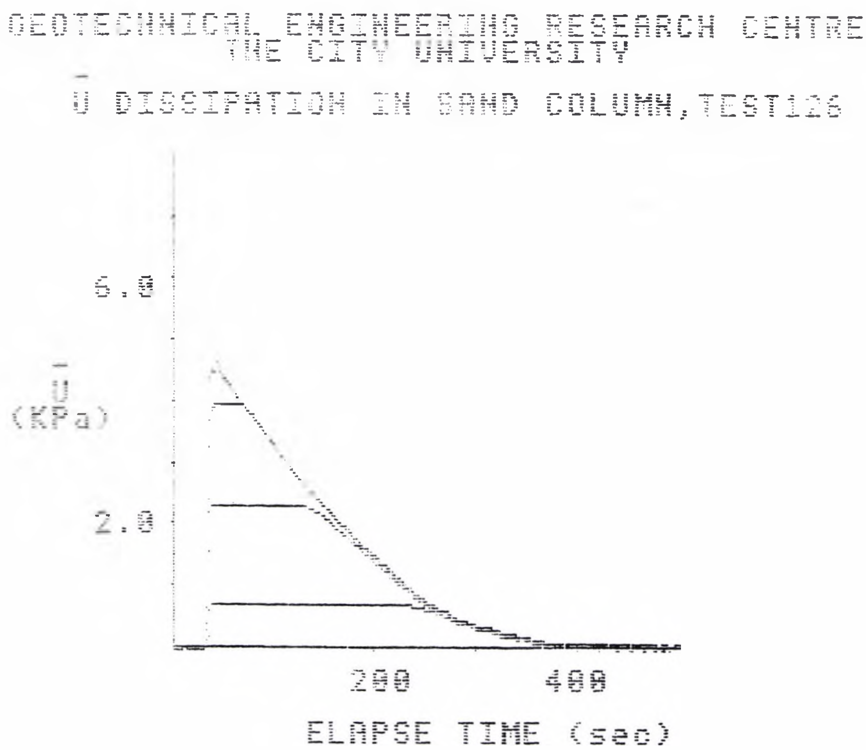

Figure B.11 Example of the output from UDISPR5

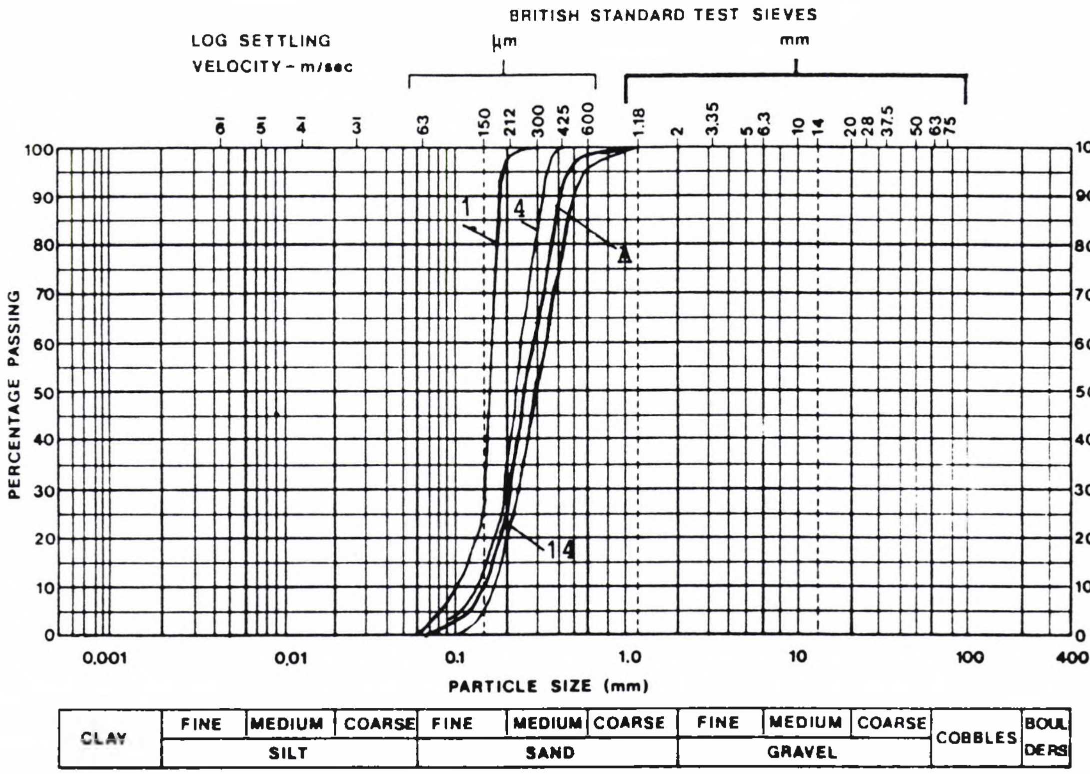

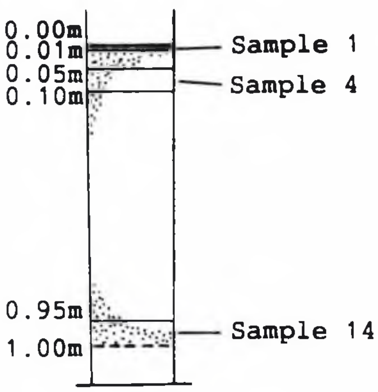

Schematic section through sand column showing the positions of samples within a 1m bed of soil 26. Curve A represents the average grading of soil 26.

Figure D.1 Differential grading within soil beds

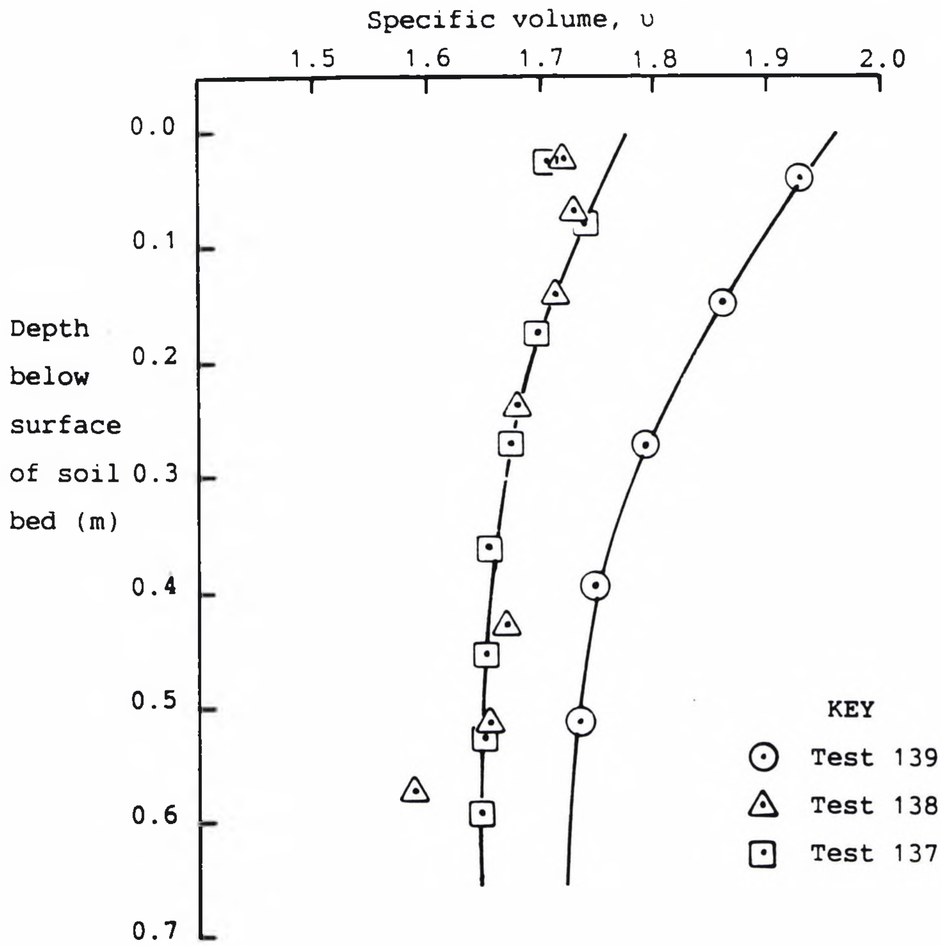

Figure D.2 Variations in soil density within soil beds